ACS APPLIED MATERIALS & INTERFACES

Editors' Choice

www.acsami.org

Review

Recent Advances in Radiative Cooling: From Fundamentals to Commercial Applications

Harit Keawmuang, Junkyeong Park, Heon Lee, Seokju Choi, Sunae So, Changhyeon Lim, Trevon Badloe, Changhwan Hyeon, Minseo Jeong, Dasol Lee, Ya Huang, Siming Zhao, Rufan Zhang, Juhoon Baek, Minkyung Kim, Fei Xie, Longnan Li, Wei Li, Xuzhe Zhao, Jiachen Li, Kaichen Dong, Saichao Dang, Qiaoqiang Gan, Shaowen Cao, Yi Long, Hyunkyu Kwak, Do Hyeon Kim, Young Min Song, Jung Bin Yang, Dong Rip Kim, Yansu Hou, Jia Zhu, Bin Zhu, Shengxi Bai, Kaixin Lin, Chi Yan Tso, Seonggon Kim, Yong Tae Kang, Qingsong Fan, Qizhang Li, Po-Chun Hsu, and Junsuk Rho*

Cite This: *ACS Appl. Mater. Interfaces* 2026, 18, 21363−21423

Read Online

ACCESS | Metrics & More | Article Recommendations

ABSTRACT: Radiative cooling (RC) is a sustainable technology that passively lowers the temperature of terrestrial objects through thermal radiation, dissipating heat into outer space via the atmospheric window, unlike conventional cooling systems that require electricity and release waste heat to the environment. In recent years, RC technologies have advanced rapidly, moving steadily toward practical implementation and commercialization. Here, this mega-review offers a comprehensive overview of RC, encompassing its fundamental background, the underlying photonic and thermal principles, and fabrication approaches for constructing efficient cooling devices. We discuss a variety of RC structures along with their design strategies and explore the diverse functionalities that adapt RC toward particular requirements. We further review emerging applications of RC, highlighting practical implementations. Finally, we outline the key challenges and future directions, offering perspectives and insights to guide continued progress in this rapidly advancing field.

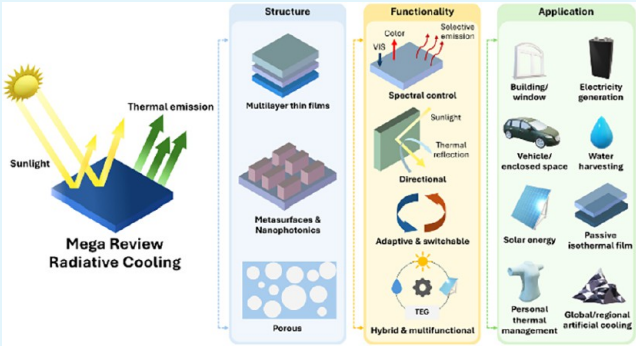

KEYWORDS: *radiative cooling, thermal radiation, photonic materials, metamaterials, thermal management, energy efficiency, sustainable technologies*

1. INTRODUCTION

Harit Keawmuang and Junsuk Rho

The accelerating pace of urbanization and global warming has led to an unprecedented rise in global cooling demand.[1] Cooling is no longer a luxury but a necessity for health, productivity, and comfort in many regions of the world, with the urban population projected to reach 66% of the world's total by 2050,[2] while cooling energy demand for air conditioning is expected to increase by 750% over the same period.[3] Conventional air conditioning requires large amounts of electricity, necessitating major expansions in energy infrastructure. It also drives significant carbon emissions, and the refrigerants it uses have a high global warming potential that further worsens the climate burden.[1] Growing awareness of these energy and environmental challenges has stimulated interest in both improving conventional cooling systems and developing alternatives.

Radiative cooling (RC) has emerged as one of the most promising alternatives. It is a passive process in which a hot object loses heat by emitting thermal radiation toward a colder environment.[4−6] Through this photon exchange, both energy and entropy are carried away, allowing the object to cool without external energy input, unlike conventional systems that consume electricity and release waste heat into the environment.[7] However, the process requires coupling to a colder heat sink that can absorb the emitted radiation. RC is a process that occurs naturally in daily life. For instance, the human body, being warmer than its surroundings, continually releases heat to the environment through thermal radiation. On a larger scale, Earth

Received: January 3, 2026
Revised: March 18, 2026
Accepted: March 23, 2026
Published: April 12, 2026

Downloaded via NATL KAPODISTRIAN UNIV OF ATHENS on June 2, 2026 at 13:46:34 (UTC).
See https://pubs.acs.org/sharingguidelines for options on how to legitimately share published articles.

ACS Publications © 2026 American Chemical Society

https://doi.org/10.1021/acsami.6c00074
ACS Appl. Mater. Interfaces 2026, 18, 21363−21423

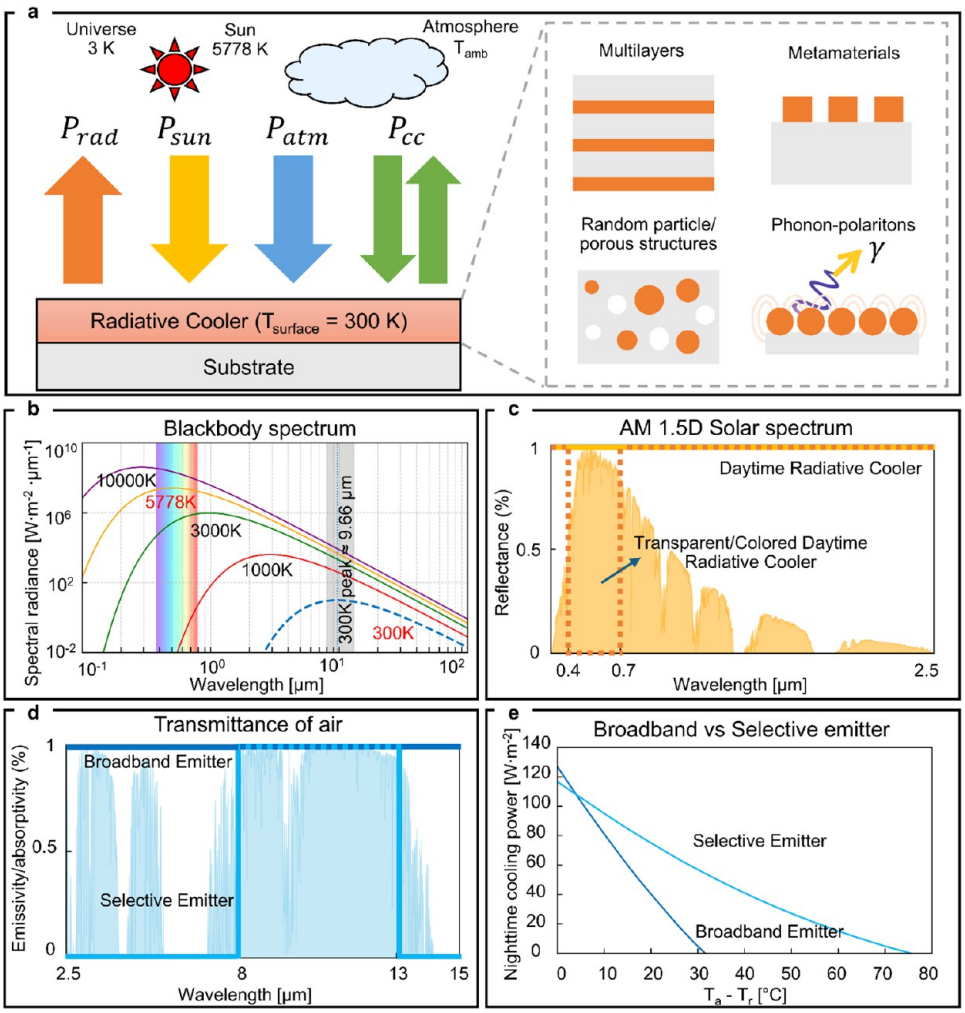

Figure 1. Principle and performance of radiative cooling systems. (a) Schematic illustration of the radiative cooling process, where the device exchanges heat with the universe (3 K), the Sun (5778 K), and the ambient atmosphere. The radiative cooler is typically realized through multilayers, metamaterials, random particle/porous structures, or phonon-polariton-based designs. (b) Blackbody radiation spectra at various temperatures with the 300 K emission highlighted, showing the overlap with the atmospheric window (AW). (c) Solar irradiance spectrum (AM 1.5D, 0.3−2.5 μm, orange shaded area) indicating the spectral range relevant for daytime radiative cooling, including transparent or colored radiative coolers. When the Sun is directly overhead (90° solar altitude), the air mass (AM) is defined as AM 1.0. At oblique incidence, sunlight passes through a thicker atmospheric path, resulting in higher AM values. AM1.5 is the most widely used standard condition on the ground (corresponding to latitudes of approximately 30−40°). Standard AM1.5D data set (ASTM G173) was normalized to their maximum value (set to 1) in order to compare the relative magnitudes across wavelengths. (d) Comparison of air transmittance (2.5−15 μm, blue shaded area) with broadband and selective emitters, emphasizing the importance of matching emissivity with the AW. (e) Nighttime cooling power as a function of temperature difference between the atmosphere and the cooler ($T_{amb} - T_{surface}$), comparing the performance of selective and broadband emitters. Reproduced with permission from ref 42. Available under a CC-BY 4.0 license. Copyright 2020 The Author(s).

(about 300 K) continuously radiates heat to the cold universe, which is at about 3 K, through the mid-infrared atmospheric window (8−13 μm).[8] This spectral range coincides with the peak thermal emission of objects near ambient temperature, allowing a substantial portion of Earth's heat to escape directly into outer space, which effectively acts as the ultimate heat sink.[9,10] Through this concept, a technology known as nighttime RC has been realized, in which a black emitter exposed to the sky radiates its internal heat to the cold universe and cools below the ambient temperature.[11−16] Although RC occurs naturally, its practical implementation requires careful design and control. This becomes especially critical during the daytime, when the greatest cooling demand arises and the challenge is to achieve cooling even under direct solar irradiation. Traditional black emitters used in nighttime studies are ineffective in this case, as they readily absorb sunlight and heat up instead of providing cooling.

Daytime RC addresses the limitation by employing spectrally selective structures that minimize absorption of solar radiation in the range $0.3 \leq \lambda \leq 2.5$ μm while maintaining strong thermal emission in the mid-infrared atmospheric window.[17−23] This spectral selectivity allows radiative coolers to function not only at night but also under direct sunlight during the day. The first demonstration of daytime RC is reported in 2014 by Raman et al.,[24] they use a multilayer photonic structure that reflects incoming solar radiation while emitting strongly in the atmospheric window. Following this breakthrough, the field of RC has rapidly advanced, with the development of diverse structural designs,[25] the expansion of key functionalities,[26−31] and the emergence of a wide range of applications,[32−38]

https://doi.org/10.1021/acsami.6c00074
ACS Appl. Mater. Interfaces 2026, 18, 21363−21423

establishing it as a leading direction in energy-efficient technologies.

This mega-review presents a comprehensive overview of RC, covering its background, principles, structures, functionalities, and applications. We begin by introducing the fundamental photonic and thermal concepts that govern RC, and representative fabrication strategies for realizing radiative coolers. We then explore diverse structural configurations of radiative coolers, along with their design strategies and essential characteristics. Next, we highlight the key functionalities that tailor RC performance for specific needs, with a focus on physical principles, design approaches, and key performance metrics. Then, we further survey emerging applications across diverse domains, such as energy-efficient buildings, solar energy systems, and electricity generation, highlighting practical implementations of RC across these fields. Particular emphasis is placed on system-level performance, integration strategies, and real-world impact. Lastly, we discuss the remaining challenges and future outlook, aiming to offer both a broad perspective and useful insights for further development in this rapidly evolving field.

2. FUNDAMENTALS AND PRINCIPLES OF RC

2.1. Thermal Balance of RC

Junkyeong Park and Junsuk Rho

Heat transport originates from the nonequilibrium energy distributions of four fundamental carriers: phonons, electrons, fluid particles, and photons.[6,39] Microscopic heat transfer phenomena can thus be interpreted through the behavior of these fundamental carriers. Phonons, representing quantized lattice vibrations, are responsible for thermal conduction in dielectric materials. Electrons contribute to thermal conduction particularly in conductors and semiconductors, where their concentration may be constant or vary with temperature. Fluid particles, whether monatomic or polyatomic, transfer heat through collisions with neighboring fluid particles, a process known as convection. Photons, the only carriers capable of transporting energy across a vacuum, span a broad energy range relevant to heat transport, from far-infrared to ultraviolet (UV). They interact with electric and magnetic entities, thereby defining material-specific electromagnetic responses. In general, heat transfer occurs through the transport of these carriers, whereas energy conversion arises from their inelastic interactions.

To examine photons in more detail, a photon can be interpreted not only as a particle but also as an electromagnetic wave. A blackbody is an idealized emitter that radiates electromagnetic energy solely as a function of its temperature. By introducing the concepts of quantized radiation energy and the Planck constant, Max Planck formulated the spectral distribution of blackbody radiation and demonstrated that the peak emission wavelength shifts with temperature (Figure 1b). The equation of this principle is as follows:[9]

$$I_{BB}(\lambda, T) = \frac{2hc^2}{\lambda^5}\frac{1}{e^{hc/\lambda k_B T} - 1} \tag{1}$$

where $h = 6.626 \times 10^{-34}$ Js is Planck's constant, $k_B = 1.381 \times 10^{-23}$ J/K is the Boltzmann constant, $c = 2.998 \times 10^8$ m/s is the speed of light. In this sense, every object at a temperature above 0 K continuously radiates thermal energy into its surroundings.

Radiative cooling technologies aim to enhance and control this naturally occurring process for efficient thermal management. The Sun, at a temperature of around 5778 K, emits predominantly in the visible (VIS) range (Figure 1c), whereas the Earth, at approximately 300 K, emits primarily in the mid-infrared, particularly within 8−13 μm. Importantly, at the same time, Earth's atmosphere exhibits selective transparency in this range (Figure 1d). While water vapor strongly absorbs radiation below 8 μm and both water vapor and CO_2 absorb above 13 μm, the 8−13 μm region, known as the "atmospheric window (AW)", allows infrared radiation to escape into outer space with minimal absorption. This spectral overlap between terrestrial blackbody emission and the AW forms the physical basis of passive radiative cooling.

To describe the thermal behavior of a radiative cooler at the macroscopic level, heat transfer is governed by the heat flux P, which includes contributions from conduction, convection, and radiation (Figure 1a). These mechanisms are generally treated under the assumption of local thermodynamic equilibrium, where thermal energy is stored and exchanged in a quasi-static manner. Based on this framework, the net thermal behavior of a radiative cooling system can be expressed as[4]

$$P_{cool}(T, T_{amb}) = P_{rad}(T) - P_{sun} - P_{atm}(T_{amb}) - P_{cc}(T, T_{amb}) \tag{2}$$

Here, P_{cool} denotes the total cooling power of the system. P_{rad} is the thermal radiation emitted by the cooler, P_{sun} is the absorbed solar power, P_{atm} is the downwelling atmospheric thermal radiation absorbed by the cooler, and P_{cc} accounts for nonradiative energy exchange via conduction and convection. These terms are expressed as follows:

$$P_{rad}(T) = \int d\Omega \cos\theta \int_0^\infty d\lambda I_{BB}(T, \lambda)\epsilon(\lambda, \theta) \tag{3}$$

$$P_{sun} = \int_0^\infty d\lambda I_{sun}(\lambda)\epsilon(\lambda, \theta_{sun}) \tag{4}$$

$$P_{atm}(T_{amb}) = \int d\Omega \cos\theta \int_0^\infty d\lambda I_{BB}(T_{amb}, \lambda)\epsilon_{atm}(\lambda, \theta)\epsilon(\lambda, \theta) \tag{5}$$

The solid angle integral $\int d\Omega$ spans the hemisphere above the surface, and θ denotes the zenith angle. I_{BB} refers to the spectral radiance (W m^{-2} sr^{-1} μm^{-1}) of a blackbody. I_{sun} refers to the spectral irradiance (W m^{-2} μm^{-1}) of the sun, assuming that the structure is facing the sun at a fixed angle θ_{sun}. For I_{sun}, the AM1.5 solar spectrum ($I_{AM1.5}$) is commonly used as the standard terrestrial condition. $\varepsilon(\lambda,\theta)$ is the directional spectral emissivity of the cooler, and $\varepsilon_{atm}(\lambda,\theta)$ describes the angular and spectral dependence of atmospheric emissivity. The latter can be related to the zenith-direction transmittance (λ) through:

$$\varepsilon_{atm}(\lambda, \theta) = 1 - \tau(\lambda)^{1/\cos\theta} \tag{6}$$

Finally, nonradiative heat exchange with the ambient environment is modeled as

$$P_{cc}(T, T_{amb}) = h_{cc}(T_{amb} - T) \tag{7}$$

where h_{cc} is an effective heat transfer coefficient encompassing both convective and conductive contributions.

For applications that demand cooling power either close to the ambient temperature or significantly below it, the emissivity of the radiative cooling surface can be tuned in various ways.[4,40] A representative comparison can be made between a broadband emitter, which exhibits high emissivity over all infrared

https://doi.org/10.1021/acsami.6c00074
ACS Appl. Mater. Interfaces 2026, 18, 21363−21423

wavelengths, and a selective emitter, which exhibits high emissivity only within the AW (Figure 1d). A broadband emitter enables large cooling power output. However, based on Kirchhoff's law, such a surface not only emits thermal radiation through the AW but also absorbs incoming radiation outside this range. This reciprocal effect limits its ability to reach temperatures lower than the ambient environment. In contrast, a selective emitter, characterized by near-unity emissivity solely within the AW, reduces absorption of downward atmospheric radiation and thereby enables deeper subambient cooling. Consequently, broadband emitters are advantageous for maximizing cooling power when the device temperature is above or near ambient, whereas selective emitters are better suited for achieving significantly lower surface temperatures. As illustrated in Figure 1e, the selective design reaches substantially lower equilibrium temperatures. The calculation assumes an ambient temperature of 27.15 °C under ideal conditions, with solar absorption and parasitic nonradiative losses neglected, and an atmospheric transmission spectrum corresponding to 60% relative humidity.

Additionally, the angular dependence of atmospheric emissivity can also be considered in cooler design to minimize P_{atm}. Atmospheric emissivity is highest at grazing angles (θ = 90°) within the 4−20 μm range, but lowest at normal incidence (θ = 0°) in the 8−13 μm window. Thus, tailoring the cooler's emissivity profile to account for angular variations in atmospheric radiation enhances its performance.[4,40,41]

2.2. Photonic Concepts of RC

Junkyeong Park and Junsuk Rho

Nighttime radiative cooling,[43,44] which enables thermal emission into outer space, has been studied and utilized since the 1970s. For decades, radiative cooling during the daytime was considered impossible because the solar radiation term (P_{sun}) is overwhelmingly large. However, in 2014, the concept of daytime radiative cooling[24,45] was introduced, demonstrating that radiative cooling can also be achieved under direct sunlight. This is made possible by employing photonic structures capable of reflecting both visible and near-infrared (NIR) radiation. The key to daytime RC lies in minimizing solar absorption while maximizing thermal emission within the AW.

Recent progress in nanophotonics has enabled precise manipulation of electromagnetic properties using engineered nano- and microscale structures.[9] Photonic structures of radiative coolers reported to date can be broadly classified into four categories: multilayer structures, metamaterials, random particles, and porous structures. Multilayer designs consist of stacked materials with carefully tuned sequences and thicknesses to achieve desired spectral responses. For example, dielectric-metal-dielectric layers can induce surface plasmon effects,[46] whereas alternating dielectric layers form Bragg mirrors;[47] both structures can be utilized to achieve reflection. Metal-dielectric-metal layers are often employed to design absorbers or emitters.[48] Metamaterials, composed of subwavelength structures, allow fine control of light-matter interactions, including the excitation of resonances and the creation of effective gradient refractive indices.[49−51] By employing the photonic concepts of these structures, various radiative cooler designs that are transparent, colored, or tunable have also been proposed (dashed region in Figure 1c).

For practical deployment, scalability, cost-effectiveness, and optical robustness are critical. Unlike periodic designs, random particle and porous structures exploit multiple scattering in disordered configurations to yield inherently broadband, polarization-independent, and angle-insensitive optical responses.[52] Such characteristics are advantageous under incoherent and broadband illumination, for example, solar radiation. These structures can be fabricated from dielectric or metallic materials through scalable and low-cost techniques, including coating,[53] casting,[54] and spraying.[55] Collectively, these attributes constitute a practical platform that combines spectral control, manufacturability, and durability for large-scale radiative cooling applications.

The choice of materials is primarily determined by refractive index and absorption characteristics within the AW. High index materials such as titanium dioxide (TiO_2) and silicon (Si), low index materials such as polytetrafluoroethylene (PTFE) and silicon dioxide (SiO_2), are commonly employed. Materials such as polydimethylsiloxane (PDMS) and silicon nitride (Si_3N_4) exhibit strong phonon-polariton resonances within the 8−13 μm AW, enabling efficient thermal absorption in this spectral range. According to Kirchhoff's law of thermal radiation, their high absorptivity directly translates into high emissivity, making them effective radiative cooling materials. Since they are transparent in the visible range, their spectral properties can also be tailored for use as coatings in transparent or colored radiative cooling devices.[28,56,57]

Metals such as silver (Ag) and aluminum (Al) exhibit high reflectivity and are widely used as underlying substrates or back reflectors in radiative cooling devices to suppress solar absorption and enhance cooling performance. Furthermore, by tailoring the metal layer thickness or nanostructure, plasmonic resonances can be engineered to enable selective transmission at desired wavelengths, produce desired colors, or tailor spectral absorption and therefore emissivity.

Biomimetic approaches have also been investigated, drawing inspiration from desert beetles,[58,59] butterfly wings,[60] and plant cuticles[61,62] to enhance radiative cooling. These structures provide passive thermal regulation, multifunctionality, and hierarchical ordering, improving solar reflectance and mid-infrared emissivity while ensuring scalability and environmental compatibility. Extending these principles to wearable devices, textiles have recently been proposed as a pathway for personal thermal management.[32,63] Detailed examples and material-specific discussions will be presented in the following section.

2.3. Representative Fabrication Strategies

Heon Lee

The first passive daytime radiative cooling device was fabricated by vacuum-depositing a thin metallic silver film on a silicon wafer substrate to reflect incident solar radiation, and then repeatedly depositing thin films of silicon oxide and hafnium oxide with varying thicknesses to emit (absorb) infrared radiation in the atmospheric window region. This experiment was the first to experimentally demonstrate cooling below ambient temperature during the day via radiative cooling.[24] Subsequently, extensive research has focused on implementing selective emissions in the atmospheric window. Hossain et al. maximized selective emission in the window region using a photonic structure containing multilayer metamaterials of chromium and aluminum.[49] Zou et al. enhanced atmospheric window emissivity by forming a periodic metasurface structure using phosphorus-doped n-type silicon and silver.[64] Sequential deposition of different kinds of ceramic thin films also significantly increases infrared emission in the atmospheric window. Chae et al. fabricated a radiative cooling

https://doi.org/10.1021/acsami.6c00074
ACS Appl. Mater. Interfaces 2026, 18, 21363−21423

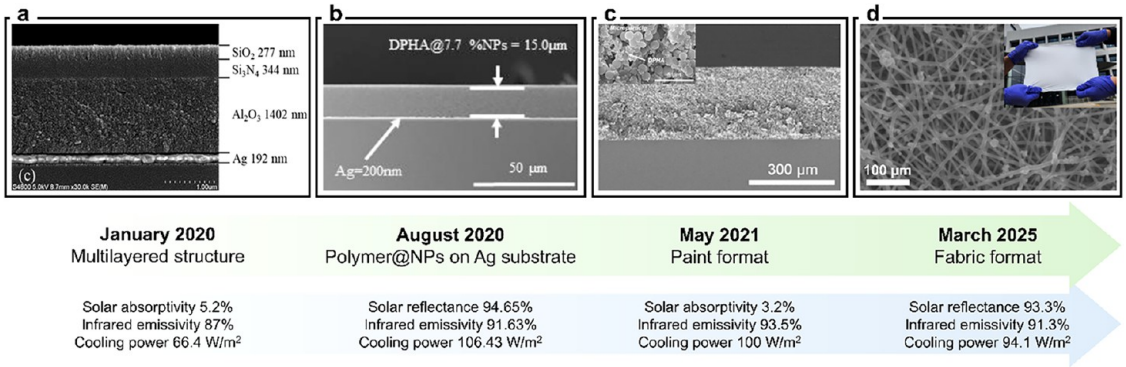

Figure 2. Evolution and performance progression of radiative cooling devices. (a) Multilayered thin film structure (January 2020). Adapted with permission from ref 22. Copyright 2020 American Chemical Society. (b) Dispersed nanoparticles in polymer matrix of Ag thin film (August 2020). Adapted with permission from ref 53. Copyright 2020 Elsevier. (c) Dispersed nanoparticles in polymer matrix (paint format, May 2021). Adapted with permission from ref 66. Copyright 2021 Elsevier. (d) Dispersed nanoparticles in polymer fiber (fabric format, March 2025). Adapted with permission from ref 67. Copyright 2025 Elsevier. The timeline and annotations summarize the reported optical/thermal performance for each generation, including solar absorptivity/reflectance, infrared emissivity, and cooling performance, to highlight performance improvements across successive device formats.

device by depositing aluminum oxide, silicon nitride, and silicon oxide at thicknesses of 1402, 344, and 277 nm, respectively, achieving a solar absorption rate of 5.2% and atmospheric window emissivity of 87%.[22] Ma et al. improved atmospheric window emission by multiple-layer deposition of silicon oxide and silicon nitride, excluding alumina, and used a silver thin film for solar reflection.[65] However, multilayer ceramic film composition is not always effective, facing disadvantages such as high processing cost and restrictions on substrate types due to high temperature processes.

Dispersing ceramic microparticles in a polymer matrix can boost emissivity in the window region through the covalent bonds of the polymer and the resonant infrared absorption of the ceramic particles, potentially replacing multilayer ceramic thin films. Forming a polymer layer with dispersed ceramic microparticles over a silver thin film results in a simpler radiative cooling device. Professor Yin at the University of Colorado developed an advanced radiative cooling material by dispersing silica microparticles in a polymethylpentene (TPX) polymer.[52] Professor Lee's research group at Korea University mixed alumina, silica, and silicon nitride—previously thin-film materials—in particle form into dipentaerythritol penta-hexa-acrylate (DPHA) polymer and coated it on a silver layer to implement a radiative cooling device.[53] However, this method makes it difficult to achieve selective high emissivity only in the atmospheric window; instead, it achieves high reflectance across the entire long-wave infrared region, including the window (Figure 2).

A method to achieve over 96% solar reflectance without using metallic silver was proposed. Son et al. secured high reflectance across all solar wavelengths by employing microscopic pore scattering formed from blends of different polymer matrices, instead of mirror reflection with silver films. Using poly(vinylidene fluoride) (PVDF) powder and polyurethane acrylate (PUA), they achieved 93% solar reflectance and 93% average atmospheric window emissivity.[68] Yet, such methods have drawbacks: the polymer matrices are expensive, and the presence of micropores can compromise device durability. Alternatively, ceramic particles with high whiteness, reflectance, and refractive index—capable of strong solar scattering—are dispersed in more common polymer matrices for radiative cooling devices. Barium sulfate and calcium carbonate particles were first explored, leading to the development of paint-type radiative cooling devices. Professor Ruan at Purdue University published a white paint using $BaSO_4$ and an acrylic binder, showing excellent cooling performance with 97.6% solar reflectance and 96% atmospheric window emissivity.[69] The research group also created a device utilizing $CaCO_3$ particles, achieving 95.5% solar reflectance and 94% window emissivity.[70] Subsequently, research utilizing various ceramic particles or combinations of particles has been actively conducted.[23,66,71,72] These paint-type radiative cooling devices are a form where ceramic particles are dispersed in a liquid polymer resin. When applied as a paint film on various substrates, this film reflects the incident sunlight by scattering with ceramic particles, while the polymer resin and dispersed ceramic particles within the coating show high absorption for long-wavelength infrared, including the atmospheric window region, thereby enabling radiative cooling. Compared to conventional paint, which maxes out at 88% solar reflectance, the high incident solar reflectance of over 96% makes it possible for radiative cooling to achieve temperatures lower than the ambient temperature even during the sunny daytime. Paint-type radiative cooling devices offer lower manufacturing costs by using inexpensive ceramic particles with no degradation from silver oxidation, high versatility as coatings can be directly applied to metals, resins, concrete, wood, and more, and direct applicability to large-area objects. Despite these advantages, practical deployment of paint-type RC devices still faces several challenges. One of the primary concerns is the long-term outdoor durability. Among these, soiling can reduce solar reflectance over time by depositing contaminants on the coating surface.[33,73] In this regard, hydrophobic or self-cleaning RC designs[73−76] that can withstand physical cleaning are promising for mitigating soiling, maintaining cooling performance, and extending operational lifetime. Furthermore, prolonged exposure to solar UV irradiation can gradually degrade RC performance over time.[77] To mitigate this issue, fluoropolymer-based coatings can be integrated into RC systems, as their relatively low UV absorption helps preserve solar reflectance, hence preserving long-term outdoor stability.[78] Adhesion to different substrates is another important practical consideration for paint-type RC systems, particularly for architectural coating applications, as insufficient interfacial stability can lead to peeling, cracking, or delamination

https://doi.org/10.1021/acsami.6c00074
ACS Appl. Mater. Interfaces 2026, 18, 21363−21423

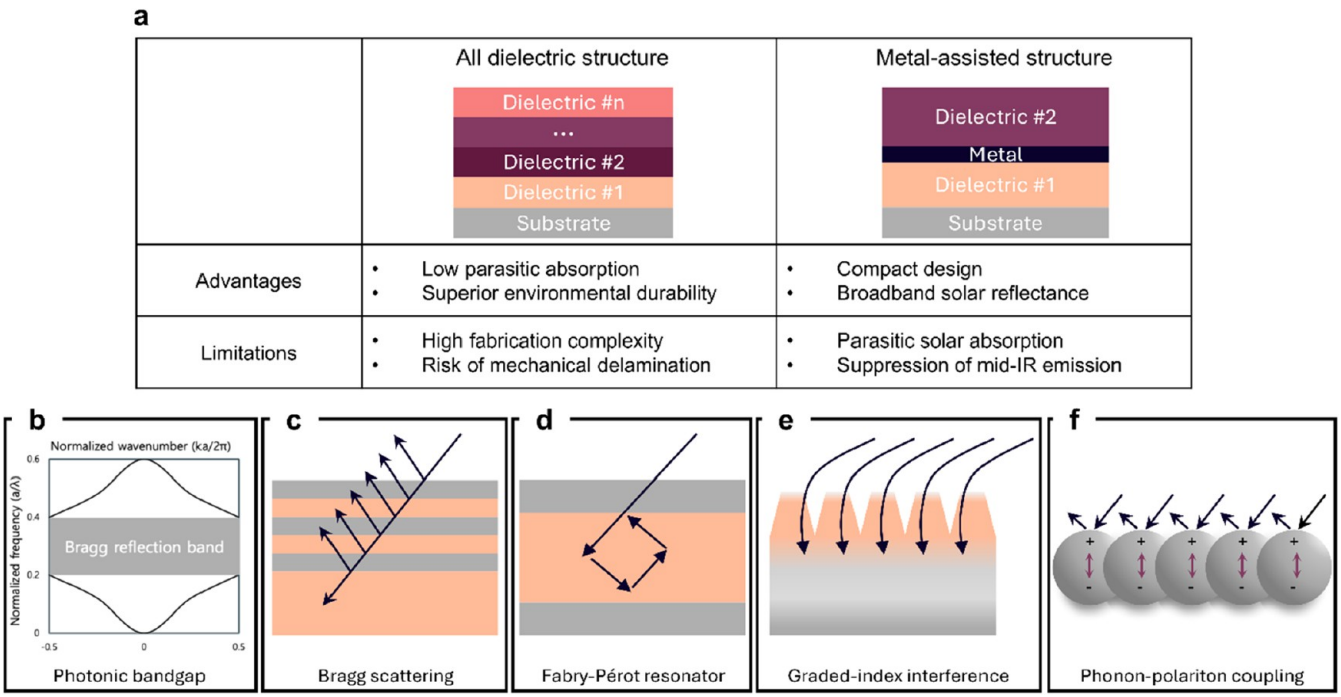

Figure 3. An overview of multilayer designs and their physical mechanisms for radiative cooling. (a) Comparative summary of all-dielectric multilayer structures and metal-assisted structures. (b) Photonic bandgap in a 1D photonic crystal. (c) Bragg scattering and interference effects. (d) Fabry−Pérot resonance between two reflective surfaces. (e) Interference in a graded refractive index. (f) Phonon-polariton resonance.

during long-term outdoor use.[79] Accordingly, recent RC coating designs have increasingly sought to improve substrate adhesion together with outdoor durability and optical performance.[80,81]

Another form is radiative cooling fabrics. By incorporating ceramic nanoparticles during polymer fiber fabrication, fibers embedded with these particles can be woven into fabrics with radiative cooling properties (i.e., high solar reflectance and high atmospheric window emissivity). A simpler method is to create fabric using electrospinning by mixing ceramic nanoparticles such as TiO_2 and Al_2O_3 into polymer resins like PU, PAN, or PVDF.[82,83] Subsequently, treatments such as pressing can be applied to ensure the fabric has appropriate mechanical properties, thereby producing a fabric with radiative cooling function.[84] Textile-form radiative cooling materials have great industrial and economic potential because they can be used directly in clothing and hats to enhance thermal comfort. Iqbal et al. embedded ZnO in a polyethylene matrix to fabricate textiles by electrospinning, yielding personal thermal management material that reflects sunlight while allowing body heat emission.[38] Park et al. reported electrospun fibers with excellent radiative cooling performance, based on PMMA, thermoplastic polyurethane (TPU), and Al_2O_3 nanoparticles.[85] However, the ceramic nanoparticles and nanopores added to realize the radiative cooling function can potentially impair the inherent properties of the fabric. For example, deterioration in the fabric's mechanical strength, flexibility, wrinkle recovery, and texture are typical problems. Various researchers are working on producing fabrics with excellent radiative cooling ability while minimizing these problems. For instance, Lim et al. developed a fabric-type cover sheet using PU and TiO_2 materials via an electrospinning process, and their research team confirmed that the mechanical strength and optical properties were maintained even after over 1000 cycles of tension and contraction.[67]

3. STRUCTURES OF RC

3.1. Multilayer Thin Film Structures

Seokju Choi and Sunae So

Multilayer thin films, composed of alternating layers of materials with distinct optical properties, are among the earliest and most extensively investigated approaches for RC (Figure 3a). Their primary function is to suppress solar energy absorption while simultaneously enhancing thermal emission within the atmospheric transparency window. This dual spectral control is governed by well-established photonic mechanisms, including photonic bandgaps[86] arising from Bragg scattering,[87] Fabry−Pérot resonances,[88] graded-index interference[89] and, in some cases, phonon-polariton coupling[90] (Figure 3b−f). Owing to their rigorous theoretical foundation, compatibility with mature thin-film fabrication methods, and adaptability across a wide range of substrates, multilayer thin films continue to serve both as benchmark systems and as practical platforms for scalable RC.

The operating principles of multilayer structures are rooted in classical optics. Periodic stacks of high- and low-refractive-index materials generate Bragg scattering and associated photonic bandgaps, where light propagation is strongly suppressed. When aligned with the solar spectrum (0.3−2.5 μm), such bandgaps enable broadband reflection, thereby effectively minimizing parasitic solar heating.[22,24] Fabry−Pérot resonances provide another route to spectral control:[91−94] placing a dielectric spacer between two reflective interfaces creates standing-wave modes that selectively enhance emissivity in the mid-infrared. By adjusting cavity thickness, these emissivity peaks can be positioned within the atmospheric window (8−13 μm), allowing for efficient thermal emission. Beyond such discrete mechanisms, graded-index multilayer structures,[45,95,96] where refractive index or layer thickness changes gradually across the stack, produce broadened reflection bands. In practice, high-

https://doi.org/10.1021/acsami.6c00074
ACS Appl. Mater. Interfaces 2026, 18, 21363−21423

performance multilayer films typically combine multiple mechanisms, often supplemented by the intrinsic vibrational resonances of the chosen materials.

Materials are central to performance. Transparent dielectric oxides such as SiO_2, TiO_2, HfO_2, Al_2O_3, and ZrO_2 are widely employed due to their generally low optical losses across most of the solar spectrum and good thermal stability, making them ideal for alternating high/low-index layers in Bragg-type designs. Low-index fluorides such as MgF_2 and CaF_2 further increase refractive index contrast, thereby strengthening interference effects in the solar band. These fully dielectric multilayers can achieve excellent solar reflectance and robust mid-infrared emissivity, though typically at the expense of requiring many layers, increasing fabrication complexity.

Incorporating metals into multilayer structures offers a more compact route to broadband solar reflection. Metal-assisted multilayer designs take several forms, including metal-backed dielectric stacks,[24] dielectric-metal-dielectric (DMD) structures[97,98] and hyperbolic metamaterials (HMMs).[99,100] DMD stacks place a thin metal film between dielectric layers, providing broadband reflection across the solar spectrum with only a few layers, while the dielectrics tune interference effects and protect the metal surface. Metal-backed dielectric stacks adopt a simpler geometry in which a reflective metal substrate serves as the bottom mirror upon which dielectric multilayers are deposited to tailor mid-infrared emission. HMMs, composed of deeply subwavelength alternating metal and dielectric layers, exploit extreme optical anisotropy to control spectral response across distinct wavelength bands. Despite these structural advantages, metallic layers paradoxically introduce several practical limitations that compromise their overall performance and longevity. They introduce parasitic absorption, converting a fraction of incident sunlight into heat. In addition, metals generally exhibit low intrinsic emissivity in the mid-infrared, meaning that efficient thermal emission must be achieved through careful design of the surrounding dielectric or resonant structures. A common workaround has been to add an emissive polymer overlayer, which restores emission in the mid-infrared.[101,102] However, these polymers complicate fabrication workflows by requiring separate processing routes (e.g., spin coating or dip coating) that are not directly compatible with vacuum-based thin-film deposition. Furthermore, polymers degrade under long-term UV exposure, leading to yellowing, cracking, or reduced emissivity, ultimately shortening device lifetime.[103] Thus, while metal-assisted multilayers remain attractive for transparent RC applications such as smart windows, their reliance on metals continues to impose fundamental limitations.

An alternative approach involves incorporating polar dielectrics such as SiC, SiO_2, and $BaSO_4$ into multilayer stacks. These materials support phonon−polariton resonances in the mid-infrared, producing selective emissivity peaks that naturally align with the atmospheric window. By coupling interference effects with vibrational resonances, such multilayers achieve strong thermal emission without relying on polymers or suffering from metallic absorption losses.

Fabrication of multilayer films leverages well-established thin-film deposition techniques. Physical vapor deposition, where a solid source material is physically converted into a vapor through processes such as evaporation such as evaporation[24,104] and sputtering,[105] are most widely used offering nanometer-scale thickness control and high film uniformity.[106] Chemical vapor deposition, which involves introducing precursor gases that chemically react or decompose on the substrate surface to form the desired film, is also used for dielectric layers, especially when low-temperature growth is required.[107−110] Atomic layer deposition provides angstrom-level precision and excellent conformality, making it particularly attractive for hybrid or graded-index designs where exact layer control is critical. More recently, sol−gel processing[111,112] and solution-based spin-coating[113] have been explored as low-cost alternatives, though their reproducibility and precision are still limited. For practical deployment, industrial-scale methods such as roll-to-roll sputtering[114] and glass-coating lines[115] are promising, yet achieving defect-free interfaces and thickness precision across tens of alternating layers remains a formidable technical challenge.

Despite significant progress, multilayer thin films present ongoing design and fabrication challenges. Fabrication can be complex and costly, especially when many alternating layers are required to achieve broadband reflectivity. This can increase manufacturing time and may lead to mechanical stress within the film, potentially causing delamination.[116] Interference-based optical responses are inherently angle-dependent, reducing cooling effectiveness under diffuse or oblique sunlight. Additionally, there are material constraints: high-refractive-index dielectrics that are both perfectly nonabsorbing across the entire solar spectrum and stable under environmental conditions are scarce. Finally, while thin-film deposition is scalable in principle, achieving large-area, defect-free multilayer structures with precise thickness control across many layers remains a bottleneck for mass production.

Looking forward, several research directions appear especially critical. Improving angular robustness through graded-index designs[117−119] will be crucial for stable performance under realistic outdoor conditions. Enhancing durability by replacing polymer overlayers with inorganic emissive coatings,[120,121] or by employing alloyed[122] and encapsulated[120,123,124] metallic films, could significantly extend device lifetimes. At the same time, discovering or engineering new dielectric compounds with tailored refractive indices would expand the design space beyond the relatively narrow set of oxides and fluorides currently available.[125−127] The integration of polar dielectrics is particularly attractive, as their intrinsic phonon-polariton resonances align naturally with the atmospheric window, offering selective emissivity without reliance on metals or polymers.[128−131] Employing scalable fabrication strategies are also important. Hybrid approaches that combine precision thin-film layers with solution-based or roll-to-roll coatings may offer a path toward affordable large-area deployment.[56,132,133] Finally, computational optimization techniques and AI-driven inverse design are expected to further accelerate progress, as the optical response of multilayer films can be readily modeled.[21,57,134] Leveraging such tools to achieve multiobjective, high-performance structures that not only maximize RC performance but also integrate additional functions such as durability, self-cleaning, and aesthetic control will open opportunities for multifunctional coatings with real-world relevance.[27,135−137]

3.2. Metasurfaces and Nanophotonic Structures

Changhyeon Lim and Trevon Badloe

Metasurfaces are two-dimensional structures with precisely arranged subwavelength features that enable complete control of the optical properties of light.[138,139] As the optical response of a metasurface can be finely tuned by adjusting the material and geometrical parameters of its constituent structures, known as

https://doi.org/10.1021/acsami.6c00074
ACS Appl. Mater. Interfaces 2026, 18, 21363−21423

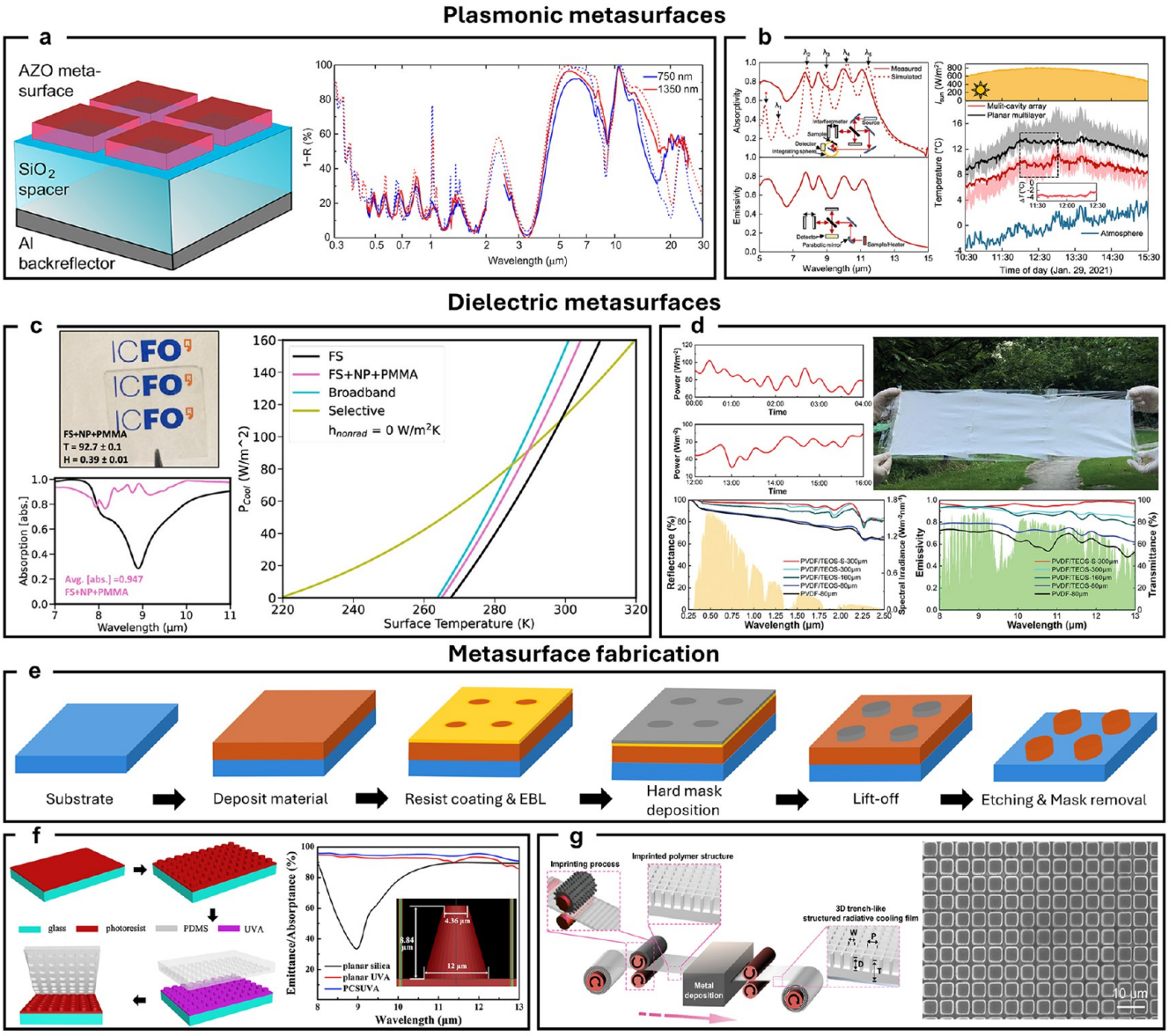

Figure 4. Metasurfaces and nanophotonic structures of RC. (a) Schematic cross-section of the metasurface-based radiative cooler for space applications (left) and measured absorption spectra (right). Adapted with permission from ref 144. Copyright 2018 American Chemical Society. (b) Absorption and emissivity spectra within the atmospheric window (left) and comparison of daytime cooling performance between planar and multicavity structures (right). Adapted with permission from ref 146. Copyright 2021 American Chemical Society. (c) Photos of transparent metasurface-based radiative cooler (top left) and absorption spectra (bottom left). Calculated cooling power (left). Adapted with permission from ref 147. Copyright 2022 American Chemical Society. (d) RC power throughout the day (top left) and large radiator pasted on a transparent membrane (top right). Reflectance and emissivity spectra in atmospheric window (bottom). Adapted with permission from ref 149. Copyright 2020 Wiley-VCH. (e) Schematic of a standard metasurface fabrication method. (f) Schematic of nanoimprint fabrication method (left) and simulated absorptance spectra (right). Adapted with permission from ref 157. Copyright 2019 Elsevier. (g) Schematic of the roll-to-roll nanofabrication process (left) and scanning electron microscope (SEM) image showing the uniform meta-atoms. Adapted with permission from ref 133. Copyright 2023 Springer Nature.

meta-atoms, they have shown extreme applicability for RC applications, where the manipulation of the absorption/emission across the spectrum from the visible to the mid-infrared region is required. This is generally designed through multipole resonances designed at specific locations through plasmonics or high refractive index dielectrics. With these versatile properties, metasurfaces have emerged as a powerful tool for managing thermal radiation and enabling daytime RC.[9,40,140]

Since metasurfaces can be designed with resonance characteristics at specific wavelengths, they allow for direct implementation of efficient emission through the atmospheric window and simultaneous modulation of visible and NIR wavelengths, the keys for daytime RC. Plasmonic metasurfaces are engineered to modulate the spectral response through various mechanisms at metal/dielectric interfaces[141] and have been proven for RC purposes.[142,143] Sun et al. developed a metasurface-based optical solar reflector using aluminum-doped zinc oxide (AZO) as a transparent conductive oxide for the RC of spacecraft (Figure 4a).[144] The AZO is a plasmonic material in the infrared, while staying transparent in the visible, providing a high thermal emissivity of 79% in the infrared region and a low solar

https://doi.org/10.1021/acsami.6c00074
ACS Appl. Mater. Interfaces 2026, 18, 21363−21423

absorptance of 16% in the visible range. Not only the optical performance of the AZO, but also its mechanical and thermal robustness prove it to be a strong choice for spacecraft solar reflectors. In space applications, however, the requirement for selective emission through the atmospheric window is relaxed, reducing one of the design requirements for metasurface-based daytime radiative coolers.

Gap plasmon resonances in metal−dielectric−metal cavities have been proposed as an effective strategy for RC due to their broadband thermal emission.[145] Cho et al. demonstrated a multicavity Cu/ZnS/Cu metasurface that supports multiple gap plasmon resonances, providing 62% emissivity in the atmospheric window (Figure 4b).[146] Experiments showed a substrate temperature reduction of up to 4 °C compared with a planar Cu/ZnS/Cu thin film. This highlights the potential of plasmonic metasurfaces in RC applications compared to simple multilayer structures. While the control of emission spectra with multiple plasmonic meta-atoms exhibiting low-Q resonances is a powerful answer to terrestrial- and space-based cooling applications, recently, there has been a rise in the use of all-dielectric materials for the creation of metasurfaces.

The main drawback of using metals in RC metasurfaces is the inherent absorption that they possess, which will reduce the efficiency of the device through Ohmic heating. Therefore, all-dielectric metasurfaces have been demonstrated as solutions to daytime RC.[64,119] In one example, Arrés Chillón et al. proposed a lithography-free approach for RC using a transparent glass surface decorated with randomly distributed nanopillars in (Figure 4c).[147] The nanopillars are randomly distributed but approximating a periodic arrangement. The addition of the nanopillars suppresses the infrared reflection of SiO_2 at 9 μm, achieving a near unit emissivity. Furthermore, an additional PMMA polymer coating was applied to mitigate haze caused by the deep nanopillar structures in the visible spectrum by reducing the surface scattering. This resulted in a high transmittance of T = 93.1%, producing a radiative cooler with a P_{cool} = 138.74 W m^{-2} while maintaining the transparency of glass.

When the wavelength of incident light is comparable to the geometric dimensions of the meta-atom, oscillations in the electromagnetic field are induced, leading to Mie scattering.[148] This scattering reduces solar absorption and can be harnessed for various RC applications. Wang et al. incorporated nanopores with diameters in the range of 100−200 nm into a flexible metasurface-based radiative cooler, inducing Mie scattering that resulted in a solar reflectance of 97% and an infrared emissivity of 96% (Figure 4d).[149] Experimental measurements demonstrated a daytime temperature reduction of up to 6 °C and a RC power of 61 W m^{-2}, while also exhibiting excellent flexibility and mechanical strength, indicating strong potential for large-scale practical deployment. While solar reflectance depends on the areal coverage ratio, cooling performance within the atmospheric window is most sensitive to geometric parameters such as pattern size, spacing, and shape.[150]

The design of RC structures faces interesting photonic challenges due to the order of magnitude wavelength mismatch between the visible regime (100s of nanometers) and the mid-infrared (micrometers). This makes the design process a multiscale problem, which can be difficult to achieve heuristically; therefore, artificial intelligence (AI) has been implemented in the design and optimization process.[151] Su et al. applied the k-nearest neighbor algorithm to construct regression models for optimizing the parameters of both quasi-periodic metasurfaces and cross-trapezoidal cavity metasurfaces.[152] The optimized configurations achieved high emissivity within the atmospheric window of 96.98 and 97.81%, respectively, while maintaining low solar absorptances of 9.34 and 7.21%, respectively. Under ambient conditions, these designs yielded net cooling powers of 63.48 and 90.13 W m^{-2}. Meanwhile, Ding et al. reported a biomimetic metasurface using AI-driven inverse design.[153] Three types of SiO_2-based photonic structures, truncated cones, cylinders, and cones were modeled with varying geometric parameters, and simulated data were used to train a generative deep learning model. The resulting inverse-designed truncated-cone arrays experimentally exhibited an average emissivity of 95% within the atmospheric window, 95% reflectance in the solar spectrum, and a cooling of 8.5 °C, all while maintaining robust manufacturability due to low aspect ratios. These AI-assisted inverse design schemes for metasurface-based RC show that the multiscale and multidimensional problems can be successfully solved through advanced computational methods that consider the materials and fabrication constraints directly into their optimization function.

After the metasurface-based radiative cooler has been designed, it should be physically realizable for real-world use. Generally, metasurfaces are fabricated using standard lithography techniques (Figure 4e), which gives them a huge advantage in terms of fabrication compared to three-dimensional metamaterials. However, the manufacturability of large-scale metasurfaces for RC is still one of the main challenges. Efficient modulation of the solar spectrum with meta-atoms requires precise nanoscale fabrication, which is in complete contrast with the physical size required for radiative coolers that should be at least centimeter, if not meter-scale in size, for any meaningful application. Electron beam lithography has been generally utilized to realize such nanometer resolution, as it offers a significantly shorter effective wavelength compared to conventional photolithography techniques (e.g., ArF, KrF).[154] Despite the resolution advantages of electron beam lithography, its low throughput and high operational costs remain significant limitations for large scale fabrication.

Nanoimprint lithography, which replicates patterned molds directly onto a substrate via physical contact, offers reduced fabrication costs and scalability for mass production of metasurfaces.[155,156] Nanoimprint lithography has been used to fabricate truncated cone-shaped 2D photonic crystal structures of a UV-curable adhesive, serving as a versatile and large-area manufacturing method for high-resolution nanopattern transfer (Figure 4f).[157] The truncated cone geometry was produced via a photopolymerization reaction of the UV-curable resin. Subsequently, a composite structure comprising a polyethylene terephthalate substrate and Ag reflective layer was utilized to achieve thermal emission. The fabricated RC film exhibited an emissivity of 95% within the infrared atmospheric transparency window and achieved a maximum temperature reduction of 7.7 ± 0.2 °C in outdoor experiments. This fabrication method does not require high-temperature processing or chemical etching, enabling its facile application to flexible polymer substrates such as PET, allowing it to be adapted for various applications.

Recently, high-throughput nanoimprinting of large-scale metasurfaces has been demonstrated using roll-to-plate[158] and roll-to-roll (R2R) techniques. For RC, Lin et al. proposed a polymer-based metasurface through R2R nanoimprinting (Figure 4g).[133] After the R2R process, a physical vapor deposition process was followed to coat a 100 nm silver layer on the backside of the film to enhance the reflectivity. Owing to

https://doi.org/10.1021/acsami.6c00074
ACS Appl. Mater. Interfaces 2026, 18, 21363−21423

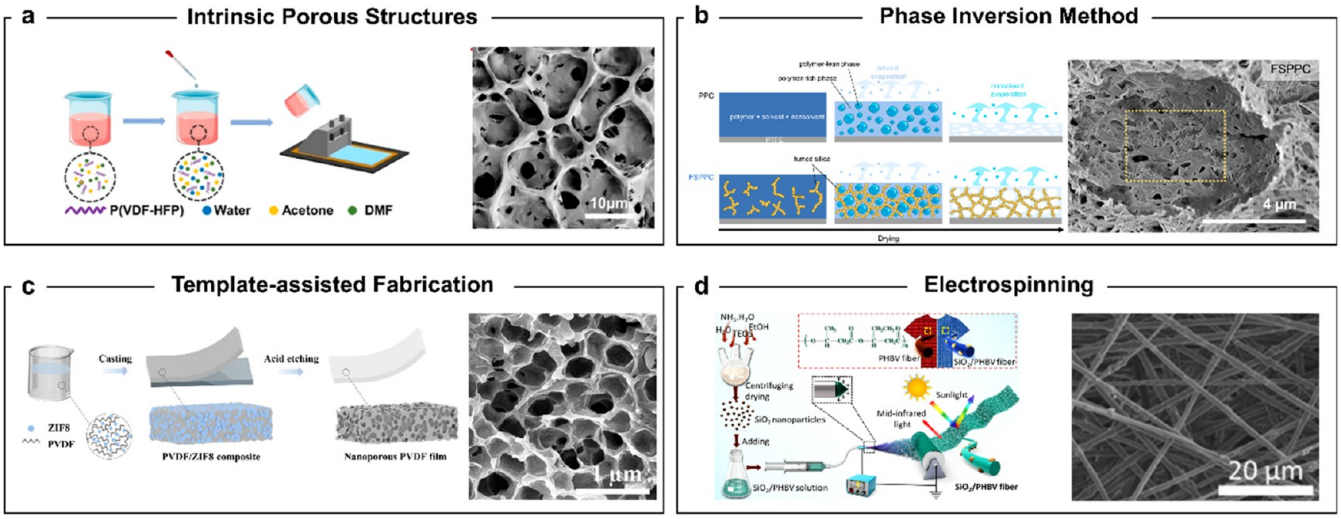

Figure 5. Representative fabrication routes for nanoporous radiative cooling materials. (a) Intrinsic porous PVDF−HFP films fabricated via a nonsolvent-induced phase separation (NIPS) process, showing the fabrication schematic and the resulting hierarchically interconnected porous structure of the optimized PVDF−HFP-5 film. Reproduced from ref 163. Copyright 2024 American Chemical Society. (b) Phase inversion via solvent−nonsolvent exchange, yielding asymmetric membranes with interconnected micropores and macrovoids, with SEM morphology highlighting their broadband scattering capability. Reproduced from ref 186. Available under a CC-BY 4.0 license. Copyright 2024 Author(s). (c) Fabrication process of a $PVDF_{NP}$ film and a cross-sectional SEM view of the resulting structure, characterized by an average pore diameter of ∼400 nm. Reproduced from ref 168. Copyright 2024 American Chemical Society. (d) Schematic of the preparation process for the Poly(3-hydroxybutyrate-*co*-3-hydroxyvalerate) (PHBV) and SiO_2/PHBV fiber membranes, with SEM image of SiO_2/PHBV fiber membranes 15 wt % SiO_2 concentrations. Reproduced from ref 209. Copyright 2025 American Chemical Society.

the flexibility of the polymer film, the metasurface-based radiative cooler exhibited a low solar absorptance of 4.8% and an excellent omnidirectional absorptance/emissivity of 96.1% in the atmospheric window. This continuous, large-area manufacturing approach is advantageous for practical applications and is expected to meet demanding requirements for metasurface-based RC performance in the future.

In summary, metasurfaces provide an attractive solution to RC due to their potential for multispectral manipulation through resonance engineering with metal and dielectric materials. However, due to the large disparity in wavelength scales between the visible and mid-infrared regimes, it is challenging to achieve ideal solar reflection and infrared emission simultaneously using a single material or a single pattern. Furthermore, the angular-dependent nature of standard metasurfaces limits full emission to the atmospheric window and could have a profound effect on the performance of metasurface-based radiative coolers. These limitations necessitate the adoption of complex designs such as multiscale architectures, multiple patterned layers, and combinations of hybrid material resonators,[159] while AI has been proven as a useful tool for photonic design and optimization. Recent research has increasingly focused on improving the durability and environmental stability of metasurfaces under diverse weather conditions, including high humidity, temperature fluctuations, and prolonged ultraviolet exposure,[63] as well as color-preserving radiative coolers for aesthetic outdoor purposes.[57] Such advancements are critical to ensuring long-term performance and reliability in real-world outdoor applications. Considering the unique advantages that metasurfaces offer, alongside the advancements in computational design and large-scale nanofabrication techniques, metasurface-based radiative coolers could still prove to be one of the go-to solutions for passive RC devices.

3.3. Porous Structures

Changhwan Hyeon, Minseo Jeong, and Dasol Lee

Nanoporous architectures have emerged as a promising and scalable platform for RC materials due to their ability to manipulate light−matter interactions through engineered multiscale porosity.[24,160] Within a single metal-free layer, broadband solar reflectance (0.3−2.5 μm) and strong mid-infrared (MIR) emissivity (8−13 μm) can be achieved without metallic back reflectors or complex multilayer stacks, provided that sufficient optical thickness, hierarchical nanoto-micro porosity, and optically nonabsorbing or highly reflective substrates are employed.[161] These combined optical responses enable subambient operation with temperature drops up to ≈10 °C under sunlight.[132] Such passive cooling provides energy-free thermal management for applications ranging from wearable electronics to buildings and biomedical devices.[162]

The cooling performance is governed by optical, structural, and material factors.[163] Based on Mie scattering principles, the peak scattering wavelength scales with the void diameter; submicron pores predominantly scatter UV and visible light, and micron-scale voids shift the scattering peak to extend scattering into the NIR.[20] Their hierarchical integration ensures uniformly high solar reflectance without spectral gaps.[164] High dielectric contrast between matrix and voids amplifies scattering, and interconnected pore architectures induce dependent scattering that broadens the resonance profile, while minimizing absorption reduces heat gain.[137] Structurally, porosity (60−90%) lowers effective refractive index and boosts MIR emissivity though excessive porosity weakens durability.[165] Pore connectivity, isotropy, and morphology also govern angular stability and can impart hydrophobicity or self-cleaning.[166] Materials must pair low solar absorption with strong MIR phonon−polariton resonances, as in fluoropolymers, cellulose, and ceramics, while resisting degradation for outdoor reliability.[167]

The realization of these attributes depends critically on fabrication methodology, which determines pore morphology, size hierarchy, connectivity, and scalability. Several representa-

https://doi.org/10.1021/acsami.6c00074
ACS Appl. Mater. Interfaces 2026, 18, 21363−21423

tive strategies have been widely adopted. Intrinsic porous structures, arising from natural morphologies or stress-induced voids in semicrystalline polymers, enable facile processing and low cost; however, they often require nonmetallic auxiliary reflectors, such as highly reflective substrates, dielectric backings, or white polymer supports, to compensate for limited scattering strength or insufficient layer thickness and thereby achieve high radiative cooling performance, rather than metallic mirror back reflectors.[168] Phase inversion, based on solvent−nonsolvent exchange, generates hierarchical porosity in polymers, yielding large-area coatings with high reflectance and emissivity.[169] Template-assisted methods use sacrificial particles to form tunable voids in poly(methyl methacrylate) (PMMA) or PDMS, while hard templates such as anodic aluminum oxide (AAO) membranes can guide ordered pore architectures with precise control.[170] Finally, electrospinning creates fibrous networks with nano/micropores, combining strong scattering with flexibility and textile-scale production.[171]

Here, we review these four fabrication routes, emphasizing processing−structure−property relationships that dictate optical performance, mechanical stability, and durability. We systematically compare intrinsic porous structures, phase inversion, template-assisted fabrication, and electrospinning, highlight recent advances, and propose guidelines for scalable RC materials in energy and healthcare.

3.3.1. Intrinsic Porous Structures. Intrinsic porous structures exploit the inherent crystalline morphology and deformation behavior of semicrystalline polymers to generate hierarchical porosity without sacrificial templates.[172] In polyethylene (PE) and polypropylene (PP), crystalline lamellae and tie molecules act as stress concentrators where voids nucleate during stretching or controlled phase rearrangement. Cavitation under uniaxial or biaxial deformation produces micro- to mesoscale voids, while thermal or chemical modulation of lamellar spacing introduces nanopores.[173] This distribution—nanopores (<100 nm) for UV scattering, submicron pores (≈200−800 nm) for visible backscattering, and micron-scale voids (≈1−10 μm) for NIR reflection—enables broadband solar reflection.[174] Furthermore, vibrational resonances of the polymer backbone yield strong emissivity within the 8−13 μm atmospheric transparency window, a prerequisite for RC.[175]

For instance, Li et al.[163] reported an intrinsically porous radiative cooling film based on PVDF−HFP, fabricated via a nonsolvent-induced phase separation (NIPS) process with rationally tuned solvent compositions. During solvent evaporation, spontaneous phase separation between polymer-rich and polymer-poor domains generated a hierarchically interconnected porous structure spanning nano- to microscale length regimes, as confirmed by scanning electron microscopy (SEM) (Figure 5a). By adjusting the solubility parameter mismatch between the polymer and mixed solvents, the pore size distribution and overall porosity were effectively controlled, enabling efficient broadband solar scattering. The optimized PVDF−HFP film exhibited a high solar reflectance of 97.7% and a mid-infrared (MIR) emissivity of 96.7%, without the use of any inorganic fillers or auxiliary reflective layers. As a result, the film achieved a subambient temperature reduction of approximately 5.4 °C under a solar irradiance of ∼945 W m^{-2}, along with a daytime net radiative cooling power of up to ∼80 W m^{-2}. These results indicate that intrinsic hierarchical porosity in polymeric films provides a scalable and effective structural route for passive radiative cooling applications. Hsu et al.[176] further demonstrated nanoporous PE films with solar reflectance exceeding 0.9, achieving an outdoor personal cooling of ≈2−3 °C. More recently, Li et al.[150] reported that naturally abundant wood can be processed to form randomized porous structures that result in strong solar backscattering and MIR emissivity leading to 20−60% reductions in building energy consumption. Together, these studies establish intrinsic porosity as a versatile and scalable route for passive RC.

Processing parameters play a decisive role in dictating both the performance and durability of intrinsically porous structures. These parameters refer to the controllable mechanical and thermal conditions applied during polymer deformation—most notably draw ratio, strain rate, and drawing temperature—that govern the processes of void nucleation, growth, and stabilization.[177] Optimized draw ratios (3−10×, ratio of stretched to initial length) and strain rates (0.1−5 s^{-1}), when applied at drawing temperatures of ∼0.6−0.9 Tm (relative to the polymer melting point, Tm), facilitate stable pore formation while mitigating premature collapse. In semicrystalline polymers such as PE and PP, porosity levels of 60−90% have been reported to reduce the effective refractive index without compromising tensile strength, and crystallinity values of 45−70% provide a balanced compromise between void generation and structural robustness.[178] Importantly, these ranges should be viewed as representative rather than universal benchmarks, as the optimal processing conditions are highly dependent on polymer type, crystalline morphology, and deformation pathway. Postannealing is often employed as a supplementary treatment to stabilize pore geometry and enhance long-term environmental durability.[179] By enabling stress relaxation and partial recrystallization, annealing reduces pore collapse, suppresses defect propagation, and improves resistance to external stresses such as humidity fluctuations and thermal cycling.[180] Typical annealing conditions at 0.4−0.7 Tm allow pore walls to consolidate while preserving the hierarchical network essential for broadband solar scattering.[181] Effectiveness, however, depends on polymer type and prior history, so annealing is not universally required.[182] Intrinsic approaches remain limited by narrow processing windows and trade-offs between optical efficiency and mechanical integrity.[73]

3.3.2. Phase Inversion Method. The phase inversion method is a solution-based approach that generates porous architectures through solvent−nonsolvent exchange, in which liquid−liquid demixing induces polymer precipitation and pore formation.[183] In a typical process, polymers such as poly(vinylidene fluoride-*co*-hexafluoropropylene), poly(ether sulfone), or cellulose acetate are dissolved in a polar solvent (e.g., Dimethylformamide, Dimethylacetamide, or acetone) and deposited by doctor blading, dip-coating, or spraying.[184] Immersion into a nonsolvent bath (commonly water or alcohol) initiates phase separation: rapid solvent−nonsolvent diffusion creates finger-like macrovoids and interconnected channels, whereas slower diffusion produces sponge-like micro/nanoporous networks.[185]

Hong et al.[186] demonstrated humidity-tolerant porous polymer coatings fabricated using phase inversion (Figure 5b). The schematic depicts solvent−nonsolvent diffusion that drives polymer-rich and polymer-lean phase separation, and the SEM micrograph shows a heterogeneous porous morphology with interconnected macrovoids and micropores. These hierarchical features provided broadband solar reflectance of 0.93 and the MIR emissivity of 0.96, enabling stable subambient cooling of ≈6.5 °C under humid outdoor conditions. Mandal et al.[78] further developed hierarchically porous cellulose acetate films

https://doi.org/10.1021/acsami.6c00074
ACS Appl. Mater. Interfaces 2026, 18, 21363−21423

that exhibited solar reflectance in excess of 0.92 and cooling powers exceeding 100 W m^{-2}, highlighting their potential for sustainable large-scale deployment. Zhai et al.[52] introduced a roll-to-roll nonsolvent-induced phase separation process that achieved ≈5 °C subambient cooling, demonstrating manufacturability at industrial scales. More recently, Hu et al.[187] reported coral-like polyvinylidene fluoride (PVDF) porous films with broadband solar reflectance (∼0.95), strong MIR emissivity, and antibacterial activity, underscoring the adaptability of this method to multifunctional RC applications.

Optimization requires control of demixing kinetics—solvent out-diffusion and nonsolvent in-diffusion—which shape macrovoids and nanopores.[188] Polymer concentrations of 8−20 wt % balance porosity and stability. Solvent−nonsolvent miscibility determines pore type, bath temperatures (5−40 °C) tune distributions, and polyethylene glycol additives enhance porosity while preventing collapse.[189] Post-treatments such as humidity-controlled drying, mild stretching, and surface functionalization further refine porosity and durability.[190] Despite challenges in solvent recovery and humidity sensitivity, phase inversion offers unmatched scalability, tunability, and compatibility, making it one of the most practical RC fabrication methods.

3.3.3. Template-Assisted Fabrication. Template-assisted fabrication is a bottom-up technique enabling precise nanoscale control over a material's geometric morphology. This control enhances the performance of RC materials, which require the simultaneous optimization of high solar reflectance and selective thermal emissivity.[167] The approach uses two methods: the use of hard templates, forming the final structure's framework, and sacrificial templates, removed after formation.

In hard-template synthesis, the template is fabricated to possess desired properties, acting as the final material's core functional component. AAO is a representative hard template created via an electrochemical process yielding nanoporous alumina membranes.[165,167,191] The process controls geometry: the interpore distance is determined by the acidic electrolyte, while the pore diameter and film thickness are controlled by the applied voltage and anodization time.[167,191] A two-step anodization process produces a highly ordered hexagonal pore arrangement, using an initial oxide layer as a pattern for subsequent growth.[167,191] For RC applications, this method forms a dual-function structure: a transparent infrared emitter (porous alumina) and a solar reflector (the underlying substrate).[167,191]

Scientific understanding of AAO for RC has progressed. Initial studies by Fu et al.[165] demonstrated porous alumina's cooling potential. Subsequent work focused on performance enhancement. Lee et al.[167] broadened the material's high-emissivity spectrum across the MIR by applying a thin SiO_2 coating via atomic layer deposition. Diaz-Lobo et al. resolved conflicting literature results through chemical control. Their research showed optical properties are tunable, with counterions (e.g., phosphates, sulfates) incorporated from the electrolyte during anodization acting as critical factors. These ions create specific infrared absorption bands that directly shape the material's emissivity profile, establishing design principles for optimizing radiative performance without additional coatings.[191]

In the sacrificial-template method, porous structures are fabricated by embedding a removable template within a matrix, later eliminated to create a porous network (Figure 5c). This method offers high structural flexibility for tailored pore structures.[161,168,192−198] Template material selection involves a trade-off between structural precision, cost, scalability, and process complexity. For low-cost and scalable production, Chen et al. used water-soluble sodium chloride as a template,[199] whereas Yang et al.[194] used sucrose. These materials, mixed with a polymer precursor like PDMS, dissolve in water, leaving a porous structure.

Ordered porous PMMA structures are created by infiltrating a SiO_2 sacrificial template with polymer, followed by hydrofluoric acid etching. Zhang et al.[192] fabricated a periodic inverse opal structure using a 3D colloidal crystal template, achieving 0.94 solar reflectance, significantly outperforming a disordered counterpart (0.77). This showed ordered porous structures provide higher solar reflectance, emphasizing structural control. However, inorganic templates pose challenges like facile removal and precise nanoscale architectural control.[168] To address these limitations, Huang et al. optimized optical properties by forming uniform nanopores in PVDF using metal−organic framework sacrificial templates (Figure 5c). With an optimal pore size of approximately 400 nm and a porosity of 37%, they maximized the solar reflectance from 9.5 to 94.9% and achieved 92.8% thermal emissivity.[168] This demonstrated that precise control over pore size and density is the key to high-performance radiative cooling.[168,197] In essence, both template approaches confirm a fundamental principle: precise nanoscale architectural control enables high solar reflectance and selective thermal emissivity, providing a robust pathway for RC material design and optimization.

3.3.4. Electrospinning. Electrospinning is a versatile technique using a high-voltage electric field to draw polymer solutions into interconnected microfiber/nanofiber networks. This nanofiber network provides the necessary characteristics for RC. Strong Mie scattering, which results in high solar reflectance, is induced because the fiber diameters are comparable to the wavelengths of sunlight, and this effect is amplified by the network's high porosity and the fiber−air refractive index mismatch[75,200−209] (Figure 5d). The constituent polymers, such as PVDF and poly(vinyl alcohol), also provide high thermal emissivity in the MIR via molecular vibrations.[204,206−214] Based on these properties, research has progressed beyond simple cooling films, focusing on improving durability, stability, and integrating multifunctionality.

Electrospinning's material versatility is crucial for robust materials in demanding outdoor/extreme environments. To address polymer fragility/degradation, Xin et al. fabricated durable flexible alumina nanofiber mats (FAFM). As an inorganic material, FAFM resists UV aging and fire while demonstrating strong RC.[211] To withstand extreme space environments, Song et al. developed molecularly engineered polyimide nanofibers with solar reflectance of 99.6% and MIR emissivity of 0.93. This performance is highly durable for space applications. After exposure to severe thermal shock (−196 to 150 °C) and corrosive atomic oxygen, the solar reflectance showed minimal degradation (2.2−2.6%) and the material retained ∼92% of its mechanical strength.[200]

Electrospinning facilitates composite/multilayered structure fabrication, ideal for integrating new capabilities. Techniques such as coaxial (core−shell), blended, or roll-to-roll electrospinning are used to develop dynamic and intelligent systems. Zhang et al. developed a textile with high wash stability to improve wearability. After a high-speed (1000 rpm) washing test, the textile's radiative heating performance did not show significant degradation. This study incorporated a Janus

https://doi.org/10.1021/acsami.6c00074
ACS Appl. Mater. Interfaces 2026, 18, 21363−21423

Table 1. Summary of Representative Structural Classes for Radiative Cooling, together with Their Fabrication Routes, Scale-Up Potential, and Representative Use Scenarios

	Multilayer thin film structures	Metasurfaces/nanophotonic structures	Porous structures
Representative fabrication routes	Chemical vapor deposition,[47,65] physical vapor deposition,[229] and others	Photolithography,[230] Nanoimprint lithography,[157] Electron beam lithography,[49] and others	Electrospinning,[231] phase-inversion,[78] and others
Scale-up potential	Limited	Limited to Moderate	High
Representative use scenarios	Buildings, vehicles, and enclose spaces	Photovoltaic integration	Paints/coatings, textiles

structure for stability and selectable heating/cooling.[206] Some systems enhance personal comfort by combining radiative cooling with moisture management. Yan et al. used a two-step roll-to-roll electrospinning method to engineer a dual-gradient Janus textile that provides an additional 2.5 °C skin temperature drop through moisture desorption.[202] Chen et al. employed microfluidic electrospinning to incorporate hollow microspheres into a double-layer textile, achieving a "self-pumping" effect that promotes evaporation.[215] For more controllable systems, Pyun et al. demonstrated dynamic radiative cooling with a PDMS nanofiber matrix fabricated via a core−shell electrospinning process. Mechanical pressure reversibly collapses its porous structure, enabling dynamic switching between reflective cooling and transparent noncooling states. The cooling mode achieved subambient cooling of approximately 3.8 °C during the daytime and up to 7.9 °C at night.[201] In conclusion, electrospinning's ability to fabricate composite/multilayered nanofiber structures from diverse materials enables direct integration of durability, multifunctionality, and dynamic responsiveness, meeting advanced application demands beyond static cooling.

This review examined four fabrication routes for porous radiative cooling materials, each defined by a fundamental trade-off between optical performance, production scalability, and structural precision. Scalable methods (e.g., phase inversion) offer high throughput but limited microstructural control, whereas template-assisted fabrication provides high precision but is hindered by complexity and cost. Electrospinning serves as a versatile intermediate, offering a platform for the durable and multifunctional systems that are a focus of current research.

Looking forward, material evolution will overcome current design/functionality limitations. Future perspectives include material and structural innovation, such as developing multifunctional composites with integrated properties such as UV resistance, self-cleaning, and flame retardancy.[216−219] Simultaneously, intelligent/switchable systems will advance, aiming to create adaptive materials for diverse climates, preventing overcooling for year-round efficiency.[214,220−224]

The practical application of these advanced materials, however, depends on advancements in cost-effective and scalable manufacturing. This requires the adoption of new mass-production technologies such as 3D printing and melt processing. Unlike conventional multistep methods, these approaches enable the continuous and scalable production of digitally designed porous structures, ideal for industrial applications.[225,226] These manufacturing innovations are expected to expand the role of porous RC materials beyond buildings to diverse fields such as automobiles, electronics, and smart textiles, establishing them as a key technology for an energy-efficient and sustainable future.[163,203,207,226−228]

To facilitate cross-comparison among the representative RC structural classes discussed above, Table 1 summarizes their representative fabrication routes, scale-up potential, and representative use scenarios. This qualitative overview highlights the distinct structural characteristics associated with multilayer thin film, metasurface/nanophotonic, and porous RC platforms.

4. FUNCTIONALITIES OF RC

4.1. Spectral Control-Based RC

4.1.1. Selective Mid-Infrared Regulation. *Ya Huang, Siming Zhao, and Rufan Zhang*

RC emitters were typically classified into three types, i.e., nonselective emitters, monoselective emitters, and dual-selective emitters according to their MIR emissivity (Figure 6a).[232] Nonselective emitters exhibited high emissivity across the entire MIR range, not only enabling large radiative heat loss but also including wavelengths strongly absorbed by atmospheric gases. Monoselective emitters confined high emissivity within the first AW, 8−13 μm while suppressing emission elsewhere, thereby maximizing net cooling under clear-sky conditions. Dual-selective emitters extended this strategy by exhibiting high emissivity in both the first (8−13 μm) and the second (16−25 μm) AWs, with low emissivity outside these windows. Because the radiative effectiveness of each strategy was strongly influenced by atmospheric transparency and humidity, its relative advantages became climate-dependent. Consequently, monoselective designs were effective in moderately humid environments, and dual-selective designs were particularly advantageous in arid or low-humidity climates. The underlying design principles and representative material systems of the monoand dual-selective approaches are discussed in this section.

4.1.1.1. Mono-Selective RC Emitter. Monoselective RC materials exhibit high emission in the first AW regions, while maintaining low emission in nonfirst AW regions.[233] Specifically, the monoselective materials should have three characteristics in the spectrum: (1) high solar reflectivity to minimize the solar absorption and the resulted heating effects; (2) high emissivity in the first AW regions to enhance the thermal radiation dissipation; (3) low emissivity in nonfirst AW regions to resist the parasitic heat from surroundings. According to their material composition, monoselective RC materials can be divided into two types: polymer-based and inorganic oxide-based materials. In 2014, Fan et al. first reported the monoselective RC materials composed of SiO_2 and HfO_2 via the multilayer photonic structure. They achieved a high emissivity of 0.75 in the first AW regions and a high solar reflectivity of 0.97, thus resulting in the first report of subambient cooling effect under the sunlight.[24] Since then, numerous efforts have been devoted to increasing the solar reflectivity and the first AW emissivity, while decreasing the cost of the material preparation[17,234] In 2022, Huang et al. developed a solution-processed inorganic emitter to achieve subambient RC, which showed a high solar reflectance (96.4%) and strong infrared-selective emittance (94.6%) with superior spectral selectivity (1.46).[235] The all-inorganic narrowband emitter comprised the SiO_xN_y and a self-assembly monolayer of SiO_2 via

https://doi.org/10.1021/acsami.6c00074
ACS Appl. Mater. Interfaces 2026, 18, 21363−21423

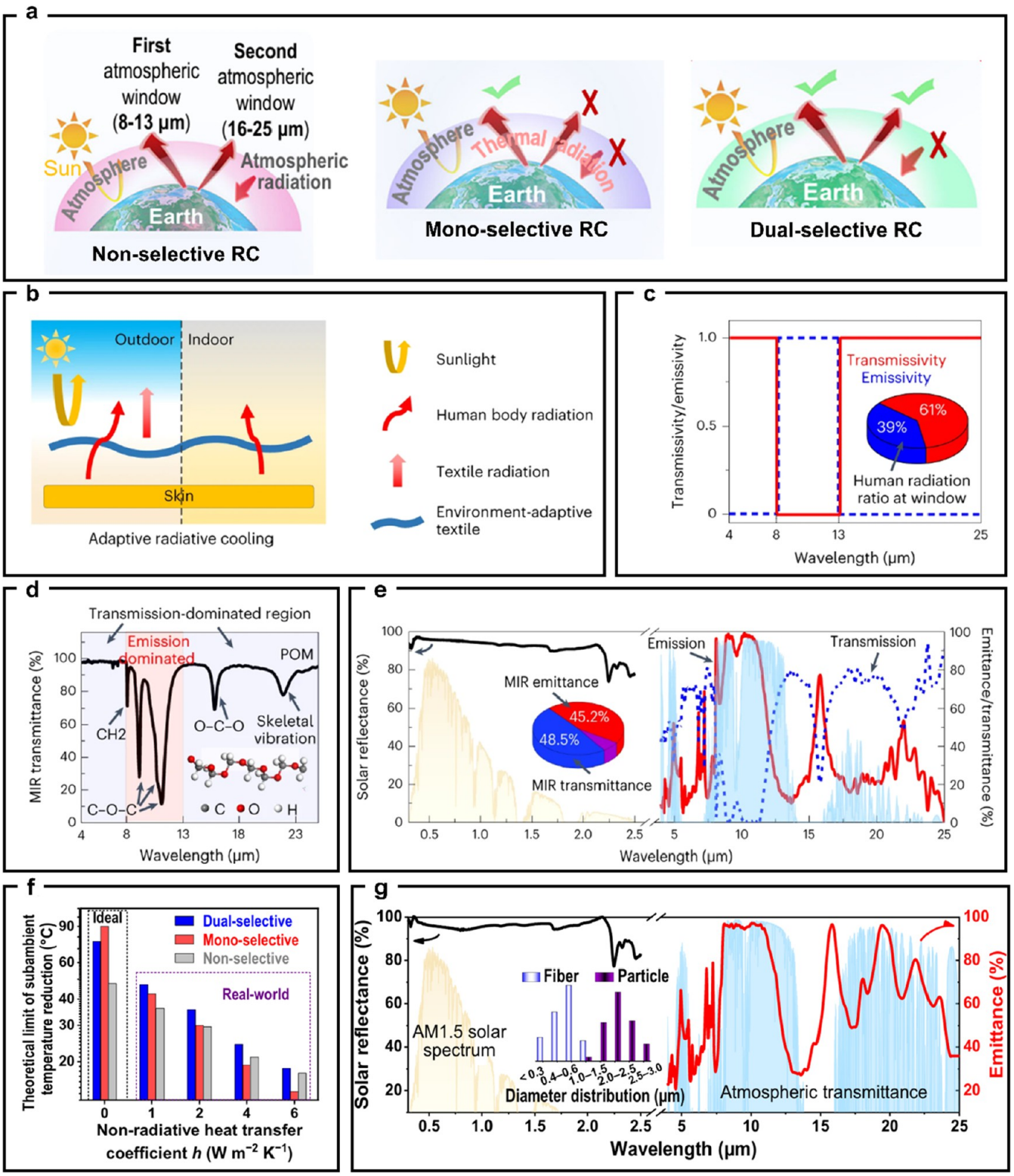

Figure 6. (a) Schematic of the radiative heat transfer process of a nonselective, a monoselective, and a dual-selective radiative emitters. (b) Schematic of the monoselective radiative emitters. (c) Spectral in the MIR band of the monoselective radiative emitters. (d) The FTIR of the POM fabrics. (e) Spectral of the POM film in the 0.3−25 μm. (f) Theoretical calculation of subambient cooling of the three radiative emitters at different heat transfer coefficients (h = 0−6 W m^{-2} K). (g) Spectral of the POM−PTFE-Al film in the 0.3−25 μm. (b−e) Reproduced with permission from ref 238. Copyright 2023 Springer Nature. (a) and (f, g) Reproduced with permission from ref 132. Available under CC BY 4.0 license. Copyright 2024 The Author(s).

a simple method rather than the delicate methods. Polymer-based monoselective RC materials were also widely reported for their high processability and scalability. Typically, Zhu et al. developed the poly(ethylene oxide) (PEO)-based electrospinning nanofibers, which showed great solar reflectivity (96.3%) and the first AW emissivity (78%).[236] Except for the

https://doi.org/10.1021/acsami.6c00074
ACS Appl. Mater. Interfaces 2026, 18, 21363−21423

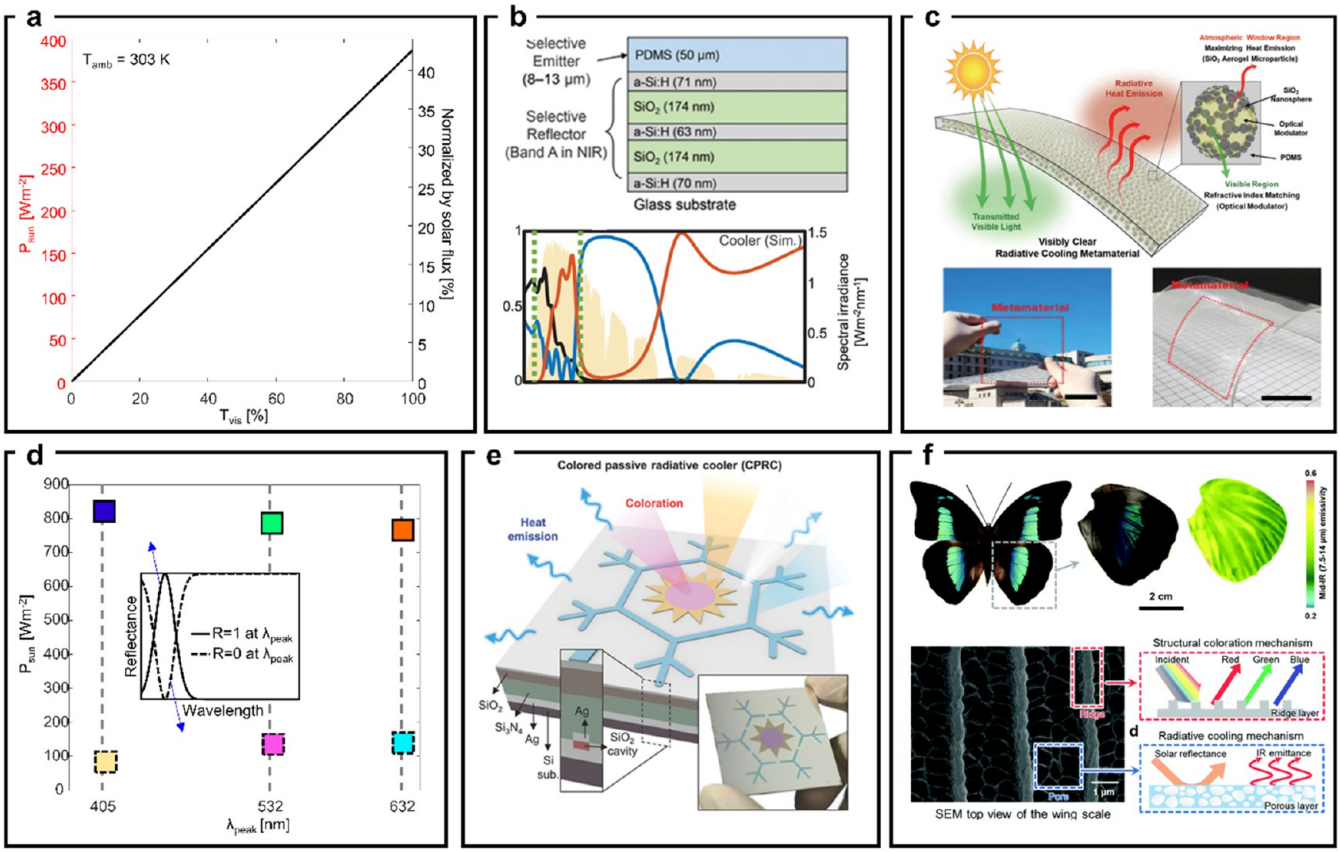

Figure 7. Transparent and colored radiative cooler. (a) P_{sun} for various average visible transmittance with perfect UV and NIR reflection and perfect absorption in the 8−13 μm range. The right axis shows P_{sun} normalized by that of a perfect absorber. (b) A multilayer-based transparent radiative cooler and simulated optical response. Adapted with permission from ref 47. Copyright 2021 John Wiley and Sons. (c) Particle-based transparent radiative cooler and its photographs. Adapted with permission from ref 34. Copyright 2022 John Wiley and Sons. (d) P_{sun} of a colored radiative cooler with various resonant spectra and a bandwidth of 100 nm. The color of markers indicates the reflected color. (e) A multilayer-based radiative cooler with a color printing and its photograph. Adapted with permission from ref 31. Copyright 2018 John Wiley and Sons. (f) A colored radiative cooler inspired by butterfly wing scales. Reproduced with permission from ref 196. Copyright 2022 Royal Society of Chemistry.

material preparation, the property in nonfirst AW regions of the selective monoselective RC materials was also important when applied in practical applications, which attracts much research interest.[237] The low emission in the nonfirst AW region can exhibit high reflection or high transmission, which plays different roles in different scenarios. Taking personal thermal management as an example, our group reported a selective emission model to achieve heat dissipation indoors and outdoors (Figure 6b).[238] It achieved the cooling effects outdoors via heat dissipation in the first AW regions and sunlight reflection, while it achieved temperature reduction indoors via the heat transmission from the human body in nonfirst AW regions (Figure 6c). Due to the backbone chain consisting only of C−O−C bonds, we selected polyformaldehyde (POM) to combine both working modes of emission and transmission (Figure 6c). The POM textile showed a selective emittance (75.7%) in the first AW and a transmittance of 48.5% in the 4−25 μm (Figure 6d), exhibiting enhanced radiative human body cooling performance. Moreover, as the heat-island effects become more and more severe, the surroundings become heating resources for human beings in the city. Hsu et al. developed a selectively emissive and reflective fabric with a high spectral selectivity ratio of 2.23 and an average emissivity of 0.85 in the first AW to achieve the heat dissipation to outer space, while it had high reflectivity outside the first AW to resist the heat transfer.[239]

4.1.1.2. Dual-Selective RC Emitter. Although numerous efforts to monoselective RC materials have been made, the cooling contribution of the second AW (16−25 μm) was often neglected in previous studies, as its atmospheric transparency decreased with increasing humidity due to the strong absorption of thermal radiation by water vapor in this spectral range.[44] However, we demonstrated that under practical conditions (heat transfer coefficient $h \geq 1$ W m^{-2} K), the dual-selective RC model exhibited markedly superior subambient cooling compared with both nonselective and monoselective RC models.[132] Specifically, at h = 1−6 W m^{-2} K, it achieved temperatures 1.0−10.9 °C lower than the nonselective model and 4.2−5.5 °C lower than the monoselective model. Based on this, we developed a scalable polyformaldehyde−polytetrafluoroethylene−aluminum (POM−PTFE−Al) dual-selective thermal emitter. Specifically, POM exhibits strong C−O−C bond vibrations in the first AW, while PTFE shows pronounced C−F bond absorption in the second AW. Both polymers display negligible absorption outside atmospheric windows, enabling the emitter to achieve an emittance of 83.2% in 8−13 μm, 67.5% in 16−25 μm, and a high solar reflectance of 95.4% in 0.3−2.5 μm. It achieved ∼9 °C daytime subambient cooling and 151.8 W m^{-2} net cooling power, outperforming mono- and nonselective designs.

Beyond intrinsic molecular vibrational selectivity, ordered nanophotonic architectures could further enhance RC through

https://doi.org/10.1021/acsami.6c00074
ACS Appl. Mater. Interfaces 2026, 18, 21363−21423

precise spectral control, such as photonic crystals and metamaterials. Mira et al. designed a multilayer cooler composed of three dielectric layers (SiN, SiC, SiO_2) on an Ag back reflector, with thicknesses optimized via a genetic algorithm.[240] The device exhibited high emittance in both the first and second AW, delivering strong cooling performance across diverse environments, particularly in arid regions. Its pronounced angle-dependent emittance in the second AW helped suppress ground emission absorption, thereby improving cooling efficiency. Similarly, Yin et al. developed an emitter with triangular prism metamaterials atop a multilayer stack for RC.[241] The surface features with two triangular prisms acting as an absorption layer on Si_3N_4 and TiO_2 films, while an underlying SiO_2 metamaterial layer extends the absorption band, with its geometry tuning the emission peak. The base slit of the prisms enhances selective emission in the second AW, whereas the Si_3N_4 layer boosts absorption in the first AW. As a result, the emitter achieves absorptances of 98.56 and 96.31% in the 8−13 μm and 16−25 μm bands, respectively, while maintaining solar reflectance above 93%.

As discussed above, numerous studies have been devoted to establishing and developing high-performance selective PC materials, including the monoselective and dual-selective materials. However, an easy, cost, large-scale, stable, and accessible method to obtain the materials is also the biggest obstacle in the way to achieve the practical application of selective PC materials.

4.1.2. Spectral Control-Based RC. *Juhoon Baek and Minkyung Kim*

4.1.2.1. Transparent RC. While perfect solar reflection is essential for an ideal radiative cooler, it restricts implementation of coolers into applications that require visible transparency, such as windows, displays, and photovoltaic modules. To overcome this limitation, transparent radiative coolers that emit thermal radiation through the atmospheric window while remaining transparent in the visible range have been proposed. Unlike the night-time radiative coolers reported in the 1970s and 1980s,[11,12,242−244] transparent radiative coolers generally employ spectrally selective control in the solar regime. Thus, while transmitted visible light gives rise to heat gain and reduces the cooling effect, leading to an inevitable trade-off between transparency and cooling (Figure 7a), they can still achieve effective daytime cooling by reflecting the solar spectrum outside the visible.

The early stage of the visibly transparent radiative coolers focused on their integration into solar cells.[230,245] Since 2020, multiple groups have reignited the interest independently by implementing silica microspheres in a PET film,[246] using an ITO layer,[247] and employing a Bragg reflector.[47] These coolers exhibit common optical characteristics across broad wavelength ranges: visible transparency, NIR reflection, and high emissivity within the atmospheric window. Multilayer structures have been widely studied to realize selective NIR reflection. Kim et al. demonstrated that a Bragg reflector, composed of alternating low- and high-refractive-index layers on a PDMS substrate, reduced the temperature by up to 14.4 °C under direct sunlight, compared with bare PDMS (Figure 7b).[47] Other strategies include the use of optical topological transition in metal−dielectric multilayers, which creates a sharp transition between visible transmission and NIR reflection,[99,100] or utilizing the intrinsic optical properties of ITO.[59] The design of multilayers has benefited from various optimization techniques such as quantum computing,[248,249] genetic algorithms,[102,250] binary optimization−based active learning,[251] particle swarm optimization,[47] and deep reinforcement learning.[134] In addition, multilayer-based transparent radiative coolers have been engineered to enhance color neutrality,[56] introduce diffusive properties,[136] and provide multifunctionality—for example, switching between radiative conduction and barrier under different thermal conditions[97] or serving as direction-dependent MIR emitters.[28] Multilayer-based coolers often maintain high transmittance in the entire solar spectrum, not limited to the visible, yet they have demonstrated subambient cooling throughout the day.[65] Beyond multilayers, photonic crystals have also been applied to achieve selective solar reflection.[98]

Fabrication of multilayer and periodic structures typically requires patterning, multiple manufacturing steps, and/or vacuum-based techniques, which makes low-cost scalability challenging. As such, intensive efforts have been devoted to developing transparent radiative coolers using cost-effective approaches such as roll-to-roll processing[247] and colloidal self-assembly.[252] To induce strong absorption in the atmospheric window while keeping visible transparency, particle- and porous-based structures have been widely investigated. For example, when placed on top of a solar cell, silica aerogel microparticles in a silicone elastomer showcased a temperature reduction of up to 6.2 °C, under direct sunlight, compared with a bare cell (Figure 7c).[34] Other approaches include embedding SiO_2 micro/nanoparticles in polymer matrices,[54,131,253] using delaminated aerogel films,[254] and implementing pyramidal patterning.[255,256] While such particle- or porous-based coolers are not ideal for cooling since they lack spectral selectivity and remain generally transparent in the broad solar spectrum, similar to night-time radiative coolers, they offer practical advantages. Their compatibility with scalable fabrication methods makes real-world deployment more feasible, and their flexible and foldable forms demonstrate potential for applications in displays.[131]

4.1.2.2. Colored RC. More sophisticated spectral control within the solar range—for instance, introducing a resonant reflection peak or dip in the visible region—enables coloration of radiative coolers. Vivid coloration, however, requires a narrow reflection peak, which typically accompanies absorption at other wavelengths, leading to a trade-off between coloration and cooling (Figure 7d). Using a reflection dip at a same target wavelength reduces solar absorption and is therefore advantageous for cooling but results in less vivid, subtractive colors. However, the one-to-many relationship between color and spectrum indicates that the vividness of colors does not necessarily lead to a reduced cooling effect, which demonstrates the potential of photonic spectral control for thermal applications.[257]

Colored radiative coolers can be realized by integrating spectrally selective photonic structures with pigments or dyes,[78,132,258−260] in which the photonic structures provide cooling via thermal radiation through the atmospheric window and NIR reflection, while preserving the colors from the pigments or dyes. Beyond these pigment-based coolers, various photonic concepts such as multilayer-based spectral selectivity and structural coloration have been demonstrated. To avoid an intensive solar heating, the first proposal of colored radiative coolers used printing, in which only a small portion of the cooler surface exhibits color (Figure 7e).[31] Tuning a thin-film optical cavity within a multilayer structure enabled the realization of cyan, magenta, and yellow colors and resulted in subambient cooling of 3.9 °C under daylight conditions. More recently, diverse photonic structures including multilayers and periodic

https://doi.org/10.1021/acsami.6c00074
ACS Appl. Mater. Interfaces 2026, 18, 21363−21423

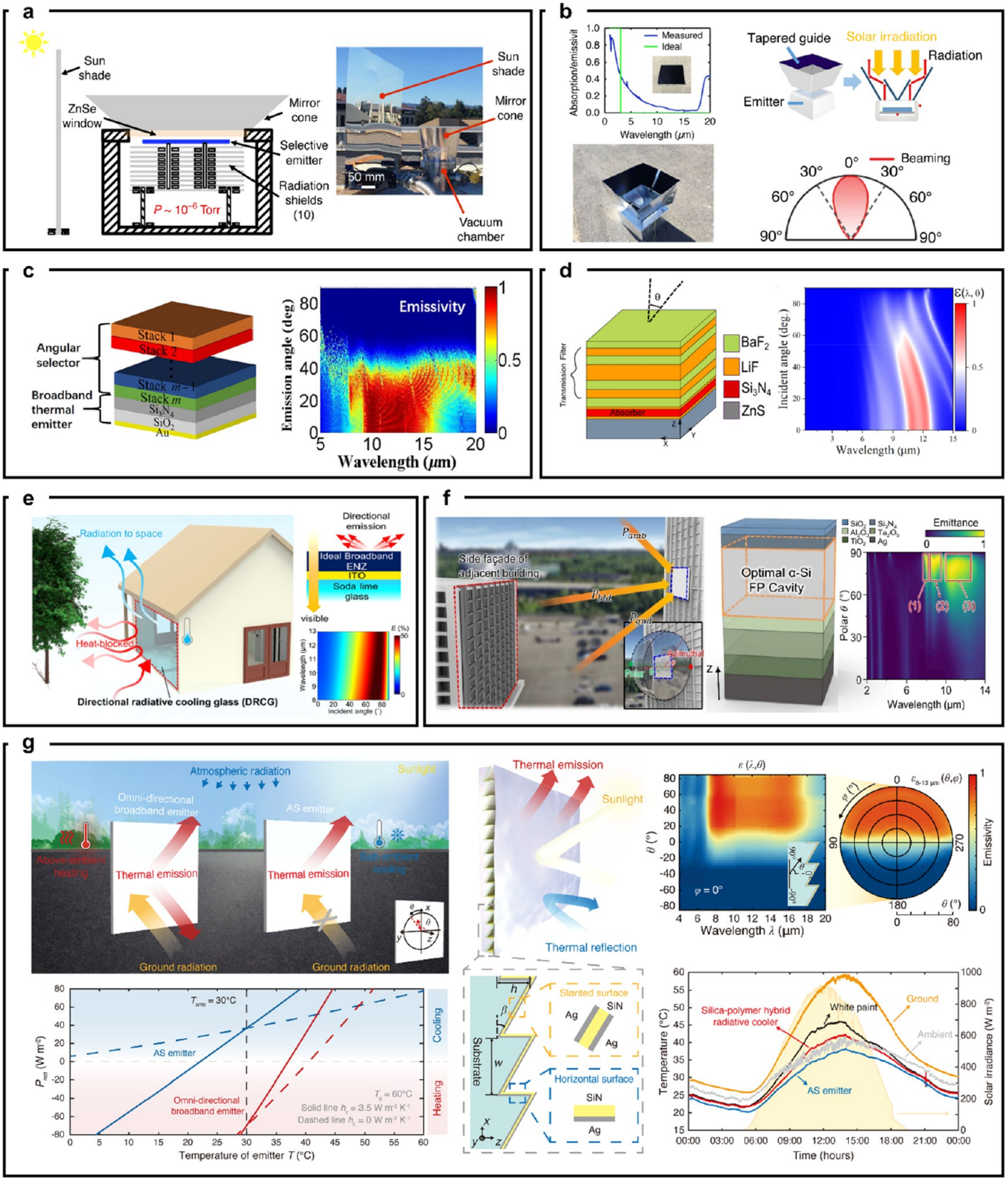

Figure 8. Directional radiative cooling. (a) Schematic of the radiative cooling setup designed to minimize parasitic heat losses, solar irradiance and sky radiation from higher zenith angles. Adapted from ref 44. Available under a CC-BY 4.0 license. Copyright 2016 The Author(s). (b) Schematic of the cooling system with tapered waveguide structure for thermal emission beam control and suppression of solar input. Adapted with permission from ref 276. Copyright 2019 Springer Nature. (c) Left: Schematic of a directional radiative cooler consisting of a broadband thermal emitter at the bottom and a multilayer angular selector on the top. Right: Spectral and angular emissivity of the cooler. Adapted with permission from ref 286. Copyright 2020 American Physical Society. (d) Left: Schematic of a spectrally and angularly selective radiative cooler consisting of a transmission filter on top of a thermal emitter. Right: Spectral and angular emissivity of the cooler. Adapted from ref 287. Available under a CC-BY 4.0 license. Copyright 2022 The Author(s). (e) Schematic of the directional radiative cooling glass for energy-saving windows. Adapted with permission from ref 300. Copyright 2024 De-Gruyter. (f) Schematic of the directional radiative cooler with the oblique radiation-angled photonic structure for building façade. Adapted from ref

https://doi.org/10.1021/acsami.6c00074
ACS Appl. Mater. Interfaces 2026, 18, 21363−21423

Figure 8. continued

301. Available under the Optica Open Access Publishing Agreement. Copyright 2024 Optica Publishing Group. (g) Left: Design considerations for subambient daytime radiative cooling of vertical surfaces. Middle: Schematic of the AS emitter consisting of a sawtooth grating covered by a UV−vis−reflective, IR-transparent nanoPE film. Right: Spectral and angular emissivity distribution and subambient daytime radiative cooling performance of the AS emitter. Adapted with permission from ref 20. Copyright 2024 The American Association for the Advancement of Science.

patterns have been designed for selective absorption of visible light to realize coloration, aided by parametric sweeps,[261,262] iterative parameter optimization,[57,263] and AI-based inverse design.[135,264]

A colored radiative cooler consisting of a monolayer polystyrene microspheres on a PDMS film was demonstrated, where the diameter of the microspheres determined the resulting color.[265] The cooler achieved a temperature reduction of 9−27 °C compared with commercial paints of similar colors. In other study, truncated SiO_2 microcones fabricated by a self-assembly method, when coated with an Ag layer, showed subambient cooling under sunlight along with angle-dependent color variation between incidence and observation, after coated by an Ag layer.[266] Design strategies have often involved biomimetic approaches inspired by natural structures,[267] diffusion using cholesteric liquid crystals,[268] the use of phase-change materials,[269,270] or the photonic bandgap effect.[271] A hybrid design that combines a PDMS photonic grating with a porous structure inspired by butterfly wing scales was also reported (Figure 7f).[196] Precise pitch control of the grating, combined with the porous structure, produced vivid coloration and solar reflection, which in turn enabled subambient cooling of up to 8.45 °C under sunlight. Very recently, inspired by the scarab beetle, a layered porous nested structure composed of 3D spherical photonic crystal on a PMMA substrate was proposed.[272] The structure demonstrated subambient cooling accompanied by angle-dependent color variation. These studies demonstrate that integration of radiative cooling with structural coloration provides a promising pathway to broaden the functionality of radiative coolers and to accelerate their translation into real-world applications.

4.2. Directional RC

Fei Xie, Longnan Li, and Wei Li

Beyond spectral selectivity, the design of directional thermal emission is equally crucial for achieving high-power subambient radiative cooling, particularly in environments where surrounding objects are hotter than the radiative cooler itself. Conventional radiative coolers typically exhibit omnidirectional thermal emission, radiating heat uniformly in all directions. Consequently, they also absorb thermal radiation from all directions according to Kirchhoff's law. This leads to unwanted heat absorption from specific directions, significantly limiting cooling power. For instance, even within the atmospheric transparency window (8−13 μm), the angle dependence of atmospheric transmittance results in significant downward atmospheric radiation at high zenith angles that can exceed the cooler's outgoing radiation.[4,41] Furthermore, in practical applications like building facades, conventional coolers readily absorb heat from relatively warm ground surfaces and adjacent objects, rendering them ineffective for cooling. Directional thermal emission control can address these limitations by tailoring the spatial distribution of emitter's thermal emission to specific scenarios. Fan et al. highlight the central role of the emissivity profile in controlling the performance of the radiative cooler.[4] This approach concentrates thermal radiation in the most transparent direction of the atmosphere while minimizing absorption from undesired directions, thereby maximizing net cooling power and unlocking new opportunities for radiative cooling.

Over the past decade, the thermal emission distribution of radiative coolers has been tailored using external devices or by engineering nano/microstructures on emitter surfaces. On the one hand, various types of external devices have been employed to block downward atmospheric radiation originating from high zenith angles.[35,44,273−278] Chen et al. utilized a mirror-cone to restrict the thermal emission of the emitter to around the zenith direction where the sky is most transparent, thereby preventing relatively high-intensity incoming sky radiation from high zenith angles (Figure 8a).[44] Zhou et al. integrated a spectrally selective film with a tapered waveguide to achieve the beaming effect on the mid-infrared radiation and the suppression of the solar input (Figure 8b). This system can collimate and confine thermal radiation from the planar emitter within a relatively narrow angular range, thereby reducing the surrounding environment's impact on cooling performance.[276] In addition, V-shaped structure has also been demonstrated as an effective means of tailoring the spatial distribution of thermal emission, thereby enhancing radiative cooling performance.[277−280] On the other hand, thanks to significant advances in thermal radiation control over the past two decades, a range of approaches have been explored to tailor the angular response of thermal emission.[281−285] This development has enhanced the net cooling power of directional radiative coolers in various application scenarios. For instance, Qu et al. theoretically designed a directional thermal emitter featuring a multilayer angular selector made of anisotropic material placed atop a three-layer broadband thermal emitter (Figure 8c).[286] This directional thermal emitter exhibits high emissivity at emission angles between 0 and 40°, enabling it to reflect the strong thermal emission from the surrounding buildings and achieve higher cooling efficiency than conventional radiative coolers with omnidirectional thermal emission. Chamoli et al. designed a 16-μm-thick thin film stack comprising an angle dependent transmission filter overlaid on a selective thermal emitter, achieving both angularly and spectrally selective emission under s- and p-polarized light without the use of anisotropic layers (Figure 8d).[287] Fan et al. developed a compact pixelated directional microemitter that exhibits polarization independent thermal emission with strong directionality. Through delicate structure designing, the emitter confines thermal radiation to a narrow angular range across an ultrawide working wavelength range, enabling efficient thermal energy transfer and offering the potential to enhance the capabilities of radiative cooling.[288]

While radiative cooling has traditionally been applied to horizontal surfaces like rooftops, recent efforts have extended its use to vertical surfaces such as building facades and windows. These vertical applications require more stringent directional control of thermal emission due to their complex heat transfer

https://doi.org/10.1021/acsami.6c00074
ACS Appl. Mater. Interfaces 2026, 18, 21363−21423

processes. The concept of directional thermal emission control based on gradient epsilon-near-zero (ENZ) materials has been explored for use on vertical surfaces. ENZ materials support a leaky p-polarized electromagnetic mode near their resonance pole, known as the Berreman mode, which can couple to propagating free-space modes at a range of wave vectors and certain angles of incidence.[289−299] Bae et al. designed a directional radiative cooling glass (DRCG) consisting of a multilayer angular selector based on epsilon-near-zero materials (Si_3N_4 and Al_2O_3) deposited on an indium−tin−oxide thermal reflector (Figure 8e).[300] The DRCG provides directional emissivity confined to high incident angles while maintaining a visible transmittance above 84%, and its use as a window improves space-cooling performance by approximately 1.5 °C compared with conventional glass. Ryu et al. designed an angular selective broadband emitter by stacking the ENZ layers using a Fabry-Pérot (FP) optical cavity, achieving high emittance at high polar angles (70−90 °) while reflecting radiative heat incident perpendicularly from adjacent buildings (Figure 8f).[301]

Although the approach based on ENZ materials can effectively suppress thermal radiation from adjacent objects, the spatial symmetry and polarization dependence of its thermal radiation pose significant obstacles to achieving subambient radiative cooling on vertical surfaces. To overcome this limitation, several studies[302−305] have demonstrated relative cooling effects by employing asymmetric directional emitters compared to conventional omnidirectional emitters. To further address the challenge of achieving cooling below ambient temperature, Xie et al. comprehensively analyzed underlying constraints for vertical surfaces and hierarchically designed an angularly asymmetric spectrally selective thermal emitter, demonstrating daytime subambient radiative cooling on vertical surfaces for the first time (Figure 8g).[20] These advances underscore the potential of asymmetric directional thermal radiation to enhance radiative cooling performance and highlight its promise for practical building applications.

Overall, the development of directional radiative coolers offers a pivotal solution for overcoming the limitations of traditional horizontal surfaces while unlocking new possibilities for radiative cooling. Current research advances demonstrate that directional thermal radiation is extending radiative cooling applicability to multidimensional scenarios—from rooftops to vertical walls, and from open areas to densely built areas. Moreover, directional thermal radiation shows considerable potential for further development in applications such as vehicles and textiles, where most exterior surfaces are vertical. This enhanced spatial adaptability, combined with optimized spectral selectivity, creates significant opportunities for building energy conservation, electronic thermal management, and sustainable energy systems.

4.3. Adaptive and Switchable RC

Xuzhe Zhao, Jiachen Li, and Kaichen Dong

RC technology utilizes the atmospheric window to exchange heat with the cold outer space, achieving continuous cooling without energy consumption. With the advancement of nanophotonics and the maturation of spectral regulation technologies, RC films have achieved nearly perfect atmospheric emissivity and solar reflectivity, making their cooling power sufficient to meet market demands. With the fast industrialization and real-world applications of RC, new practical requirements emerge and quickly attract wide attention. For example, in high-latitude or midlatitude regions with cold winters, the heat loss associated with static RC contributes to unwanted heating burden during cold days.[306] Consequently, the year-round energy savings of RC are substantially reduced with additional carbon emissions—contrary to the original intention of the RC technology.

To address the above issue, the concept of adaptive and switchable RC (ASRC) was proposed, which involves designing RC devices with tunable atmospheric window emissivity.[30] ASRC technologies aim at switching to a thermal insulation mode at low temperatures, and reverting to a RC mode at high temperatures, thereby realizing cooling in summer and keeping warm in winter.

ASRC technologies are generally categorized based on whether external control or actuation is required. Passive ASRC technologies operate autonomously, responding to environmental stimulus such as temperature or humidity without additional energy input. On the other hand, active ASRC technologies require external control—such as mechanical actuation or electrical bias—to modulate thermal emissivity rapidly and precisely.

Among passive ASRC technologies, temperature-adaptive ASRC[307] is the most widely adopted due to its direct temperature-emissivity response characteristics, which naturally meets the all-season energy-saving requirements of RC. The working principle of temperature-adaptive ASRC lies in responsive materials or structures whose emissivity varies with temperature. When the ambient temperature falls below a preset threshold, the temperature-adaptive ASRC maintains a low emissivity to minimize thermal loss. Conversely, when the temperature rises beyond the threshold, ASRC autonomously switches to high emissivity to boost RC.

Based on the employed materials or structural mechanisms, temperature-adaptive ASRC can be broadly classified into shape memory material-based technologies[317] and phase-change material (PCM)-based technologies.[318] Shape memory materials primarily include shape memory alloys[319] and shape memory polymers.[317] For instance, shape memory polymer-based structures integrate a polymer-based mechanical actuation layer between RC and solar heating layers, enabling automatic emissivity switching in response to temperature changes.[320] Zhang et al. developed a dual-mode thermal management device using shape memory polymers that achieved self-switching between heating (859.8 W m^{-2}) and cooling (126.0 W m^{-2}) modes.[320] Shape memory alloys are also commonly used to fabricate mechanical actuators such as memory springs for reversible switching between heating and cooling modes.[319]

PCM-based thermally adaptive ASRC generally employs PCMs like GST,[321] perovskites,[322] lanthanum strontium manganese oxide (LSMO),[323] and vanadium dioxide (VO_2),[324] which have all been extensively explored owing to their drastic infrared refractive index change with temperature changes. With the advancement of nanophotonics and microfabrication technologies, a growing number of photonic structures, such as 1D photonic crystals,[24] Fabry-Pérot (F−P) cavities,[30] core−shell structures,[325] and optical antennas[309] have been developed to amplify the emissivity modulation performance of PCMs. Among all the above PCMs, VO_2, in particular, stands out because of its reversible metal−insulator transition near ambient temperature and pronounced changes in infrared refractive index across its phase transition.[326] In 2018, an F−P cavity photonic structure based on VO_2 was theoretically demonstrated to achieve a modulation depth of 0.6 in emissivity.[30] However, early VO_2-based ASRC designs were

https://doi.org/10.1021/acsami.6c00074
ACS Appl. Mater. Interfaces 2026, 18, 21363−21423

mostly theoretical or small-scale laboratory prototypes, lacking extensive outdoor testing and validation.[327] In 2021, Wang et al.[308] and Tang et al.[307] independently proposed VO_2-based smart window and roof coatings. As shown in Figure 9a(i),

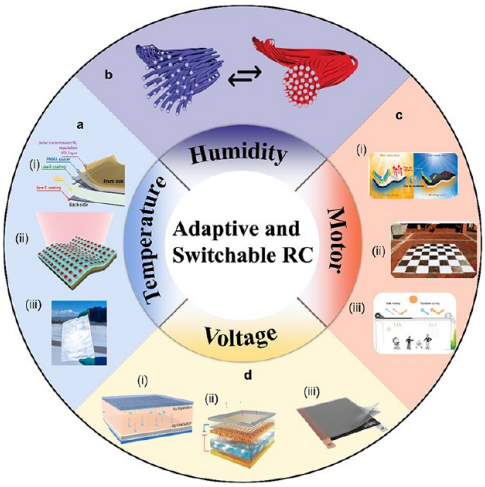

Figure 9. ASRC Technologies with Four Modulation Approaches. (a) Temperature-adaptive ASRC. (i) F−P cavity (ii) metasurface (iii) optical antenna. (b) Humidity-adaptive ASRC. (c) Motor-controlled ASRC. (i) flipping type (ii) sliding type (iii) overlapping type. (d) Voltage-controlled ASRC. (i) reversible deposition of silver (ii) reversible deposition of copper (iii) electro-intercalation. Adapted with permission from ref 307. Copyright 2021 American Association for the Advancement of Science. Adapted with permission from ref 308. Copyright 2021 American Association for the Advancement of Science. Adapted with permission from ref 309. Copyright 2023 Elsevier. Reprinted with permission from ref 310. Copyright 2019 American Association for the Advancement of Science. Adapted with permission from ref 311. Copyright 2022 Springer Nature. Adapted with permission from ref 312. Copyright 2022 American Chemical Society. Adapted with permission from ref 313. Copyright 2020 Springer Nature. Adapted with permission from ref 314. Copyright 2022 John Wiley and Sons. Adapted with permission from ref 315. Copyright 2023 Springer Nature. Adapted with permission from ref 316. Copyright 2021 Springer Nature.

Wang et al.[308] proposed a smart window based on a F−P cavity composed of VO_2, PMMA, and a low-emissivity coating, achieving an infrared emissivity modulation depth of 0.4. Tang et al.[307] and Li et al.[309] realized switchable emissivity with three-layer metasurface and optical antenna structures using VO_2/BaF_2/Ag and PE/VO_2/Al configurations, as shown in Figure 9a(ii) and Figure 9a(iii), respectively, enhancing the emissivity modulation depth to around 0.7. Through year-round energy simulations and outdoor field tests, it was validated that ASRC can reduce overall energy consumption across multiple climate zones worldwide compared with traditional static RC. This is especially effective in regions with large temperature fluctuations, laying the foundation for future ASRC development.

In addition to temperature-adaptive ASRC, humidity-adaptive ASRC offers an alternative passive route for adaptive thermal regulation. Humidity-adaptive ASRC technologies do not respond directly to temperature fluctuations, but instead to the associated changes in ambient humidity.[310] Given that sweating typically accompanies a rise in human body temperature, humidity-adaptive ASRC materials are often applied in personal thermal management.[310] Under cool or thermally neutral conditions, limited perspiration keeps humidity-adaptive ASRC in an "off" state, maintaining low emissivity and conserving body heat. When sweating occurs with a rise in body or ambient temperature, the resulting increase in local humidity activates these materials to an "on" state, raising their emissivity to enhance RC. As illustrated in Figure 9b, Zhang et al. developed a humidity-responsive metafiber by combining carbon nanotubes with hydrophobic triacetate and hydrophilic cellulose, achieving an emissivity modulation depth of 0.35.[310] Furthermore, Mandal et al. infused porous polymers with volatile liquids such as ethanol or isopropanol, reaching an emissivity modulation depth of 0.64, illustrating strong potential in personal thermal management.[328]

Compared with passive ASRC, active ASRC offers distinct advantages in terms of response speed and control precision. Among them, motor-controlled ASRC systems have attracted considerable attention due to their design flexibility and large emissivity modulation depths.[311] These systems typically operate by integrating distinct surfaces with high and low emissivity, switching between them via mechanical structures or manual manipulation. Depending on the switching mechanism, they can be further categorized into flipping-type[311] and sliding-type configurations.[312]

As illustrated in Figure 9c(i), Xiang et al. developed a Janus all-polymer ASRC material with flipping functionality, utilizing poly(vinylidenefluoride-*co*-hexafluoropropene) (PVDF-HFP) and polypyrrole (PPy) on opposite surfaces. The chemical bonding differences between the two materials produce spectral contrasts in both the solar and mid-infrared ranges, enabling emissivity modulation via manual flipping.[311] In addition to flipping-based systems, sliding-type structures have also been demonstrated. For example, as shown in Figure 9c(ii), Ke et al. designed a reconfigurable interwoven surface tailored for building thermal regulation, capable of manually sliding to alternate between high and low emissivity.[312] Li et al. adopted a similar approach as shown in Figure 9c(iii), substituting manual operation with a motorized mechanism to enable emissivity modulation by dynamically overlapping two different roofing materials.[313]

Similar to motor-controlled ASRC, voltage-controlled ASRC also requires additional energy input to switch between states. Owing to their compact architecture and high response speed, voltage-controlled ASRC has demonstrated broad applicability in aerospace thermal management and smart windows.[315] Voltage-controlled ASRC can be realized using transition metal oxides,[329] conductive polymers,[330] or reversible metal deposition.[331] Among them, transition metal oxides such as WO_3 can significantly increase infrared reflectance upon the intercalation of small cations,[332] thereby enabling emissivity modulation via electrical control. Besides, voltage-controlled ASRC based on conductive polymers offers flexibility and processability that are not achievable with the former. Voltage-controlled ASRC relying on reversible metal electrodeposition typically utilizes infrared-transparent electrodes and aqueous electrolytes.[314] Without an applied voltage, the device exhibits high emissivity, enabling effective RC at high ambient temperatures; conversely, applying a reverse voltage drives metal layer deposition, lowering the emissivity and thereby promoting heat retention at low ambient temperatures. As illustrated in Figure 9d(i) and Figure 9d(ii), Tao et al.[314] and Sui et al.[315] reported emissivity modulation depths of 0.48 and 0.8 using reversible deposition of silver and copper, respectively. Beyond reversible metal electrodeposition, other strategies such as electro-intercalation of lithium ions into graphene layers[316] as shown in Figure 9d(iii)

https://doi.org/10.1021/acsami.6c00074
ACS Appl. Mater. Interfaces 2026, 18, 21363−21423

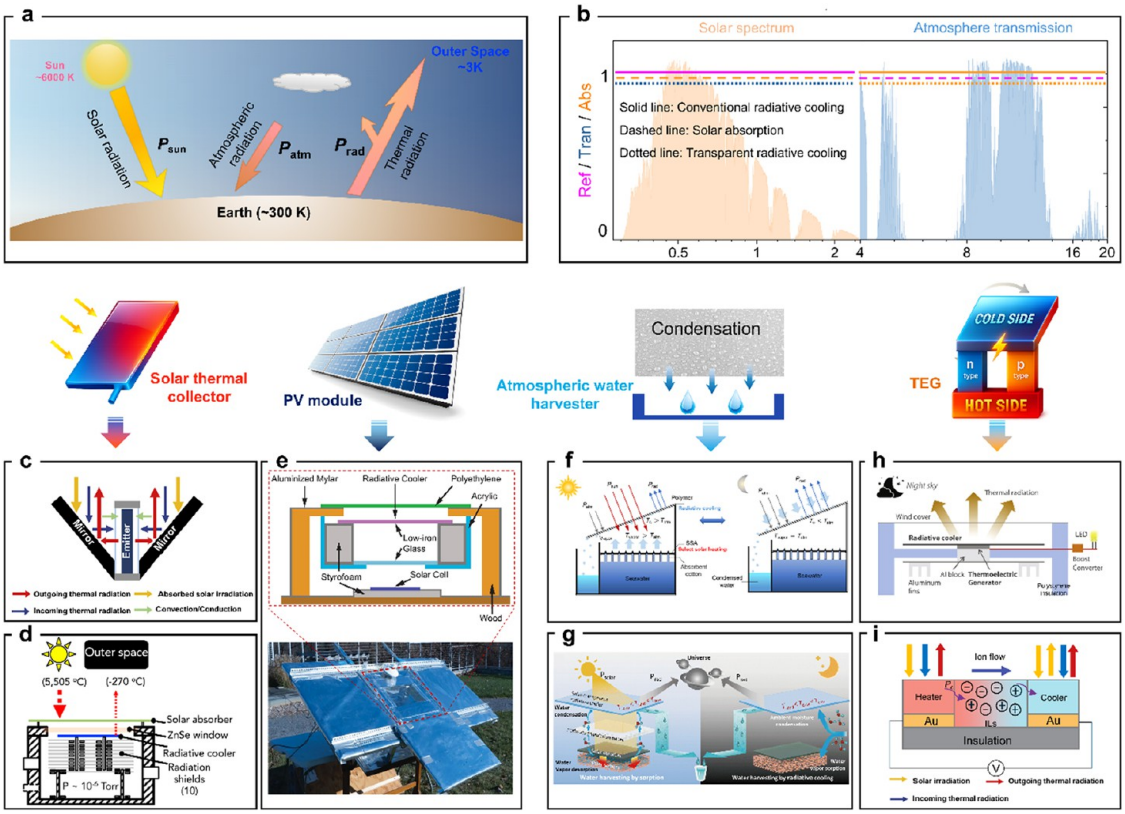

Figure 10. Hybrid and multifunctional radiative cooling (RC) platforms. (a) Schematic illustration of RC coupled with four representative functions on Earth: solar thermal collectors, photovoltaic (PV) modules, atmospheric water collectors, and thermoelectric generators (TEGs). (b) Spectral requirements for conventional radiative cooling, solar absorption and transparent radiative cooling. For solar thermal collectors: (c) vertical RC configurations enabling coutilization of heat and cooling. Reproduced with permission from ref 277. Copyright 2021 Elsevier. (d) Vacuum-assisted RC systems enhancing heat harvesting. Adapted with permission from ref 338. Copyright 2019 Elsevier. For PV modules: (e) transparent RC layers integrated with solar energy conversion. Reproduced with permission from ref 343. Copyright 2024 Elsevier. For atmospheric water collectors: (f) all-day freshwater production via solar-driven interfacial desalination combined with transparent RC. Adapted with permission from ref 339. Copyright 2022 American Chemical Society. (g) Continuous sorption−desorption cycles coupling solar heating with transparent RC. Adapted with permission from ref 341. Copyright 2024 Royal Society of Chemistry. For TEGs: (h) nighttime RC-driven power generation for lighting. Adapted with permission from ref 347. Copyright 2019 Elsevier. (i) Hybrid RC−solar heating architectures for enhanced electrical output. Reproduced from ref 345 under the terms of the CC-BY 4.0 license. Copyright 2023 The Author(s), published by John Wiley and Sons.

and dynamic modulation of intersubband transitions in n-type quantum wells[333] have also enabled fast and broadband electrical tuning of emissivity.

In conclusion, both passive ASRC (triggered by either temperature or humidity) and active ASRC (operated via mechanical or electrical control) offer distinct advantages tailored to specific applications. Compared with static RC, the dynamic emissivity modulation of ASRC enhances adaptability to varying ambient conditions and facilitates thermal stability. Consequently, ASRC technologies are promising for diverse scenarios, including spacecraft thermal regulation,[334] personal thermal management,[310] and building energy conservation.[307] Nevertheless, their widespread deployment will depend on addressing critical challenges, particularly with respect to durability, scalable manufacturing, and cost-effectiveness. To this end, future research should investigate long-term material stability under realistic operating environments, establish scalable and economically viable fabrication methods, and evaluate integration strategies that enable reliable performance across diverse application scenarios.

4.4. Hybrid and Multifunctional RC

Saichao Dang and Qiaoqiang Gan

Mitigating global warming requires technologies capable of alleviating thermal loads without consuming additional energy.[32,63,335] RC offers such a pathway by channeling terrestrial heat into outer space through strong mid-infrared (mid-IR) emission within the 8−13 μm atmospheric transparency window, enabling passive—and even subambient—cooling under direct sunlight (Figure 10a). However, the performance of RC is inherently constrained by environmental and spectral conditions. Its cooling power depends strongly on sky clarity, humidity, and ambient temperature, while daytime operation demands stringent solar-band suppression to prevent parasitic heating. As a result, superwhite or spectrally selective coolers must reject most incident solar photons to maintain radiative cooling performance (Figure 10b, solid lines).

In the context of a decarbonizing world, discarding the solar resource represents a profound inefficiency,[336,337] Furthermore, pure RC systems struggle to meet variable thermal demands across diurnal and seasonal cycles or under fluctuating cloud cover—conditions that limit their practical deployment. These challenges underscore a fundamental reality: no single passive cooling technology can satisfy all thermal management needs across diverse weather and usage scenarios.

https://doi.org/10.1021/acsami.6c00074
ACS Appl. Mater. Interfaces 2026, 18, 21363−21423

The emerging opportunity lies in hybrid and multifunctional RC platforms that preserve the mid-IR radiative channel to the sky while strategically harnessing or redirecting the solar spectrum toward complementary energy services—such as heating,[277,338] water harvesting,[339−342] and electricity generation.[343−349] Recent advances demonstrate that the perceived conflict between radiative cooling and solar utilization is not fundamental, but rather a matter of spectral and thermal management.[344,350] By spectrally separating the solar and mid-IR bands and minimizing unwanted heat exchange, hybrid RC systems can simultaneously reject excess thermal energy to outer space while capturing useful solar energy for other processes. Building on this framework, the following sections examine four representative directions in RC integration:

(i) Solar thermal collectors,[277,338]
(ii) Photovoltaic (PV) modules,[343,344]
(iii) Atmospheric water collectors,[339−342] and
(iv) Thermoelectric generators (TEGs).[345−349]

Each category is discussed in terms of its governing physical principles, material and structural design strategies, and key performance metrics. Together, these examples illustrate how RC can evolve from a single-function passive cooler into a multifunctional thermal−water−energy management platform, offering a more holistic response to the planet's rising thermal and energy challenges.

4.4.1. RC and Solar Thermal Collectors. *4.4.1.1. Physical Principles.* RC requires surfaces with high mid-infrared emissivity and strong solar reflectance (Figure 10b, solid lines), while solar thermal absorbers demand the opposite—strong shortwave absorption and suppressed mid-infrared emission (Figure 10b, dashed lines). This inherent spectral conflict can be resolved by decoupling the solar and mid-infrared channels so that one element captures solar heat while another maintains radiative cooling.[344]

4.4.1.2. Design Strategies. One strategy is the vertical mirror−emitter configuration (Figure 10c).[277] Here, two solar-absorbing wings with high solar absorptivity and mid-infrared reflectivity act as heaters, while a central emitter, designed for high solar reflectivity and strong mid-infrared emissivity, radiates to the sky as a cooler. This geometry separates solar absorption from radiative emission, allowing both processes to operate without interference. Another approach is vacuum-assisted integration (Figure 10d), where a mid-infrared-transparent solar absorber is placed above a radiative cooler inside a vacuum chamber.[338] The vacuum environment minimizes parasitic conduction and convection, preserving large thermal contrasts between the hot and cold elements.

4.4.1.3. Key Performance Metrics. The vertical mirror−emitter system demonstrated enhanced subambient cooling of 6.2 °C (double-sided RC) compared to 4.2 °C (single-sided RC), alongside simultaneous solar heating of ∼40 °C above ambient on the absorbers.[277] In vacuum-assisted platforms, absorber temperatures reached 24 °C above ambient, while the radiative cooler simultaneously achieved 29 °C below ambient.[338] These results underscore the capability of RC-based architectures to achieve coharvesting of solar heat and sky-coupled cooling within the same footprint

4.4.2. RC AND PVs. *4.4.2.1. Physical Principles.* RC and PV modules impose opposite spectral requirements: RC relies on reflecting sunlight to remain cool, while PV requires absorbing sunlight for power generation. This competition can be reconciled through transparent RC layers (Figure 10b, dotted lines), which transmit most of the solar spectrum to the PV cell while maintaining strong mid-infrared emission to the sky.[344] In this configuration, the PV continues to harvest sunlight for electricity, while the RC layer simultaneously harvests cold from outer space, enabling colocated solar energy conversion and passive thermal management.

4.4.2.2. Design Strategies. One straightforward strategy employs low-iron glass radiators with high solar transmittance and strong mid-infrared emissivity, laminated above solar cells (Figure 10e).[343] In this configuration, the glass not only transmits sunlight to the PV absorber but also establishes a subambient cavity between the cover and the cell, effectively storing "harvested cold" that can be used to dissipate excess heat from the module. An alternative strategy is to apply transparent RC coatings directly onto the PV cover surface.[14,230,280,351−353] These coatings—ranging from silica−polymer composites[34,352] and porous dielectrics[230] to multilayer thin films[351] and engineered micro/nanostructured textures[353] are designed to enhance the infrared emissivity of the solar cell surface while maintaining high solar transmittance (>90%). By enabling the cell itself to radiatively shed heat to the sky, this approach lowers operating temperature, mitigates thermal degradation, and improves long-term performance.

4.4.2.3. Key Performance Metrics. Outdoor experiments on laminated RC−PV modules demonstrate subambient temperature reductions of approximately 5 °C, with radiative cooling power densities of 60−90 W m^{-2} under peak solar irradiance.[343] Importantly, these systems maintain PV electrical outputs exceeding 150 W m^{-2}, evidencing that effective thermal management does not compromise photovoltaic conversion. The corresponding radiative cooling flux has been measured at 63.8 W m^{-2} under full sunlight and 87.0 W m^{-2} at night, confirming robust 24-h radiative performance. Such thermal regulation translates into efficiency improvements of up to ∼30%, along with mitigated thermal degradation and extended module lifetime. Collectively, these findings establish transparent RC coatings and laminates as practical, scalable, and durable solutions for passive thermal regulation in solar energy systems, simultaneously enhancing performance, stability, and sustainability.

4.4.3. RC and Atmospheric Water Collectors. *4.4.3.1. Physical Principles.* In atmospheric water harvesting (AWH), the introduction of transparent radiative coolers plays a crucial role in reconciling condensation with daytime solar heating.[339−342] Transparent RC layers are engineered to be highly emissive in the mid-infrared, ensuring continuous radiative cooling to the sky, while at the same time transmitting most of the solar spectrum to underlying absorbers or sorbent beds.[354] This dual function establishes a spectral separation of roles: the solar channel is directed downward to drive evaporation or desorption, while the mid-infrared channel remains open upward to sustain subambient cooling and condensation. In this way, transparent RC components act simultaneously as optical windows and radiative condensers, creating the thermodynamic conditions needed for all-day water harvesting.

4.4.3.2. Design Strategies. In practice, transparent radiative coolers made from polymers such as PDMS and PMMA have been widely employed as the top condenser layer in hybrid water-harvesting modules.[339,340,355] A representative approach is the all-in-one configuration, where the transparent RC cover both maintains radiative cooling and allows solar radiation to reach an underlying absorber or sorbent bed within an insulated

https://doi.org/10.1021/acsami.6c00074
ACS Appl. Mater. Interfaces 2026, 18, 21363−21423

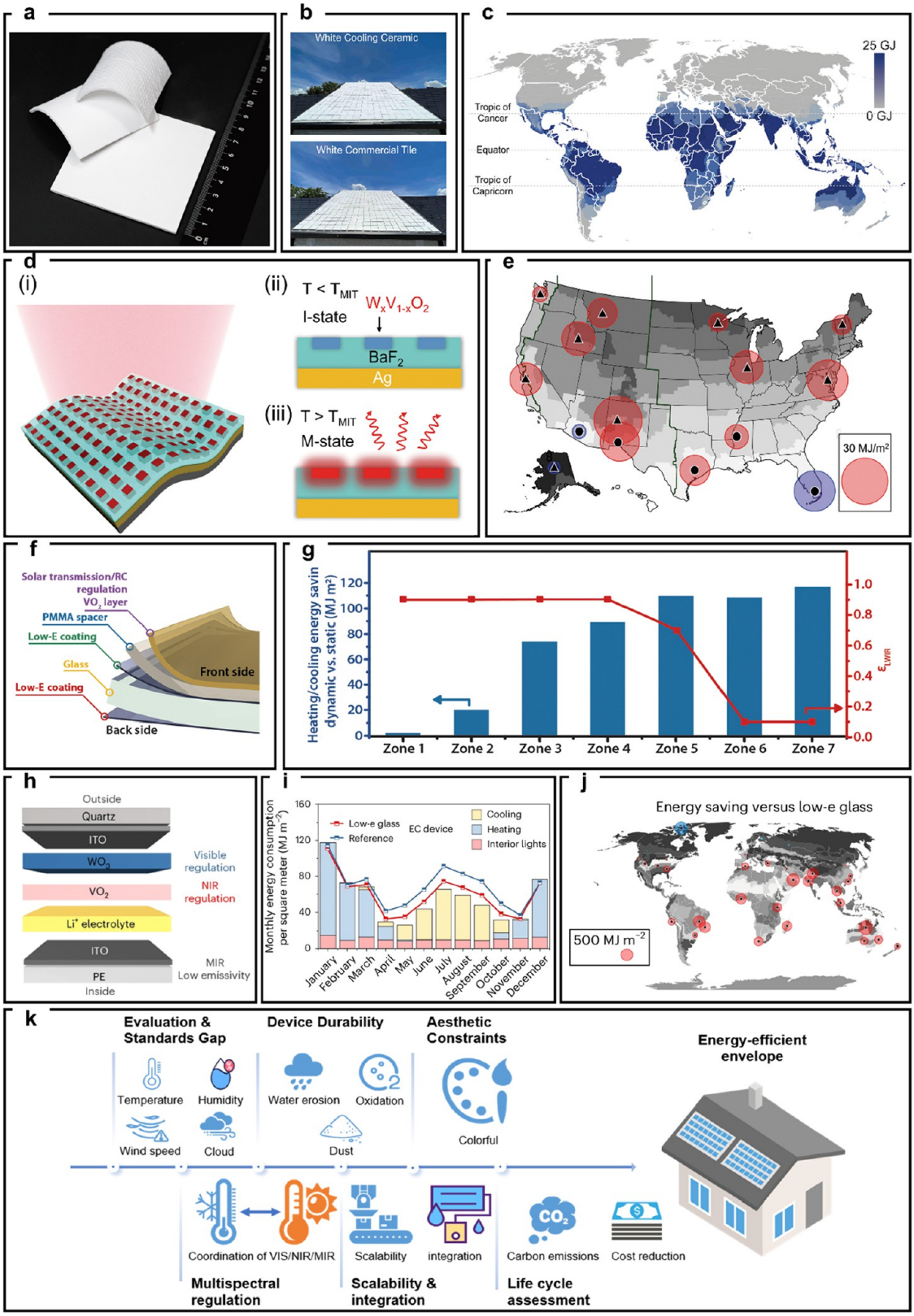

Figure 11. Energy-efficient buildings and smart windows. (a) Photograph of the cooling ceramics with flat and curved shapes. Patterns can also be applied on the cooling ceramic surface. (b) Photograph of the model houses, with the white cooling ceramic and white commercial tile applied on the roof (area: ~1.15 m^2). The model houses were installed 2 m apart during the experiment to eliminate interference. (c) Energy-saving performance on a worldwide scale considering the energy consumed by cooling systems, fans, and heating equipment. Adapted with permission from ref 164. Copyright 2023 AAAS. (d) Schematics of the structure (i), materials composition and working mechanism (ii and iii) of the Temperature-adaptive radiative coating. (e) Minimum space-conditioning source energy savings ($SCSES_{min}$) of TARC compared with other existing roof-coating materials for different cities representing the 15 climate zones in the United States. Red and blue circles indicate positive and negative $SCSES_{min}$ values, respectively. The values are scaled to the area of the circles. Adapted with permission from ref 307. Copyright 2021 AAAS. (f) Schematic structure of the RC

https://doi.org/10.1021/acsami.6c00074
ACS Appl. Mater. Interfaces 2026, 18, 21363−21423

Figure 11. continued

regulating thermochromic window. (g) Heating and cooling energy saving (blue columns) of simulated optimized dynamic samples against optimized static samples (red square) from zones 1 to 7. In this simulation, T_{sol} was fixed to 30%. The optimized static ε sample is derived from the point of minimum total energy consumption by adding heating and cooling in seven climate zones by fixing ε. The optimized dynamic ε window has a ε_{LWIR} of 0.9 for cooling and 0.1 for heating. The optimized dynamic ε window has lower energy consumption than optimized static ε window from zones 2 to 7. Adapted with permission from ref 308. Copyright 2021 AAAS. (h) Schematics of the optimizing-multispectral EC device with a low-e surface. (i) Monthly energy consumption of the EC device, low-e glass and normal glass window in the climate condition of Shanghai. To provide a clearer representation of the data for this EC device (j) Estimated heating and cooling energy saving of a triband-optimized EC device against a commercial low-e glass as the baseline for different cities representing different climate zones. Adapted with permission from ref 377. Copyright 2024 Springer Nature. (k) Current limitations and future potential of RC for energy-efficient envelopes.

chamber (Figure 10f).[339,340] This enables daytime vapor generation beneath the cover and condensation on its subambient surface, while at night the same RC layer directly condenses atmospheric moisture. An alternative route is the sorption−desorption cycle, in which hygroscopic materials (e.g., salt−polymer composites,[341] hydrogels[356−358]) are combined with transparent RC condensers (Figure 10g). Here, the RC layer provides continuous cooling to enhance nighttime vapor uptake, while solar heating during the day regenerates the sorbent and directs the released vapor to the RC surface for condensation. Key considerations across these designs include the optical transparency and mid-infrared emissivity of the RC layer, the durability of polymeric materials under outdoor conditions, and the optimization of surface wettability and vapor transport channels to maximize condensation efficiency and water yield.

4.4.3.3. Key Performance Metrics. Hybrid RC−AWH systems have demonstrated daily water yields of 0.2−3.6 L m^{-2} day^{-1}, with instantaneous condensation fluxes up to 0.36 L m^{-2} h^{-1} under favorable humidity conditions.[339−341,356−358] Transparent RC layers, typically composed of polymers such as PDMS or PMMA, serve both as condensers and spectral separators, enhancing subambient cooling and extending dew-point margins by several degrees compared with conventional passive designs.[339,340,355] Performance assessment typically involves dew-point margin ($\Delta T_{surface} - T_{dew}$), net cooling power, areal yield (L m^{-2} day^{-1}), and sorbent productivity (kg H_2O per kg sorbent per cycle). Multiday cyclic experiments confirm stable water output and minimal degradation, underscoring the long-term feasibility and operational robustness of RC-assisted atmospheric water harvesting. Collectively, these findings establish RC as a sky-coupled thermal component that enables sustainable, diurnal freshwater generation across a wide range of climatic conditions.[35,358,359]

4.4.4. RC and Thermoelectric Generators (TEGs). *4.4.4.1. Physical Principles.* TEGs convert a temperature gradient into electricity by driving charge carriers across n−p legs, and their output scales directly with the magnitude and stability of the temperature difference (ΔT).[347,348] RC provides a natural cold sink: surfaces with high mid-infrared emissivity can emit thermal radiation through the 8−13 μm atmospheric window, allowing them to cool below ambient temperature, particularly under clear skies. However, the ΔT achievable with RC alone is typically modest (∼1−5 °C relative to ambient air), which limits the electrical output of a TEG if RC is used in isolation.[348] Hybrid RC−TEG systems overcome this limitation by pairing the RC surface as the cold side with a dedicated hot side, such as a solar-heated absorber[345,360,361] or the hot ground.[362] This configuration maintains a continuous temperature bias: at night, the RC surface cools below ambient, while the hot side—often the surrounding air or residual thermal mass—remains warmer; during the day, solar heating further elevates the hot side temperature. In this way, RC provides a persistent cold reservoir that sustains ΔT, enabling round-the-clock thermoelectric power generation.[345,347,349,360,361]

4.4.4.2. Design Strategies. Nighttime configurations typically use a sky-facing RC radiator as the cold side and ambient air as the hot side (Figure 10h).[347] Design improvements include enlarging the radiator-to-TEG area ratio, applying IR-transparent covers to suppress convective exchange, and reducing thermal/electrical contact resistances. For daytime operation, spectral separation is critical: solar photons are routed to a selective absorber or thermal mass (hot side), while the RC element remains optically coupled to the sky (cold side).[345,360,361] Recent advances employ dual-material designs such as cellulose-based composites with opposite optical properties: a solar-reflective, high-emissivity radiator as the cold surface, paired with a solar-absorbing, MIR-suppressing heater as the hot surface (Figure 10i).[345] This arrangement maintains a stable ΔT over day−night cycles.

4.4.4.3. Key Performance Metrics. Prototype RC−TEG systems have demonstrated $\Delta T \approx 2-5$ °C, producing open-circuit voltages of 80−100 mV and power outputs around tens of mW m^{-2}, sufficient to drive small electronics or LEDs.[347] Cellulose-based day−night systems reported a ΔT of ∼10 °C under solar irradiance of ∼400 W m^{-2}, generating thermovoltages above 60 mV. Modeling further indicates that with optimized convective management, minimized parasitic losses, and proper thermal impedance matching, outputs could exceed 0.5 W m^{-2} in hot, arid climates.[345] Although far below photovoltaics in power density, RC−TEG hybrids uniquely provide continuous 24-h trickle power for sensors, off-grid electronics, and distributed Internet of Things (IoT) devices without external energy input.

5. POTENTIAL APPLICATIONS OF RC

5.1. Energy-Efficient Buildings and Smart Windows

Shaowen Cao and Yi Long

Buildings account for ∼30% of global final energy use, and spectral thermal management of envelopes and glazing is increasingly regarded as a priority pathway to reduce carbon emissions.[8,363] RC provides a continuous and stable passive "cold source" for buildings. For opaque envelopes, RC applied to roofs and walls has demonstrated appreciable temperature reductions and energy savings under real conditions in low-latitude regions.[364] In midlatitude climates with distinct seasons, dynamical envelopes that integrate RC and radiative heating are emerging, enabling reversible switching between "cooling" and "heating" states to optimize annual energy performance.[365] For transparent systems, thermal-management materials used in smart windows must preserve visible transmittance and daylighting, which demands more complex and precise spectral

https://doi.org/10.1021/acsami.6c00074
ACS Appl. Mater. Interfaces 2026, 18, 21363−21423

control across the VIS, NIR, and MIR bands. In cooling-dominated low-latitude regions, static RC windows are suitable, whereas in midlatitude regions dynamically tunable smart windows are needed to accommodate seasonal variation. It is worth mentioning the recent radiative warming for high latitude regions have been developed with the broadband mode,[366,367] which is not covered in this review. Consequently, this section reviews RC applications and energy benefits in roofs/walls and smart windows for energy-efficient buildings and examines the system-level potential and engineering challenges for real-world deployment.

For opaque static building envelopes, i.e., RC roofs and walls, the outer layer typically employs coatings, films, ceramic panels, or cementitious components with high solar reflectance (R_{sol}) and high MIR emittance (ε_{MIR}), integrated with existing insulation and waterproofing to lower surface temperature and cooling loads without altering building functions. Because roofs and walls are continuously exposed to UV radiation, precipitation, and soiling, long-term durability is critical for real-world deployment. Addressing this need, Tso et al. fabricated hierarchically porous Al_2O_3 cooling ceramics via phase inversion and sintering (Figure 11a,b). The ceramic exhibits weatherability, mechanical stability, and long-term performance. For a four-story apartment prototype in tropical cooling-dominated climates, simulations indicate >10% annual heating, ventilating, and air conditioning (HVAC) energy savings, equivalent to ∼25 GJ yr^{-1} (Figure 11c).[164] Hu et al. reported a solution-processed dual-particle inorganic porous architecture that combines durability with applicator-friendly processing and delivers near-optimal high R_{sol}/high ε_{MIR}. In humid climates it achieves ∼3.5 °C subambient cooling and ∼8−10% reductions in building cooling-related emissions.[368] Recently, Li et al. developed a water-borne cementitious integrated cooling paint by embedding nano-$BaSO_4$ into a porous C−S−H network. The paint reaches ∼93% R_{sol} and ∼95% atmospheric-window emittance under routine brush application and maintains high mechanical and weathering robustness. Field tests in Singapore show 30−40% reductions in air-conditioning electricity use relative to a commercial cool-roof paint.[369]

Static RC is effective in cooling-dominated low-latitude regions, yet it can cause winter overcooling penalty in midlatitude climates with distinct seasons and in heating-dominated high-latitude regions.[32] This risk increases heating demand and motivates the use of tunable thermal management. VO_2 is a prototypical thermochromic material whose metal−insulator transition enables temperature-dependent emissivity. Leveraging this property, Wu et al. designed a temperature-adaptive radiative coating (TARC) that reversibly switches near 22 °C from low emissivity ($\varepsilon_{LWIR} \approx 0.2$) to high emissivity ($\varepsilon_{LWIR} \approx 0.9$)[307] (Figure 11d). Annual whole-building simulations across 15 U.S. zones show energy savings of about 22.4 $MJ{\cdot}m^{-2}{\cdot}y^{-1}$ for a typical single-family house in mixed climates such as Baltimore when compared with a static RC coating (Figure 11e). Extending this concept, Wu et al. developed a roll-to-roll flexible overlayer with tunable ε_{LWIR} and optimized solar absorption for energy-efficient building envelopes.[309] Compared with a standard cool roof it yields additional annual energy reductions in most climate zones, for example ∼12.6 GJ per year for a typical San Francisco residence, while mitigating winter overcooling and cool-roof condensation. In addition, Long et al. proposed a switchable interwoven surface for dynamic cooling−heating regulation.[312] The surface is assembled from modules with distinct R_{sol} and ε_{LWIR} pairs: Phase 0 exhibits a black, high absorptance state with $A_{sol} = 0.87$ and $\varepsilon_{LWIR} = 0.39$, whereas Phase 1 exhibits a white, low-absorptance high-emittance state with $A_{sol} = 0.05$ and $\varepsilon_{LWIR} = 0.91$. Spatial reconfiguration between the two module types enables meter-scale deployment and achieves up to 9.5% annual HVAC energy savings in ASHRAE Climate Zone 4 relative to a conventional roof.

Compared with opaque materials for roofs and walls, thermal management for transparent glazing must preserve daylighting while coordinating spectral control across the VIS, NIR, and MIR bands. From practical considerations, simultaneously achieving high visible transmittance, environment-dependent near-infrared dynamic modulation, and tailored mid-infrared emissivity is challenging. If relatively independent spectral regulation is desired in the VIS, NIR, and MIR bands, at least three optical design degrees of freedom are generally required. In reported transparent glazing structures, common implementations often involve about 4 to 7 design degrees of freedom. This range is not a fixed standard, and it is closely related to the adopted spectral regulation mechanism. If a single functional layer can contribute to multiband regulation, the required degrees of freedom may be reduced accordingly. In contrast, when additional electrochemical circuit elements are introduced to enable multiple states or larger modulation amplitude, the required design freedom typically increases.

Rho et al. reported a static RC window that employs an emitter−reflector stack comprising a PDMS emissive top layer to enhance ε_{LWIR}, a TiO_2/MgF_2 Bragg reflector engineered to maintain high T_{VIS} and selectively reflect NIR radiation, and an apertured Ag reflector to suppress A_{sol} without compromising a neutral appearance or T_{VIS}.[56] Outdoor measurements showed a 22.1 °C temperature reduction relative to a PDMS-coated glass reference. Zhou et al.[370] proposed a transparent delignified-bamboo/epoxy glazing that integrates a PMMA-protected AgNW low-emissivity face ($\varepsilon_{LWIR} = 0.3$) opposite a high-emissivity epoxy face ($\varepsilon_{LWIR} = 0.95$) delivering high transmittance ($T_{lum} = 80\%$) and, in Singapore building-energy simulations, up to ∼89% annual energy savings relative to commercial low-e glass. Richards et al. demonstrated a transparent, self-cleaning polymeric photonic metamaterial based on PDMS micropyramids with $T_{VIS} \sim 95\%$ and ∼0.98 emissivity in 8−13 μm, yielding a theoretical cooling power of ∼97 $W{\cdot}m^{-2}$ and ∼6 °C subambient cooling under humid outdoor conditions in Karlsruhe, highlighting practical potential for passive building cooling and energy reduction.[136]

Compared with static RC windows that provide cooling only, dynamically tunable smart windows are more effective for improving whole-building annual efficiency because they enable high-performance thermal management across diverse climates and weather conditions. Long et al. reported a VO_2-based smart window[308] (Figure 11f). The device comprises a VO_2 thin film, a transparent PMMA spacer, and a glass substrate coated with ITO on both sides, forming a Fabry−Perot cavity. VO_2 serves as the NIR modulation layer, while PMMA and ITO act as MIR-transparent and MIR-opaque layers. Leveraging the VO_2 phase transition and F−P resonance, the window dynamically tunes the T_{sol} and ε_{LWIR} with $\Delta T_{sol} = 9.3\%$ and $\Delta\varepsilon_{LWIR} = 0.4$. Relative to a "static-optimal-emissivity" window, it yields up to 115.9 $MJ{\cdot}m^{-2}{\cdot}yr^{-1}$ savings in heating and cooling source energy over a full year. Using commercial low-e glass as the baseline, whole-building simulations report up to 324.6 $MJ{\cdot}m^{-2}{\cdot}yr^{-1}$ annual energy savings and superior performance across climate zones

https://doi.org/10.1021/acsami.6c00074
ACS Appl. Mater. Interfaces 2026, 18, 21363−21423

(Figure 11g). In a related thermochromic advance, Long et al. also demonstrated a smart window composed of glass/ITO low-e layers and an hydroxypropyl cellulose (HPC) hydrogel encapsulated in polyethylene.[371] Outdoor tests show a ∼5.4 °C reduction in summer relative to clear glass. Building-energy modeling indicates ∼37.4% annual HVAC reduction in Singapore, ∼18.8% reduction during the heating season in Beijing, and ∼9.2−19.1% total annual energy savings for large office buildings across multiple cities. Despite the promising thermal regulation performance, hydrogel-based smart windows face nontrivial outdoor durability challenges, which directly affect long-term optical stability and practical scalability. Hydrogel-based smart windows face four dominant outdoor durability risks. Dehydration and moisture migration can cause shrinkage and state drift, and commonly reported approaches include device-level encapsulation and edge sealing, as well as hygroscopic modification through hygroscopic functional groups or salt systems.[372,373] UV and oxidative aging may induce chain scission, yellowing, and network embrittlement, and mitigation approaches include incorporating UV-shielding nanoparticles to enhance UV absorption or scattering.[374] Thermal cycling fatigue can trigger microcracks and reduce state stability, and common strategies include network reinforcement and device-level encapsulation.[375] Freeze−thaw and overheating can cause irreversible degradation, and organo-hydrogel designs using low-volatility solvents such as glycerol have been reported to improve freezing and drying tolerance.[376] These approaches are typically accompanied by constraints including interfacial reflection and sealing reliability, salt crystallization or ion migration, increased process complexity, and viscosity or processability changes.

Apart from thermochromics, Cao et al. introduced a triband electrochromic smart window consisting of quartz/ITO/WO_3/VO_2/solid electrolyte/ITO/PE (Figure 11h).[377] The device enables independent control of visible and NIR transmittance and establishes ε_{LWIR} outside and low ε_{LWIR} inside. Simulations show up to ∼596.7 MJ·m^{-2} annual heating plus cooling savings versus commercial low-e glass across many climate zones, and for Shanghai the HVAC energy use is reduced by ∼23.9% compared with clear glass (Figure 11i,j).

From the perspectives of system integration and commercialization, static RC roofs and walls have already matured into replicable product lines and engineering pathways in cooling-dominated climates, reflecting comparatively high readiness.[378,379] Static RC glazing has undergone outdoor trials and whole-building energy simulations at multiple sites, yet large-scale market adoption has not emerged. Dynamically tunable roofs/walls and smart windows exhibit year-round energy savings in laboratory but overall remain in an engineering scale-up phase. The key bottlenecks fall into two areas (Figure 11k). 1. Deployment and industrialization constraints persist: long payback periods, poor weatherability, antisoiling and robust cycling[380] require rigorous qualification; achieving low-cost, large-area manufacturing with high uniformity and yield remains challenging; compatibility with existing roofing, wall, as well as city-scale aesthetic requirements, limits its applications. 2. Evaluation and standards are insufficient: the translation from material-level temperature reduction to building-level energy savings is not well-defined as the performance is highly sensitive to convection, humidity and cloudy weather, as well as mounting details and sensor placement.

Collectively, these considerations suggest a pragmatic development pathway. In cooling-dominated regions, prioritize scaling static RC roofs and walls while completing weathering, fire certifications, and life-cycle carbon footprint assessment. In midlatitude regions with pronounced seasonality, dynamically tunable building envelopes and smart windows should be developed with large modulation in both solar (0.25−2.5 μm) and MIR (2.5−25 μm) bands. In parallel, shift evaluation from short-term temperature modulation to hourly loads and annual whole-building energy simulation under transient outdoor conditions. On the technological side, cost-effective and environmentally friendly materials together with scalable and compatible process are the keys to lab to fab transfer.

Assessing deployment readiness for radiative cooling building envelopes and smart windows hinges on manufacturability, durability, and climate-specific constraints. Static opaque RC envelopes are relatively scalable because they can use low-cost solution processing such as brush coating.[368,369] By contrast, dynamically tunable smart windows are limited by expensive active materials such as VO_2 and WO_3 and by complex multilayer deposition and integration.[308,377] In real environments, performance is challenged by UV exposure and soiling, and hydrogel-based systems additionally face dehydration and freezing, with reported mitigation routes including robust cementitious binders, hygroscopic salt doping, and UV-shielding nanoparticles.[164,369,372,373,375,376,381] A key barrier for opaque envelopes is winter overcooling in midlatitudes, motivating temperature-adaptive radiative coatings.[307,312] For glazing, maintaining daylighting while enabling NIR modulation and tailored MIR behavior often requires multilayer asymmetric stacks of roughly four to seven functional layers.[56,377] Overall maturity differs markedly: static opaque roofs are closest to deployment, static RC glazing is moving through field testing, and dynamically tunable smart windows remain in engineering scale-up.

5.2. Vehicles and Enclosed Spaces

Hyunkyu Kwak, Do Hyeon Kim, and Young Min Song

Thermal regulation technologies in enclosures are essential for ensuring thermal comfort of human lives and durability of electronic devices. The ideal temperature range where humans experience thermal comfort is typically known as 22−26 °C.[382] In addition, various electronic devices (e.g., smartphones, laptops, and electric vehicles) can effectively operate from 20 to 40 °C due to the ideal operating temperature range for Li-ion batteries.[383] However, during summer, the enclosure temperature can rise extremely higher than that range without any cooling source. For instance, the indoor temperature of a vehicle parked under direct sunlight can even reach ∼90 °C in summer,[384] causing a risk of heat-related illnesses and ∼degradation of device performance.[385] Moreover in winter, the indoor temperature of buildings can drop to near 0 °C or even lower,[386] inducing hypertension-related and respiratory disease, depression, and anxiety.[387] In general, HVAC systems can provide thermal comfort in enclosures but require a significant amount of energy for operation. According to the previous report, the energy used for thermal regulation accounts for ∼20% of building energy consumption, and if this trend continues, it is predicted to increase to 50% by 2050.[388] Such energy demands lead to serious environmental problems such as greenhouse gas emissions and an acceleration of global warming. To realize energy-efficient thermal regulation in enclosures, passive radiative cooling/heating has been explored in various ways. A common method for passive radiative cooling to mitigate the overheating issues is applying radiative coolers to

https://doi.org/10.1021/acsami.6c00074
ACS Appl. Mater. Interfaces 2026, 18, 21363−21423

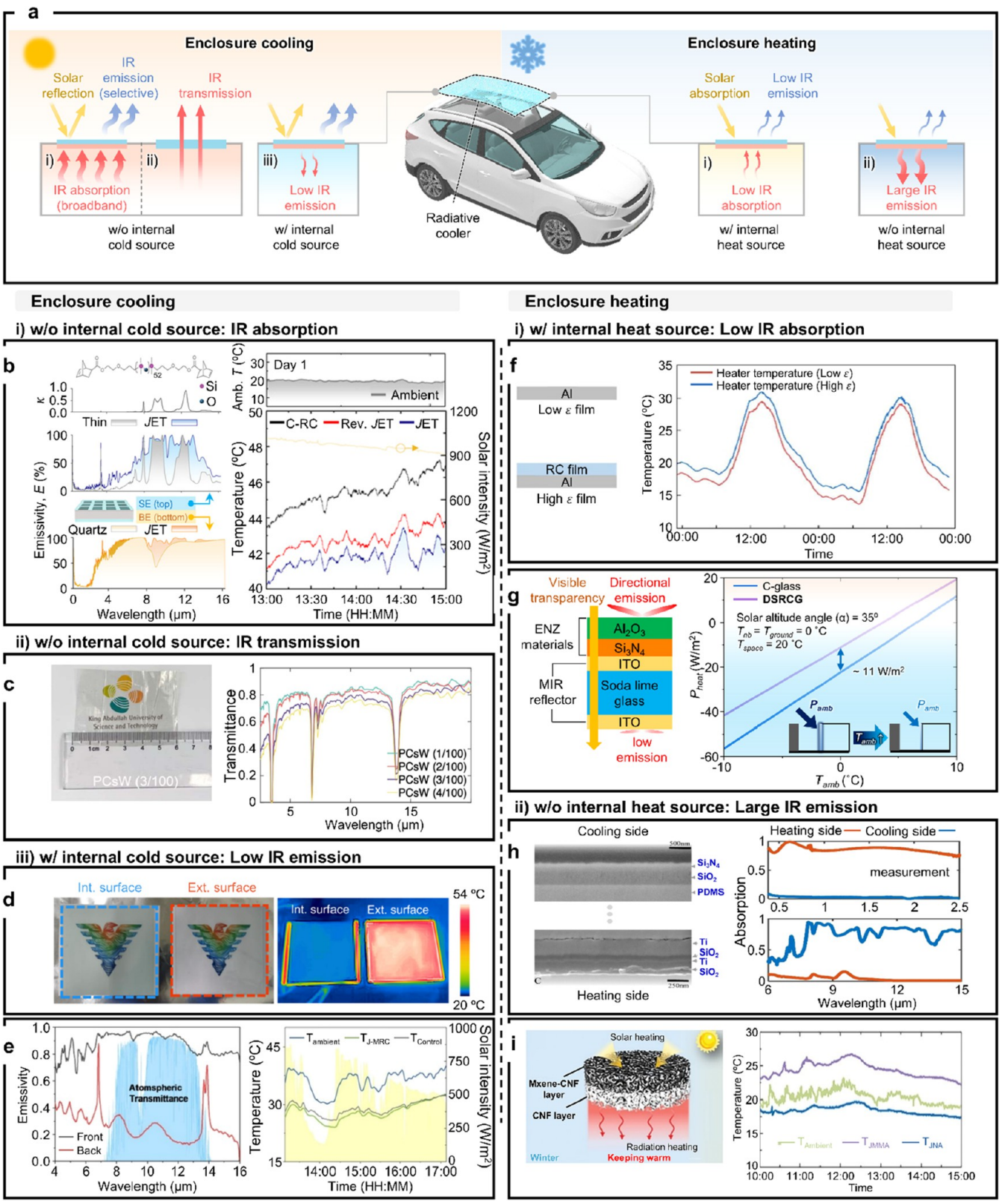

Figure 12. Thermal management methods for enclosures. (a) Schematic illustration of desirable thermal management methods under each condition. (b−e) Radiative coolers applicable for enclosure cooling. (b) The emissivity spectra of *Janus* emitter (JET) and the enclosure temperature measurement result of radiative objects. Adapted with permission from ref 405. Copyright 2020 AAAS. (c) The photograph of polyethylene (PE) film infused with cesium tungsten oxide ($Cs_{0.33}WO_3$) nanoparticles (PCsW cover) and MIR transmittance spectra depending on $Cs_{0.33}WO_3$ nanoparticles to PE weight ratio. Adapted with permission from ref 411. Copyright 2025 Elsevier. (d) The photograph and IR image of a pattern covered by interior (Int.) and exterior (Ext.) surface of enhanced color-preserving radiative cooling (ECRC) strategy. Adapted with permission from ref 262. Available under CC BY 4.0 license. (e) The IR emissivity spectra of the radiative cooling film with *Janus* optical properties (*J*-MRC) and the result of the enclosure temperature measurement. Adapted with permission from ref 415. Available under CC BY 4.0 license. (f-i) Thermal regulators applicable for

https://doi.org/10.1021/acsami.6c00074
ACS Appl. Mater. Interfaces 2026, 18, 21363−21423

Figure 12. continued

enclosure heating. (f) The schematics of the low-emissivity (low ε) and high-emissivity (high ε) films and the measured temperatures of the heaters in the experimental setups. Adapted with permission from ref 416. Copyright 2023 Elsevier. (g) The schematic of dual-sided radiative cooling glass (DSRCG) structure and the calculated power transferred to the enclosure (P_{heat}) under winter urban conditions. Adapted with permission from ref 417. Available under CC BY 4.0 license. (h) The structure and the absorption spectra of the *Janus* multilayer. Adapted with permission from ref 418. Copyright 2021 American Chemical Society. (i) The schematic of *Janus* structured MXene-nanofibrils aerogel (JMNA) and the result of enclosure temperature measurement. Adapted with permission from ref 419. Copyright 2023 John Wiley and Sons.

the outer surfaces (e.g., wall, roof, and window) of enclosures, including vehicles,[47,389−391] buildings,[164,313,392,393] greenhouses,[394−396] and spacecraft.[144] Meanwhile, several groups have developed solar absorbers with minimal IR emission to provide enclosure heating in winter or at nighttime.[313,397,398] For year-round thermal regulation, recent works also have proposed radiative coolers for adaptive thermal control, whose optical properties can be properly adjusted (i.e., solar absorptivity and IR emissivity) in response to surrounding temperatures.[334,371,399]

Specifically, the enclosure temperature is strongly affected by the temperature and optical properties of the inner surface.[400] In particular, the desired IR emission property of the inner surface for efficient enclosure cooling depends on the relations between the indoor and outdoor temperatures of the enclosure and its surfaces. Additionally, the impact of the inner surface becomes more important under several practical conditions, such as a limited sky-view factor (SVF) (e.g., urban areas)[401,402] and a high convective heat transfer coefficient (i.e., windy conditions).[403] Under these cases, the enclosure cooling performance can be further enhanced by incorporating inner-surface IR control, rather than utilizing a single-sided emitter alone. In summertime, the enclosure is typically cooler than the outer surface, and low wall thermal resistance causes heat conduction into the enclosure, hindering temperature regulation.[404] In this case, the inner surface exhibiting a low emissivity is suitable for minimizing heat radiation into the enclosure. Accordingly, this section highlights the suitable IR emission properties of the inner surface required for ideal thermal regulation under various conditions, along with the notable strategies to achieve these properties. Figure 12a summarizes the desirable IR emission properties of the inner surface depending on the presence of internal cold and heat sources. Without an internal cold source (e.g., air conditioner and water chiller), a significant amount of heat can be accumulated in the enclosure, remarkably increasing the enclosure temperature. This is because the windows and films of enclosures transmit the incoming solar radiation, while the windows and inner walls are opaque to outgoing IR emission from interior objects. Such heat accumulation can be mitigated by designing the inner surface to (i) absorb IR emission from the enclosure or (ii) transmit the emission directly to the outdoors. However, if the enclosure is cooled by an internal cold source, these strategies may instead induce unwanted IR emission from the comparably hot inner surface to the enclosure. This phenomenon can degrade the cooling performance as well as increase cooling energy consumption. Thus, (iii) minimizing the IR emissivity of the inner surface can suppress undesirable heat emission to the enclosure, facilitating the enclosure temperature control. Similarly, tailoring the emission properties of the inner surface can also improve enclosure heating performance. When an internal heat source is operating, the enclosure temperature becomes sufficiently higher than the cold ambient. Thus, (i) minimizing heat absorption to the inner surface prevents heat loss of the enclosure. On the other hand, without an internal heat source, the enclosure can be cooled to a temperature similar to the ambient. Therefore, (ii) designing the inner surfaces to exhibit high IR emissivity promotes heat supply to the enclosure, raising its temperature.

As shown in Figure 12b, Heo et al. proposed a *Janus* emitter (*J*ET) whose bottom side absorbs heat from the enclosure within a broadband IR range while the top side selectively emits heat within the AW.[405] The broadband emission of the bottom side was accomplished by integrating PDMS and quartz layers. On the other hand, the selective emission of the top side was realized via spoof surface plasmon polariton (sSPP) resonance induced by the Ag−PDMS layer on the micropatterned quartz substrate. Under direct sunlight, the enclosure temperature of the experimental setup with the *J*ET was ∼4 and ∼1 °C cooler than the reverse-*J*ET (Rev. *J*ET) and conventional radiative cooler (C-RC), respectively. The experimental result indicates that the strategy of drawing heat from an enclosure can be an effective way to cool a comparably hot enclosure. Moreover, lowering the thermal resistance of emitters could be a promising strategy to further facilitate heat transfer to the outdoor environment and enhance the enclosure cooling performance.[406−410]

For greenhouses, the cover is required to allow high transmission in photosynthetically active radiation (PAR; 0.4−0.7 μm) for sufficient plant growth. The cover should also prevent solar-induced overheating by minimizing near-infrared (NIR; 0.7−2.5 μm) transmission. In addition, especially when highly emissive objects such as soil and leaves are present inside, a film with high IR transmittance can improve enclosure cooling.[411,412] Tian et al. recently suggested a solution for passive greenhouse cooling by combining a spectrally selective cover (PCsW cover) with a cellulose ground mulch (Figure 12c).[412] The PCsW cover is composed of polyethylene (PE) film infused with cesium tungsten oxide ($Cs_{0.33}WO_3$) nanoparticles. The PE film exhibits high solar transmittance (>90%) while $Cs_{0.33}WO_3$ nanoparticles provide NIR absorption property induced by the small polaron effect.[413] Therefore, the PCsW cover effectively blocks unnecessary incoming near-infrared sunlight and prevents excessive solar heating. Especially, the PCsW cover with a $Cs_{0.33}WO_3$ weight ratio of 3/100 (3%) maintains its PAR transmittance at 73%, while its NIR transmittance decreases to 50%. Considering that the PAR transmittance of ∼70% is regarded as a sufficient value for seedling growth,[414] the PCsW cover is expected to transmit enough PAR to sustain plant growth. On the other hand, the cover maintains a high MIR transmittance (0.73), facilitating efficient heat dissipation by transmitting the IR emission from the cellulose ground mulch, which features a high MIR emissivity (0.92). Although the solar reflectivity of the cellulose mulch (0.93) is similar to that of the aluminized mulch (0.89), the integration of the PCsW cover with the cellulose mulch showed a maximum enclosure temperature reduction of 14.7 °C, compared to the integration of a sunshine board with an aluminized mulch. Since the PCsW cover has ∼0.72 higher MIR

https://doi.org/10.1021/acsami.6c00074
ACS Appl. Mater. Interfaces 2026, 18, 21363−21423

transmittance compared to the aluminized mulch, the result confirms that transmitting IR emission from interior objects can be an advantageous strategy for passive greenhouse cooling.

As previously mentioned, the enclosures can maintain cool conditions by operating cooling systems such as air conditioners during summer. In this case, reducing the IR emission from the inner surface provides a beneficial approach for enclosure temperature control. Zhu et al. designed an enhanced color-preserving radiative cooling (ECRC) strategy to lower the cooling energy consumption of an actively temperature-regulated enclosure (Figure 12d).[262] Both the exterior (Ext.) and interior (Int.) surfaces of the ECRC strategy utilize visibly transparent materials to preserve the aesthetics of buildings. Simultaneously, their contrasting MIR emission properties maximize enclosure cooling performance. The Ext. surface, composed of 30 layers of TiO_2 and SiO_2, exhibits high MIR emissivity (0.88). On the other hand, the Int. surface employs an ITO film as a radiant barrier, featuring a low MIR emissivity (0.21) and minimizing the heat emission to the enclosure. With an internal thermoelectric cooler, the enclosure temperature of the roof with ECRC was 9.6 and 3.6 °C lower than those of the bare roof and the roof with only a hot mirror (i.e., with only the Ext. surface of the ECRC), respectively. Furthermore, the roof with ECRC reduced the cooling power consumption by up to 63% compared to the bare roof at a fixed enclosure temperature of ∼26 °C. In 2024, Yang et al.[415] fabricated a radiative cooling film with *Janus* optical properties (*J*-MRC) (Figure 12e) and confirmed its enclosure cooling performance. The outer surface of *J*-MRC comprises a nano-PE film and a hot-pressed PEO film (HP-PEO), exhibiting strong emissions within the broadband MIR range. Meanwhile, the inner surface consists of a nano-PE film with low MIR emissivity and an AgNWs layer that thermally isolates the inner and outer surfaces. Specifically, when ∼100 g of ice is installed as an internal cold source, the chamber with *J*-MRC was able to cool the enclosure temperature maximally 1.4 °C lower than that of the control group (outer surface of *J*-MRC). Such works indicate that the method involving a low-emissivity inner surface can be practical for cooling and energy saving in actively temperature-regulated enclosures.

Employing an inner surface with a low IR emissivity can also be advantageous for enclosure heating cases, especially when an internal heat source keeps the enclosure warm. The low-emissivity inner surface absorbs less heat from the enclosure compared with conventional building materials, thus reducing the heating demand of enclosures. Zhao et al. demonstrated the applicability of low-emissivity inner surface for minimizing heat loss of enclosures (Figure 12f).[416] They simply fabricated a low-emissivity (low ε) film with Al foil and a high-emissivity (high ε) film by depositing a polyethylene terephthalate (PET) layer onto Al foil. With an internal heater applied in the setup, the average nighttime heater temperature in the low ε case was 1.8 °C higher than that in the high ε case. In addition, the simulated heat loss of Beijing buildings in the low ε case showed a 33.2% reduction compared to that in the high ε case. Similarly, Kwak et al. designed dual-sided radiative cooling glass (DSRCG) incorporating a low-emissivity inner surface composed of an ITO layer (Figure 12g).[417] Under simulated winter urban conditions, the calculated power transferred from the glass to the enclosure (P_{heat}) of the DSRCG was ∼11 W m^{-2} higher than that of the soda-lime glass (C-glass). Moreover, the difference in P_{heat} between the two glasses increased as the ambient temperature (T_{amb}) dropped. These encouraging results demonstrate the possibility of a low-emissivity inner surface for maintaining mild enclosure temperatures under cold outdoor conditions.

As mentioned already, when no internal heat source is operating, the enclosure temperature can decrease closely to cold ambient. To realize enclosure heating for such conditions, several studies have integrated solar absorbers to the outer surface and transferred the absorbed heat into the enclosure via inner surfaces with high IR emissivity. Wang et al. proposed an applicable method by fabricating a *Janus* multilayer including both heating and cooling sides (Figure 12h).[418] Enclosure heating can be achieved by orienting the heating and cooling sides as outer and inner surfaces, respectively. The cooling side, composed of Si_3N_4, SiO_2, PDMS, and an Ag layer, exhibits broadband IR emission and low solar absorption. Meanwhile, Ti and SiO_2 were integrated as the heating side to reduce IR absorptivity (i.e., emissivity) and increase solar absorptivity. As a result, the cooling side features solar and IR absorptivity of 0.04 and 0.66, respectively, whereas the heating side has corresponding values of 0.87 and 0.05. Another approach developed by Yang et al. is *Janus* structured MXene-nanofibrils aerogel (JMNA) featuring an asymmetric design (Figure 12i).[419] The outer MXene-CNF layer strongly absorbs sunlight and converts it into thermal energy while minimizing IR emission and heat loss. The generated heat is then transferred to the enclosure via the inner porous CNF layer with high IR emissivity. As a result, the enclosure temperature of the chamber with JMNA was ∼6 and ∼4 °C higher than those of the chamber with CNF aerogel (JNA) and ambient, respectively. The measurement results indicate that JMNA enables efficient heat transfer from the heated outer surface to the enclosure through the emissive inner surface.

Enclosure thermal regulation based on passive radiative cooling can facilitate enclosure temperature control as well as reduce cooling and heating energy consumption. Nevertheless, the studies applying radiative coolers to vehicles,[47,389−391,405] greenhouses,[394−396,411,412] and spacecraft[144,399] remain relatively unexplored compared to building applications.[164,262,313,334,392,393,397,398,415−419] In this section, several promising strategies for enclosure thermal regulation under various internal and external conditions are provided. These strategies present the potential of radiative cooling for broader applications in enclosure thermal regulation.

Manufacturing and cost drivers are important considerations for practical deployment. To reduce the production cost of emitters and facilitate large-scale production, it is essential to utilize cost-effective fabrication methods. The processes such as electrophoretic deposition of multilayer structures,[420] phase transition method for porous structure,[421] and electrospinning to form fiber membrane[231] are promising technologies to reduce fabrication cost. Notably, the roll-to-roll method[52] and paint-like facile fabrication[78] can offer production methods for large-scale surface coatings of outdoor structure exteriors.

Reliability and lifetime in real environments are also critical for real-world applications. The emitters should exhibit sufficient outdoor durability for applications in buildings or vehicles. Especially, the emitters are required to maintain their original structure and optical properties (e.g., high solar reflectance and infrared emissivity) under continuous UV exposure, weathering induced by rain or wind, and temperature cycling. In this context, hydrophobic coatings like 1*H*,1*H*,2*H*,2*H*-Perfluorodecyltriethoxysilane,[422] aluminum oxide nanoparticles,[423] and a mixture of (heptadecafluoro-1,1,2,2-tetrahydrodecyl) trichlorosilane and hexane[28] can

https://doi.org/10.1021/acsami.6c00074
ACS Appl. Mater. Interfaces 2026, 18, 21363−21423

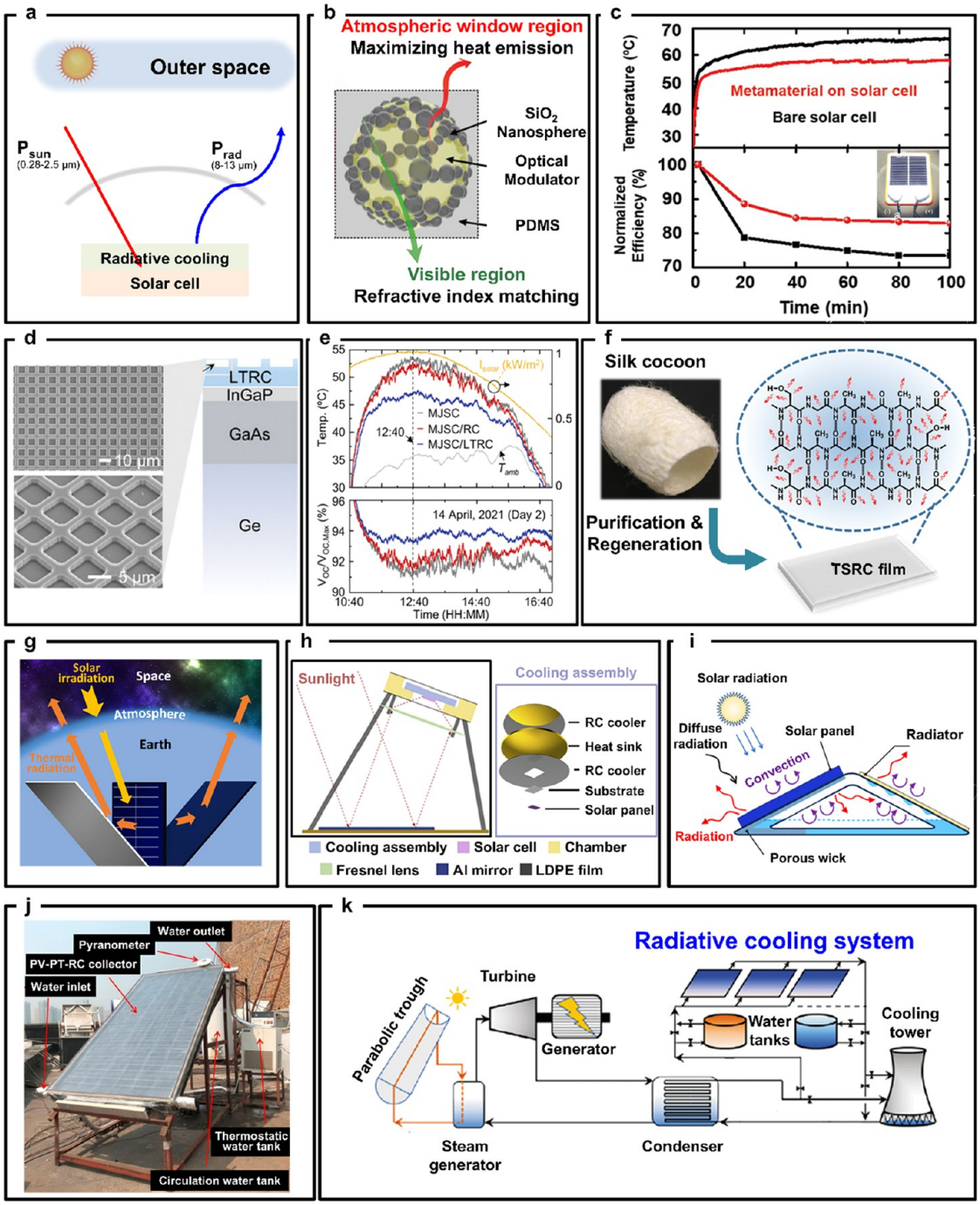

Figure 13. Various efforts to apply RC technology to high-performance solar energy systems. (a) Schematic diagram for the integration of RC and solar cells. Reproduced from ref 428. Available under a CC-BY 4.0 license. Copyright 2024 The Author(s). (b) Schematic illustration of the working principle and (c) RC performance of visibly clear RC metamaterials. Reproduced with permission from ref 34. Copyright 2021 Wiley-VCH. (d) Schematic diagram of multijunction solar cells with micrograting structures for light trapping and RC, and (e) their performance of outdoor field tests. Reproduced with permission from ref 444. Copyright 2021 Wiley-VCH. (f) Schematic illustration of the transformation of opaque cocoons into a transparent silk fibroin RC (TSRC) film. Reproduced with permission from ref 445. Copyright 2023 Wiley-VCH. (g) Schematic illustration of the working principle of v-PV system, which combines a V-shaped aluminum mirror and a vertical PV system. Reproduced from ref 280. Available under a CC-BY 4.0 license. Copyright 2024 Authors. (h) Schematic illustration of reverse concentrating PV panel for double-sided RC. Reproduced with permission from ref 352. Copyright 2020 Elsevier. (i) Schematic illustration of loop heat pipe integrated RC solar panel. Reproduced with permission from ref 446. Copyright 2024 Elsevier. (j) Photograph of a practical-scale photovoltaic/thermal collector installation. Reproduced with permission from ref 432. Copyright 2018 Elsevier. (k) Schematic diagram of a RC integrated solar thermal power plant. Reproduced from ref 434. Available under a CC-BY 4.0 license. Copyright 2022 The Author(s).

prevent emitters from rainwater erosion. Moreover, trimethylchlorosilane-modified inorganic SiO_2[424] and mixed Al_2O_3 and TiO_2 nanoparticles[423] can offer UV resistance to the emitters.

Application-specific barriers and representative solution pathways should also be considered. In particular, the high thermal resistance in the Janus emitter concept can hinder heat

https://doi.org/10.1021/acsami.6c00074
ACS Appl. Mater. Interfaces 2026, 18, 21363−21423

removal from the enclosure and degrade enclosure cooling performance. Several research groups reduced the thermal resistance of emitters by incorporating thermally conductive materials such as hexagonal boron nitride (h-BN) nanoplates,[406] nickel−titanium spring,[407] graphene,[409,410] or diamane nanosheets.[408] These strategies can further facilitate heat removal from the enclosure and enhance the cooling performance.

In terms of deployment maturity, the reliability of thermal regulation performance and outdoor durability of the emitters have been validated at the laboratory scale. The manufacturing methods that enable scalable production have also been introduced by several research groups. Nevertheless, the cost-effective materials still need to be further explored, and emitters' compatibility with conventional building materials should be demonstrated for building and vehicle applications.

5.3. High-Performance Solar Energy System

Jung Bin Yang and Dong Rip Kim

Solar energy has emerged as one of the most promising energy sources to meet the growing global demand for environmentally friendly and renewable power generation.[425−427] Considerable research has been conducted to improve the efficiency and performance of solar energy systems, including (concentrating) solar panels,[34,280,428,429] the photovoltaic/thermal collector (PV−PT) systems,[430−432] and concentrating solar thermal power (CSP).[433−435] However, these systems face a common challenge: elevated operating temperatures caused by solar radiation absorption, which reduces energy conversion efficiency.[425,426,434,436] Active cooling technologies, such as forced air cooling and liquid cooling, can effectively lower device temperature but require additional energy input, increasing operational costs and maintenance burdens.[280,425] Passive cooling methods, such as natural convection cooling,[437,438] integrated heat sinks,[439,440] and phase change materials,[441] have been extensively studied. RC is emerging as a promising passive thermal management strategy for high-performance solar energy systems. RC works by directly emitting thermal radiation into cold outer space through the atmospheric transparency window (with a wavelength range of 8 to 13 μm), thereby significantly reducing the device temperature without additional energy input. This environmentally friendly and cost-effective approach offers significant potential for sustainable solar power generation. In this section, we present research on applying RC technology to solar energy systems. Specifically, we discuss integration strategies, system-level efficiency improvements, limitations, and future outlook.

Despite various efforts to improve RC performance, most RC materials have adopted opaque designs, such as white or silver coatings, which limit direct application to solar panels.[40] For integration with solar modules, RC materials must combine high transparency in the visible wavelengths of solar spectrum with strong emissivity in the MIR range (Figure 13a).[428] To meet these criteria, researchers have explored strategies such as refractive index matching,[34,131] multilayer architectures,[56,442] and silica photonic crystal structures.[40,147,443] For example, Lee et al.[34] successfully fabricated an RC metamaterial using PDMS, SiO_2, and *n*-hexadecane, which have similar refractive indices and low extinction coefficients in the visible wavelength (Figure 13b). *n*-hexadecane infiltrated the micropores of the SiO_2 aerogel, acting as an optical modulator, resulting in excellent photonic cooling performance while remaining transparent. In addition, the high flexibility and scalability of the PDMS substrate further enhance its applicability to solar cells. To verify the performance change due to RC of a solar cell, a commercial Si solar cell (efficiency 10.35%, open-circuit voltage 3.65 V, short-circuit current density 27.69 mA/cm^2) was subjected to light soaking using an AM 1.5G solar simulator as shown in Figure 13c. The metamaterial-covered solar cell suppressed the temperature increase by about 8.5 °C during 100 min of light absorption compared to the control cell, showing about 1.5 times lower degradation (The normalized efficiency decrease of the metamaterial-covered solar cell was 17%, while that of the control solar cell was 26%). Heo et al.[444] analyzed the effectiveness of radiative coolers integrated with various types of solar cells and demonstrated that multijunction solar cells (MJSC, InGaP/GaAs/Ge) benefited most from RC due to their higher temperature-efficiency sensitivity. They designed and fabricated a light-trapping radiative cooler (LTRC) using micrograting of quartz and integrated it into MJSC as shown in Figure 13d. As a result, the MJSC/LTRC exhibited a near-unity thermal emission in the long-wave infrared region, enhancing solar energy gain across the solar spectrum. Outdoor field tests (solar irradiation of ∼900 W m^{-2}) experimentally demonstrated that the MJSC/LTRC effectively suppressed the temperature increase of the cell by ∼6.1 °C, while enhancing photon absorption due to the light trapping effect and minimizing open-circuit voltage degradation (2% increase of $V_{OC}/V_{OC,max}$ compared to the control sample) as shown in Figure 13e. Chen et al.[445] developed a transparent silk radiative cooling (TSRC) film and applied it to the solar panel. During the purification/regeneration process of silk (*Bombyx mori*), the fibrous morphology was transformed and the secondary structure of silk fibroin protein was disrupted to improve transparency in visible wavelengths, while securing high broadband emissivity in the MIR region by maintaining the molecular structure of the backbone and side chains (Figure 13f). Sericin, which adversely affected adhesion to substrate, was removed during the purification process, resulting in effective adhesion to commercial poly-Si solar panels. The performance of the TSRC-coated solar panels was investigated in an outdoor environment of ∼900 W m^{-2}. The steady-state temperature of the TSRC film-coated solar panel (61 °C) was 14 °C lower than that of the bare panel (75 °C). This improved the open circuit voltage of the solar panel from 5.7 V (Bare) to 6.0 V (TSRC film-coated), resulting in a 7% improvement in solar cell efficiency of the TSRC film-coated solar panel (9.52%) compared to the bare one (8.91%).

In addition, RC can be implemented through indirect cooling designs.[280,352,431] In typical monofacial PV modules, deploying RC onto the rear-side of PV modules can be ineffective because the temperature difference between the backside and the ground is small, reducing net radiative heat flux. For example, when the temperature of the PV module (assumed to be a blackbody) is 323 K, the net radiative heat flux using a 300 K ground heat sink was about 60% of the heat flux using a zenith heat sink.[280] To solve this problem, Fang et al.[280] proposed a V-shaped PV (v-PV) system combining a vertical PV module with aluminum mirrors to reflect and radiate rear-side emissions to the sky (Figure 13g). They optimized the angle between the panel and the mirror through simulations to improve the solar irradiance and RC efficiency (modified v-PV). Outdoor test (Thuwal, Saudi Arabia, on Nov. 13, 2022) showed that the modified v-PV increased average irradiance by ∼15% (1065 W m^{-2}) and maximum power output by ∼17% (5.77 W) compared to the control (modified h-PV, 929 W m^{-2} and 4.94 W). They also predicted that their proposed design would have a lower

https://doi.org/10.1021/acsami.6c00074
ACS Appl. Mater. Interfaces 2026, 18, 21363−21423

degradation rate (reduction of 0.043%/year) and LCOE (levelized cost of energy) of 0.3411 USD/kWh (13% reduced compared to the bare one) by lowering the temperature and increasing the power output. Wang et al.[352] integrated a heat sink on the rear of a concentrating photovoltaic (CPV) cell and applied soda-lime glass radiative coolers to both the front and back surfaces (Figure 13h). They also used aluminum reflectors to reverse the CPV panel so that the back side faced the zenith, which enabled double-sided RC. They verified the cooling performance with and without the radiative cooler through outdoor tests (direct normal irradiance of 1019 W m^{-2}). As a result, they confirmed that the presence of the cooler resulted in a temperature of up to 36 °C lower than that without it, which led to a significant increase (27%) in the open-circuit voltage. Hamdan et al.[446] combined RC with a loop heat pipe (LHP) system (Figure 13i), transferring heat from the sun-facing surface to a shaded RC surface through the LHP, and the radiative cooler then dissipates the heat load to the sky. They numerically verified that their proposed LHP RC system can reduce the maximum temperature by more than 10 °C (weather for June 1, 2022 in Sharjah, United Arab Emirates) and improve the electrical efficiency by 4.6% compared to the control (without LHP and radiator), and such a system can achieve an annual energy saving of 8.7 kWh/m^2.

Meanwhile, in addition to solar panels, various solar energy systems require various cooling loads. In this regard, RC is one of the attractive strategies for achieving high-efficiency solar energy systems using passive methods.[431−435] PV−PT is a system that can simultaneously produce thermal and electrical energy by converting solar energy into usable forms, which draws much attention for its high overall efficiency and dual function by extracting the excess heat of PV modules.[430] Specifically, the integration of RC can further highlight the advantages of PV−PT systems by adding a night-time cooling function. They can not only generate electricity, but also provide hot water, cooling, and heating, which is attractive in building energy management.[430] Hu et al.[432] designed and fabricated a practical-scale PV−PT-RC collector (total area 1.12 m^2 with 72 monocrystalline silicon solar cells) and systematically analyzed its electricity generation, heating, and cooling performance through outdoor experiments (Figure 13j). Their experimental results showed that the electrical efficiency of the PV-PT-RC collector in daily system mode was 9.69 — 11.7%, the RC power on a clear night was 72 W m^{-2}, and the total cooling energy gain of the PV−PT-RC system was reported to be 2.9 MJ in night-time operation. In CSP plants, wet cooling is widely used to condense steam and maintain high turbine power conversion efficiency, but water scarcity limits its application in arid, high-irradiance regions.[434,435] In one innovative approach, Ali et al.[434] integrated RC into the precooling to reduce the cooling load on the cooling tower of the CSP system (Figure 13k). Specifically, using the Mojave Solar Project's CSP solar plant (280 MW) as a reference power generation and the National Solar Irradiance Database (NSRDB) weather data of 3000 locations in the contiguous U.S, the performance of an RC-integrated CSP plant was numerically analyzed. As a result, they confirmed that for the southwestern U.S. region, a suggested RC-integrated CSP system could save 65 to 85% of water compared to the conventional system. However, they found that the evaluated cost of this technology is $55 to 110 per kW, which was significantly higher than that of conventional alternatives. Therefore, further investigation is needed to explore high-performance and low-cost RC technologies that can reduce this cost. Zeyghami et al.[433] proposed the integration of RC to an air-cooled CSP plant to reduce its cooling load. The RC system was added between the air cooling and the main compressor both in the simple and recompression supercritical carbon dioxide (CO_2) cycle, thereby further reducing the fluid temperature entering the compressor. This allowed the RC system to decrease the cooling load, improving overall cycle performance. Consequently, for the recompression supercritical CO_2 cycle operating at a maximum temperature of 550 °C, the net output power increased by 7.5%, when using 18.26 m^2/kW_e of RC.

Despite the progress in RC integration strategies for high-performance solar energy systems, several challenges remain for future research. First, large-scale system-level integrated performance analysis through outdoor experiments is necessary. Existing studies, with a few exceptions,[432] have been limited to the cell level.[34,280,445] In addition, comprehensive outdoor field tests under real-world conditions are necessary to verify the performance enhancement of RC, since high humidity can significantly degrade RC performance and cloudy days can adversely affect the performance of solar energy systems.[426] Therefore, comparing performance under various outdoor conditions will provide valuable insights into practical application considerations. From this perspective, large-scale application of RC technology and performance verification through outdoor experiments will increase the feasibility of its practical application in high-performance solar energy systems. Second, the development of novel materials and manufacturing that achieve high RC performance at lower costs is necessary. While numerous studies have demonstrated high-performance RC properties, reports that also consider cost are limited.[426,427] Despite its high performance of RC, cost remains a major obstacle to its practical application. Therefore, significant progress in cost reduction can make RC technology an attractive option for solar energy devices. Furthermore, research is needed on the manufacturing side for applying those materials to complex geometries or large-area applications. In summary, high-performance RC research that considers cost, materials, and applicability (manufacturing) is necessary. Finally, durability research is essential. All solar energy systems are operating outdoors, suggesting the necessity of long-term durability tests under various climatic conditions, such as UV-induced degradation, thermal cycling-induced aging, dust accumulation-induced performance degradation, and corrosion. Addressing these challenges through large-scale outdoor tests, low-cost material development, and durability studies will be key to realizing the full potential of RC in advancing global renewable energy goals.

From a deployment perspective, several additional practical considerations should also be noted. Manufacturing and cost drivers are important considerations for PV-related RC integration. The main cost drivers of direct PV integration are the integration of transparent RC layers with simultaneous high solar transmittance and strong MIR emissivity,[34,428,444,445] whereas indirect RC-PV/CPV systems shift cost toward auxiliary devices such as mirrors, heat sinks, loop heat pipes, and cooling towers.[280,352,434,446] Reliability and lifetime in real environments are also critical, as all target systems operate outdoors. Their lifetime will depend on resistance to UV exposure, thermal cycling, humidity, dust/soiling, corrosion, and retention of optical selectivity over time.[426,427] At the same time, several application-specific barriers remain. The main barriers are the transparency-cooling trade-off in front-side PV integration, limited sky access for conventional rear-side PV

https://doi.org/10.1021/acsami.6c00074
ACS Appl. Mater. Interfaces 2026, 18, 21363−21423

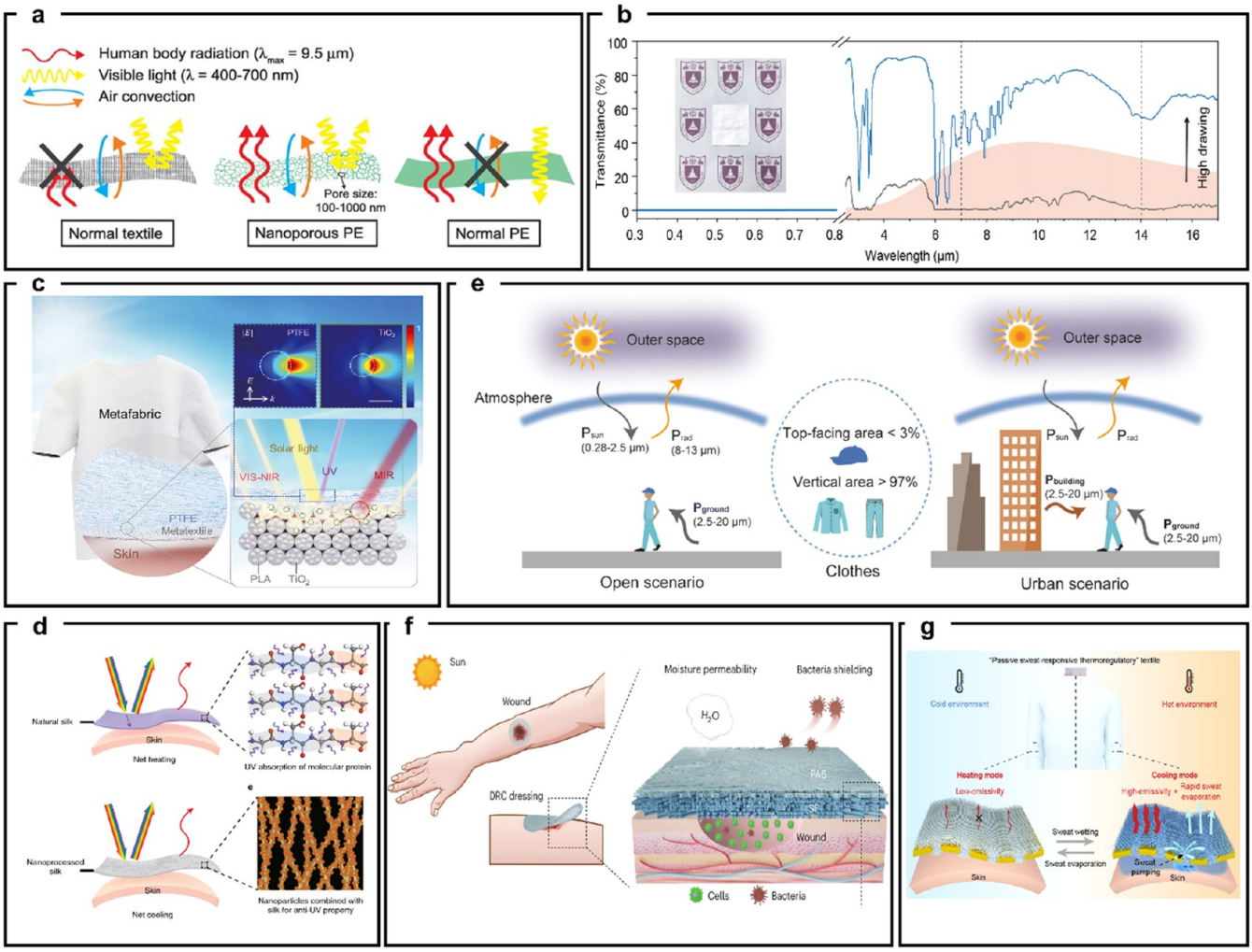

Figure 14. Radiative cooling applications for personal thermal management. (a) Schematics of comparison between nanoPE, normal PE, and cotton. Reproduced with permission from ref 176. Copyright 2016 The American Association for the Advancement of Science. (b) The total transmittance of infrared and visible light for the IRT-PA6 textiles (blue curves) and the IR transmittance of drop-casting films (gray curves) that are obtained from the volatilization of spinning solution. Reproduced from ref 456. Available under a CC-BY license. Copyright 2025 The Author(s). (c) Schematic of a metafabric for daytime radiative cooling. Adapted with permission from ref 457. Copyright 2021 The American Association for the Advancement of Science. (d) Subambient daytime radiative cooling design for nanoprocessed silk. Reproduced from ref 458. Available under a CC-BY license. Copyright 2021 The Author(s). (e) Schematic of wearable fabrics in an open scenario and an urban scenario. Adapted with permission from ref 239. Copyright 2024 The American Association for the Advancement of Science. (f) Schematic of the structural design of daytime RC dressings for local wound environment management under sunlight. Reproduced from ref 459. Available under a CC-BY license. Copyright 2024 The Author(s). (g) The PSRT textile maintains human body temperature stability in a dynamic environment with temperature variations. Reproduced from ref 460. Copyright 2025 American Chemical Society.

layouts, the scarcity of system-level outdoor validation, and the high added cost of RC hardware in CSP integration.[280,426,432−434] Several representative solution pathways have been proposed to address these barriers. Promising pathways include transparent index-matched or structured RC coatings for front-side integration,[34] V-shaped or double-sided sky-coupled PV/CPV configurations,[280] remote radiators assisted by loop heat pipes,[446] and hybrid PV−PT/CSP design where RC is integrated at the subsystem level.[432,434] In terms of deployment maturity, transparent PV coating/film integration remains at the prototype or limited outdoor validation stage, while microstructure-assisted PV/CPV systems are still at the early engineering prototype stage. By comparison, PV−PT-RC has reached practical-scale field demonstration, whereas CSP integration remains largely at the simulation and technoeconomic stage.

5.4. Personal Thermal Management

Yansu Hou and Jia Zhu

Over the past few decades, greenhouse gas emissions have accelerated global warming.[447,448] High summer temperatures pose a serious threat to human health, leading to heat-induced illnesses and related complications such as heatstroke, skin cancer, and cardiovascular diseases.[449] Therefore, the development of personal cooling technologies has become particularly important and has attracted extensive attention and research efforts in recent years. Specifically, radiative cooling fabrics optimize the thermal exchange pathways between the human body, the fabric, and the environment through optical regulation of emission, transmission, and reflection, thereby achieving passive all-day cooling without any additional energy input.[450]

Existing radiative cooling fabrics can be classified into three distinct types based on their thermal management mechanisms.

https://doi.org/10.1021/acsami.6c00074
ACS Appl. Mater. Interfaces 2026, 18, 21363−21423

The first type is transmission-type fabrics, which optimize high infrared transmission within the human body's radiation bands, establishing efficient thermal radiation channels to enhance heat dissipation from the body surface, primarily for indoor environments.[176,451] The second type is emission-type fabrics, which enhance solar reflectivity to inhibit external heat gain, along with high mid-infrared emissivity to promote radiative cooling.[452,453] The third type is selective emission/transmissive fabric that employs precise spectral design to achieve high emissivity in atmospheric windows and high transmissivity in nonatmospheric windows, thereby enabling all-weather thermal comfort regulation.[205,454,455]

Due to the fundamental differences between indoor and outdoor application scenarios, extensive research has been devoted to exploring this distinction. Indoor cooling fabrics depend on high infrared radiation transmission to reduce heat buildup and promote cooling. Intrinsic MIR transparent materials are not common, Hsu et al. demonstrated nanoporous polyethylene (nanoPE) as a novel candidate material for human body radiative cooling (Figure 14a). Nanoscale pores ranging from 50 to 1000 nm are embedded in the polyethylene film, strongly scattering visible light while the mismatch with the mid-infrared wavelength range ensures that mid-infrared transparency is not compromised.[176] Furthermore, Chen et al. designed an infrared-transparent PA6 textile based on the common polymer nylon-6 (PA6) by employing a high-stretching process combined with rapid solvent evaporation (Figure 14b). By altering the chain conformation and crystalline structure, the molecular vibrations (infrared absorption) of PA6 in the infrared region were significantly weakened. Meanwhile, this process reduced the fiber diameter to the nanoscale and minimized infrared reflection. Compared with cotton textiles, the PA6 fabric achieved a cooling effect of up to 2.1 °C, corresponding to an estimated ∼20% reduction in the energy required for indoor cooling.[456]

By contrast, outdoor radiative cooling fabrics require high solar reflectance and the ability to strongly absorb and emit human heat. By minimizing the solar heat absorption and maximizing the emission of heat from the human body to the environment, textiles can cool the human body even under intense solar exposure. Zeng et al. developed a metamaterial fabric with a hierarchical morphological structure, achieving a high solar reflectance of 92.4% in the solar spectrum and a high emissivity of 94.5% within the atmospheric window (Figure 14c).[457] Through scalable industrial textile manufacturing routes, the fabric maintains efficient radiative cooling performance while exhibiting excellent mechanical strength, water resistance, and breathability required for commercial apparel. Practical application tests demonstrated that when covered with this metamaterial fabric, the human body temperature was approximately 4.8 °C lower than when covered with commercial cotton fabric. To achieve the radiative cooling effect, nanostructures are required. Unlike the design of the aforementioned metamaterial cooling fabric, Zhu et al. realized daytime radiative cooling below ambient temperature based on textiles (silk) (Figure 14d). Due to the inherent absorption of proteins in the ultraviolet region, natural silk is prevented from achieving net cooling under sunlight. This study explored the nanoprocessing of silk through molecular bonding design and scalable coupling agent-assisted dip-coating methods. Results demonstrated that the simulated skin temperature covered with nanoprocessed silk was reduced by 8 °C compared to natural silk. Furthermore, the study provided a comprehensive evaluation of the impacts of nanoprocessing on human comfort. The nanoprocessed silk exhibited a water vapor transmission rate (WVTR) comparable to that of natural silk and commercial Tyvek, even slightly outperforming cotton. Regarding the wicking rate-a critical measure of moisture transport-the silk maintained excellent hydrophilicity with a wicking distance of 10 mm, significantly superior to the hydrophobic Tyvek, which lacks wicking capability entirely. Additionally, by employing a single-sided screen-printing technique to coat nanoparticles exclusively on the outer surface of the fabric, the inherent "cool-to-touch" tactile property of silk was preserved, while ensuring robust durability to endure 50 cycles of accelerated washing and drying. This research further provides a customizable strategy for the convenient and scalable design of natural materials.[458] Most radiative cooling textiles are often designed as broadband emitters in the entire MIR region, without considering heat from the heated ground and urban buildings. Wu et al. designed a mid-infrared spectrally selective hierarchical textile (SSHF) (Figure 14e), achieving high emission in the AW, while high reflection in the non-AW to suppress parasitic heat from the ground or buildings.[239] The rational optical design and fiber nanofabrication enable substantial cooling effects: The SSHF is 2.3 °C cooler than the broadband emitter when placed vertically and 6.2 °C cooler than the ambient temperature when placed horizontally. This spectrally selective design for vertically oriented fabrics offers an innovative solution to tacking urban heat islands.

Currently, much research is focused on developing radiative cooling textiles that can operate effectively under various environmental conditions and possess additional functionalities. Example include antimicrobial radiative cooling textiles that protect wounds under sunlight. Zhang et al. demonstrated a daytime radiative cooling dressing based on a polyamide 6/silk fibroin bilayer structure (Figure 14f), which can reduce the thermal load on skin wounds under sunlight exposure.[459] Polyamide 6 with mid-infrared transparency and silk fibroin with biocompatibility jointly endow the dressing with a high mid-infrared emissivity (about 0.94) and solar reflectance (about 0.96), thus its temperature can be about 7 °C lower than the ambient temperature under direct sunlight. Under sunlight, this dressing can accelerate the wound healing rate. Furthermore, to address the challenges posed by fluctuating temperatures, such as substantial day-to-night variations, people have developed active and passive thermal-regulating textiles. For example, a sweat-responsive thermal-regulating textile based on unidirectional moisture wicking has been developed that can regulate mid-infrared radiation and sweat evaporation while remaining wearable to achieve the widest thermal comfort range (8.3−33.0 °C) currently available in dynamic environments (Figure 14g).[460]

From a commercialization perspective, the transition of RC textiles from laboratory prototypes to commercial products hinges on scalable manufacturing and cost-effective strategies. Current research demonstrates compatibility with industrial processes through techniques like coupling agent-assisted dip-coating, single-sided screen-printing, and high-throughput fiber drawing. By utilizing low-cost polymers like PA6 or natural materials (silk, cotton, and wood), additional material overhead is minimized. Environmental reliability is a critical benchmark; for instance, nanoprocessed silk has proven to maintain its optical and cooling performance through 50 cycles of accelerated washing and drying while preserving mechanical strength and breathability. To overcome application-specific

https://doi.org/10.1021/acsami.6c00074
ACS Appl. Mater. Interfaces 2026, 18, 21363−21423

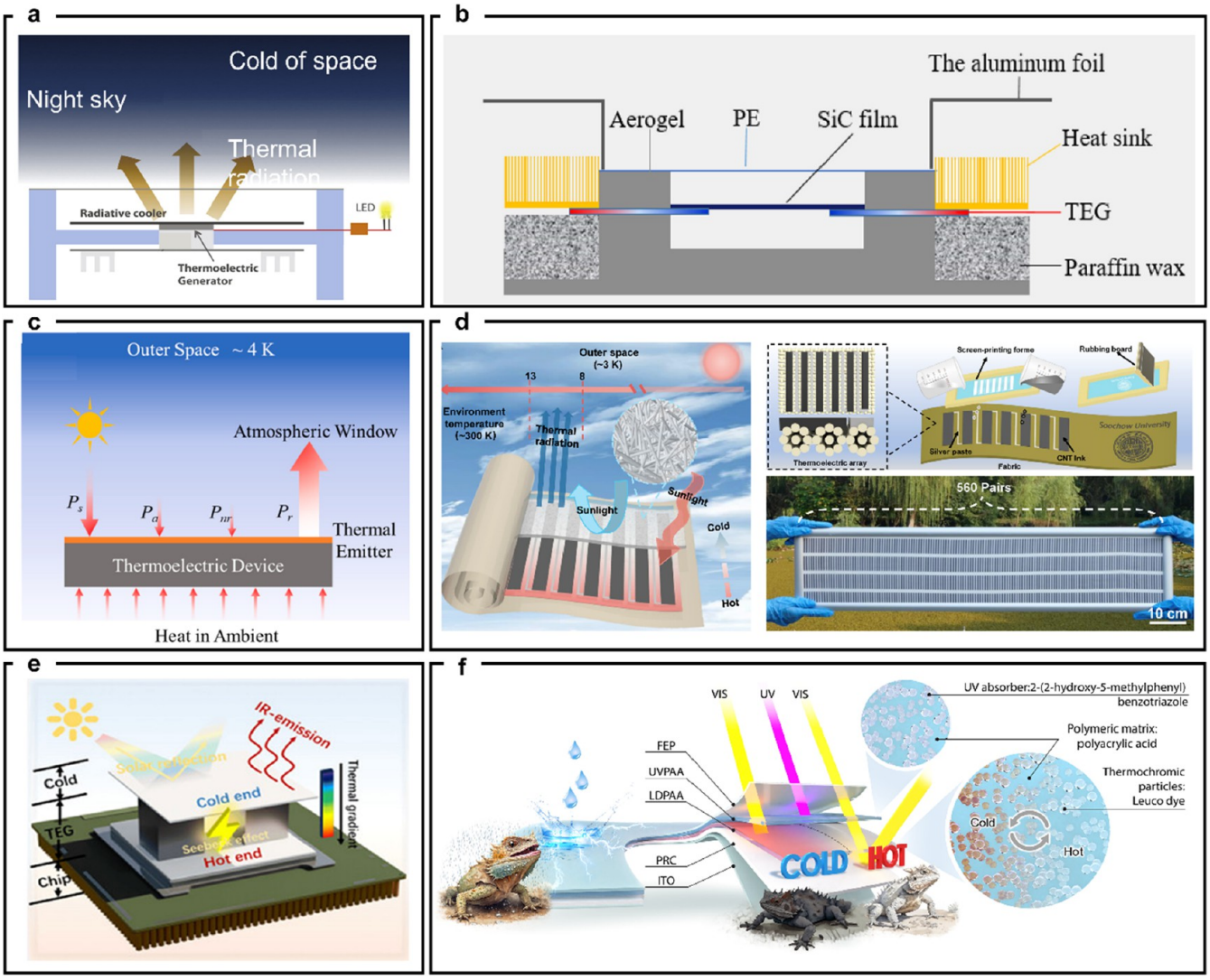

Figure 15. Radiative cooling applications for boosting electricity generation via thermoelectric systems. (a) Schematic of the nighttime thermoelectric system. Reproduced with permission from ref 347. Copyright 2019 Elsevier. (b) Main view of the structural scheme of the designed thermoelectric generator. Reproduced with permission from ref 475. Copyright 2020 Elsevier. (c) Schematic of TEG working mechanism based on radiative cooling. Reproduced with permission from ref 477. Copyright 2018 Elsevier. (d) Principle and the structures of wearable thermoelectrical device, schematic diagram of screen-printing process, and display of large-area fabric. Reproduced with permission from ref 478. Copyright 2025 The American Association for the Advancement of Science. (e) Principle and structure of B-TEG. Reproduced with permission from ref 479. Copyright 2025 John Wiley and Sons. (f) Design of bioinspired all-weather energy harvesting metafilms. Adapted with permission from ref 480. Copyright 2025 The American Association for the Advancement of Science.

barriers, such as parasitic heat from urban buildings, spectrally selective designs (e.g., SSHF) offer a solution by suppressing nonatmospheric window absorption. Furthermore, specialized solution pathways like antimicrobial bilayer dressings are expanding RC technology into healthcare. While the deployment maturity is supported by a solid theoretical foundation in material design, achieving a complete industrial value chain requires the coordinated optimization of visual aesthetics, washability, and thermal comfort to meet diverse market demands.

In summary, although radiative cooling fabrics have achieved foundational advances in material design principles that laid a solid theoretical basis, their successful commercialization still requires coordinated optimization of breathability, moisture permeability, washability, visual aesthetics, and thermal performance. Future directions will focus on advancing technological innovation in materials science, integrating multifunctional systems, broadening cross-disciplinary applications, promoting environmental sustainability, and responding to evolving market demands. In addition, sustainable cooling fabrics can contribute to the low-carbon transformation of the textile industry. Natural materials like bamboo, wood, cotton, and linen can be used to design and develop environmentally friendly cooling fabrics. By innovating materials, advancing equipment technology, and strengthening industry standards, radiative cooling fabrics are expected to evolve into products with complete industrial value chains in the future.

5.5. Electricity Generation

Yansu Hou and Bin Zhu

The current fossil fuel-dominated power sector accounts for nearly 40% of global annual energy-related CO_2 emissions.[461] The low-carbon transition of the power sector is crucial to tackling climate change and ensuring the future supply of

https://doi.org/10.1021/acsami.6c00074
ACS Appl. Mater. Interfaces 2026, 18, 21363−21423

energy.[462,463] Traditional power generation methods, mainly relying on fossil fuels and even including some renewable energy sources such as solar and wind power,[464,465] are facing severe challenges: Fossil fuel power plants account for about 30% of global carbon dioxide emissions, solar photovoltaic systems experience efficiency decline in high temperatures (for every 1 °C increase above 25 °C, efficiency drops by 0.4−0.5%),[466] and wind turbines' operation depends on unstable weather conditions.[467] To overcome these limitations, researchers are exploring innovative technologies that can enhance the sustainability and efficiency of power generation. Unlike active cooling methods that consume electricity, such as air conditioning or liquid cooling, radiative cooling utilizes the natural thermal radiation of materials to reduce heat accumulation, providing unique advantages for optimizing power generation systems.

TEGs are attractive as an environmentally clean technology for converting waste heat into electrical power through the Seebeck effect. Its advantages include minimal mechanical vibration, high scalability, and a long lifespan.[468] The output power of the TEG is directly proportional to the temperature difference between its cold and hot ends.[469] Therefore, researchers focus on methods to decrease the cold end temperature or raise the hot end temperature. However, TEG's efficiency is often limited by the temperature gradient between the hot end (exposed to waste heat) and the cold end (in contact with the ambient environment). The traditional cooling techniques involve installing air[470] or water cooling devices[471] at the cold end of the TEG, but these methods require additional energy input, which will reduce the overall efficiency of the TEG. Therefore, people are seeking a passive cooling method to increase the output power of TEGs without affecting their efficiency.[348]

In 2019, Raman et al. constructed a thermoelectric system (TES) driven by RC.[347] By radiating heat to the cold cosmic space, the radiative cooling technology maintains the cold end of the TEG below the ambient temperature (Figure 15a). The hot end is heated by the surrounding air. The temperature difference generates usable electrical energy. Their experimental findings demonstrated that the device could generate 25 mW m^{-2} of power. This demonstration shows that the device can directly power a light-emitting diode, effectively generating light from the darkness of space itself. Subsequently, many researchers also proposed many TEGs driven by radiative cooling.[472−474] However, due to the lack of strict spectral regulation of the cold end coating, the operation of the equipment was limited to nighttime. Xia et al. were the first to propose a fully weather-protected continuous electricity and water production device (Figure 15b).[475] During the day, it absorbs solar radiation, and at night, it utilizes radiation cooling. The top part acts as the hot end during the day and the cold end at night. The opposite temperature gradient during the day and night causes the reversal of the output of the positive and negative electrodes. With the rapid development of micronano manufacturing technology, various kinds of photonic devices emerged,[149,234,476] which have strict selectivity for electromagnetic wave in the region of 8−13 μm but strong thermal emission, thus effectively reflecting almost all incident sunlight. Therefore, they have been developed for daytime radiative cooling. Mu et al. have developed the first prototype of TEG utilizing RC that combines the ultrathin TEG with the thermal emitter (Figure 15c).[477] The TEG-RC using SiO_2/Si_3N_4 alternating layer thermal emitters as radiative coolers (emissivity up to 80.8%). They observed maximum temperature drop of 4 K was achieved by using the thermal emitter. The output voltage of the TEG-RC reached up to 0.5 mV, and the TEG-RC exhibited a continuous average 0.18 mV output more than 24 h.

In addition to developing high-efficiency TEG prototypes based on radiative cooling, Liu et al. integrated this concept into wearable thermoelectric textiles (Figure 15d).[478] They screen-printed large-area carbon nanotube (CNT)-based thermoelectric arrays onto conventional fabrics, which were then combined with electrospun poly(vinylidene fluoride-*co*-hexafluoropropylene) (PVDF-HFP) films serving as radiative modulation layers. The resulting thermoelectric fabric (0.2 m^2) achieves a substantial ΔT of 37 K under a solar intensity of ∼800 W per square meter, yielding a peak power density of 0.20 milliwatt per square meter. Shi et al. integrated a fully biomass-based radiative cooling material into a thermoelectric device with a gradient structure (Figure 15e).[479] The device achieved a power density of 7.61 W m^{-2} under a temperature difference of ΔT = 30 °C by harvesting waste heat from electronic components. This study provides an innovative approach for carbon-neutral cooling and sustainable energy applications.

The different demands for radiative cooling during day and night provide a direction for exploring how to achieve the switching of the spectral characteristics of cooling materials with the lowest energy consumption or in a completely passive manner. Optimizing the geometric characteristics of the thermoelectric system (especially the areas of the radiative cooler, solar absorber, and thermoelectric generator (TEG), and integrating the passive thermoelectric system with photovoltaic (PV), frictional nanogenerators (collecting energy from raindrops),[27] are potential strategies for achieving stable and continuous power generation. For instance, Chen et al. designed a biomimetic metafilm that achieved sustainable power supply in unfavorable weather (Figure 15f).[480]

The commercial viability of radiative cooling-driven thermoelectric systems (RC-TESs) depends on transitioning from idealized laboratory setups to robust, scalable manufacturing. Current progress in large-area screen-printing of thermoelectric arrays and the use of biomass-based materials offers a clear pathway to reduce cost drivers while ensuring environmental sustainability. However, reliability and lifetime in real-world environments remain significant hurdles. Performance is often degraded by application-specific barriers, such as high thermal contact resistance at the device-skin interface in wearable textiles and restricted radiative view factors in dense urban building envelopes. To bridge this gap, representative solution pathways involve developing advanced, flexible interface materials with high thermal conductivity to minimize impedance, and optimizing device orientation to maximize sky exposure. Furthermore, the deployment maturity of RC-TES can be significantly enhanced by synergistic integration with other energy harvesters, such as PV for daytime boost or triboelectric nanogenerators for rainy conditions, evolving into all-weather power units. Such maintenance-free, self-powered systems are approaching readiness for critical low-power applications, including remote IoT sensors and implantable medical devices.

Overall, the autonomous energy-harvesting capability of RC-TESs positions them as transformative power solutions for low-energy electronics, ranging from wireless IoT sensors to wearable health monitors.[481,482] To bridge the gap between laboratory-scale demonstrations and practical deployment, future research must shift from maximizing theoretical efficiency to mitigating the dominant loss terms inherent in real-world

https://doi.org/10.1021/acsami.6c00074
ACS Appl. Mater. Interfaces 2026, 18, 21363−21423

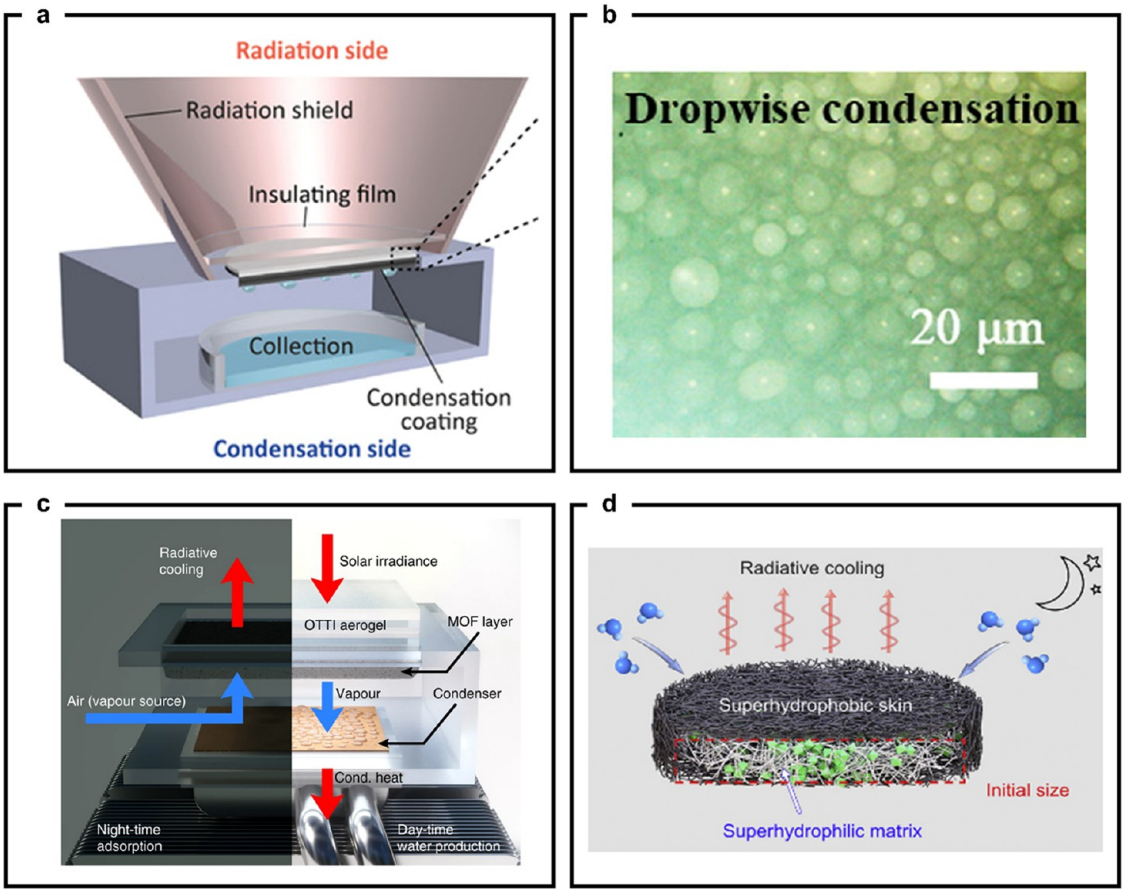

Figure 16. Radiative cooling applications for atmospheric water harvesting via direct condensation or adsorption assistance. (a) Working principle of the RCon with separated radiation and condensation side, where the radiation shield can substantially improve the dew harvesting potential. Reproduced with permission from ref 35. Available under a CC BY-NC 4.0 license. Copyright 2021 The Author(s). (b) An image of dropwise vapor condensation on a hydrophilic-superhydrophobic patterned surface (F-SiO2/TiO2, 1:3 w/w). Reproduced with permission from ref 491. Available under a CC BY-NC-ND 4.0 license. Copyright 2021 The Author(s). (c) Working principle of the RC-assisted SAWH system using MOF-801 with night-time adsorption (left half) and day-time solar-assisted water production (right half), where the OTTI aerogel suppresses convective heat loss from the solar absorber. Reproduced from ref 495. Available under a CC BY 4.0 license. Copyright 2018 The Author(s). (d) Schematic of the bioinspired heterogeneous wetting AWH device with fibrous skin for night-time RC-assisted sorption. Reproduced with permission from ref 496. Available under a CC BY-NC-ND 4.0 license. Copyright 2022 The Author(s).

environments. In particular, the thermal contact resistance at the device-source interface is a critical bottleneck for the conformal integration of wearable textiles, while the radiative view factor often limits performance due to complex installation geometries. Addressing these challenges requires a synergistic approach: developing advanced interface materials with high thermal conductivity and mechanical flexibility to minimize impedance, while simultaneously optimizing device orientation and spectral selectivity (8−13 μm) to maximize sky exposure. By integrating these adaptive configurations with complementary energy-harvesting modalities, such as photovoltaics or triboelectric nanogenerators, RC-TESs can evolve into robust, all-weather power units. Such advancements will facilitate the realization of truly maintenance-free, self-powered electronics, extending their applicability to critical systems like implantable medical sensors and remote environmental nodes.

5.6. Atmospheric Water Harvesting

Shengxi Bai, Kaixin Lin, and Chi Yan Tso

With freshwater resources dwindling with population growth, urbanization and climate change, RC has emerged as a promising approach for enabling AWH. This technology offers solutions for decentralized freshwater production, particularly in water-scarce regions where freshwater transport and delivery are challenging. AWH holds great potential for alleviating water stress, given the vast amount of water vapor in the atmosphere (12,900 km^3 fresh water).[483] Among AWH methods, dew water collection stands out as more viable than cloud seeding or fogwater collection due to its cost-effectiveness and lower dependence on geographical conditions.[484]

RC can facilitate dew water collection either directly through dew-point condensation or indirectly by coupling with other AWH systems. First introduced in the late 20th century,[485] radiative condensers (RCons), as a direct method, employ a subambient cooling surface to achieve direct water condensation at the dew point. Theoretically, RCons are engineered with high solar reflectivity and strong MIR emissivity to maximize radiative condensation power. Common designs include porous polymers, metamaterials, multilayer structures or randomly distributed structures.[486] Unlike conventional RC designs that require selective infrared emission for subambient cooling, RCons leverage broadband infrared emission from 4 μm to over 13 μm. As the water vapor generated in most passive AWH systems is at or above ambient temperature, broadband infrared

https://doi.org/10.1021/acsami.6c00074
ACS Appl. Mater. Interfaces 2026, 18, 21363−21423

emission maximizes radiative heat dissipation to the atmosphere and thus enhances radiative condensation.[487]

Several RCon designs and applications have been reported in recent years. Zhou et al.[487] developed an RCon composed of a PDMS layer, a silver layer, and an aluminum plate to passively accelerate water vapor condensation. By pumping humidified air (RH = 90−95%) at ambient temperature into the condenser, the device achieved a daily water production of 0.8 mL with a surface area of 0.05 m^2 at UW−Madison in September 2017. Based on coalescence-induced water removal mechanism, Haechler et al.[35] demonstrated uninterrupted 24-h AWH by integrating thermal radiative shielding and cooling with a superhydrophobic RCon (Figure 16a). The radiative shield minimizes absorption of horizon-sourced atmospheric radiation while directing thermal emission toward low zenith angles, to optimize cooling efficiency. The system achieved a mean dew mass flux of 50 g m^{-2} h^{-1} under high humidity (RH > 90%) and moderate solar irradiation (>200 W m^{-2}) conditions during the field tests at ETH Zurich in August 2019. Apart from standalone operation, RCons can be integrated with other AWH systems, such as sorption-based AWH (SAWH) systems. SAWH systems capture water vapor from ambient air using hygroscopic sorbents, release it via heating/regeneration (desorption), then condense the vapor into liquid water. Bai et al.[488,489] demonstrated a dual single-bed SAWH system using MIL-101-Cr (HF) sorbent materials and poly(vinylidene fluoride-*co*-hexafluoropropylene) [P(VdF-HFP)] RCons for decentralized freshwater production. Such system could achieve a water condensation productivity of 678 mL m^{-2} per day during clear days in Hong Kong based on field test results.

Apart from the investigation on radiative condensation power, more research is needed on the surface wettability modification to facilitate condensate collection. Dai et al.[490] proposed that multifunctional coatings favorable for both droplet nucleation and removal can greatly improve AWH efficiency, and demonstrated a hydrophilic directional slippery rough surface for rapid nucleation and water droplets removal. Chen et al.[491] developed a wettability and spectral selectivity engineered coating using hydrophobic SiO_2 and hydrophilic TiO_2 nanospheres for efficient water collection. This surface wettability modification enhanced dropwise collection to a maximum droplet harvesting rate of 1047 mg cm^{-2} h^{-1} (Figure 16b). Bioinspired approaches show particular promise for advancing condensate collection. By mimicking biological structures, researchers aim to achieve mesoscale droplet nucleation and condensation and enable efficient water collection at macroscales. However, this remains a significant challenge. Wang et al.[492] suggested that multidimensional bionic structure design[493] could be an effective approach, potentially promoting bionic AWH.

As an indirect method, RC can enhance dew water collection when integrated with other AWH systems. One typical example is utilizing RC to provide cooling effect during sorption process to maintain optimal RH, as the exothermic nature of moisture capture typically reduces sorption capability due to increased local temperature and decreased local RH.[494] The potential of RC in improving the sorption efficiency has been demonstrated by several studies. Kim et al.[495] developed a SAWH device using metal−organic framework (MOF)-801, employing night-time RC to lower the adsorber layer temperature and thereby increase the effective RH to facilitate water vapor uptake (Figure 16c). This approach reduced the temperature by ∼3 °C during adsorption phase, increased the RH by 5−7% near the MOF layer, and resulted in an equilibrium water uptake of 0.25 kg kg^{-1}. Similarly, Wang et al.[496] utilized the RC properties of the carbon black-doped P(VdF-HFP)/polydimethylsiloxane fibrous skin to increase the effective RH during sorption. This modification accelerated the sorption rate and increased the water uptake capacity of their composite sorbent (i.e., active carbon felt-lithium chloride) (Figure 16d). Recently, Huang et al.[497] demonstrated a passive SAWH system coupling composite hydrogel with RC and solar heating. Their field test showed that RC increased the night-time water uptake rate from 0.242 kg m^{-2} h^{-1} (using the sorbent only) to 0.310 kg m^{-2} h^{-1} (using both the sorbent and RC), representing a great performance improvement.

From an implementation perspective, industry analyses estimate the AWH market's base valuation at USD 2.8 billion in 2024, and it is expected to grow at a compound annual growth rate of 8% from 2025 to 2034.[498] Cost-effective AWH powered by RC is still under investigation. Li et al. proposed an RC fabric for AWH with an estimated annual water production cost of \$5.2/L at 60% RH and \$0.01/L at 90% RH.[499] Regarding reliability and lifetime in real environments, more attention should be paid on the optical degradation from UV thermal aging and surface soiling of RC materials. Compared with traditional AWH designs, RCon increases water collection in low RH environments and reduces system energy consumption, which offers an environmentally friendly and sustainable AWH solution.[500] However, RC performance relies on weather and climatic conditions, which limits the applications of RCon and RC-assisted sorption process. The key application-specific barriers include low specific yield and sorption kinetics mismatch, parasitic heat gains and atmospheric transmittance. Certain progress has been made regarding these barriers, such as angular shielding and enhanced spectral selectivity, continuous 24-h transmissive RC architectures. Currently, AWH by RCon and RC-assisted sorption process remains heavily constrained by complex synthesis costs, operating primarily at the pilot scale.

Overall, RC contributes to AWH via two primary mechanisms: directly by condensing water using RCons and indirectly by enhancing sorption in SAWH systems. While RC-assisted SAWH systems generally demonstrate higher specific water productivity due to the utilization of hygroscopic sorbents and larger condensation capacity, RCons offer the distinct advantage of completely passive operation under suitable weather conditions. Current limitations of RCons, particularly their relatively low water productivity and efficiency caused by insufficient RC capacity and substantial heat loss,[484,501] highlight the need for more research efforts. Future research could focus on developing advanced RCon materials with optimized radiative properties, improving condenser designs to enhance condensation efficiency and refining surface structures to maximize water collection performance. For RC-assisted SAWH systems, research priorities should include optimizing sorption efficiency through careful material selection of both RC coatings and sorbents, as well as adjusting system-level parameters tailored to specific climatic conditions. Addressing these challenges will be crucial for advancing both approaches toward practical implementation in water-scarce regions, offering sustainable solutions to global water stress.

5.7. Passive Isothermal Film

Seonggon Kim and Yong Tae Kang

Radiative coolers typically operate by reflecting solar energy in the ultraviolet, visible, and near-infrared regions during the

https://doi.org/10.1021/acsami.6c00074
ACS Appl. Mater. Interfaces 2026, 18, 21363−21423

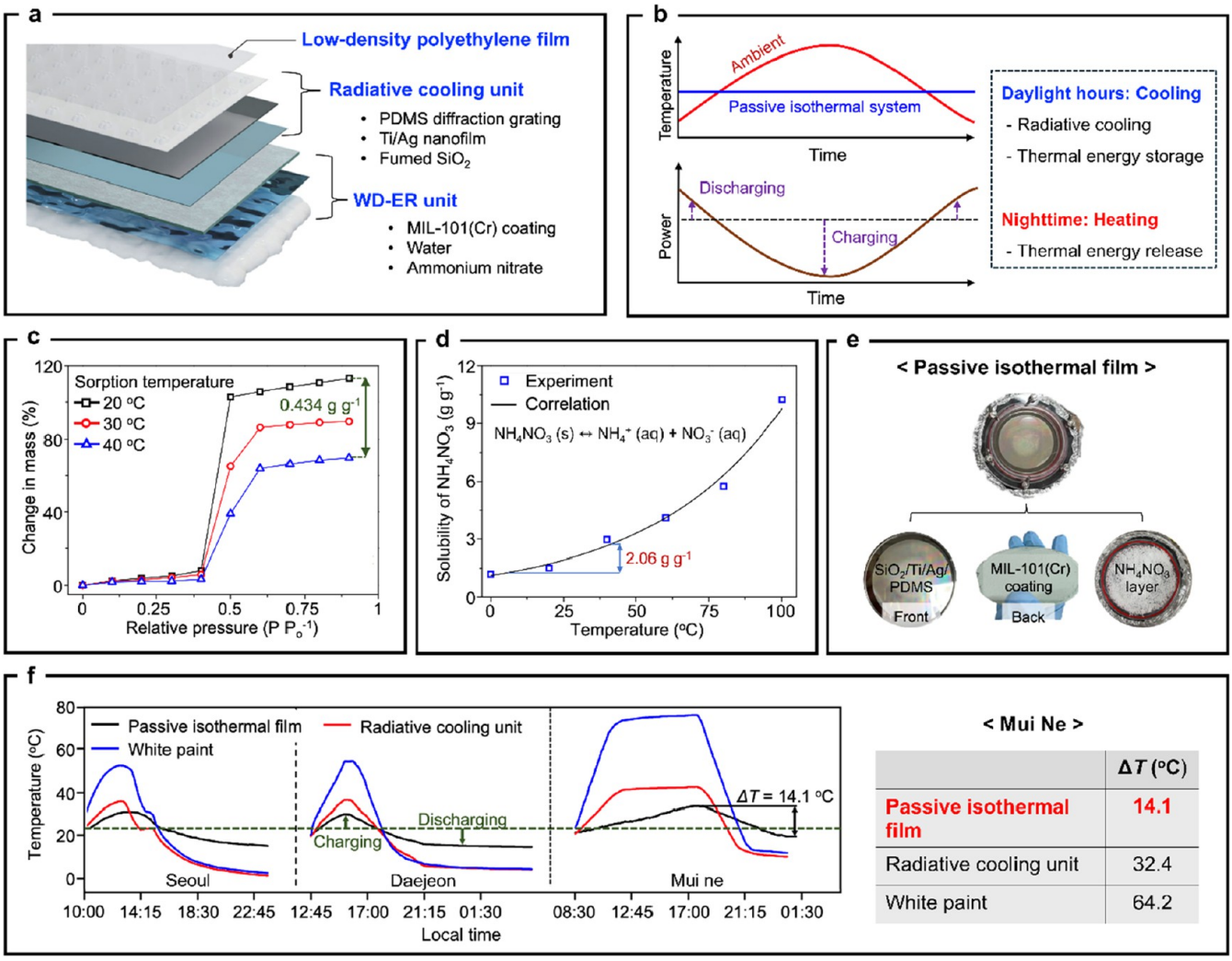

Figure 17. Radiative cooler-based passive isothermal film for arid climate applications. (a) Schematic of the system configuration, consisting of RC and water desorption-driven endothermic reaction (WD-ER) layers. (b) Idealized cooling and heating operations for maintaining an isothermal temperature of 25 °C over a full day. (c) Water adsorption isotherm of chromium(III) terephthalate metal−organic frameworks (MIL-101(Cr)). (d) Temperature-dependent solubility curve of ammonium nitrate. (e) Photographs of the passive isothermal film. (f) Temperature profile of the passive isothermal film throughout a full day. Adapted with permission from ref 502. Available under a Creative Common CC BY 4.0 License. Copyright 2024 The Author(s).

daytime while emitting thermal radiation in the mid-infrared to achieve subambient temperatures. Recent advances have enabled practical applications through cost-effective material designs such as hierarchically structured poly(methyl methacrylate),[197] polydimethylsiloxane-coated metal structures,[276] delignified wood,[150] and three-dimensional porous cellulose acetate matrices with internally deposited SiO_2.[174] However, continuous thermal emission could increase heating loads rather than provide a benefit in cold climates or during nighttime in regions with large diurnal temperature variations, which limits the applicability of radiative coolers. In response to this challenge, temperature-responsive materials capable of self-switching thermal emission have been proposed as a means of selectively enabling cooling only when needed.[307,309]

A radiative cooler-based passive isothermal film has been developed to reduce both cooling and heating energy consumption in arid climates with large diurnal temperature variations, maintaining 25 °C solely through natural processes without any external energy input,[502] as presented in Figure 17a. This film is composed of a low-density polyethylene cover, a RC unit containing PDMS with a diffraction grating and fused SiO_2/Ti/Ag sublayers, and a water desorption-driven endothermic reaction (WD-ER) unit including chromium(III) terephthalate metal−organic frameworks (MIL-101(Cr)) and ammonium nitrate.

During daylight hours as illustrated in Figure 17b, the low-density polyethylene layer minimizes forced/natural convection heat transfer through intermittent air. The PDMS diffraction grating allows solar irradiation to pass through, while the SiO_2/Ti/Ag layers reflect it to prevent overheating. The PDMS diffraction grating is designed to achieve an emissivity close to 1.0 within the temperature range of 30−60 °C (typical of daytime temperatures in arid climates). The WD-ER unit absorbs the net thermal energy input through a chain reaction involving water desorption from the MIL-101(Cr) coating layer for latent cooling and an endothermic reaction by the dissolution of ammonium nitrate in water. This process sustains indoor temperatures by utilizing the principles that the water sorption capacity of porous materials decreases as temperature increases, and the solubility of solutes rises with temperature.

https://doi.org/10.1021/acsami.6c00074
ACS Appl. Mater. Interfaces 2026, 18, 21363−21423

During nighttime, when the PDMS diffraction grating is exposed to lower outdoor temperatures than indoors, its emissivity decreases, minimizing thermal emission heat loss. Additionally, the reverse reaction in the WD-ER unit releases heat, which aids in temperature maintenance. While conventional passive RC systems focus on minimizing solar irradiation (reducing absorptivity in the ultraviolet−visible range) and enhancing thermal emission power (achieving emissivity close to 1 in the infrared spectrum), in this study, some energy input from nature is utilized to operate the WD-ER unit to store energy during daylight hours. This enables the passive isothermal system to discharge the stored energy during nighttime, which minimizes heating and cooling energy loads in arid climates by utilizing the diurnal energy balance.

Figure 17c presents the isothermal water sorption capacity of MIL-101(Cr). As the passive isothermal film operates in a moisture-containing environment, the capture capacity depending on the temperature variation is examined at a point where the relative pressure is close to 1. MIL-101(Cr) in the WD-ER unit exhibits a water sorption capacity of 1.12 g g^{-1} at 20 °C, and as the temperature rises to 40 °C, approximately 0.434 g g^{-1} of water is desorbed (This value is calculated from the chemical equilibrium state. However, the WD-ER unit operates in a quasi-steady state with a full-day cycle.). Linear regression of the isothermal water sorption capacity enables the prediction of working capacity with respect to temperature changes. The average water desorption enthalpy reaches 53 kJ mol^{-1}. Figure 17d displays the solubility of ammonium nitrate in water as a function of temperature. The dissolution enthalpy for ammonium nitrate is 28.1 kJ mol^{-1}, and its solubility can be fitted with an exponential function.

The configuration of the passive isothermal film is summarized in Figure 17e. Ammonium nitrate crystals were dispersed onto a waterproof surface, and a moisture environment was formed. A SiO_2/Ti/Ag/PDMS film coated on the back with MIL-101(Cr) was attached to the H_2O/NH_4NO_3 layer. The temperature variation of the passive isothermal film was tested throughout a full day under various climatic conditions, as presented in Figure 17f. As a result of the experiment in Seoul, the temperature of white paint increases to 52.5 °C during daylight hours and drops to 0.8 °C at night. The maximum temperature of the RC unit is 35.8 °C, which is 16.7 °C lower than that of the white paint. However, a significant heating load is still required to achieve 25 °C at night. The passive isothermal film demonstrates a reduction of 4.8 °C in the maximum daytime temperature compared to the RC unit while presenting a significant increase in nighttime temperature by 13.6 °C. The relatively large temperature difference of 17.5 °C is attributed to the difficulty of preserving equilibrium between the charging and discharging of the WD-ER unit, especially due to the relatively short daytime duration in the test region compared to nighttime.

The results from tests conducted at the White Sand Dunes in Vietnam (Mui Ne) indicate that the temperature of white paint rises to 76.0 °C during daylight hours and drops to 11.8 °C at night, resulting in a temperature difference of 64.2 °C. Although the RC unit reduces the maximum temperature to 42.5 °C, the minimum temperature at night is lower than that of the white paint due to thermal emission. The passive isothermal film significantly reduces the maximum temperature difference to 14.1 °C and generates a cooling power of −1.1 kW m^{-2} during the daytime and a heating power of 0.28 kW m^{-2} at nighttime (The cooling and heating power of the passive isothermal film was obtained by calculating the power required to maintain the temperature difference between the indoor air in the system with a white paint surface and that with the passive isothermal film). By integrating the heating and cooling power generated throughout a full day and adding the solar energy absorbed by the white paint, the diurnal energy balance is established with an error margin of 9.7%.

RC-based isothermal film hold promise as a viable passive thermal management solution, particularly for buildings in arid or high-insolation regions. When integrated into building skins such as roofs or exterior panels, these systems could contribute to heating, ventilation, and air conditioning energy savings without the need for active control.[503] Their passive operation aligns with net-zero energy building goals and off-grid applications. Future work should explore architectural integration strategies, durability under long-term environmental exposure, and compatibility with existing construction materials to assess scalability.

The passive isothermal film combines a radiative cooling unit (SiO_2/Ti/Ag/PDMS) with water desorption-driven endothermic reaction unit (MIL-101(Cr)/H_2O/NH_4NO_3). The main cost drivers are the multilayer optical coating and the use of metal−organic frameworks. In practice, scalable radiative cooling films and sorbents such as zeolites could reduce fabrication cost, while their selection can be optimized depending on the operating conditions. Regarding reliability and lifetime in real environments, the passive isothermal film was tested for multiple cycles in different regions including South Korea and Vietnam, demonstrating stable performance. Since the system is composed of stable materials, it is suitable for scale-up in real environments. However, system performance depends on local climate conditions such as diurnal temperature variation and solar intensity, and the limited flexibility of the passive isothermal film makes its application to curved surfaces difficult. To overcome these barriers, optimization based on the thermophysical properties of the materials may enable operation in a wider range of environments, while integration of small units into building envelopes may improve practical applicability. Although current demonstrations remain at the prototype level, the individual components are based on well-established materials, suggesting that, with scalable fabrication and improved durability, applications in building envelopes are feasible.

It is also essential to consider alternative materials within the WD-ER unit to improve economic feasibility. Zeolites such as 13X, 5A, 3A, Y, SAPO-34, and SSZ-13 offer lower-cost, scalable options with reasonable water sorption performance.[504] Similarly, alternative salts like NH_4Cl or KCl, could still provide useful thermal buffering effects when coupled with appropriate sorbents. Additionally, recent advances in low-cost RC designs, such as delignified wood structures or polymer-based multilayers, could be integrated to reduce fabrication complexity and material costs. These substitutions, if optimized for performance and reliability, would facilitate broader deployment in cost-sensitive or resource-limited settings.

5.8. Global- and Regional-Scale Artificial RC

Qingsong Fan, Qizhang Li, Po-Chun Hsu

Global warming is caused by the decreased atmospheric transparent window caused by anthropogenic greenhouse gas emissions. Although it is urgent to decarbonize all energy sectors and eventually reverse the CO_2 level back to the preindustrial period, human civilization may not have enough time to prevent

https://doi.org/10.1021/acsami.6c00074
ACS Appl. Mater. Interfaces 2026, 18, 21363−21423

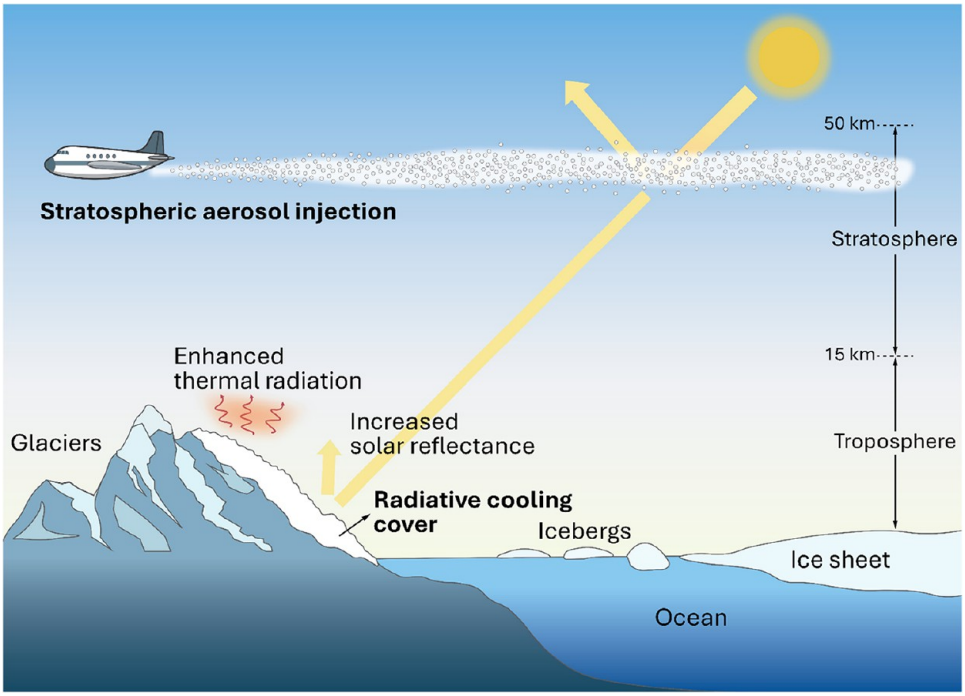

Figure 18. Schematic showing the artificial radiative cooling at the regional and global scales.

the catastrophic impact of global climate change if we only rely on decarbonization. Just like passive daytime radiative cooling is widely employed to enhance cooling without work input, there are emerging research efforts to conduct artificially enhanced radiative cooling at the regional or even global scale. Theoretically, mitigating the solar heat gain can have a more drastic effect than increasing the radiative heat loss (by restoring the atmospheric transparent window via decarbonization), making it a critical approach that warrants more scientific research and discussion. This Chapter will focus on two topics: glacier preservation and solar geoengineering (Figure 18).

5.8.1. Glacier Preservation. Glaciers, which cover approximately 10% of the Earth's land surface, hold profound geological, biological, and economic importance.[505] However, the continuous increase in greenhouse gas emissions has led to an unprecedented rate of glacial melting since the beginning of the 21st century. This has resulted in an estimated annual mass loss of 260 gigatons between 2003 and 2009.[506] Predictions indicate that by 2100, glaciers could lose approximately 26% of their 2015 mass, contributing to a mean sea-level rise of about 90 mm.[507] This projection assumes an optimiztic scenario where the global temperature increase is limited to 1.5 °C, a target that appears increasingly unlikely under current conditions.[508] The accelerated retreat of glaciers not only raises sea levels but also threatens freshwater supplies, compromises the security of infrastructure due to events like ice avalanches and glacial lake outbursts, and negatively impacts the tourism industry.[509] In recognition of the urgency, the United Nations has designated 2025 as the International Year of Glaciers' Protection.

Since the early 2000s, considerable theoretical and experimental efforts have been made to develop methods for artificially slowing the melting of snow and ice to preserve glacier mass.[510−515] Understanding the mechanisms behind these methods requires an analysis of the energy balance at the glacier surface. According to the energy balance equation:[516]

$$Q_{melt} = Q_{sens} + Q_{lat} + Q_{rad}$$

Here Q_{melt} is the net energy available for melting, Q_{sens} is the sensible heat flux from convection and conduction, which accounts for 15−20% of the net energy. Q_{lat} is the latent heat flux from phase change of water, which is often negligible as it contributes less than 10% to the energy budget. The dominant term, Q_{rad}, is the net radiation, which accounts for 75−80% of the energy driving the melting process. It is the sum of net shortwave (Q_{SW}, 0.3−2.5 μm) and longwave (Q_{LW}, 8−13 μm) radiation:[517]

$$\begin{aligned} Q_{rad} &= Q_{SW} + Q_{LW} \\ &= (1 - R_{solar})Q_{SW,in} + (Q_{LW,in} - \varepsilon_{IR}\sigma T^4) \end{aligned}$$

Here R_{solar} is the solar reflectance in the shortwave band (albedo), Q_{SW} and $Q_{LW,in}$ are the incoming radiation in the shortwave and longwave bands, respectively. ε_{IR} is the emissivity in the longwave band, σ is the Stefan−Boltzmann constant and T is the surface temperature in K.

Early glacier preservation efforts focused on increasing surface albedo. A glacier's albedo varies significantly: fresh snow exhibits a high albedo of 0.8−0.9, whereas the albedo of clean ice drops below 0.4. The accumulation of dust and debris further reduces albedo.[516,517] Therefore, artificially creating a layer of fresh snow is a simple yet effective method to enhance reflectivity. For instance, a natural summer snowfall on the Morteratsch Glacier (Switzerland) in July 2000 resulted in a net preservation of 13 cm water equivalent by the end of the melt season.[509] Similarly, an artificial snowfall experiment in the Altai region of China during summer 2018 demonstrated a 40% reduction in glacier mass loss,[518] further demonstrating the effectiveness of this method. However, this method is limited by its reliance on a substantial water source and a narrow window of favorable weather conditions for snow production.

To overcome these challenges, researchers have explored using high-albedo blankets, known as geotextiles, to cover glaciers. A 2012 experiment on the Presena Ovest Glacier (Italy)

https://doi.org/10.1021/acsami.6c00074
ACS Appl. Mater. Interfaces 2026, 18, 21363−21423

demonstrated a 69% reduction in snow and ice melt in areas covered by a nonwoven polypropylene geotextile compared to uncovered areas.[519] This success was attributed to the geotextile's high mean albedo (0.64) versus the bare ice surface (0.43). The long-term effectiveness of the geotextile for glacier protection was confirmed by 15-year study in Switzerland.[520] The result showed that coverage of glaciers using geotextiles can reduce the ice melt up to 350,000 m^3 per year, corresponding to a 59% efficiency in ice melt reduction. With their effectiveness demonstrated in field tests, geotextiles have already been commercialized and widely used in glacier protection projects. However, most currently available geotextiles are made from petroleum-based polymers such as polypropylene and polyester, raising concerns about potential environmental impacts, particularly when deployed at large scale. In addition, the solar reflectance (albedo) of these materials is only moderate, suggesting that further improvements in reflectivity could enhance their overall cooling performance and melt-reduction efficiency.

A significant advance occurred in 2014 with the demonstration of passive radiative cooling, achieving temperatures ∼5 °C below ambient even under direct sunlight.[24] This was accomplished using a multilayer photonic structure with a solar reflectance of 0.97 and strong thermal emissivity. However, the complex structure consisting of alternating nanometer-precision layers of HfO_2 and SiO_2 makes large-scale application impractical, as fabricating such a device in a cost-effective manner is highly challenging. Consequently, research has focused on developing more scalable materials with similar properties.

In 2022, Li et al. designed a hierarchical film based on cellulose acetate (CA), an abundant and eco-friendly material.[521] This film's porous structure yields a solar reflectivity of 0.974, while the vibrations of molecular bonds provide a mid-IR emissivity of 0.92. These properties result in an excellent cooling power of up to 110 W m^{-2} and enable the material to maintain a surface temperature below 0 °C for extended periods. In addition, the CA film is more hydrophobic compared to the traditional polypropylene and polyester geotextiles, which helps keep its surface clean from dust that would otherwise reduce reflectance. With its cooling performance, antisoiling properties, mechanical strength, biodegradability, and potential for scalable production, this CA film is a promising candidate for glacier protection. However, the fabrication of the CA film via electrospinning remains relatively energy-intensive and time-consuming, posing challenges for large-scale manufacturing. As a result, the current production cost is expected to be higher than that of conventional geotextiles.[517] In addition, the long-term durability and large-scale effectiveness of this material for glacier protection still require validation through field experiments. Further efforts to develop scalable and cost-effective fabrication processes will therefore be essential for its practical deployment.

The accelerated melting of glaciers demands urgent and effective intervention. Mitigation strategies have evolved from applying artificial snow to employing durable high-albedo geotextiles. The future of glacier preservation likely resides in advanced materials engineered for passive radiative cooling, which offer superior performance and environmental compatibility. Future work must focus on validating the large-scale efficacy of these novel materials and developing cost-effective manufacturing processes to enable their widespread deployment. Overcoming these hurdles will be crucial in the ongoing effort to protect Earth's vital ice reserves.

5.8.2. Solar Geoengineering. In recent decades, scientists have been discussing global-scale approaches that could rapidly stop the Earth temperature increase through solar radiation management (SRM), also known as solar geoengineering. SRM aims at cooling the Earth by reflecting a portion of incoming solar radiation back into space. Among the proposed techniques, stratospheric aerosol injection (SAI) is the most widely studied, which seeks to enhance the solar reflectivity of the upper atmosphere by introducing fine aerosol particles into the stratosphere (about 15−20 km in altitude).[522] The efficacy of SAI has been showcased in the volcanic eruption of Mount Pinatubo in 1991, which released about 20 million tons of sulfur dioxide into the stratosphere, forming reflective sulfate aerosols that cooled the global climate by ∼0.5 °C for about a year.[523] Essentially, SAI is to artificially create such volcanic effects by deliberate and controlled injection of aerosols into the stratosphere.

In the exploration of SAI, developing suitable aerosol materials is one of the major research focuses. It involves a comprehensive set of metrics spanning optical, microphysical, chemical, and environmental properties. The optical performance is mainly characterized by the single-scattering albedo (SSA), which quantifies the fraction of total extinction due to scattering rather than absorption. Materials with near-unity SSA and strong backscattering are preferred for maximizing solar reflectivity. Particle microphysics, including size distribution, coagulation, and sedimentation, govern both radiative efficiency and atmospheric residence time. Optimal particle radii of approximately 0.1−0.5 μm are predicted to maximize scattering efficiency while maintaining sufficient atmospheric lifetime.[524,525] Particles smaller than about 0.1 μm scatter solar radiation inefficiently and are prone to rapid coagulation, whereas larger ones settle faster and absorb more infrared radiation.[526−528] In addition to single-component particles, composite or coated aerosols have also been proposed to improve overall performance.[528,529] As an example, a recent study suggests that a thin high-index shell enclosing a low-density core can boost solar reflectivity, which also greatly lowers mass and settling rate, thus increasing their lifetime in stratosphere.[530] As for chemical and environmental aspects, the selected materials should minimize heterogeneous reactions and ozone impacts while remaining stable under high UV exposure, as well as exhibiting negligible toxicity or ecological disturbance after their deposition in the environment.

The leading candidate material for SAI is sulfur dioxide (SO_2) gas, which oxidizes to form sulfate aerosol droplets (H_2SO_4) in the atmosphere. Sulfate has a high solar reflectivity and, when largely distributed in the stratosphere, can significantly increase global albedo. However, sulfate aerosols provide surfaces for heterogeneous reactions that generate chlorine and bromine radicals and accelerate ozone depletion, as observed after the 1991 Mount Pinatubo eruption.[531] In addition, the non-negligible infrared radiation of sulfates can warm the stratosphere and disrupt its circulation, thereby influencing ozone distribution and global climate patterns.[532] These substantial side effects have motivated research on alternative aerosol materials, such as alumina (Al_2O_3) or calcite ($CaCO_3$). Compared with sulfates, injection of solid particles can largely avoid stratospheric heating and even counter ozone loss by neutralizing acidic compounds and suppressing chlorine radical formation.[533,534] For example, a modeling study suggests that using $CaCO_3$ particles with a radius of 275 nm can reduce stratospheric radiative heating by roughly an order of magnitude

https://doi.org/10.1021/acsami.6c00074
ACS Appl. Mater. Interfaces 2026, 18, 21363−21423

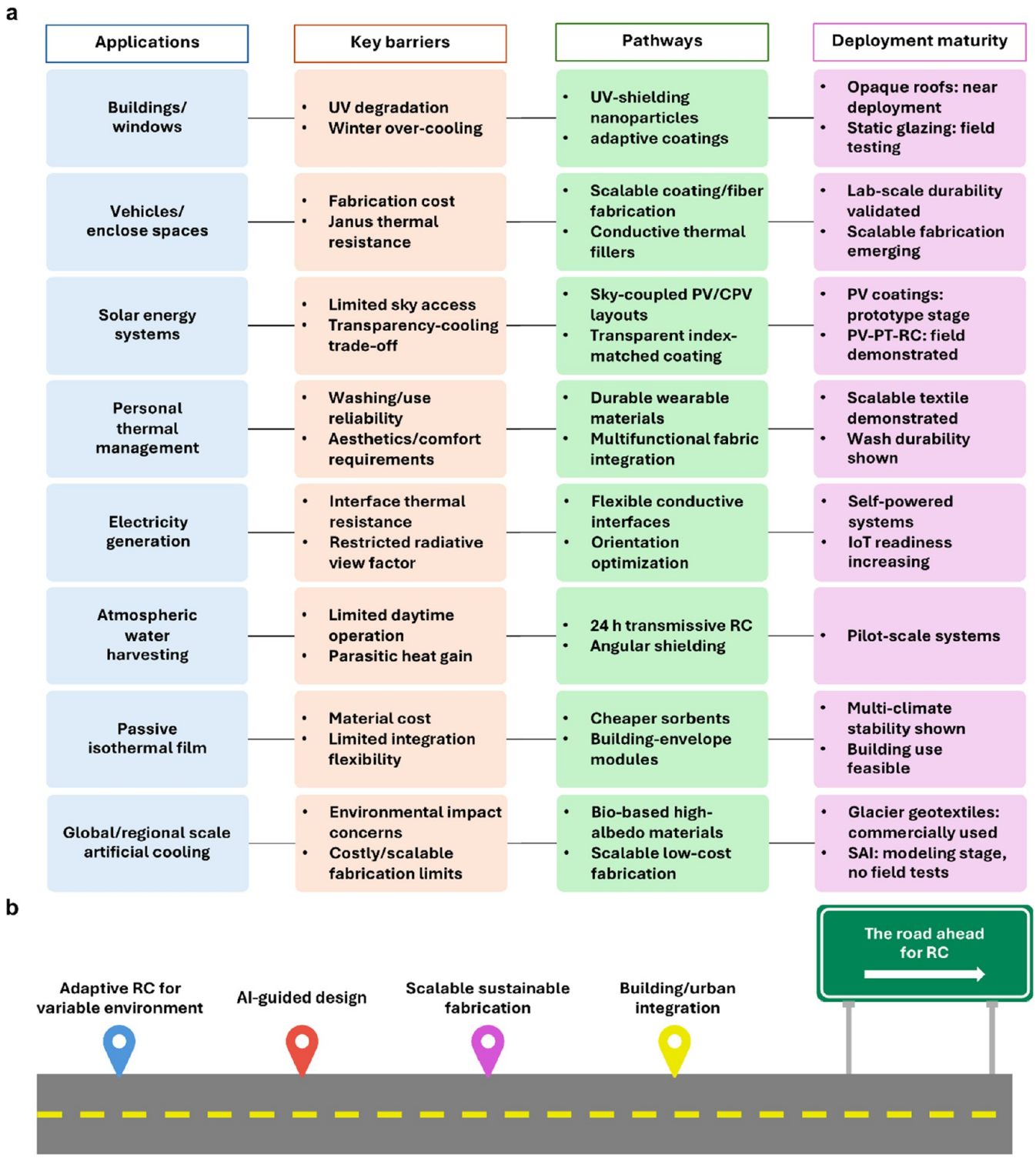

Figure 19. (a) Application-oriented roadmap of radiative cooling (RC) technologies, summarizing representative applications together with key barriers, corresponding pathways, and current deployment maturity. (b) Outlook roadmap highlighting future directions for RC.

compared with sulfate aerosols under the same radiative forcing (a benchmark for SRM performance).[534] Among various SAI materials, diamond stands out for its high refractive index and low absorption coefficient, which ensures strong solar reflection and greatly limits stratospheric heating.[532] Although dispersing million tons of diamond would be economically infeasible, it serves as a benchmark for developing more advanced material candidates of SAI implementation.

In addition to technical challenges, such as determining what (e.g., aerosol materials),[533] how (e.g., delivery methods),[535] and where (e.g., injection locations)[536] for SAI implementation, the major concern remains its potential global side effects.[532] The inevitable stratospheric heating can accelerate ozone depletion and change tropical atmospheric circulation. Moreover, SAI is expected to reduce the global mean precipitation. Historical observations after the Mt. Pinatubo eruption showed a

https://doi.org/10.1021/acsami.6c00074
ACS Appl. Mater. Interfaces 2026, 18, 21363−21423

significant decrease in land precipitation and river discharge, suggesting a potential risk for widespread drought under SAI scenarios.[537,538] Modeling studies show that many regions, especially monsoonal areas like Central India, could experience significant drying and reduced summer rainfall after SAI deployment.[532,539] It is also noteworthy that SAI does not address the root causes of global warming — greenhouse gas emissions. Without effective and sustained CO_2 mitigation, a sudden termination of SAI would trigger an unprecedentedly rapid temperature rebound, posing severe risks to ecosystems and societies.[540]

Due to significant ethical and governance concerns, the real-world implementation of SAI has remained largely stalled. For instance, the Stratospheric Controlled Perturbation Experiment (SCoPEx) proposed by Harvard researchers planned a small-scale test in Kiruna, Sweden in 2021, but the experiment was finally canceled in 2024 after opposition from environmental groups and local stakeholders.[541] As a result, no stratospheric field experiment of SAI has been conducted to date, and most research remains confined to modeling and laboratory studies. The absence of field experiments means that many practical engineering challenges and potential environmental impacts remain unverified, which is considered one of the key factors limiting the further development and evaluation of SAI technologies.

Although being greatly debated due to its potential risks, SAI is regarded as perhaps the only feasible fast track for achieving the Paris Agreement's 1.5 °C temperature increase target.[542] Climate model experiments consistently show that SAI could induce rapid global cooling within just a few years of implementation, much faster than emission-mitigation methods.[532] Indeed, SAI is not intended to replace mitigation strategies, but rather to serve as a temporary emergency approach to quickly cool the planet and potentially buy time for effective emissions cuts to be fully implemented.

6. CHALLENGES AND FUTURE OUTLOOK

Harit Keawmuang and Junsuk Rho

While RC technologies have achieved remarkable progress in recent years, important challenges still remain to be overcome in order to fully realize their potential in research innovation and practical implementation. Figure 19a summarizes the application-oriented roadmap of RC by highlighting representative applications together with their key barriers, corresponding pathways, and current deployment maturity. Building on these practical considerations, this section discusses broader challenges and future directions for advancing RC toward real-world implementation and long-term impact.

(1) The effectiveness of radiative cooling is strongly influenced by ambient factors such as humidity, cloud coverage, solar irradiance, and wind speed, which vary substantially across different regions and weather conditions. For example, high humidity can reduce cooling performance by absorbing mid-infrared radiation within the 8−13 μm transparency window.[15] Cloudy skies also suppress radiative cooling. Although clouds reduce incoming solar radiation, they simultaneously enhance atmospheric re-emission in the infrared, which weakens the overall cooling effect.[543] As a result, clear skies are generally required for radiative coolers to achieve their maximum performance. Such environmental variability highlights the need for radiative cooling strategies that remain effective across different regions and weather conditions. One promising direction to address these challenges is the development of adaptable radiative cooling systems that can dynamically tune their optical and thermal properties in response to changing environments. Such adaptive systems can respond to diverse environmental stimuli, for example, temperature-adaptive RC[222,307,317,544] and humidity-adaptive RC.[267,310,373]

(2) The use of artificial intelligence (AI) has become an increasingly powerful approach for accelerating and optimizing the design of photonic structures.[545−547] AI techniques, including machine learning (ML) and optimization algorithms like genetic algorithms (GA) and particle swarm optimization (PSO), can efficiently explore large and complex design spaces by learning or evolving the relationships between structural parameters and optical responses.[548,549] In the field of radiative cooling, these AI-driven approaches has started to play an important role in guiding design and performance optimization.[550] For the optimization methods, PSO has been widely employed to optimize multilayer structures for achieving desired optical functionalities, such as in conventional RC[22] and transparent RC.[27,47,56] Similarly, GA is most often utilized for material selection and multilayer structure optimization in RC designs.[21,102,551] ML has also emerged as an effective approach for the design and optimization of RC structures including multilayer,[57,134,552,553] randomly distributed particle-based,[554,555] and metasurface designs.[119,152,153,556] For example, Zhang et al.[119] adopt ML to inversely design hybrid metasurface-based thermal emitters with enhanced selectivity and wide-angle emissivity. Recently, several RC studies have combined optimization algorithms with ML to enhance design efficiency.[553,555] For instance, Li et al.[553] present a hybrid design framework that combines ML and GA to accelerate the discovery of high-performance multilayer RC structures, where GA explores the design space and ML guides the search toward the optimal configuration. This hybrid strategy is expected to play a key role in the future development of AI-assisted radiative cooling technologies.

(3) Another key challenge for the broad deployment of radiative cooling technologies lies in the development of cost-effective, environmentally sustainable, and scalable fabrication methods. Despite significant progress in cooling performance, many state-of-the-art RC structures still rely on complex photonic structures, vacuum deposition, or lithographic techniques that are difficult to scale and costly to produce.[47,56,476] Promising scalable pathways include films,[52,557] paint-type coatings,[33,78] and fabrics/textiles.[176,236,457] However, their long-term durability under real-world conditions and mechanical robustness still need to be improved to ensure stable and reliable operation in practical applications. Furthermore, the use of biodegradable or naturally derived materials such as cellulose- or silk- based systems can help mitigate the environmental impact associated with polymer waste.

(4) Lastly, a promising path for future development lies in integrating RC technologies into existing architectural and urban infrastructures. Embedding RC systems into building envelopes, windows, and roofs can provide passive thermal regulation and reduce energy consump-

https://doi.org/10.1021/acsami.6c00074
ACS Appl. Mater. Interfaces 2026, 18, 21363−21423

tion without altering existing power systems. To achieve this, further efforts are needed to ensure mechanical durability, environmental stability, and aesthetic compatibility of RC materials under real outdoor conditions. The integration of scalable fabrication and adaptive control with infrastructure-oriented design will be key to realizing practical, building-integrated radiative cooling solutions.

The roadmap outlook of these perspectives is illustrated in Figure 19b.

7. CONCLUSION

Harit Keawmuang and Junsuk Rho

RC has rapidly evolved into a multidisciplinary field that bridges photonics, materials science, and thermal engineering. The research progress summarized in this mega-review highlights how RC has advanced from a fundamental concept to a versatile platform for sustainable thermal management and energy applications. In this article, we review the fundamental principles that govern RC, examine a wide range of structural designs and material systems, and discuss their diverse functionalities and emerging applications across various domains. Finally, we outline the key challenges and future perspectives that guide the continued development of RC toward practical, scalable, and environmentally sustainable technologies. We hope that this review serves as both a comprehensive reference and an inspiration for future research that will further expand the potential and impact of radiative cooling.

■ AUTHOR INFORMATION

Corresponding Author

Junsuk Rho − *Department of Mechanical Engineering, Pohang University of Science and Technology (POSTECH), Pohang 37673, Republic of Korea; Department of Chemical Engineering and Department of Electrical Engineering, Pohang University of Science and Technology (POSTECH), Pohang 37673, Republic of Korea; POSCO−POSTECH-RIST Convergence Research Center for Flat Optics and Metaphotonics, Pohang 37673, Republic of Korea;* orcid.org/0000-0002-2179-2890; Email: jsrho@postech.ac.kr

Authors

Harit Keawmuang − *Department of Mechanical Engineering, Pohang University of Science and Technology (POSTECH), Pohang 37673, Republic of Korea*

Junkyeong Park − *Department of Mechanical Engineering, Pohang University of Science and Technology (POSTECH), Pohang 37673, Republic of Korea*

Heon Lee − *Department of Materials Science and Engineering, Korea University, Seoul 02841, Republic of Korea; ZERC, Seoul 02841, Republic of Korea;* orcid.org/0000-0001-6635-1880

Seokju Choi − *Department of Control and Instrumentation Engineering, Korea University, Sejong 30019, Republic of Korea*

Sunae So − *Department of Control and Instrumentation Engineering, Korea University, Sejong 30019, Republic of Korea*

Changhyeon Lim − *Department of Electronics and Information Engineering, Korea University, Sejong 30019, Republic of Korea*

Trevon Badloe − *Department of Electronics and Information Engineering and Division of Smart Energy Convergence Engineering, Korea University, Sejong 30019, Republic of Korea;* orcid.org/0000-0001-9458-6062

Changhwan Hyeon − *Department of Biomedical Engineering, Yonsei University, Wonju 26493, Republic of Korea*

Minseo Jeong − *Department of Biomedical Engineering, Yonsei University, Wonju 26493, Republic of Korea; School of Electrical Engineering, Korea Advanced Institute of Science and Technology (KAIST), Daejeon 34141, Republic of Korea;* orcid.org/0009-0002-8250-0588

Dasol Lee − *Department of Biomedical Engineering, Yonsei University, Wonju 26493, Republic of Korea*

Ya Huang − *Beijing Key Laboratory of Green Chemical Reaction Engineering and Technology, Department of Chemical Engineering, Tsinghua University, Beijing 100084, China*

Siming Zhao − *Beijing Key Laboratory of Green Chemical Reaction Engineering and Technology, Department of Chemical Engineering, Tsinghua University, Beijing 100084, China*

Rufan Zhang − *Beijing Key Laboratory of Green Chemical Reaction Engineering and Technology, Department of Chemical Engineering, Tsinghua University, Beijing 100084, China;* orcid.org/0000-0003-1774-0550

Juhoon Baek − *Department of Mechanical and Robotics Engineering, Gwangju Institute of Science and Technology (GIST), Gwangju 61005, Republic of Korea*

Minkyung Kim − *Department of Mechanical and Robotics Engineering, Gwangju Institute of Science and Technology (GIST), Gwangju 61005, Republic of Korea;* orcid.org/0000-0001-5229-4520

Fei Xie − *GPL Photonics Laboratory, State Key Laboratory of Luminescence Science and Technology, Changchun Institute of Optics, Fine Mechanics and Physics, Chinese Academy of Sciences, Changchun, Jilin 130033, P. R. China; University of Chinese Academy of Sciences, Beijing 100049, China*

Longnan Li − *GPL Photonics Laboratory, State Key Laboratory of Luminescence Science and Technology, Changchun Institute of Optics, Fine Mechanics and Physics, Chinese Academy of Sciences, Changchun, Jilin 130033, P. R. China; University of Chinese Academy of Sciences, Beijing 100049, China;* orcid.org/0000-0003-0225-3303

Wei Li − *GPL Photonics Laboratory, State Key Laboratory of Luminescence Science and Technology, Changchun Institute of Optics, Fine Mechanics and Physics, Chinese Academy of Sciences, Changchun, Jilin 130033, P. R. China; University of Chinese Academy of Sciences, Beijing 100049, China;* orcid.org/0000-0002-2227-9431

Xuzhe Zhao − *Institute of Data and Information, Tsinghua Shenzhen International Graduate School and Center of Double Helix, Tsinghua Shenzhen International Graduate School, Tsinghua University, Shenzhen 518055, China; Intelligent Passive Thermal Control Center, Research Institute of Tsinghua University in Shenzhen, Shenzhen 518057, China*

Jiachen Li − *Department of Mechanical Engineering, Massachusetts Institute of Technology, Cambridge, Massachusetts 02139, United States;* orcid.org/0000-0002-0368-3551

Kaichen Dong − *Institute of Data and Information, Tsinghua Shenzhen International Graduate School and Center of Double Helix, Tsinghua Shenzhen International Graduate School, Tsinghua University, Shenzhen 518055, China; Intelligent Passive Thermal Control Center, Research Institute of*

https://doi.org/10.1021/acsami.6c00074
ACS Appl. Mater. Interfaces 2026, 18, 21363−21423

Tsinghua University in Shenzhen, Shenzhen 518057, China; orcid.org/0000-0001-5334-4243

Saichao Dang − *Sustainable Photonics Energy Research Laboratory, Material Science Engineering, Physical Sciences and Engineering Division, King Abdullah University of Science and Technology, Thuwal 23955-6900, Saudi Arabia*

Qiaoqiang Gan − *Sustainable Photonics Energy Research Laboratory, Material Science Engineering, Physical Sciences and Engineering Division, King Abdullah University of Science and Technology, Thuwal 23955-6900, Saudi Arabia*

Shaowen Cao − *Department of Electronic Engineering, The Chinese University of Hong Kong, Hong Kong, China*

Yi Long − *Department of Electronic Engineering, The Chinese University of Hong Kong, Hong Kong, China*

Hyunkyu Kwak − *School of Electrical Engineering, Korea Advanced Institute of Science and Technology (KAIST), Daejeon 34141, Republic of Korea*

Do Hyeon Kim − *School of Electrical Engineering, Korea Advanced Institute of Science and Technology (KAIST), Daejeon 34141, Republic of Korea;* orcid.org/0000-0003-3060-1192

Young Min Song − *School of Electrical Engineering, Korea Advanced Institute of Science and Technology (KAIST), Daejeon 34141, Republic of Korea; GIST InnoCORE AI-Nano Convergence Institute for Early Detection of Neurodegenerative Diseases, Gwangju Institute of Science and Technology (GIST), Gwangju 61005, Republic of Korea;* orcid.org/0000-0002-4473-6883

Jung Bin Yang − *School of Mechanical Engineering, Hanyang University, Seoul 04763, Republic of Korea*

Dong Rip Kim − *School of Mechanical Engineering, Hanyang University, Seoul 04763, Republic of Korea;* orcid.org/0000-0001-6398-9483

Yansu Hou − *National Laboratory of Solid State Microstructures, College of Engineering and Applied Sciences, Jiangsu Key Laboratory of Artificial Functional Materials, Collaborative Innovation Center of Advanced Microstructures, Frontiers Science Center for Critical Earth Material Cycling, Nanjing University, Nanjing 210093, China*

Jia Zhu − *National Laboratory of Solid State Microstructures, College of Engineering and Applied Sciences, Jiangsu Key Laboratory of Artificial Functional Materials, Collaborative Innovation Center of Advanced Microstructures, Frontiers Science Center for Critical Earth Material Cycling, Nanjing University, Nanjing 210093, China;* orcid.org/0000-0002-2871-4369

Bin Zhu − *National Laboratory of Solid State Microstructures, College of Engineering and Applied Sciences, Jiangsu Key Laboratory of Artificial Functional Materials, Collaborative Innovation Center of Advanced Microstructures, Frontiers Science Center for Critical Earth Material Cycling, Nanjing University, Nanjing 210093, China;* orcid.org/0000-0002-0466-7692

Shengxi Bai − *School of Energy and Environment, City University of Hong Kong, Hong Kong, China*

Kaixin Lin − *School of Energy and Environment, City University of Hong Kong, Hong Kong, China*

Chi Yan Tso − *School of Energy and Environment, City University of Hong Kong, Hong Kong, China;* orcid.org/0000-0002-7725-2172

Seonggon Kim − *School of Mechanical Engineering, Sungkyunkwan University, Suwon, Gyeonggi-do 16419, Republic of Korea*

Yong Tae Kang − *Research Center for Plus Energy Building Innovative Technology, Seoul 02841, Republic of Korea; School of Mechanical Engineering, Korea University, Seoul 02841, Republic of Korea*

Qingsong Fan − *Pritzker School of Molecular Engineering, University of Chicago, Chicago, Illinois 60637, United States;* orcid.org/0000-0001-8555-769X

Qizhang Li − *Pritzker School of Molecular Engineering, University of Chicago, Chicago, Illinois 60637, United States;* orcid.org/0000-0002-5454-4578

Po-Chun Hsu − *Pritzker School of Molecular Engineering, University of Chicago, Chicago, Illinois 60637, United States;* orcid.org/0000-0002-6509-9377

Complete contact information is available at: https://pubs.acs.org/10.1021/acsami.6c00074

Author Contributions

J.R. conceived the idea of a mega-review in radiative cooling. J.R. and H.K. outlined the mega-review structure. H.K. integrated parts for each section and conducted revision and editing. Sections 2.1 and 2.2: J.P. and J.R. wrote the photonic concepts of RC and thermal balance of RC sections. Section 2.3: H.L. wrote the representative fabrication strategies for the RC section. Section 3.1: S.C. and S.S. wrote the multilayer thin-film structures section. Section 3.2: C.L. and T.B. wrote the metasurfaces and nanophotonic architectures section. Section 3.3: C.H., M.J., and D.L. wrote the porous structures section. Section 4.1.1: Y.H., S.Z., and R.Z. wrote the monoselective RC emitter and dual-selective RC emitter sections. Section 4.1.2: J.B. and M.K. wrote the transparent radiative cooler and colored radiative cooler sections. Section 4.2: F.X., L.L., and W.L. wrote the directional and anisotropic RC section. Section 4.3: X.Z., J.L., and K.D. wrote the adaptive and switchable RC section. Section 4.4: SD and Q.G. wrote the hybrid and multifunctional RC section. Section 5.1: S. Cao and Y.L. wrote the energy-efficient buildings and smart windows section. Section 5.2: H. Kwak, D.H.K., and Y.M.S. wrote the vehicles and enclosed spaces section. Section 5.3: J.B.Y. and D.R.K. wrote the high-performance solar energy systems section. Section 5.4: Y. Hou and J.Z. wrote the personal thermal management section. Section 5.5: Y. Hou and B.Z. wrote the electricity generation section. Section 5.6: S.B., K.L., and C.Y.T. wrote the atmospheric water harvesting section. Section 5.7: S.K. and Y.T.K. wrote the passive isothermal film section. Section 5.8: Q.F., Q.L., and P.-C.H. wrote the global- and regional-scale artificial RC section. H.K. and J.R. wrote the abstract, introduction, challenges and future outlook, and conclusion sections.

Notes

The authors declare no competing financial interest.

■ ACKNOWLEDGMENTS

This work was financially supported by the POSCO-POSTECH-RIST Convergence Research Center program funded by POSCO, the National Research Foundation (NRF) grant (RS-2022-NR068140) funded by the Ministry of Science and ICT (MIST) of the Korean government. H.K. acknowledges the POSCO Asia fellowship, and the Yuhan Foundation *New Ilhan* fellowship. Section 2.3: This work was supported by the DIPS 1000+ Program (20270659) funded by Korea Electric Power Corporation (KEPCO). Section 3.1: S.S. acknowledges the NRF Sejong Science fellowships (NRF-2022R1C1C2009430) funded by the MSIT of the Korean

government. Section 3.3: D.L. acknowledges the National Research Foundation (NRF) grant (RS-2025-00556856) funded by the Ministry of Science and ICT (MSIT) of the Korean government. Section 4.1.1: This work was supported by the China National Petroleum Corporation Innovation Fund (2024DQ02-0409), the National Key Research Program (2020YFC2201103 and 2020YFA0210702), and the National Natural Science Foundation of China (220375163). Section 4.1.2: This work was supported by the NRF grant (RS-2025-23524064) funded by the MSIT of the Korean government. Section 4.2: National Natural Science Foundation of China (grant nos. T2525033, 62134009, 62121005, 62475261), the International Partnership Program of Chinese Academy of Sciences for Future Network (Grant No. 171GJHZ2023038FN), Jilin Provincial Scientific and Technological Development Program (Grant No. SKL202401020) and the Postdoctoral Fellowship Program and China Postdoctoral Science Foundation (Grant No. BX20250359). Prof. Wei Li acknowledges the support from the New Cornerstone Science Foundation through the XPLORER PRIZE. Section 4.3: X.Z. and K.D. acknowledge the support from the National Natural Science Foundation of China (Grant 62375151), the Shenzhen Science and Technology Program (Grant KJZD20240903095721028), the National Key R&D Program of China (grant 2023YFB3208700), and the Start-up funding in Tsinghua Shenzhen International Graduate School, Tsinghua University. Section 5.1: Y.L. wishes to thank for the funding support from the Global STEM Professorship Scheme sponsored by the Government of Hong Kong Special Administrative Region, Start-up funding from the Chinese University of Hong Kong, the 2024 Shenzhen-Hong Kong-Macau Science and Technology Program (Category C) (SGDX20230821094659005), and the Innovation and Technology Fund (ITS/221/23). Y.L. also thanks the Hong Kong Environment and Conservation Fund under Grant No. 96/2024. Section 5.2: This work was supported by the InnoCORE program of the Ministry of Science and ICT (GIST InnoCORE KH0830). This work was also supported by the National Research Foundation of Korea (NRF) funded by the Korea government (MSIT) (RS-2022-NR068140). Section 5.3: This study was supported by Nano-Material Technology Development Program (NRF-2022M3H4A1A02046445) of the National Research Foundation of Korea (NRF), funded by the Ministry of Science and ICT of Korea. This study was also financially supported by the Korea Institute of Energy Technology Evaluation and Planning (KETEP) and the Ministry of Trade, Industry & Energy (MOTIE) of the Republic of Korea (RS-2023-00236325). Sections 5.4 and 5.5: We acknowledge the microfabrication center of the National Laboratory of Solid State Microstructures (NLSSM) for the technical support. This work was jointly supported by the National Key Research and Development Programme of China (2022YFA1404704 and 2020YFA0406104), the National Natural Science Foundation of China (52372197, 52303323, 51925204, 52002168), the Natural Science Foundation of Jiangsu Province (BK20231540), the Excellent Research Programme of Nanjing University (ZYJH005), the research foundation of Frontiers Science Center for Critical Earth Material Cycling (14380214), the Fundamental Research Funds for the Central Universities (021314380184, 021314380208, 021314380190, 021314380140, and 021314380150), Department of Science and Technology of Hubei Province (2021CSA076), and the State Key Laboratory of New Textile Materials and Advanced Processing Technologies (Wuhan Textile University, No. FZ2022011). Section 5.6: The atmospheric water harvesting section was supported by the Hong Kong Research Grant Council via Research Fellow Scheme with the reference number of RFS2425-1S06, and via the General Research Fund (GRF) account 11200022. Section 5.7: This research was supported by National Research Foundation of Korea (NRF) grant funded by the Korean government (MSIT) (No. NRF-2020R1A5A1018153). Section 5.8: The authors thank the funding support from the Climate Systems Engineering Initiative (CSEi) at the University of Chicago.

REFERENCES

(1) Davis, L.; Gertler, P.; Jarvis, S.; Wolfram, C. Air conditioning and global inequality. *Glob. Environ. Change* **2021**, *69*, No. 102299.

(2) Frayssinet, L.; Merlier, L.; Kuznik, F.; Hubert, J.-L.; Milliez, M.; Roux, J.-J. Modeling the heating and cooling energy demand of urban buildings at city scale. *Renewable Sustainable Energy Rev.* **2018**, *81*, 2318−2327.

(3) Santamouris, M. Cooling the buildings−past, present and future. *Energy Build.* **2016**, *128*, 617−638.

(4) Fan, S.; Li, W. Photonics and thermodynamics concepts in radiative cooling. *Nat. Photonics* **2022**, *16* (3), 182−190.

(5) Howell, J. R.; Mengüç, M. P.; Daun, K.; Siegel, R. *Thermal radiation heat transfer*; CRC Press, 2020.

(6) Modest, M. F.; Mazumder, S. *Radiative heat transfer*; Academic Press, 2021.

(7) Steven Brown, J.; Domanski, P. A. Review of alternative cooling technologies. *Appl. Therm. Eng.* **2014**, *64* (1−2), 252−262.

(8) Liu, R.; Wang, S.; Zhou, Z.; Zhang, K.; Wang, G.; Chen, C.; Long, Y. Materials in radiative cooling technologies. *Adv. Mater.* **2025**, *37* (2), No. 2401577.

(9) So, S.; Yun, J.; Ko, B.; Lee, D.; Kim, M.; Noh, J.; Park, C.; Park, J.; Rho, J. Radiative cooling for energy sustainability: from fundamentals to fabrication methods toward commercialization. *Adv. Sci.* **2024**, *11* (2), No. 2305067.

(10) Zhao, B.; Hu, M.; Ao, X.; Chen, N.; Pei, G. Radiative cooling: A review of fundamentals, materials, applications, and prospects. *Appl. Energy* **2019**, *236*, 489−513.

(11) Granqvist, C. G.; Hjortsberg, A. Surfaces for radiative cooling: Silicon monoxide films on aluminum. *Appl. Phys. Lett.* **1980**, *36* (2), 139−141.

(12) Granqvist, C. G.; Hjortsberg, A. Radiative cooling to low temperatures: General considerations and application to selectively emitting SiO films. *J. Appl. Phys.* **1981**, *52* (6), 4205−4220.

(13) Gentle, A. R.; Smith, G. B. Radiative heat pumping from the earth using surface phonon resonant nanoparticles. *Nano Lett.* **2010**, *10* (2), 373−379.

(14) Li, W.; Dong, M.; Fan, L.; John, J. J.; Chen, Z.; Fan, S. Nighttime radiative cooling for water harvesting from solar panels. *ACS Photonics* **2021**, *8* (1), 269−275.

(15) Dong, M.; Chen, N.; Zhao, X.; Fan, S.; Chen, Z. Nighttime radiative cooling in hot and humid climates. *Opt. Express* **2019**, *27* (22), 31587−31598.

(16) Zeyghami, M.; Goswami, D. Y.; Stefanakos, E. A review of clear sky radiative cooling developments and applications in renewable power systems and passive building cooling. *Sol. Energy Mater. Sol. Cells* **2018**, *178*, 115−128.

(17) Zhang, Q.; Wang, S.; Wang, X.; Jiang, Y.; Li, J.; Xu, W.; Zhu, B.; Zhu, J. Recent progress in daytime radiative cooling: Advanced material designs and applications. *Small Methods* **2022**, *6* (4), No. 2101379.

(18) Chen, M.; Pang, D.; Chen, X.; Yan, H.; Yang, Y. Passive daytime radiative cooling: Fundamentals, material designs, and applications. *EcoMat* **2022**, *4* (1), No. e12153.

(19) Bhatia, B.; Leroy, A.; Shen, Y.; Zhao, L.; Gianello, M.; Li, D.; Gu, T.; Hu, J.; Soljačić, M.; Wang, E. N. Passive directional sub-ambient daytime radiative cooling. *Nat. Commun.* **2018**, *9* (1), No. 5001.

https://doi.org/10.1021/acsami.6c00074
ACS Appl. Mater. Interfaces 2026, 18, 21363−21423

(20) Xie, F.; Jin, W.; Nolen, J. R.; Pan, H.; Yi, N.; An, Y.; Zhang, Z.; Kong, X.; Zhu, F.; Jiang, K.; et al. Subambient daytime radiative cooling of vertical surfaces. *Science* **2024**, *386* (6723), 788−794.
(21) So, S.; Yang, Y.; Son, S.; Lee, D.; Chae, D.; Lee, H.; Rho, J. Highly suppressed solar absorption in a daytime radiative cooler designed by genetic algorithm. *Nanophotonics* **2022**, *11* (9), 2107−2115.
(22) Chae, D.; Kim, M.; Jung, P. H.; Son, S.; Seo, J.; Liu, Y.; Lee, B. J.; Lee, H. Spectrally Selective Inorganic-Based Multilayer Emitter for Daytime Radiative Cooling. *ACS Appl. Mater. Interfaces* **2020**, *12* (7), 8073−8081.
(23) Yun, J.; Chae, D.; So, S.; Lim, H.; Noh, J.; Park, J.; Kim, N.; Park, C.; Lee, H.; Rho, J. Optimally designed multimaterial microparticle−polymer composite paints for passive daytime radiative cooling. *ACS Photonics* **2023**, *10* (8), 2608−2617.
(24) Raman, A. P.; Anoma, M. A.; Zhu, L.; Rephaeli, E.; Fan, S. Passive radiative cooling below ambient air temperature under direct sunlight. *Nature* **2014**, *515* (7528), 540−544.
(25) Wang, Y.; Ji, H.; Liu, B.; Tang, P.; Chen, Y.; Huang, J.; Ou, Y.; Tao, J. Radiative cooling: structure design and application. *J. Mater. Chem. A* **2024**, *12* (17), 9962−9978.
(26) Son, S.; Jeon, S.; Chae, D.; Lee, S. Y.; Liu, Y.; Lim, H.; Oh, S. J.; Lee, H. Colored emitters with silica-embedded perovskite nanocrystals for efficient daytime radiative cooling. *Nano Energy* **2021**, *79*, No. 105461.
(27) Lee, G.; Kang, H.; Yun, J.; Chae, D.; Jeong, M.; Jeong, M.; Lee, D.; Kim, M.; Lee, H.; Rho, J. Integrated triboelectric nanogenerator and radiative cooler for all-weather transparent glass surfaces. *Nat. Commun.* **2024**, *15* (1), No. 6537.
(28) Park, J.; Lim, H.; Keawmuang, H.; Chae, D.; Lee, H.; Rho, J. Flexible Self-Cleaning Janus Emitter for Transparent Radiative Cooling in Enclosed Spaces. *Small* **2025**, *21* (32), No. 2501840.
(29) Kim, M.; Lee, D.; Yang, Y.; Rho, J. Switchable diurnal radiative cooling by doped VO2. *Opto-Electron. Adv.* **2021**, *4* (5), No. 200006.
(30) Ono, M.; Chen, K.; Li, W.; Fan, S. Self-adaptive radiative cooling based on phase change materials. *Opt. Express* **2018**, *26* (18), A777−A787.
(31) Lee, G. J.; Kim, Y. J.; Kim, H. M.; Yoo, Y. J.; Song, Y. M. Colored, daytime radiative coolers with thin-film resonators for aesthetic purposes. *Adv. Opt. Mater.* **2018**, *6* (22), No. 1800707.
(32) Yang, K.; Wu, X.; Zhou, L.; Wu, P.; Gereige, I.; Gan, Q. Towards practical applications of radiative cooling. *Nat. Rev. Clean Technol.* **2025**, *1*, 235−254.
(33) Mandal, J.; Yang, Y.; Yu, N.; Raman, A. P. Paints as a scalable and effective radiative cooling technology for buildings. *Joule* **2020**, *4* (7), 1350−1356.
(34) Lee, K. W.; Lim, W.; Jeon, M. S.; Jang, H.; Hwang, J.; Lee, C. H.; Kim, D. R. Visibly clear radiative cooling metamaterials for enhanced thermal management in solar cells and windows. *Adv. Funct. Mater.* **2022**, *32* (1), No. 2105882.
(35) Haechler, I.; Park, H.; Schnoering, G.; Gulich, T.; Rohner, M.; Tripathy, A.; Milionis, A.; Schutzius, T. M.; Poulikakos, D. Exploiting radiative cooling for uninterrupted 24-h water harvesting from the atmosphere. *Sci. Adv.* **2021**, *7* (26), No. eabf3978.
(36) Omair, Z.; Assawaworrarit, S.; Fan, L.; Jin, W.; Fan, S. Radiative-cooling-based nighttime electricity generation with power density exceeding 100 mW/m2. *iScience* **2022**, *25* (8), No. 104858.
(37) Lv, Y.; Huang, A.; Yang, J.; Xu, J.; Yang, R. Improving cabin thermal environment of parked vehicles under direct sunlight using a daytime radiative cooling cover. *Appl. Therm. Eng.* **2021**, *190*, No. 116776.
(38) Iqbal, M. I.; Lin, K.; Sun, F.; Chen, S.; Pan, A.; Lee, H. H.; Kan, C.-W.; Lin, C. S. K.; Tso, C. Y. Radiative cooling nanofabric for personal thermal management. *ACS Appl. Mater. Interfaces* **2022**, *14* (20), 23577−23587.
(39) Kaviany, M. *Heat transfer physics*; Cambridge University Press, 2014.
(40) Lee, M.; Kim, G.; Jung, Y.; Pyun, K. R.; Lee, J.; Kim, B.-W.; Ko, S. H. Photonic structures in radiative cooling. *Light: Sci. Appl.* **2023**, *12* (1), No. 134.
(41) Jeon, S.; Shin, J. Directional radiation for optimal radiative cooling. *Opt. Express* **2021**, *29* (6), 8376−8386.
(42) Chen, M.; Li, W.; Tao, S.; Fang, Z.; Lu, C.; Xu, Z. A pragmatic and high-performance radiative cooling coating with near-ideal selective emissive spectrum for passive cooling. *Coatings* **2020**, *10* (2), 144.
(43) Li, W.; Fan, S. Radiative cooling: harvesting the coldness of the universe. *Opt. Photonics News* **2019**, *30* (11), 32−39.
(44) Chen, Z.; Zhu, L.; Raman, A.; Fan, S. Radiative cooling to deep sub-freezing temperatures through a 24-h day−night cycle. *Nat. Commun.* **2016**, *7* (1), No. 13729.
(45) Rephaeli, E.; Raman, A.; Fan, S. Ultrabroadband photonic structures to achieve high-performance daytime radiative cooling. *Nano Lett.* **2013**, *13* (4), 1457−1461.
(46) Kim, J.; Baek, S.; Park, J. Y.; Kim, K. H.; Lee, J. L. Photonic multilayer structure induced high near-infrared (NIR) blockage as energy-saving window. *Small* **2021**, *17* (29), No. 2100654.
(47) Kim, M.; Lee, D.; Son, S.; Yang, Y.; Lee, H.; Rho, J. Visibly transparent radiative cooler under direct sunlight. *Adv. Opt. Mater.* **2021**, *9* (13), No. 2002226.
(48) Ijaz, S.; Kang, D.; Rana, A. S.; Kim, J.; Chani, M. T. S.; Zubair, M.; Abbassi, Q. H.; Mehmood, M. Q.; Rho, J. Metasurface Absorber−Emitter Pair-Integrated High-Efficiency Thermophotovoltaic System. *ACS Photonics* **2025**, *12* (7), 3829−3839.
(49) Hossain, M. M.; Jia, B.; Gu, M. A metamaterial emitter for highly efficient radiative cooling. *Adv. Opt. Mater.* **2015**, *3* (8), 1047−1051.
(50) Shi, N. N.; Tsai, C.-C.; Camino, F.; Bernard, G. D.; Yu, N.; Wehner, R. Keeping cool: Enhanced optical reflection and radiative heat dissipation in Saharan silver ants. *Science* **2015**, *349* (6245), 298−301.
(51) Song, J.; Seo, J.; Han, J.; Lee, J.; Lee, B. J. Ultrahigh emissivity of grating-patterned PDMS film from 8 to 13 μm wavelength regime. *Appl. Phys. Lett.* **2020**, *117* (9), No. 094101, DOI: 10.1063/5.0017838.
(52) Zhai, Y.; Ma, Y.; David, S. N.; Zhao, D.; Lou, R.; Tan, G.; Yang, R.; Yin, X. Scalable-manufactured randomized glass-polymer hybrid metamaterial for daytime radiative cooling. *Science* **2017**, *355* (6329), 1062−1066, DOI: 10.1126/science.aai7899.
(53) Liu, Y.; Son, S.; Chae, D.; Jung, P.-H.; Lee, H. Acrylic membrane doped with Al2O3 nanoparticle resonators for zero-energy consuming radiative cooling. *Sol. Energy Mater. Sol. Cells* **2020**, *213*, No. 110561.
(54) Chen, G.; Wang, Y.; Qiu, J.; Cao, J.; Zou, Y.; Wang, S.; Ouyang, J.; Jia, D.; Zhou, Y. A visibly transparent radiative cooling film with self-cleaning function produced by solution processing. *J. Mater. Sci. Technol.* **2021**, *90*, 76−84.
(55) Chen, G.; Wang, Y.; Qiu, J.; Cao, J.; Zou, Y.; Wang, S.; Jia, D.; Zhou, Y. Robust inorganic daytime radiative cooling coating based on a phosphate geopolymer. *ACS Appl. Mater. Interfaces* **2020**, *12* (49), 54963−54971.
(56) Ko, B.; Noh, J.; Chae, D.; Lee, C.; Lim, H.; Lee, H.; Rho, J. Neutral-Colored Transparent Radiative Cooler by Tailoring Solar Absorption with Punctured Bragg Reflectors. *Adv. Funct. Mater.* **2024**, *34* (52), No. 2410613, DOI: 10.1002/adfm.202410613.
(57) Keawmuang, H.; Badloe, T.; Lee, C.; Park, J.; Rho, J. Inverse design of colored daytime radiative coolers using deep neural networks. *Sol. Energy Mater. Sol. Cells* **2024**, *271*, No. 112848.
(58) Wang, Q.; Yang, F.; Wu, D.; Guo, Z. Radiative cooling layer boosting hydrophilic-hydrophobic patterned surface for efficient water harvesting. *Colloids Surf., A* **2023**, *658*, No. 130584.
(59) Zhang, X.; Li, X.; Wang, F.; Yuan, W.; Cheng, Z.; Liang, H.; Yan, Y. Low-Cost and Large-Scale Producible Biomimetic Radiative Cooling Glass with Multiband Radiative Regulation Performance. *Adv. Opt. Mater.* **2022**, *10* (23), No. 2202031.
(60) Xu, N.; Wang, J.; Cui, Y.; Ren, S.; Deng, J.; Gou, Q.; Chen, Z.; Wang, K.; Geng, Y.; Cui, J.; Li, M. Butterfly wing-inspired micro-structured film with high reflectivity for efficient passive radiative cooling. *Renewable Energy* **2024**, *229*, No. 120732.
(61) Anusuyadevi, P. R.; Singha, S.; Banerjee, D.; Jonsson, M. P.; Hedenqvist, M. S.; Svagan, A. J. Synthetic plant cuticle coating as a

biomimetic moisture barrier membrane for structurally colored cellulose films. *Adv. Mater. Interfaces* **2023**, *10* (7), No. 2202112.
(62) Heredia, A.; Benítez, J. J.; Gonzalez Moreno, A.; Domínguez, E. Revisiting plant cuticle biophysics. *New Phytol.* **2024**, *244* (1), 65−73.
(63) Lin, C.; Li, K.; Li, M.; Dopphoopha, B.; Zheng, J.; Wang, J.; Du, S.; Li, Y.; Huang, B. Pushing radiative cooling technology to real applications. *Adv. Mater.* **2025**, *37* (23), No. 2409738.
(64) Zou, C.; Ren, G.; Hossain, M. M.; Nirantar, S.; Withayachumnankul, W.; Ahmed, T.; Bhaskaran, M.; Sriram, S.; Gu, M.; Fumeaux, C. Metal-Loaded dielectric resonator metasurfaces for radiative cooling. *Adv. Opt. Mater.* **2017**, *5* (20), No. 1700460.
(65) Ma, H.; Yao, K.; Dou, S.; Xiao, M.; Dai, M.; Wang, L.; Zhao, H.; Zhao, J.; Li, Y.; Zhan, Y. Multilayered SiO2/Si3N4 Photonic Emitter to Achieve High-Performance All-day Radiative Cooling. *Sol. Energy Mater. Sol. Cells* **2020**, *212*, No. 110584.
(66) Chae, D.; Son, S.; Lim, H.; Jung, P.-H.; Ha, J.; Lee, H. Scalable and paint-format microparticle−polymer composite enabling high-performance daytime radiative cooling. *Mater. Today Phys.* **2021**, *18*, No. 100389.
(67) Lim, H.; Lee, T. Y.; Chae, D.; Park, J.; Sung, H.; Park, C.; Park, S.; Kim, Y. K.; Lee, H. Development of a highly stretchable and detachable radiative cooling cover to facilitate radiative cooling of outdoor object in various type. *Sol. Energy* **2025**, *288*, No. 113254.
(68) Son, S.; Liu, Y.; Chae, D.; Lee, H. Cross-linked porous polymeric coating without a metal-reflective layer for sub-ambient radiative cooling. *ACS Appl. Mater. Interfaces* **2020**, *12* (52), 57832−57839.
(69) Li, X.; Peoples, J.; Yao, P.; Ruan, X. Ultrawhite BaSO4 paints and films for remarkable daytime subambient radiative cooling. *ACS Appl. Mater. Interfaces* **2021**, *13* (18), 21733−21739.
(70) Li, X.; Peoples, J.; Huang, Z.; Zhao, Z.; Qiu, J.; Ruan, X. Full daytime sub-ambient radiative cooling in commercial-like paints with high figure of merit. *Cell Rep. Phys. Sci.* **2020**, *1* (10), No. 100221, DOI: 10.1016/j.xcrp.2020.100221.
(71) Lim, H.; Park, J.; Chae, D.; Park, S.; Kim, S.; Lee, H. Zeolitic Imidazolate Framework-8-Based Passive Daytime Radiative Cooling Paint for Energy-Efficient Cooling. *Adv. Energy Sustainability Res.* **2024**, *5* (10), No. 2400087.
(72) Felicelli, A.; Katsamba, I.; Barrios, F.; Zhang, Y.; Guo, Z.; Peoples, J.; Chiu, G.; Ruan, X. Thin layer lightweight and ultrawhite hexagonal boron nitride nanoporous paints for daytime radiative cooling. *Cell Rep. Phys. Sci.* **2022**, *3* (10), No. 101058, DOI: 10.1016/j.xcrp.2022.101058.
(73) Song, J.; Zhang, W.; Sun, Z.; Pan, M.; Tian, F.; Li, X.; Ye, M.; Deng, X. Durable radiative cooling against environmental aging. *Nat. Commun.* **2022**, *13* (1), No. 4805, DOI: 10.1038/s41467-022-32409-7.
(74) Barber, E.; Feng, D.; Fang, Z.; Carne, D.; Gonzalez, O. R.; Lee, W.-J.; Vansal, N.; Raykova, K.; Ruan, X. Efficient, hydrophobic, and weather-resistant radiative cooling paints with silicone-based binders. *ACS Appl. Opt. Mater.* **2025**, *3* (5), 1137−1144.
(75) Fan, H.; Wang, K.; Ding, Y.; Qiang, Y.; Yang, Z.; Xu, H.; Li, M.; Xu, Z.; Huang, C. Core−Shell Composite Nanofibers with High Temperature Resistance, Hydrophobicity and Breathability for Efficient Daytime Passive Radiative Cooling. *Adv. Mater.* **2024**, *36* (40), No. 2406987, DOI: 10.1002/adma.202406987.
(76) Aljwirah, A. K.; Liu, X.; Rivera Gonzalez, O.; Alhammadi, K.; Lee, W.-J.; Katsamba, I.; Ruan, X. Water-based hydrophobic paints for daytime radiative cooling. *ACS Appl. Mater. Interfaces* **2025**, *17* (22), 32914−32927.
(77) Bretz, S. E.; Akbari, H. Long-term performance of high-albedo roof coatings. *Energy Build.* **1997**, *25* (2), 159−167.
(78) Mandal, J.; Fu, Y.; Overvig, A. C.; Jia, M.; Sun, K.; Shi, N. N.; Zhou, H.; Xiao, X.; Yu, N.; Yang, Y. Hierarchically porous polymer coatings for highly efficient passive daytime radiative cooling. *Science* **2018**, *362* (6412), 315−319, DOI: 10.1126/science.aat9513.
(79) Yang, S.; Wang, F.; Ou, J.; Li, C. Yellow self-cleaning radiative cooling paint for building exterior with high adhesion. *Prog. Org. Coat.* **2025**, *204*, No. 109200.
(80) Xu, Z.; Zhang, X.; Yao, Y.; Chen, M. Superhydrophobic cement-based radiative cooling paint for durable and scalable applications. *Appl. Therm. Eng.* **2025**, *281*, No. 128770.
(81) Ying, J.; Chai, Y.; Ye, Y.; Suo, Y.; Zhang, Z. High-adhesion aluminum-cement composite coating for efficient passive daytime radiative cooling. *Sol. Energy Mater. Sol. Cells* **2026**, *296*, No. 114069.
(82) Xu, M.; Li, J.; Ren, J.; Wang, J.; Xu, L.; Wang, W.; Sun, S.; Li, H.; Zhang, J.; Wu, J. Superhydrophobic and recyclable passive daytime radiative cooling fabric prepared via electrospinning. *Chem. Eng. J.* **2025**, *509*, No. 161274.
(83) Fan, C.; Zhang, Y.; Long, Z.; Mensah, A.; Wang, Q.; Lv, P.; Wei, Q. Dynamically tunable subambient daytime radiative cooling metafabric with Janus wettability. *Adv. Funct. Mater.* **2023**, *33* (29), No. 2300794.
(84) Son, S.; Lee, T. Y.; Chae, D.; Lim, H.; Ha, J.; Kim, Y. K.; Lee, H. Efficient daytime radiative cooling cover sheet with dual-modal optical properties. *Adv. Opt. Mater.* **2022**, *10* (24), No. 2201771.
(85) Park, J.; Chae, D.; Lim, H.; Ha, J.; Park, S.; Sung, H.; Park, C.; Lee, H. Daytime Radiative Cooling Sheet Functionalized by Al2O3-Assisted Organic Composite. *Adv. Sci.* **2025**, *12* (12), No. 2417584.
(86) Yablonovitch, E. Inhibited Spontaneous Emission in Solid-State Physics and Electronics. *Phys. Rev. Lett.* **1987**, *58* (20), 2059−2062.
(87) Bragg, W. H.; William Lawrence, B. The reflection of X-rays by crystals. *Proc. R. Soc. London Ser. A* **1913**, *88* (605), 428−438.
(88) Perot, A.; Fabry, C. On the Application of Interference Phenomena to the Solution of Various Problems of Spectroscopy and Metrology. *Astrophys. J.* **1899**, *9*, 87.
(89) Xi, J. Q.; Schubert, M. F.; Kim, J. K.; Schubert, E. F.; Chen, M.; Lin, S. Y.; Liu, W.; Smart, J. A. Optical thin-film materials with low refractive index for broadband elimination of Fresnel reflection. *Nat. Photonics* **2007**, *1* (3), 176−179.
(90) Kun, H. On the interaction between the radiation field and ionic crystals. *Proc. R. Soc. London, Ser. A, Math. Phys. Sci.* **1951**, *208* (1094), 352−365.
(91) Li, X.; Zhang, W.; Liu, M.; Pei, G.; Zhao, B. Adaptive spectral multilayer structure based on VO2/Ge resonant cavity for thermal management of buildings in cold regions. *Infrared Phys. Technol.* **2025**, *151*, 106054.
(92) Hervé, A.; Drévillon, J.; Ezzahri, Y.; Joulain, K. Radiative cooling by tailoring surfaces with microstructures: Association of a grating and a multi-layer structure. *J. Quant. Spectrosc. Radiat. Transfer* **2018**, *221*, 155−163.
(93) Liu, D.; Xu, Y.; Xuan, Y. Fabry−Perot-resonator-coupled metal pattern metamaterial for infrared suppression and radiative cooling. *Appl. Opt.* **2020**, *59* (23), 6861−6867.
(94) Xie, H.; Yin, H.; Fan, C. Realization of an Adaptive Radiative Cooler with a Multilayer-Filter VO2-Based Fabry-Pérot Cavity. *Chin. Phys. Lett.* **2024**, *41* (4), No. 044202, DOI: 10.1088/0256-307X/41/4/044202.
(95) Osuna Ruiz, D.; Lezaun, C.; Torres-García, A. E.; Beruete, M. Metal-free design of a multilayered metamaterial with chirped Bragg grating for enhanced radiative cooling. *Opt. Express* **2023**, *31* (14), 22698.
(96) De Luca, D.; Kortge, D.; Di Gennaro, E.; Russo, R.; Bermel, P. Ultra-thin sputter-deposited infrared rugate mirror for enhancing solar-to-thermal energy conversion. *Opt. Lett.* **2022**, *47* (2), 230−233.
(97) Li, Y.; Chen, X.; Yu, L.; Pang, D.; Yan, H.; Chen, M. Janus Interface Engineering Boosting Visibly Transparent Radiative Cooling for Energy Saving. *ACS Appl. Mater. Interfaces* **2023**, *15* (3), 4122−4131.
(98) Dang, S.; Wang, X.; Ye, H. An Ultrathin Transparent Radiative Cooling Photonic Structure with a High NIR Reflection. *Adv. Mater. Interfaces* **2022**, *9* (30), No. 2201050, DOI: 10.1002/admi.202201050.
(99) Nan, H.; Xiong, P.; Zhong, G.-J.; Li, Y.; Li, R.; Niu, J.-H.; Lei, J.; Li, Z.-M. Ag/SiO2 and Ag/TiO2 Nanoscale-Thick Layers as Hyperbolic Metamaterials for Transparent Radiative Cooling Glass Design. *ACS Appl. Nano Mater.* **2024**, *7* (14), 17111−17119.

(100) Jin, Y.; Jeong, Y.; Yu, K. Infrared-Reflective Transparent Hyperbolic Metamaterials for Use in Radiative Cooling Windows. *Adv. Funct. Mater.* **2023**, *33* (1), No. 2207940.
(101) Liu, G.; Chen, S.; Lin, C. Optimization of Dielectric-Metal Multilayer Structure for Color-Preserving Radiative Cooling Window. *ACS Omega* **2024**, *9* (28), 30425−30435.
(102) Zhu, G.; Yan, Z.; Meng, X.; Shi, Y.; Fan, D. Genetic algorithm-driven design of NIR-Reflective transparent colored multilayers for enhanced radiative cooling. *Sol. Energy Mater. Sol. Cells* **2025**, *285*, No. 113519, DOI: 10.1016/j.solmat.2025.113519.
(103) Song, J.; Shen, Q.; Shao, H.; Deng, X. Anti-Environmental Aging Passive Daytime Radiative Cooling. *Adv. Sci.* **2024**, *11* (10), No. 2305664, DOI: 10.1002/advs.202305664.
(104) Singh, J.; Wolfe, D. E. Nanostructured Component Fabrication by Electron Beam-Physical Vapor Deposition. *J. Mater. Eng. Perform.* **2005**, *14* (4), 448−459.
(105) Kukla, R. Magnetron sputtering on large scale substrates: an overview on the state of the art. *Surf. Coat. Technol.* **1997**, *93* (1), 1−6.
(106) Rossnagel, S. M. Thin film deposition with physical vapor deposition and related technologies. *J. Vac. Sci. Technol., A* **2003**, *21* (5), S74−S87.
(107) Cai, Z.; Liu, B.; Zou, X.; Cheng, H.-M. Chemical Vapor Deposition Growth and Applications of Two-Dimensional Materials and Their Heterostructures. *Chem. Rev.* **2018**, *118* (13), 6091−6133.
(108) George, S. M. Atomic layer deposition: An overview. *Chem. Rev.* **2010**, *110* (1), 111−131.
(109) Harbeke, G.; Krausbauer, L.; Steigmeier, E. F.; Widmer, A. E.; Kappert, H. F.; Neugebauer, G. Growth and Physical Properties of LPCVD Polycrystalline Silicon Films. *J. Electrochem. Soc.* **1984**, *131* (3), 675−682.
(110) Batey, J.; Tierney, E. Low-temperature deposition of high-quality silicon dioxide by plasma-enhanced chemical vapor deposition. *J. Appl. Phys.* **1986**, *60* (9), 3136−3145.
(111) Hazra, S.; Dahiya, S.; Bijarniya, J. P.; Pramanik, S.; Sarkar, J.; Pal, B. N. Cost-Efficient Ag/Ag-TiO2 Coating-Based Flexible Transparent Heat Reflector for Energy-Saving Smart Windows. *ACS Appl. Energy Mater.* **2024**, *7* (17), 7316−7324.
(112) Hench, L. L.; West, J. K. The sol-gel process. *Chem. Rev.* **1990**, *90* (1), 33−72.
(113) Hall, D. B.; Underhill, P.; Torkelson, J. M. Spin coating of thin and ultrathin polymer films. *Polym. Eng. Sci.* **1998**, *38* (12), 2039−2045.
(114) Park, J.; Shin, K.; Lee, C. Roll-to-roll coating technology and its applications: A review. *Int. J. Precis. Eng. Manuf.* **2016**, *17* (4), 537−550.
(115) Bräuer, G. Large area glass coating. *Surf. Coat. Technol.* **1999**, *112* (1−3), 358−365.
(116) Xi, Y.; Gao, K.; Pang, X.; Yang, H.; Xiong, X.; Li, H.; Volinsky, A. A. Film thickness effect on texture and residual stress sign transition in sputtered TiN thin films. *Ceram. Int.* **2017**, *43* (15), 11992−11997.
(117) Butler, A.; Reicks, A.; Alexander, D.; Gogos, G.; Zuhlke, C.; Argyropoulos, C. Tailoring the spectral and directional emissivity of functionalized laser processed surfaces. *J. Opt. Soc. Am. B* **2024**, *41* (10), 2237.
(118) Kim, J. H.; Kim, D. I.; Lee, S. S.; An, K. S.; Yim, S.; Lee, E.; Kim, S. K. Wide-angle deep ultraviolet antireflective multilayers via discrete-to-continuous optimization. *Nanophotonics* **2023**, *12* (10), 1913−1921.
(119) Zhang, Y.; Chen, Y.; Wang, T.; Zhu, Q.; Gu, M. Ultrahigh performance passive radiative cooling by hybrid polar dielectric metasurface thermal emitters. *Opto-Electron. Adv.* **2024**, *7* (4), No. 230194.
(120) Xiao, W.; Dai, P.; Singh, H. J.; Ajia, I. A.; Yan, X.; Wiecha, P. R.; Huang, R.; de Groot, C. H.; Muskens, O. L.; Sun, K. Flexible thin film optical solar reflectors with Ta2O5-based multimaterial coatings for space radiative cooling. *APL Photonics* **2023**, *8* (9), No. 090802, DOI: 10.1063/5.0156526.
(121) Zhang, Y.-S.; Liu, B.-J.; Sun, X.-J.; Duan, W.-B.; Yang, Y.-T.; Yu, D.-M.; Cai, Q.-Y.; Zhang, H.-T.; Peng, L.; Zhang, R.-J.; Zheng, Y. X. Optimal design and preparation of high-performance multilayered thin film daytime radiative coolers. *Opt. Eng.* **2024**, *63* (09), No. 091606, DOI: 10.1117/1.OE.63.9.091606.
(122) Wan Shamsuddin, W. N. S.; Roccisano, A.; Zuber, K.; Murphy, P. J.; Llusca Jane, M. Environmentally robust Ag−Cu based low-e coatings. *Sol. Energy Mater. Sol. Cells* **2022**, *248*, No. 112033, DOI: 10.1016/j.solmat.2022.112033.
(123) Ishii, S.; Hernández-Pinilla, D.; Tanjaya, N. K.; Nagao, T. Highly reflective multilayer solar reflectors for daytime radiative cooling. *Sol. Energy Mater. Sol. Cells* **2023**, *259*, No. 112463, DOI: 10.1016/j.solmat.2023.112463.
(124) Marshall, K. N.; Breuch, R. A. Optical solar reflector: A highly stable, low alpha sub S/epsilon spacecraft thermal control surface. *J. Spacecr. Rockets* **1968**, *5* (9), 1051−1056.
(125) Chen, I.-t.; Premnath, V. A.; Chang, C.-H. Multilayer dielectric reflector using low-index nanolattices. *Opt. Lett.* **2024**, *49* (4), 1093.
(126) Li, S.; An, M.; Zheng, Z.; Gou, Y.; Lian, W.; Yu, W.; Zhang, P. Daytime radiative cooling multilayer films designed by a machine learning method and genetic algorithm. *Appl. Opt.* **2023**, *62* (16), 4359.
(127) Sreekanth, K. V.; Wu, Q. Y. S.; Jana, S.; Singh, R.; Teng, J. Tunable directional thermal emission using a phase change material-based multilayer structure. *Nanoscale Horiz.* **2025**, *10*, 2615−2620, DOI: 10.1039/D5NH00367A.
(128) Greffet, J.-J.; Carminati, R.; Joulain, K.; Mulet, J.-P.; Mainguy, S.; Chen, Y. Coherent emission of light by thermal sources. *Nature* **2002**, *416* (6876), 61−64.
(129) Ding, Z.; Li, X.; Zhang, H.; Yan, D.; Werlé, J.; Song, Y.; Pattelli, L.; Zhao, J.; Xu, H.; Li, Y. Robust radiative cooling via surface phonon coupling-enhanced emissivity from SiO2 micropillar arrays. *Int. J. Heat Mass Transfer* **2024**, *220*, No. 125004, DOI: 10.1016/j.ijheatmasstransfer.2023.125004.
(130) Shin, S.; Elzouka, M.; Prasher, R.; Chen, R. Far-field coherent thermal emission from polaritonic resonance in individual anisotropic nanoribbons. *Nat. Commun.* **2019**, *10* (1), No. 1377, DOI: 10.1038/s41467-019-09378-5.
(131) Lee, K. W.; Yi, J.; Kim, M. K.; Kim, D. R. Transparent radiative cooling cover window for flexible and foldable electronic displays. *Nat. Commun.* **2024**, *15* (1), No. 4443.
(132) Wu, X.; Li, J.; Xie, F.; Wu, X.-E.; Zhao, S.; Jiang, Q.; Zhang, S.; Wang, B.; Li, Y.; Gao, D.; et al. A dual-selective thermal emitter with enhanced subambient radiative cooling performance. *Nat. Commun.* **2024**, *15* (1), No. 815.
(133) Lin, K. T.; Nian, X.; Li, K.; Han, J.; Zheng, N.; Lu, X.; Guo, C.; Lin, H.; Jia, B. Highly efficient flexible structured metasurface by roll-to-roll printing for diurnal radiative cooling. *eLight* **2023**, *3* (1), No. 22, DOI: 10.1186/s43593-023-00053-3.
(134) Yu, S.; Yu, J.-S.; Chen, Z.; Li, Q.; Wang, Z.; Luo, X.; Kim, S.-K.; Hu, R. Ultrahigh Visible-Transparency, Submicrometer, and Polymer-Free Radiative Cooling Meta-Glass Coating for Building Energy Saving. *ACS Photonics* **2024**, *11* (8), 3412−3423.
(135) Guan, Q.; Raza, A.; Mao, S. S.; Vega, L. F.; Zhang, T. Machine learning-enabled inverse design of radiative cooling film with on-demand transmissive color. *ACS Photonics* **2023**, *10* (3), 715−726.
(136) Huang, G.; Yengannagari, A. R.; Matsumori, K.; Patel, P.; Datla, A.; Trindade, K.; Amarsanaa, E.; Zhao, T.; Köhler, U.; Busko, D.; Richards, B. S. Radiative cooling and indoor light management enabled by a transparent and self-cleaning polymer-based metamaterial. *Nat. Commun.* **2024**, *15* (1), No. 3798, DOI: 10.1038/s41467-024-48150-2.
(137) Xiong, L.; Wei, Y.; Chen, C.; Chen, X.; Fu, Q.; Deng, H. Thin lamellar films with enhanced mechanical properties for durable radiative cooling. *Nat. Commun.* **2023**, *14* (1), No. 6129, DOI: 10.1038/s41467-023-41797-3.
(138) Kuznetsov, A. I.; Brongersma, M. L.; Yao, J.; Chen, M. K.; Levy, U.; Tsai, D. P.; Zheludev, N. I.; Faraon, A.; Arbabi, A.; Yu, N.; et al. Roadmap for optical metasurfaces. *ACS Photonics* **2024**, *11* (3), 816−865.
(139) Jung, C.; Kim, G.; Jeong, M.; Jang, J.; Dong, Z.; Badloe, T.; Yang, J. K.; Rho, J. Metasurface-driven optically variable devices. *Chem. Rev.* **2021**, *121* (21), 13013−13050.
(140) Ko, B.; Lee, D.; Badloe, T.; Rho, J. Metamaterial-based radiative cooling: towards energy-free all-day cooling. *Energies* **2019**, *12* (1), 89.

(141) Meinzer, N.; Barnes, W. L.; Hooper, I. R. Plasmonic meta-atoms and metasurfaces. *Nat. Photonics* **2014**, *8* (12), 889−898.
(142) Costantini, D.; Lefebvre, A.; Coutrot, A.-L.; Moldovan-Doyen, I.; Hugonin, J.-P.; Boutami, S.; Marquier, F.; Benisty, H.; Greffet, J.-J. Plasmonic metasurface for directional and frequency-selective thermal emission. *Phys. Rev. Appl.* **2015**, *4* (1), No. 014023.
(143) Lee, H.; Kim, T.; Tolessa, M. F.; Cho, H. H. Enhancing radiative cooling performance using metal-dielectric-metal metamaterials. *J. Mech. Sci. Technol.* **2017**, *31* (11), 5107−5112.
(144) Sun, K.; Riedel, C. A.; Wang, Y.; Urbani, A.; Simeoni, M.; Mengali, S.; Zalkovskij, M.; Bilenberg, B.; De Groot, C.; Muskens, O. L. Metasurface optical solar reflectors using AZO transparent conducting oxides for radiative cooling of spacecraft. *ACS Photonics* **2018**, *5* (2), 495−501.
(145) Ding, F.; Yang, Y.; Deshpande, R. A.; Bozhevolnyi, S. I. A review of gap-surface plasmon metasurfaces: fundamentals and applications. *Nanophotonics* **2018**, *7* (6), 1129−1156.
(146) Cho, J.-W.; Park, S.-J.; Park, S.-J.; Kim, Y.-B.; Moon, Y.-J.; Kim, S.-K. Cooling metals via gap plasmon resonance. *Nano Lett.* **2021**, *21* (9), 3974−3980.
(147) Arrés Chillón, J.; Paulillo, B.; Mazumder, P.; Pruneri, V. Transparent glass surfaces with silica nanopillars for radiative cooling. *ACS Appl. Nano Mater.* **2022**, *5* (12), 17606−17612.
(148) Babicheva, V. E.; Evlyukhin, A. B. Mie-resonant metaphotonics. *Adv. Opt. Photonics* **2024**, *16* (3), 539−658.
(149) Wang, X.; Liu, X.; Li, Z.; Zhang, H.; Yang, Z.; Zhou, H.; Fan, T. Scalable flexible hybrid membranes with photonic structures for daytime radiative cooling. *Adv. Funct. Mater.* **2020**, *30* (5), No. 1907562.
(150) Li, T.; Zhai, Y.; He, S.; Gan, W.; Wei, Z.; Heidarinejad, M.; Dalgo, D.; Mi, R.; Zhao, X.; Song, J.; et al. A radiative cooling structural material. *Science* **2019**, *364* (6442), 760−763.
(151) So, S.; Mun, J.; Rho, J. Simultaneous inverse design of materials and structures via deep learning: demonstration of dipole resonance engineering using core−shell nanoparticles. *ACS Appl. Mater. Interfaces* **2019**, *11* (27), 24264−24268.
(152) Su, W.; Ding, Z.; Luo, Y.; Ye, L.; Wu, H.; Yao, H. Machine learning-enabled design of metasurface based near-perfect daytime radiative cooler. *Sol. Energy Mater. Sol. Cells* **2023**, *260*, No. 112488.
(153) Ding, Z.; Li, X.; Ji, Q.; Zhang, Y.; Li, H.; Zhang, H.; Pattelli, L.; Li, Y.; Xu, H.; Zhao, J. Machine-learning-assisted design of a robust biomimetic radiative cooling metamaterial. *ACS Mater. Lett.* **2024**, *6* (6), 2416−2424.
(154) Yang, Y.; Jeon, Y.; Dong, Z.; Yang, J. K.; Haddadi Moghaddam, M.; Kim, D.-S.; Oh, D. K.; Lee, J.; Hentschel, M.; Giessen, H.; et al. Nanofabrication for Nanophotonics. *ACS Nano* **2025**, *19* (13), 12491−12605.
(155) Oh, D. K.; Lee, T.; Ko, B.; Badloe, T.; Ok, J. G.; Rho, J. Nanoimprint lithography for high-throughput fabrication of metasurfaces. *Front. Optoelectron.* **2021**, *14* (2), 229−251.
(156) Kim, J.; Seong, J.; Kim, W.; Lee, G.-Y.; Kim, S.; Kim, H.; Moon, S.-W.; Oh, D. K.; Yang, Y.; Park, J.; et al. Scalable manufacturing of high-index atomic layer−polymer hybrid metasurfaces for metaphotonics in the visible. *Nat. Mater.* **2023**, *22* (4), 474−481.
(157) Gao, M.; Han, X.; Chen, F.; Zhou, W.; Liu, P.; Shan, Y.; Chen, Y.; Li, J.; Zhang, R.; Wang, S.; et al. Approach to fabricating high-performance cooler with near-ideal emissive spectrum for above-ambient air temperature radiative cooling. *Sol. Energy Mater. Sol. Cells* **2019**, *200*, No. 110013.
(158) Choi, M.; Kim, J.; Moon, S.; Shin, K.; Nam, S.-W.; Park, Y.; Kang, D.; Jeon, G.; Lee, K.-i.; Yoon, D. H.; et al. Roll-to-plate printable RGB achromatic metalens for wide-field-of-view holographic near-eye displays. *Nat. Mater.* **2025**, *24*, 535−543.
(159) Guan, J.; Park, J.-E.; Deng, S.; Tan, M. J.; Hu, J.; Odom, T. W. Light−matter interactions in hybrid material metasurfaces. *Chem. Rev.* **2022**, *122* (19), 15177−15203.
(160) Zhang, Y.; Sun, J.; Wang, Y.; Wu, Y.; Huang, C.; Zhang, C.; Liu, T. A Radiative-Cooling Hierarchical Aligned Porous Poly(vinylidene fluoride) Film by Freeze-Thaw-Promoted Nonsolvent-Induced Phase Separation. *Chin. J. Polym. Sci.* **2024**, *42* (7), 976−983.
(161) Zhou, L.; Zhao, J.; Huang, H.; Nan, F.; Zhou, G.; Ou, Q. Flexible Polymer Photonic Films with Embedded Microvoids for High-Performance Passive Daytime Radiative Cooling. *ACS Photonics* **2021**, *8* (11), 3301−3307, DOI: 10.1021/acsphotonics.1c01149.
(162) Li, X.; Shao, S.; Huang, M.; Zhang, S.; Guo, W. Integration of daytime radiative cooling and solar heating. *iScience* **2023**, *26*, No. 105894, DOI: 10.1016/j.isci.2022.105894.
(163) Li, L.; Liu, G.; Zhang, Q.; Zhao, H.; Shi, R.; Wang, C.; Li, Z.; Zhou, B.; Zhang, Y. Porous Structure of Polymer Films Optimized by Rationally Tuning Phase Separation for Passive All-Day Radiative Cooling. *ACS Appl. Mater. Interfaces* **2024**, *16* (5), 6504−6512, DOI: 10.1021/acsami.3c19173.
(164) Lin, K.; Chen, S.; Zeng, Y.; Ho, T. C.; Zhu, Y.; Wang, X.; Liu, F.; Huang, B.; Chao, C. Y. H.; Wang, Z.; Tso, C. Y. Hierarchically structured passive radiative cooling ceramic with high solar reflectivity. *Science* **2023**, *382* (6671), 691−697, DOI: 10.1126/science.adi4725.
(165) Fu, Y.; Yang, J.; Su, Y. S.; Du, W.; Ma, Y. G. Daytime passive radiative cooler using porous alumina. *Sol. Energy Mater. Sol. Cells* **2019**, *191*, 50−54, DOI: 10.1016/j.solmat.2018.10.027.
(166) Ma, H.; Wang, L.; Dou, S.; Zhao, H.; Huang, M.; Xu, Z.; Zhang, X.; Xu, X.; Zhang, A.; Yue, H.; et al. Flexible Daytime Radiative Cooling Enhanced by Enabling Three-Phase Composites with Scattering Interfaces between Silica Microspheres and Hierarchical Porous Coatings. *ACS Appl. Mater. Interfaces* **2021**, *13* (16), 19282−19290, DOI: 10.1021/acsami.1c02145.
(167) Lee, D.; Go, M.; Son, S.; Kim, M.; Badloe, T.; Lee, H.; Kim, J. K.; Rho, J. Sub-ambient daytime radiative cooling by silica-coated porous anodic aluminum oxide. *Nano Energy* **2021**, *79*, No. 105426, DOI: 10.1016/j.nanoen.2020.105426.
(168) Huang, L.; Hu, Y.; Yao, X.; Chesman, A. S. R.; Wang, H.; Sagoe-Crentsil, K.; Duan, W. Designing Nanoporous Polymer Films for High-Performance Passive Daytime Radiative Cooling. *ACS Appl. Mater. Interfaces* **2024**, *16* (40), 54401−54411.
(169) Yue, Q.; Zhang, L.; He, C. Y.; Liu, B. H.; Wang, W. M.; Lu, Z. W.; Liu, G.; Gao, X. H. Polymer composites with hierarchical architecture and dielectric particles for efficient daytime subambient radiative cooling. *J. Mater. Chem. A* **2023**, *11* (6), 3126−3135, DOI: 10.1039/D2TA07453B.
(170) Weng, Y.; Zhang, W.; Jiang, Y.; Zhao, W.; Deng, Y. Effective daytime radiative cooling via a template method based PDMS sponge emitter with synergistic thermo-optical activity. *Sol. Energy Mater. Sol. Cells* **2021**, *230*, No. 111205, DOI: 10.1016/j.solmat.2021.111205.
(171) Jing, W.; Zhang, S.; Zhang, W.; Chen, Z.; Zhang, C.; Wu, D.; Gao, Y.; Zhu, H. Scalable and Flexible Electrospun Film for Daytime Subambient Radiative Cooling. *ACS Appl. Mater. Interfaces* **2021**, *13* (25), 29558−29566, DOI: 10.1021/acsami.1c05364.
(172) Pawlak, A.; Galeski, A.; Rozanski, A. Cavitation during deformation of semicrystalline polymers. *Prog. Polym. Sci.* **2014**, *39*, 921−958, DOI: 10.1016/j.progpolymsci.2013.10.007.
(173) Strobl, G. *The physics of polymers: Concepts for understanding their structures and behavior*; Springer Berlin Heidelberg, 2007.
(174) Xiang, B.; Zhang, R.; Luo, Y.; Zhang, S.; Xu, L.; Min, H.; Tang, S.; Meng, X. 3D porous polymer film with designed pore architecture and auto-deposited SiO2 for highly efficient passive radiative cooling. *Nano Energy* **2021**, *81*, No. 105600.
(175) Banik, U.; Agrawal, A.; Meddeb, H.; Sergeev, O.; Reininghaus, N.; Götz-Köhler, M.; Gehrke, K.; Stührenberg, J.; Vehse, M.; Sznajder, M.; Agert, C. Efficient Thin Polymer Coating as a Selective Thermal Emitter for Passive Daytime Radiative Cooling. *ACS Appl. Mater. Interfaces* **2021**, *13* (20), 24130−24137, DOI: 10.1021/acsami.1c04056.
(176) Hsu, P. C.; Song, A. Y.; Catrysse, P. B.; Liu, C.; Peng, Y.; Xie, J.; Fan, S.; Cui, Y. Radiative human body cooling by nanoporous polyethylene textile. *Science* **2016**, *353* (6303), 1019−1023, DOI: 10.1126/science.aaf5471.
(177) Pawlak, A. Cavitation during tensile deformation of isothermally crystallized polypropylene and high-density polyethylene.

Colloid Polym. Sci. **2013**, *291* (4), 773−787, DOI: 10.1007/s00396-012-2789-5.
(178) Miranda-Muñoz, J. M.; Viaña, J. M.; Calvo, M. E.; Lozano, G.; Míguez, H. Transparent porous films with real refractive index close to unity for photonic applications. *Mater. Horiz.* **2024**, *11* (22), 5722−5731.
(179) Feng, Y.; Ren, J.; Li, H.; Zhao, D.; Sheng, L.; Wu, Y.; Zhao, W.; Deng, M. Effect of thermal annealing on gas separation performance and aggregation structures of block polyimide membranes. *Polymer* **2021**, *219*, No. 123538, DOI: 10.1016/j.polymer.2021.123538.
(180) Shin, S. H.; Nur, P. J.; Kodir, A.; Kwak, D. H.; Lee, H.; Shin, D.; Bae, B. Improving the Mechanical Durability of Short-Side-Chain Perfluorinated Polymer Electrolyte Membranes by Annealing and Physical Reinforcement. *ACS Omega* **2019**, *4* (21), 19153−19163, DOI: 10.1021/acsomega.9b02436.
(181) Sadeghi, F.; Ajji, A.; Carreau, P. J. Analysis of microporous membranes obtained from polypropylene films by stretching. *J. Membr. Sci.* **2007**, *292* (1−2), 62−71, DOI: 10.1016/j.memsci.2007.01.023.
(182) Qi, C.; Ruijie, X.; Shuqiu, W.; Changbin, C.; Haibin, M.; Caihong, L.; Liangbin, L.; Li, Z. Influence of annealing temperature on the lamellar and connecting bridge structure of stretched polypropylene microporous membrane. *Polym. Int.* **2015**, *64* (3), 446−452, DOI: 10.1002/pi.4828.
(183) Haase, M. F.; Jeon, H.; Hough, N.; Kim, J. H.; Stebe, K. J.; Lee, D. Multifunctional nanocomposite hollow fiber membranes by solvent transfer induced phase separation. *Nat. Commun.* **2017**, *8* (1), No. 1234, DOI: 10.1038/s41467-017-01409-3.
(184) Jaramillo-Fernandez, J.; Yang, H.; Schertel, L.; Whitworth, G. L.; Garcia, P. D.; Vignolini, S.; Sotomayor-Torres, C. M. Highly-Scattering Cellulose-Based Films for Radiative Cooling. *Adv. Sci.* **2022**, *9* (8), No. 2104758, DOI: 10.1002/advs.202104758.
(185) Bohr, S. J.; Wang, F.; Metze, M.; Vukušić, J. L.; Sapalidis, A.; Ulbricht, M.; Nestler, B.; Barbe, S. State-of-the-art review of porous polymer membrane formation characterization—How numerical and experimental approaches dovetail to drive innovation. *Front. Sustainability* **2023**, *4*, No. 1093911.
(186) Hong, D.; Lee, Y. J.; Jeon, O. S.; Lee, I. S.; Lee, S. H.; Won, J. Y.; Jeon, Y. P.; La, Y.; Kim, S.; Park, G. S.; et al. Humidity-tolerant porous polymer coating for passive daytime radiative cooling. *Nat. Commun.* **2024**, *15* (1), No. 4457, DOI: 10.1038/s41467-024-48621-6.
(187) Hu, W.; Zhang, F.; Tan, X.; Tu, Y.; Nie, S. Antibacterial PVDF Coral-Like Hierarchical Structure Composite Film Fabrication for Self-Cleaning and Radiative Cooling Effect. *ACS Appl. Mater. Interfaces* **2024**, *16* (15), 19828−19837.
(188) Smolders, C. A.; Reuvers, A. J.; Boom, R. M.; Wienk, I. M. Microstructures in phase-inversion membranes. Part 1. Formation of macrovoids. *J. Membr. Sci.* **1992**, *73* (2−3), 259−275, DOI: 10.1016/0376-7388(92)80134-6.
(189) Saljoughi, E.; Amirilargani, M.; Mohammadi, T. Effect of PEG additive and coagulation bath temperature on the morphology, permeability and thermal/chemical stability of asymmetric CA membranes. *Desalination* **2010**, *262* (1−3), 72−78, DOI: 10.1016/j.desal.2010.05.046.
(190) Lei, C.; Wu, S.; Xu, R.; Peng, X.; Shi, W.; Hu, B. Influence of low molecular weight tail of polypropylene resin on the pore structure by room-temperature stretching. *Polym. Eng. Sci.* **2013**, *53* (12), 2594−2602, DOI: 10.1002/pen.23527.
(191) Díaz-Lobo, A.; Martin-Gonzalez, M.; Morales-Sabio, Á.; Manzano, C. V. Suitability of Anodic Porous Alumina as a Passive Radiative Cooler: An In-Depth Study. *ACS Appl. Opt. Mater.* **2024**, *2* (6), 980−990.
(192) Zhang, Y.; Wang, T.; Mei, X.; Chen, M.; Wu, L. Ordered Porous Polymer Films for Highly Efficient Passive Daytime Radiative Cooling. *ACS Photonics* **2023**, *10* (9), 3124−3132.
(193) Yu, T.; Liu, R.; Wang, X.; Yang, Z.; Gu, X.; Yang, S.; Ye, Z.; Wen, Z.; Lu, J. Transparent Radiative Cooling Films Based on Dendritic Silica for Room Thermal Management. *Carbon Neutraliz.* **2025**, *4* (4), No. e70020, DOI: 10.1002/cnl2.70020.
(194) Yang, J. H.; Pu, Q. R.; Hu, W. J.; Liu, Q. Q.; Li, X.; Huang, W. H.; Zhang, N.; Wang, Y. "Pore in Pore" Engineering in Poly(dimethylsiloxane)/Silicon Oxide Foams for Passive Daytime Radiative Cooling. *ACS Appl. Polym. Mater.* **2025**, *7* (11), 6887−6897.
(195) Ye, Q.; Guo, N.; Chen, M. Reversible solar heating and radiative cooling coupled with latent heat for self-adaptive thermoregulation. *Appl. Phys. Lett.* **2025**, *126* (11), No. 113903, DOI: 10.1063/5.0262028.
(196) Lee, J.; Jung, Y.; Lee, M. J.; Hwang, J. S.; Guo, J.; Shin, W.; Min, J. K.; Pyun, K. R.; Lee, H.; Lee, Y.; et al. Biomimetic reconstruction of butterfly wing scale nanostructures for radiative cooling and structural coloration. *Nanoscale Horiz.* **2022**, *7* (9), 1054−1064.
(197) Wang, T.; Wu, Y.; Shi, L.; Hu, X.; Chen, M.; Wu, L. A structural polymer for highly efficient all-day passive radiative cooling. *Nat. Commun.* **2021**, *12* (1), No. 365.
(198) Zhong, H.; Meng, T.; Ding, W.; Xiao, Y.; Zhang, P. Achieving a Porous PDMS Film for Passive Cooling through the Utilization of Ultrafine NaCl Sacrificial Templates. *ACS Omega* **2025**, *10* (1), 1012−1018.
(199) Chen, M.; Pang, D.; Yan, H. Sustainable and self-cleaning bilayer coatings for high-efficiency daytime radiative cooling. *J. Mater. Chem. C* **2022**, *10* (21), 8329−8338.
(200) Song, X.; Gong, H.; Li, H.; Zhang, M.; Jiang, L.; Wang, C.; Jiang, P.; Wang, H.; Cao, K.; Liu, G.; et al. Molecularly and Structurally Designed Polyimide Nanofiber Radiative Cooling Films for Spacecraft Thermal Management. *Adv. Funct. Mater.* **2025**, *35* (2), No. 2413191, DOI: 10.1002/adfm.202413191.
(201) Pyun, K. R.; Jeong, S.; Yoo, M. J.; Choi, S. H.; Baik, G.; Lee, M.; Song, J.; Ko, S. H. Tunable Radiative Cooling by Mechanochromic Electrospun Micro-Nanofiber Matrix. *Small* **2024**, *20* (20), No. 2308572, DOI: 10.1002/smll.202308572.
(202) Yan, Z.; Zhu, G.; Fan, D.; Li, Q. Bioinspired Metafabric with Dual-Gradient Janus Design for Personal Radiative and Evaporative Cooling. *Adv. Funct. Mater.* **2025**, *35* (2), No. 2412261, DOI: 10.1002/adfm.202412261.
(203) Hyeon, C.; Jeong, M.; Kwon, S.; Baek, J.; Seong, M.; Kim, M.; Lee, D. Thermal protection of wearable devices under outdoor conditions using radiative cooling films. *Opt. Mater.* **2025**, *167*, No. 117258, DOI: 10.1016/j.optmat.2025.117258.
(204) Liang, S.; Lu, Y.; Zhang, Q.; Miao, J.; Liao, H.; Wu, Y.; Shi, X.; Zhou, Y. A Sandwich Fabric with Beaded Nanofibers Encapsulating Large-Sized SiO2 Photons for Green Radiative Cooling. *ACS Appl. Mater. Interfaces* **2025**, *17* (24), 35902−35911.
(205) Hasan, K. M. F.; Chen, J.; Chen, S.; Lin, K.; Wong, M. Y.; Liang, L.; Zhu, Y.; Pan, A.; Minale, Y. F.; Ho, T. C.; et al. Advanced Bioinspired Personal Thermoregulation Textiles for Outdoor Radiative Cooling. *ACS Appl. Mater. Interfaces* **2025**, *17* (2), 3436−3447.
(206) Zhang, J.; Dong, H.; Yu, Y.; Yin, S.; Cao, M.; Li, C.; Shen, X.; Li, J.; Xu, Y.; Chen, S.; Xu, F. An Eco-Friendly and Multifunctional Textile Integrating Radiative Heating and Cooling for Large-Temperature-Variation Personal Thermal Management. *Adv. Funct. Mater.* **2025**, *35* (24), No. 2419777, DOI: 10.1002/adfm.202419777.
(207) Wei, X.; Wang, F.; Wu, D.; Zhang, C.; Zhu, H. Radiative Cooling of Outdoor Electronic Devices by Polyimide Fiber Films Fabricated via an Electrospinning-Electrospray Process. *ACS Appl. Mater. Interfaces* **2025**, *17* (14), 21313−21322.
(208) Xu, M.; Liu, J.; Wang, J.; Hu, B.; Zhang, J.; Wang, W.; Xu, L.; Sun, S.; Lin, Z.; Yang, M.; et al. Fabrication of a Recyclable Hierarchical Superhydrophobic Radiative Cooling Fabric via Electrospinning and Electrospraying. *ACS Appl. Polym. Mater.* **2025**, *7* (15), 9784−9796.
(209) Zhu, Z. J.; Li, Z.; Wu, X.; Liu, C.; Chen, N.; Zhang, Y.; Chen, Y.; Ouyang, X.; Bashir, A.; Chen, D. Z. High-Performance Radiative Cooling Using a SiO2/PHBV Fiber Membrane with a Micronano-Multistage Structure. *ACS Appl. Mater. Interfaces* **2025**, *17* (23), 34625−34636.
(210) Zhang, Q.; Wang, T.; Du, R.; Zheng, J.; Wei, H.; Cao, X.; Liu, X. Highly Stable Polyimide Composite Nanofiber Membranes with Spectrally Selective for Passive Daytime Radiative Cooling. *ACS Appl. Mater. Interfaces* **2024**, *16* (30), 40069−40076.

(211) Xin, Y.; Wang, Q.; Fu, C.; Du, S.; Hou, L.; Wei, X.; Wang, H.; Wang, X. Alumina Fiber Membrane Prepared by Electrospinning Technology for Passive Daytime Radiative Cooling. *Adv. Funct. Mater.* **2025**, *35* (3), No. 2413813, DOI: 10.1002/adfm.202413813.

(212) Zhu, H.; Wang, Y.; Qu, M.; Pan, Y.; Zheng, G.; Dai, K.; Huang, M.; Alhadhrami, A.; Ibrahim, M. M.; El-Bahy, Z. M.; et al. Electrospun poly(vinyl alcohol)/silica film for radiative cooling. *Adv. Compos. Hybrid Mater.* **2022**, *5* (3), 1966−1975, DOI: 10.1007/s42114-022-00529-9.

(213) Thiyagarajan, D.; Li, S.; Lee, B. K. Fibrous Sphere Architectures for Efficient Daytime Radiative Cooling and Moisture Management. *Nano Lett.* **2025**, *25* (14), 5609−5615.

(214) Dai, Y.; Zhang, Y.; Ye, Z.; Zhu, Z.; Yang, L.; Wei, Y.; Qin, H.; Xiong, C. Radiative Cooling Nanohybrids with Room-Temperature Switching. *ACS Appl. Mater. Interfaces* **2025**, *17* (8), 12698−12706.

(215) Chen, K.; Ren, J.; Li, G.-X.; Li, Q.; Zhou, Y.; Yu, X.-Q.; Liu, C.; Chen, S. Flexible Dual-Layer Fabric Based on AlPO4 Hollow Microspheres toward Daytime Radiative Cooling. *ACS Appl. Polym. Mater.* **2025**, *7* (15), 9681−9692, DOI: 10.1021/acsapm.5c01170.

(216) Wu, M.; Li, Y.; Huang, G.; Xu, R.; Yin, X.; Zhang, G. A leaf-like structured membrane for highly efficient and persistent radiative cooling. *Mater. Horiz.* **2025**, *12* (9), 3024−3035.

(217) Zhu, Y. Y.; Xue, C. H.; Liu, B. Y.; Guo, X. J.; Qu, Y. Y.; Wang, H. D.; Ma, C. Q.; Huang, M. C.; Cheng, J. Superhydrophobic and Flame-Retardant Poly(vinylidene Fluoride-co-hexafluoropropylene)/SiO2/Aluminum Phosphate Composite Film for Daytime Radiative Cooling. *ACS Appl. Mater. Interfaces* **2025**, *17* (13), 20284−20295.

(218) Song, S.; Hou, C.; Yang, A.; Wei, L.; Liu, H.; Xie, D.; Song, Y. Ultraviolet durable and recyclable radiative cooling covering for efficient building energy saving. *Mater. Horiz.* **2025**, *12* (8), 2535−2544.

(219) Cai, W.; Wang, J.; Wang, W.; Li, S.; Rahman, M. Z.; Tawiah, B.; Ming, Y.; Zhou, X.; Xing, W.; Hu, Y.; et al. Colored Radiative Cooling and Flame-Retardant Polyurethane-Based Coatings: Selective Absorption/Reflection in Solar Waveband. *Small* **2024**, *20* (46), No. 2402349, DOI: 10.1002/smll.202402349.

(220) Zhao, X.; Li, J.; Dong, K.; Wu, J. Switchable and Tunable Radiative Cooling: Mechanisms, Applications, and Perspectives. *ACS Nano* **2024**, *18*, 18118−18128.

(221) Deng, Y.; Yang, Y.; Xiao, Y.; Zeng, X.; Xie, H. L.; Lan, R.; Zhang, L.; Yang, H. Annual Energy-Saving Smart Windows with Actively Controllable Passive Radiative Cooling and Multimode Heating Regulation. *Adv. Mater.* **2024**, *36* (27), No. 2401869, DOI: 10.1002/adma.202401869.

(222) Si, X.; Zhu, H.; Yang, Z.; Wei, H.; Chen, B.; Wang, R.; Bao, R.; Gu, J.; Zhan, Y. Adaptive Radiative Cooling via Spectral Decoupling in Bilayered Polymer/VO2 NP Nanocomposites. *ACS Appl. Mater. Interfaces* **2025**, *17* (8), 12117−12124.

(223) Tang, W.; Zhan, Y.; Yang, J.; Meng, X.; Zhu, X.; Li, Y.; Lin, T.; jiang, L.; Zhao, Z.; Wang, S. Cascaded Heteroporous Nanocomposites for Thermo-Adaptive Passive Radiation Cooling. *Adv. Mater.* **2024**, *36* (36), No. 2310923, DOI: 10.1002/adma.202310923.

(224) Park, S.; Choi, J.; Lee, J.; Seo, J.; Lee, J.; Kim, J.; Hong, M.; Lee, D.; Park, J.; Park, J.; Choi, W. Gradient Porous and Carbon Black-Integrated Cellulose Acetate Aerogel for Scalable Radiative Cooling. *Small* **2025**, *21* (7), No. 2409873, DOI: 10.1002/smll.202409873.

(225) Lin, H.; Shen, Q.; Ma, M.; Ji, R.; Guo, H.; Qi, H.; Xing, W.; Tang, H. 3D Printing of Porous Ceramics for Enhanced Thermal Insulation Properties. *Adv. Sci.* **2025**, *12*, No. 2412554, DOI: 10.1002/advs.202412554.

(226) Ni, J.; Zhao, B.; Zhang, Z.; Song, Z.; Wang, W.; Wang, J. Melt-Processed, One-Step, In Situ Hierarchically Structured Porous Polymer Nanocomposite for Radiative Cooling in Hot Weather. *Small* **2025**, *21* (14), No. 2500020, DOI: 10.1002/smll.202500020.

(227) Huang, K.; Du, Y.; Wang, W.; Liu, J.; Tang, H.; Wang, C.; Yang, X.; Yao, G.; Lin, Z.; Zhou, Z. Stretchable and Self-Cleaning Daytime Radiative Coolers for Human Fabric and Building Applications. *ACS Appl. Mater. Interfaces* **2024**, *16* (36), 48235−48245.

(228) Wu, W. L.; Tsai, S. Y.; Lo, Y. C.; Wang, H. C.; Chen, H. L.; Wan, D.; Ko, F. H. Design of a Multifunctional Resin-Based Outdoor Spherical Robot Shell for Ultrahigh Visible to Near-Infrared Transmittance and Mid-Infrared Radiative Cooling. *ACS Omega* **2025**, *10* (3), 3080−3089.

(229) Chae, D.; Kim, M.; Lim, H.; Lee, D.; Son, S.; Ha, J.; Rho, J.; Lee, H. Selectively emissive fluoropolymer film for passive daytime radiative cooling. *Opt. Mater.* **2022**, *128*, No. 112273.

(230) Zhu, L.; Raman, A. P.; Fan, S. Radiative cooling of solar absorbers using a visibly transparent photonic crystal thermal blackbody. *Proc. Natl. Acad. Sci. U.S.A.* **2015**, *112* (40), 12282−12287.

(231) Song, W.-Z.; Wang, X.-X.; Qiu, H.-J.; Wang, N.; Yu, M.; Fan, Z.; Ramakrishna, S.; Hu, H.; Long, Y.-Z. Single electrode piezoelectric nanogenerator for intelligent passive daytime radiative cooling. *Nano Energy* **2021**, *82*, No. 105695.

(232) Xu, J.; Xie, W.; Han, H.; Xiao, C.; Li, J.; Zhang, Y.; Chen, S.; Zhao, B.; Zhang, D.; Zhou, H. Radiative Cooling Materials for Extreme Environmental Applications. *Nano-Micro Lett.* **2025**, *17* (1), No. 324.

(233) Xie, A.-Q.; Qiu, H.; Jiang, W.; Wang, Y.; Niu, S.; Zhang, K.-Q.; Ho, G. W.; Wang, X.-Q. Recent Advances in Spectrally Selective Daytime Radiative Cooling Materials. *Nano-Micro Lett.* **2025**, *17* (1), No. 264.

(234) Xie, W.; Xiao, C.; Sun, Y.; Fan, Y.; Zhao, B.; Zhang, D.; Fan, T.; Zhou, H. Flexible photonic radiative cooling films: fundamentals, fabrication and applications. *Adv. Funct. Mater.* **2023**, *33* (46), No. 2305734.

(235) Lin, C.; Li, Y.; Chi, C.; Kwon, Y. S.; Huang, J.; Wu, Z.; Zheng, J.; Liu, G.; Tso, C. Y.; Chao, C. Y.; Huang, B. A solution-processed inorganic emitter with high spectral selectivity for efficient subambient radiative cooling in hot humid climates. *Adv. Mater.* **2022**, *34* (12), No. 2109350.

(236) Li, D.; Liu, X.; Li, W.; Lin, Z.; Zhu, B.; Li, Z.; Li, J.; Li, B.; Fan, S.; Xie, J.; Zhu, J. Scalable and hierarchically designed polymer film as a selective thermal emitter for high-performance all-day radiative cooling. *Nat. Nanotechnol.* **2021**, *16* (2), 153−158.

(237) Mandal, J.; Anand, J.; Mandal, S.; Brewer, J.; Ramachandran, A.; Raman, A. P. Radiative cooling and thermoregulation in the earth's glow. *Cell Rep. Phys. Sci.* **2024**, *5* (7), No. 102065, DOI: 10.1016/j.xcrp.2024.102065.

(238) Wu, X.; Li, J.; Jiang, Q.; Zhang, W.; Wang, B.; Li, R.; Zhao, S.; Wang, F.; Huang, Y.; Lyu, P.; et al. An all-weather radiative human body cooling textile. *Nat. Sustainability* **2023**, *6* (11), 1446−1454.

(239) Wu, R.; Sui, C.; Chen, T.-H.; Zhou, Z.; Li, Q.; Yan, G.; Han, Y.; Liang, J.; Hung, P.-J.; Luo, E.; et al. Spectrally engineered textile for radiative cooling against urban heat islands. *Science* **2024**, *384* (6701), 1203−1212.

(240) Mira, Z. F.; Heo, S.-Y.; Kim, D. H.; Lee, G. J.; Lee, G. J.; Song, Y. M. Multilayer selective passive daytime radiative cooler optimization utilizing memetic algorithm. *J. Quant. Spectrosc. Radiat. Transfer* **2021**, *272*, No. 107774.

(241) Yin, H.; Yao, H.; Jia, Y.; Wang, J.; Fan, C. Realization of efficient radiative cooling in thermal emitter with inorganic metamaterials. *J. Phys. D: Appl. Phys.* **2021**, *54* (34), No. 345501.

(242) Catalanotti, S.; Cuomo, V.; Piro, G.; Ruggi, D.; Silvestrini, V.; Troise, G. The radiative cooling of selective surfaces. *Sol. Energy* **1975**, *17* (2), 83−89.

(243) Bartoli, B.; Catalanotti, S.; Coluzzi, B.; Cuomo, V.; Silvestrini, V.; Troise, G. Nocturnal and diurnal performances of selective radiators. *Appl. Energy* **1977**, *3* (4), 267−286.

(244) Berdahl, P.; Martin, M.; Sakkal, F. Thermal performance of radiative cooling panels. *Int. J. Heat Mass Transfer* **1983**, *26* (6), 871−880.

(245) An, Y.; Sheng, C.; Li, X. Radiative Cooling of Solar Cells: Opto-Electro-Thermal Physics and Modeling. *Nanoscale* **2019**, *11* (36), 17073−17083.

(246) Yi, Z.; lv, Y.; Xu, D.; Xu, J.; Qian, H.; Zhao, D.; Yang, R. Energy saving analysis of a transparent radiative cooling film for buildings with roof glazing. *Energy Built Environ.* **2021**, *2* (2), 214−222.

(247) Zhou, Z.; Wang, X.; Ma, Y.; Hu, B.; Zhou, J. Transparent Polymer Coatings for Energy-Efficient Daytime Window Cooling. *Cell Rep. Phys. Sci.* **2020**, *1* (11), No. 100231, DOI: 10.1016/j.xcrp.2020.100231.
(248) Kim, S.; Shang, W.; Moon, S.; Pastega, T.; Lee, E.; Luo, T. High-Performance Transparent Radiative Cooler Designed by Quantum Computing. *ACS Energy Lett.* **2022**, *7* (12), 4134−4141.
(249) Kim, S.; Jung, S.; Bobbitt, A.; Lee, E.; Luo, T. Wide-angle spectral filter for energy-saving windows designed by quantum annealing-enhanced active learning. *Cell Rep. Phys. Sci.* **2024**, *5* (3), No. 101847, DOI: 10.1016/j.xcrp.2024.101847.
(250) Zhang, H.; Liu, G.; Chen, S.; Lin, C. Optimization of a stacked multilayer for use in radiative cooling window. *Opt. Quant. Electron.* **2024**, *56* (8), No. 1331.
(251) Seo, S.-B.; Lee, J.-G.; Yu, J.-S.; Kim, J.-H.; Jung, S.; Kang, G.; Ko, H.; Hu, R.; Lee, E.; Kim, S.-K. Visible transparency modulated cooling windows using pseudorandom dielectric multilayers. *Nanophotonics* **2025**, *14* (10), 1587−1595.
(252) Cho, Y.; Kim, H. H.; Ahn, S.; Lee, J.; Lee, J.; Kim, K.; Kwak, S.; Lee, H.; Choi, K.; Song, K.; Lee, S. Colloidal Opaline Composites as Throughput-Scalable, Fully Transparent, and Color-Tunable Radiative Cooling Exterior Films for Outdoor Photovoltaics. *Adv. Funct. Mater.* **2025**, *35*, No. e10833.
(253) Lei, M.-Q.; Hu, Y.-F.; Song, Y.-N.; Li, Y.; Deng, Y.; Liu, K.; Xie, L.; Tang, J.-H.; Han, D.-L.; Lei, J.; Li, Z. M. Transparent radiative cooling films containing poly(methylmethacrylate), silica, and silver. *Opt. Mater.* **2021**, *122*, No. 111651.
(254) Lian, M.; Ding, W.; Liu, S.; Wang, Y.; Zhu, T.; Miao, Y.-E.; Zhang, C.; Liu, T. Highly Porous Yet Transparent Mechanically Flexible Aerogels Realizing Solar-Thermal Regulatory Cooling. *Nano-Micro Lett.* **2024**, *16* (1), No. 131.
(255) Wang, K.; Luo, G.; Guo, X.; Li, S.; Liu, Z.; Yang, C. Radiative cooling of commercial silicon solar cells using a pyramid-textured PDMS film. *Sol. Energy* **2021**, *225*, 245−251.
(256) Gao, K.; Shen, H.; Liu, Y.; Zhao, Q.; Li, Y.; Liu, J. Random inverted pyramid textured polydimethylsiloxane radiative cooling emitter for the heat dissipation of silicon solar cells. *Sol. Energy* **2022**, *236*, 703−711.
(257) Li, W.; Shi, Y.; Chen, Z.; Fan, S. Photonic thermal management of coloured objects. *Nat. Commun.* **2018**, *9* (1), No. 4240.
(258) Chen, Y.; Mandal, J.; Li, W.; Smith-Washington, A.; Tsai, C.-C.; Huang, W.; Shrestha, S.; Yu, N.; Han, R. P. S.; Cao, A.; Yang, Y. Colored and paintable bilayer coatings with high solar-infrared reflectance for efficient cooling. *Sci. Adv.* **2020**, *6* (17), No. eaaz5413.
(259) Cho, J.-W.; Lee, E.-J.; Kim, S.-K. Full-Color Solar-Heat-Resistant Films Based on Nanometer Optical Coatings. *Nano Lett.* **2022**, *22* (1), 380−388.
(260) Li, X.; Xu, H.; Yang, Y.; Li, F.; Ramakrishna, S.; Yu, J.; Ji, D.; Qin, X. Selective spectral absorption of nanofibers for color-preserving daytime radiative cooling. *Mater. Horiz.* **2023**, *10* (7), 2487−2495.
(261) Blandre, E.; Yalçin, R. A.; Joulain, K.; Drévillon, J. Microstructured surfaces for colored and non-colored sky radiative cooling. *Opt. Express* **2020**, *28* (20), 29703−29713.
(262) Zhu, Y.; Luo, H.; Yang, C.; Qin, B.; Ghosh, P.; Kaur, S.; Shen, W.; Qiu, M.; Belov, P.; Li, Q. Color-preserving passive radiative cooling for an actively temperature-regulated enclosure. *Light: Sci. Appl.* **2022**, *11* (1), No. 122.
(263) Sheng, C.; An, Y.; Du, J.; Li, X. Colored Radiative Cooler under Optical Tamm Resonance. *ACS Photonics* **2019**, *6* (10), 2545.
(264) Ding, Z.; Pattelli, L.; Xu, H.; Sun, W.; Li, X.; Pan, L.; Zhao, J.; Wang, C.; Zhang, X.; Song, Y.; et al. Iridescent Daytime Radiative Cooling with No Absorption Peaks in the Visible Range. *Small* **2022**, *18* (25), No. 2202400.
(265) Yu, S.; Zhang, Q.; Wang, Y.; Lv, Y.; Ma, R. Photonic-Structure Colored Radiative Coolers for Daytime Subambient Cooling. *Nano Lett.* **2022**, *22* (12), 4925−4932.
(266) Wang, Q.; Fu, R.; Sun, T.; Liu, M.; Sun, S.; Jiang, H.; Li, Z.; Zhang, Y.; Liu, D.; Chen, Y.; Zhong, H. Continuously in-situ manufacture of perovskite quantum dots/POE encapsulation adhesive film for silicon solar cell enhancement application. *Sol. Energy Mater. Sol. Cells* **2023**, *259*, No. 112450.
(267) He, J.; Chen, Y.; Guo, R.; Tang, S. Bioinspired Colored Films with Humidity-Induced Dynamic Reflectivity and Emissivity for Self-Adaptive, Efficient Radiative Cooling. *ACS Nano* **2025**, *19* (33), 30361−30370.
(268) Bae, S.; Kim, M.; Kang, G.; Lee, H.-S.; Kim, I. S.; Choi, S.-W.; Kang, J. G. Efficient full-color daytime radiative cooling with diffuse-reflection-dominant cholesteric liquid crystals. *Chem. Eng. J.* **2024**, *483*, No. 149245.
(269) Wei, H.; Gu, J.; Zhao, T.; Yan, Z.; Xu, H.-X.; Dou, S.; Qiu, C.-W.; Li, Y. Tunable VO2 cavity enables multispectral manipulation from visible to microwave frequencies. *Light: Sci. Appl.* **2024**, *13* (1), No. 54.
(270) Xie, H.; Fan, C. Tunable and adaptive colored radiative cooler based on the phase transition of VO2 photonic design. *Sol. Energy Mater. Sol. Cells* **2025**, *282*, No. 113382.
(271) Zhao, Q.; Finlayson, C. E.; Snoswell, D. R. E.; Haines, A.; Schäfer, C.; Spahn, P.; Hellmann, G. P.; Petukhov, A. V.; Herrmann, L.; Burdet, P.; et al. Large-scale ordering of nanoparticles using viscoelastic shear processing. *Nat. Commun.* **2016**, *7* (1), No. 11661.
(272) Hou, X.; Zhang, K.; Lai, X.; Hu, L.; Vogelbacher, F.; Song, Y.; Jiang, L.; Li, M. Brilliant colorful daytime radiative cooling coating mimicking scarab beetle. *Matter* **2025**, *8* (1), No. 101898.
(273) Smith, G. B. Amplified radiative cooling via optimized combinations of aperture geometry and spectral emittance profiles of surfaces and the atmosphere. *Sol. Energy Mater. Sol. Cells* **2009**, *93* (9), 1696−1701.
(274) Pirvaram, A.; Cooper, T.; Leung, S. N.; O'Brien, P. G. A comprehensive study on using underside infrared reflectors to enhance the performance of radiative cooling structures. *Energy Convers. Manage.* **2024**, *304*, No. 118180.
(275) Dan, Y.; Hu, M.; Wang, Q.; Su, Y.; Riffat, S. Enhancing radiative sky cooling performance by employing crossed compound parabolic concentrating configurations. *Renewable Energy* **2025**, *239*, No. 121979.
(276) Zhou, L.; Song, H.; Liang, J.; Singer, M.; Zhou, M.; Stegenburgs, E.; Zhang, N.; Xu, C.; Ng, T.; Yu, Z.; et al. A polydimethylsiloxane-coated metal structure for all-day radiative cooling. *Nat. Sustainability* **2019**, *2* (8), 718−724.
(277) Zhou, L.; Song, H.; Zhang, N.; Rada, J.; Singer, M.; Zhang, H.; Ooi, B. S.; Yu, Z.; Gan, Q. Hybrid concentrated radiative cooling and solar heating in a single system. *Cell Rep. Phys. Sci.* **2021**, *2* (2), No. 100338.
(278) Peoples, J.; Hung, Y.-W.; Li, X.; Gallagher, D.; Fruehe, N.; Pottschmidt, M.; Breseman, C.; Adams, C.; Yuksel, A.; Braun, J.; et al. Concentrated radiative cooling. *Appl. Energy* **2022**, *310*, No. 118368.
(279) Hull, J. R.; Schertz, W. W. Evacuated-tube directional-radiating cooling system. *Sol. Energy* **1985**, *35* (5), 429−434.
(280) Fang, H.; Zhou, L.; Xu, L.; Dang, S.; De Wolf, S.; Gan, Q. Radiative cooling for vertical solar panels. *iScience* **2024**, *27* (2), No. 108806.
(281) Li, W.; Fan, S. Nanophotonic control of thermal radiation for energy applications [Invited]. *Opt. Express* **2018**, *26* (12), 15995−16021.
(282) Liu, T.; Guo, C.; Li, W.; Fan, S. Thermal photonics with broken symmetries. *eLight* **2022**, *2* (1), No. 25.
(283) Yu, J.; Qin, R.; Ying, Y.; Qiu, M.; Li, Q. Asymmetric Directional Control of Thermal Emission. *Adv. Mater.* **2023**, *35* (45), No. 2302478.
(284) Wang, C.; Chen, T.; Chen, H.; Liu, J.; Yi, H.-L. Broadband Bidirectional Thermal Emission Supported by Localized Surface Plasmons and Magnetic Polaritons. *ACS Photonics* **2025**, *12* (4), 2226−2232.
(285) Wang, J.; Li, W. Non-reciprocal thermal photonics—from fundamentals to applications: a tutorial. *Adv. Opt. Photonics* **2026**, *18* (1), 105−159.
(286) Qu, Y.; Pan, M.; Qiu, M. Directional and Spectral Control of Thermal Emission and Its Application in Radiative Cooling and Infrared Light Sources. *Phys. Rev. Appl.* **2020**, *13* (6), No. 064052.

(287) Chamoli, S. K.; Li, W.; Guo, C.; ElKabbash, M. Angularly selective thermal emitters for deep subfreezing daytime radiative cooling. *Nanophotonics* **2022**, *11* (16), 3709−3717.
(288) Fan, Z.; Hwang, T.; Lin, S.; Chen, Y.; Wong, Z. J. Directional thermal emission and display using pixelated non-imaging micro-optics. *Nat. Commun.* **2024**, *15* (1), No. 4544.
(289) Xu, J.; Mandal, J.; Raman, A. P. Broadband directional control of thermal emission. *Science* **2021**, *372* (6540), 393−397.
(290) Wang, Q.; Liu, T.; Li, L.; Huang, C.; Wang, J.; Xiao, M.; Li, Y.; Li, W. Ultra-broadband directional thermal emission. *Nanophotonics* **2024**, *13* (5), 793−801.
(291) Ma, Y.; Wang, J.; Li, L.; Liu, T.; Li, W. Broadband Unidirectional Thermal Emission. *Laser Photonics Rev.* **2025**, *19* (2), No. 2400716.
(292) Wang, J.; Liu, M.; Liu, T.; Chen, W.; Ma, Y.; Wang, Q.; Li, W. Evolution and Combination of Light Line Singularities in Planar Multilayers. *ACS Photonics* **2024**, *11* (8), 3296−3302.
(293) Ying, Y.; Ma, B.; Yu, J.; Huang, Y.; Ghosh, P.; Shen, W.; Qiu, M.; Li, Q. Whole LWIR Directional Thermal Emission Based on ENZ Thin Films. *Laser Photonics Rev.* **2022**, *16* (8), No. 2200018.
(294) Hwang, J. S.; Xu, J.; Raman, A. P. Simultaneous Control of Spectral And Directional Emissivity with Gradient Epsilon-Near-Zero InAs Photonic Structures. *Adv. Mater.* **2023**, *35* (39), No. 2302956.
(295) Cho, J.-W.; Lee, Y.-J.; Kim, J.-H.; Hu, R.; Lee, E.; Kim, S.-K. Directional Radiative Cooling via Exceptional Epsilon-Based Micro-cavities. *ACS Nano* **2023**, *17* (11), 10442−10451.
(296) Ying, Y.; Yu, J.; Shen, W.; Ghosh, P.; Qiu, M.; Li, Q. Photonic control of thermal radiation for protective windows. *Light: Adv. Manuf.* **2026**, *6* (4), 630−639.
(297) Ma, X.; Teng, X.; Xu, L.; Bao, A.; Qu, H.; Li, Q.; Zhang, S.; Zhu, J. Visible light and infrared camouflage based on epsilon near zero materials. *Adv. Opt. Mater.* **2025**, *13* (20), No. 2403438.
(298) Abraham, D. E.; Cui, D.; Liang, B.; Hwang, J. S.; Santhanam, P.; Kim, L.; Lin, R.; Raman, A. P. Directional Thermal Emission Across Both Polarizations in Planar Photonic Architectures. *arXiv preprint arXiv:2505.03905* 2025.
(299) Hwang, J. S.; Xu, J.; Raman, A. P. Thermally tunable angular selectivity of broadband directional thermal emission. *Nano Lett.* **2025**, *25* (19), 8064−8071.
(300) Bae, M.; Kim, D. H.; Kim, S.-K.; Song, Y. M. Transparent energy-saving windows based on broadband directional thermal emission. *Nanophotonics* **2024**, *13* (5), 749−761.
(301) Ryu, D. G.; Kim, J. T.; Kim, M. S.; Kim, J. J.; Nam, H. J.; Jeong, I. H.; Kim, Y. J.; Lee, G. J. Angular selective broadband radiative cooling based on Berreman mode. *Opt. Express* **2024**, *32* (19), 33016−33028.
(302) Zhou, J.; Chen, T. G.; Tsurimaki, Y.; Hajj-Ahmad, A.; Fan, L.; Peng, Y.; Xu, R.; Wu, Y.; Assawaworrarit, S.; Fan, S.; et al. Angle-selective thermal emitter for directional radiative cooling and heating. *Joule* **2023**, *7* (12), 2830−2844.
(303) Cheng, Q.; Gomez, S.; Hu, G.; Abaalkhail, A.; Beasley, J. E.; Zhang, P.; Xu, Y.; Chen, X.; Tian, S.; Mandal, J.; et al. Realizing optimal radiative cooling walls in building-energy nexus via asymmetric emissivity. *Nexus* **2024**, *1* (3), No. 100028.
(304) Kim, B.-S.; Kim, J.-H.; Kang, G.; Ko, H.; Gan, Q.; Kim, S.-K. All-optical seasonal energy saving windows. *iScience* **2025**, *28* (5), No. 112514.
(305) Degeorges, M.; Anand, J.; Tsang, Y. C. A.; Li, Z.; Varghese, N. J.; Mandal, J. Beyond cooling: Radiative thermoregulation in the Earth's glow with micropatterned directional emitters. *Joule* **2025**, *9* (6), No. 101956.
(306) Xu, X.; Gu, J.; Zhao, H.; Zhang, X.; Dou, S.; Li, Y.; Zhao, J.; Zhan, Y.; Li, X. Passive and Dynamic Phase-Change-Based Radiative Cooling in Outdoor Weather. *ACS Appl. Mater. Interfaces* **2022**, *14* (12), 14313−14320.
(307) Tang, K.; Dong, K.; Li, J.; Gordon, M. P.; Reichertz, F. G.; Kim, H.; Rho, Y.; Wang, Q.; Lin, C.-Y.; Grigoropoulos, C. P.; et al. Temperature-adaptive radiative coating for all-season household thermal regulation. *Science* **2021**, *374* (6574), 1504−1509.
(308) Wang, S.; Jiang, T.; Meng, Y.; Yang, R.; Tan, G.; Long, Y. Scalable Thermochromic Smart Windows with Passive Radiative Cooling Regulation. *Science* **2021**, *374* (6574), 1501.
(309) Li, J.; Dong, K.; Zhang, T.; Tseng, D.; Fang, C.; Guo, R.; Li, J.; Xu, Y.; Dun, C.; Urban, J. J.; et al. Printable, emissivity-adaptive and albedo-optimized covering for year-round energy saving. *Joule* **2023**, *7* (11), 2552−2567.
(310) Zhang, X. A.; Yu, S.; Xu, B.; Li, M.; Peng, Z.; Wang, Y.; Deng, S.; Wu, X.; Wu, Z.; Ouyang, M.; Wang, Y. Dynamic gating of infrared radiation in a textile. *Science* **2019**, *363* (6427), 619−623.
(311) Xiang, B.; Zhang, R.; Zeng, X.; Luo, Y.; Luo, Z. An easy-to-prepare flexible dual-mode fiber membrane for daytime outdoor thermal management. *Adv. Fiber Mater.* **2022**, *4* (5), 1058−1068.
(312) Ke, Y.; Li, Y.; Wu, L.; Wang, S.; Yang, R.; Yin, J.; Tan, G.; Long, Y. On-demand solar and thermal radiation management based on switchable interwoven surfaces. *ACS Energy Lett.* **2022**, *7* (5), 1758−1763.
(313) Li, X.; Sun, B.; Sui, C.; Nandi, A.; Fang, H.; Peng, Y.; Tan, G.; Hsu, P.-C. Integration of daytime radiative cooling and solar heating for year-round energy saving in buildings. *Nat. Commun.* **2020**, *11* (1), No. 6101.
(314) Tao, X.; Liu, D.; Liu, T.; Meng, Z.; Yu, J.; Cheng, H. A bistable variable infrared emissivity device based on reversible silver electro-deposition. *Adv. Funct. Mater.* **2022**, *32* (32), No. 2202661.
(315) Sui, C.; Pu, J.; Chen, T.-H.; Liang, J.; Lai, Y.-T.; Rao, Y.; Wu, R.; Han, Y.; Wang, K.; Li, X.; et al. Dynamic electrochromism for all-season radiative thermoregulation. *Nat. Sustainability* **2023**, *6* (4), 428−437.
(316) Ergoktas, M. S.; Bakan, G.; Kovalska, E.; Le Fevre, L. W.; Fields, R. P.; Steiner, P.; Yu, X.; Salihoglu, O.; Balci, S.; Fal'ko, V. I.; et al. Multispectral graphene-based electro-optical surfaces with reversible tunability from visible to microwave wavelengths. *Nat. Photonics* **2021**, *15* (7), 493−498.
(317) Zhang, Q.; Wang, Y.; Lv, Y.; Yu, S.; Ma, R. Bioinspired zero-energy thermal-management device based on visible and infrared thermochromism for all-season energy saving. *Proc. Natl. Acad. Sci. U.S.A.* **2022**, *119* (38), No. e2207353119.
(318) Sun, K.; Riedel, C. A.; Urbani, A.; Simeoni, M.; Mengali, S.; Zalkovskij, M.; Bilenberg, B.; De Groot, C. H.; Muskens, O. L. VO2 thermochromic metamaterial-based smart optical solar reflector. *ACS Photonics* **2018**, *5* (6), 2280−2286.
(319) Xia, Z.; Fang, Z.; Zhang, Z.; Shi, K.; Meng, Z. Easy Way to Achieve Self-Adaptive Cooling of Passive Radiative Materials. *ACS Appl. Mater. Interfaces* **2020**, *12* (24), 27241.
(320) Zhang, Q.; Lv, Y.; Wang, Y.; Yu, S.; Li, C.; Ma, R.; Chen, Y. Temperature-dependent dual-mode thermal management device with net zero energy for year-round energy saving. *Nat. Commun.* **2022**, *13* (1), No. 4874.
(321) Qu, Y.; Li, Q.; Du, K.; Cai, L.; Lu, J.; Qiu, M. Dynamic thermal emission control based on ultrathin plasmonic metamaterials including phase-changing material GST. *Laser Photonics Rev.* **2017**, *11* (5), No. 1700091.
(322) Tachikawa, S.; Ohnishi, A.; Shimakawa, Y.; Ochi, A.; Okamoto, A.; Nakamura, Y. Development of a variable emittance radiator based on a perovskite manganese oxide. *J. Thermophys. Heat Transfer* **2003**, *17* (2), 264−268.
(323) Fan, D.; Sun, S.; Guo, L. Thermal Emittance of La0.7Ca0.3-xKxMnO3 Coatings on Aluminum Substrate. *Int. J. Thermophys.* **2018**, *39* (5), No. 67.
(324) Li, G.; Xie, D.; Zhong, H.; Zhang, Z.; Fu, X.; Zhou, Q.; Li, Q.; Ni, H.; Wang, J.; Guo, E.-j.; et al. Photo-induced non-volatile VO2 phase transition for neuromorphic ultraviolet sensors. *Nat. Commun.* **2022**, *13* (1), No. 1729.
(325) Wu, X.; Yuan, L.; Weng, X.; Qi, L.; Wei, B.; He, W. Passive smart thermal control coatings incorporating CaF2/VO2 core−shell micro-sphere structures. *Nano Lett.* **2021**, *21* (9), 3908−3914.
(326) Long, L.; Taylor, S.; Ying, X.; Wang, L. Thermally-switchable spectrally-selective infrared metamaterial absorber/emitter by tuning magnetic polariton with a phase-change VO2 layer. *Mater. Today Energy* **2019**, *13*, 214−220.

https://doi.org/10.1021/acsami.6c00074
ACS Appl. Mater. Interfaces 2026, 18, 21363−21423

(327) Zhang, W.-W.; Qi, H.; Sun, A.-T.; Ren, Y.-T.; Shi, J.-W. Periodic trapezoidal VO2-Ge multilayer absorber for dynamic radiative cooling. *Opt. Express* **2020**, *28* (14), 20609−20623.
(328) Mandal, J.; Jia, M.; Overvig, A.; Fu, Y.; Che, E.; Yu, N.; Yang, Y. Porous polymers with switchable optical transmittance for optical and thermal regulation. *Joule* **2019**, *3* (12), 3088−3099.
(329) Fan, Y.; Chen, H.; Liu, X.; Zhao, Y.; Huang, Y.; Liu, J.; Wang, C. Radiative Cooling in Outer Space: Fundamentals, Advances in Materials and Applications, and Perspectives. *Adv. Mater.* **2025**, *37* (43), No. e06795.
(330) Chandrasekhar, P.; Birur, G. C.; Stevens, P.; Rawal, S.; Pierson, E. A.; Miller, K. L. Far infrared electrochromism in unique conducting polymer systems. *Synth. Met.* **2001**, *119* (1−3), 293−294.
(331) Wang, L.; Jiao, X.; Chen, D.; Wang, T. A solar water-heating smart window by integration of the water flow system and the electrochromic window based on reversible metal electrodeposition. *Adv. Sci.* **2022**, *9* (6), No. 2104121.
(332) Granqvist, C. G. Progress in electrochromics: tungsten oxide revisited. *Electrochim. Acta* **1999**, *44* (18), 3005−3015.
(333) Inoue, T.; Zoysa, M. D.; Asano, T.; Noda, S. Realization of dynamic thermal emission control. *Nat. Mater.* **2014**, *13* (10), 928−931.
(334) Sun, K.; Xiao, W.; Wheeler, C.; Simeoni, M.; Urbani, A.; Gaspari, M.; Mengali, S.; De Groot, C. H.; Muskens, O. L. VO2 metasurface smart thermal emitter with high visual transparency for passive radiative cooling regulation in space and terrestrial applications. *Nanophotonics* **2022**, *11* (17), 4101−4114.
(335) Zhou, L.; Yin, X.; Gan, Q. Best practices for radiative cooling. *Nat. Sustainability* **2023**, *6* (9), 1030−1032.
(336) Tang, H.; Guo, C.; Fan, F.; Pan, H.; Xu, Q.; Zhao, D. Both sub-ambient and above-ambient conditions: a comprehensive approach for the efficient use of radiative cooling. *Energy Environ. Sci.* **2024**, *17* (13), 4498−4507.
(337) Lin, K.-T.; Han, J.; Li, K.; Guo, C.; Lin, H.; Jia, B. Radiative cooling: Fundamental physics, atmospheric influences, materials and structural engineering, applications and beyond. *Nano Energy* **2021**, *80*, No. 105517.
(338) Chen, Z.; Zhu, L.; Li, W.; Fan, S. Simultaneously and synergistically harvest energy from the sun and outer space. *Joule* **2019**, *3* (1), 101−110.
(339) Xi, Z.; Li, S.; Yu, L.; Yan, H.; Chen, M. All-day freshwater harvesting by selective solar absorption and radiative cooling. *ACS Appl. Mater. Interfaces* **2022**, *14* (22), 26255−26263.
(340) Xu, J.; Zhang, J.; Fu, B.; Song, C.; Shang, W.; Tao, P.; Deng, T. All-day freshwater harvesting through combined solar-driven interfacial desalination and passive radiative cooling. *ACS Appl. Mater. Interfaces* **2020**, *12* (42), 47612−47622.
(341) Xu, J.; Huo, X.; Yan, T.; Wang, P.; Bai, Z.; Chao, J.; Yang, R.; Wang, R.; Li, T. All-in-one hybrid atmospheric water harvesting for all-day water production by natural sunlight and radiative cooling. *Energy Environ. Sci.* **2024**, *17* (14), 4988−5001.
(342) Liu, C.; Yan, X.-Y.; Li, S.; Zhang, H.; Deng, B.; Fang, N. X.; Habibi, Y.; Chen, S.-C.; Zhao, X. A metre-scale vertical origami hydrogel panel for atmospheric water harvesting in Death Valley. *Nat. Water* **2025**, *3*, 714−722.
(343) Ghosh, P.; Wei, X.; Liu, H.; Zhang, Z.; Zhu, L. Simultaneous subambient daytime radiative cooling and photovoltaic power generation from the same area. *Cell Rep. Phys. Sci.* **2024**, *5* (3), No. 101876, DOI: 10.1016/j.xcrp.2024.101876.
(344) Gan, Q.; Zhou, L. Synergizing radiative cooling and solar power generation. *Joule* **2024**, *8* (5), 1205−1207.
(345) Liao, M.; Banerjee, D.; Hallberg, T.; Åkerlind, C.; Alam, M. M.; Zhang, Q.; Kariis, H.; Zhao, D.; Jonsson, M. P. Cellulose-based radiative cooling and solar heating powers ionic thermoelectrics. *Adv. Sci.* **2023**, *10* (8), No. 2206510.
(346) Wang, C. H.; Chen, H.; Jiang, Z. Y.; Zhang, X. X. Design and experimental validation of an all-day passive thermoelectric system via radiative cooling and greenhouse effects. *Energy* **2023**, *263*, No. 125735, DOI: 10.1016/j.energy.2022.125735.
(347) Raman, A. P.; Li, W.; Fan, S. Generating Light from Darkness. *Joule* **2019**, *3* (11), 2679−2686.
(348) Wang, C. Radiative-cooling-driven passive thermoelectric devices. *Device* **2024**, *2* (6), No. 100424, DOI: 10.1016/j.device.2024.100424.
(349) Xia, Z.; Zhang, Z.; Meng, Z.; Ding, L.; Yu, Z. Thermoelectric Generator Using Space Cold Source. *ACS Appl. Mater. Interfaces* **2019**, *11* (37), 33941−33945.
(350) Dang, S.; Almahfoudh, H. H.; Alajlan, A. M.; Qasem, H.; Wang, J.; Zhu, Y.; Bakr, O. M.; Ooi, B. S.; Gan, Q. Sky cooling for LED streetlights. *Light: Sci. Appl.* **2025**, *14* (1), No. 100, DOI: 10.1038/s41377-024-01724-7.
(351) Li, W.; Shi, Y.; Chen, K.; Zhu, L.; Fan, S. A comprehensive photonic approach for solar cell cooling. *ACS Photonics* **2017**, *4* (4), 774−782.
(352) Wang, Z.; Kortge, D.; Zhu, J.; Zhou, Z.; Torsina, H.; Lee, C.; Bermel, P. Lightweight, passive radiative cooling to enhance concentrating photovoltaics. *Joule* **2020**, *4* (12), 2702−2717.
(353) Zhu, L.; Raman, A.; Wang, K. X.; Anoma, M. A.; Fan, S. Radiative cooling of solar cells. *Optica* **2014**, *1* (1), 32−38.
(354) Aili, A.; Wei, Z.; Chen, Y.; Zhao, D.; Yang, R.; Yin, X. Selection of polymers with functional groups for daytime radiative cooling. *Mater. Today Phys.* **2019**, *10*, No. 100127.
(355) Yang, R.; Niu, D.; Pu, J. H.; Tang, G.; Wang, X.; Du, M. Passive all-day freshwater harvesting through a transparent radiative cooling film. *Appl. Energy* **2022**, *325*, No. 119801.
(356) Shi, Y.; Ilic, O.; Atwater, H. A.; Greer, J. R. All-day fresh water harvesting by microstructured hydrogel membranes. *Nat. Commun.* **2021**, *12* (1), No. 2797.
(357) Shan, H.; Poredoš, P.; Ye, Z.; Qu, H.; Zhang, Y.; Zhou, M.; Wang, R.; Tan, S. C. All-day multicyclic atmospheric water harvesting enabled by polyelectrolyte hydrogel with hybrid desorption mode. *Adv. Mater.* **2023**, *35* (35), No. 2302038.
(358) Wilson, C. T.; Díaz-Marín, C. D.; Colque, J. P.; Mooney, J. P.; El Fil, B. Solar-driven atmospheric water harvesting in the Atacama Desert through physics-based optimization of a hygroscopic hydrogel device. *Device* **2025**, 3, No. 100798, DOI: 10.1016/j.device.2025.100798.
(359) Ahmad, S.; Siddiqui, A. R.; Yang, K.; Zhou, M.; Ali, H. M.; Hardian, R.; Szekely, G.; Daniel, D.; Yang, S.; Gan, Q. Lubricated Surface in a Vertical Double-Sided Architecture for Radiative Cooling and Atmospheric Water Harvesting. *Adv. Mater.* **2024**, *36* (51), No. 2404037, DOI: 10.1002/adma.202404037.
(360) Yu, L.; Xi, Z.; Li, S.; Pang, D.; Yan, H.; Chen, M. All-day continuous electrical power generator by solar heating and radiative cooling from the sky. *Appl. Energy* **2022**, *322*, No. 119403.
(361) Liu, Y.; Xie, Y.; Chen, H.; Liao, J.; Lu, Y.; Lan, D.; Wang, C. Design and experimental study of a compact thermoelectric device driven by solar heating and radiative cooling. *Nat. Energy* **2024**, *4*, No. 100146.
(362) Tian, Y.; Liu, X.; Chen, F.; Zheng, Y. Harvesting energy from sun, outer space, and soil. *Sci. Rep.* **2020**, *10* (1), No. 20903.
(363) Li, X.; Xie, W.; Sui, C.; Hsu, P.-C. Multispectral thermal management designs for net-zero energy buildings. *ACS Mater. Lett.* **2020**, *2* (12), 1624−1643.
(364) Abraham, D. E.; Yang, R.; Mandal, J.; Yore, M.; Huang, X.; Turner, V. K.; Wells, W.; Schwarz, K.; Eisenman, D. P.; Raman, A. P. Efficient outdoor thermal comfort via radiant cooling and infrared-reflective walls. *Nat. Sustainability* **2025**, *8*, 642−650.
(365) Zhou, Z.; Liu, R.; Wan, J.; Long, Y. Multispectral thermal management for energy-saving buildings in diverse climates: From facade to indoor personal thermal management. *Joule* **2025**, *9*, No. 102214, DOI: 10.1016/j.joule.2025.102214.
(366) Zhou, Z.; Liu, R.; Huang, Z.; Hu, B.; Long, Y. Radiative Warming Glass for High-Latitude Cold Regions. *Adv. Sci.* **2025**, *12* (9), No. 2414192.
(367) Biswas, A.; Wang, S.; Milne, C. L.; Alvarez, G. A.; Islam, M. A.; Pieshkov, T. S.; Terlier, T.; Li, T.; Murukeshan, J.; Gray, T.; et al. Carbon Doped Boron Nitride Nano-Coatings for Durable, Low Emissivity Glass Windows. *Adv. Mater.* **2025**, *37* (38), No. 2507557.

(368) Zhao, X.; Li, T.; Xie, H.; Liu, H.; Wang, L.; Qu, Y.; Li, S. C.; Liu, S.; Brozena, A. H.; Yu, Z.; et al. A solution-processed radiative cooling glass. *Science* **2023**, *382* (6671), 684−691.
(369) Fei, J.; Zhang, X.; Han, D.; Lei, Y.; Xie, F.; Zhou, K.; Koh, S.-W.; Ge, J.; Zhou, H.; Wang, X.; et al. Passive cooling paint enabled by rational design of thermal-optical and mass transfer properties. *Science* **2025**, *388* (6751), 1044−1049.
(370) Zhou, C.; Julianri, I.; Wang, S.; Chan, S. H.; Li, M.; Long, Y. Transparent bamboo with high radiative cooling targeting energy savings. *ACS Mater. Lett.* **2021**, *3* (6), 883−888.
(371) Wang, S.; Zhou, Y.; Jiang, T.; Yang, R.; Tan, G.; Long, Y. Thermochromic smart windows with highly regulated radiative cooling and solar transmission. *Nano Energy* **2021**, *89*, No. 106440.
(372) Tu, H.; Wang, T.; Chen, M.; Wu, L. Isotope-driven hydrogel smart windows for self-adaptive thermoregulation. *Nat. Commun.* **2025**, *16* (1), No. 6952.
(373) Galib, R. H.; Tian, Y.; Lei, Y.; Dang, S.; Li, X.; Yudhanto, A.; Lubineau, G.; Gan, Q. Atmospheric-moisture-induced polyacrylate hydrogels for hybrid passive cooling. *Nat. Commun.* **2023**, *14* (1), No. 6707.
(374) Wang, K.; Liu, S.; Yu, J.; Hong, P.; Wang, W.; Cai, W.; Huang, J.; Jiang, X.; Lai, Y.; Lin, Z. Hofmeister Effect-Enhanced, Nanoparticle-Shielded, Thermally Stable Hydrogels for Anti-UV, Fast-Response, and All-Day-Modulated Smart Windows. *Adv. Mater.* **2025**, *37* (14), No. 2418372.
(375) Jiang, F.; Yu, K.; Kieffer, R.; de Jong, D.; Parker, R. M.; Vignolini, S.; Aubin-Tam, M.-E. Thermochromic hydrogel with high transmittance modulation and fast response for flexible smart windows. *Commun. Mater.* **2025**, *6* (1), No. 239.
(376) Liu, B.; Li, F.; Niu, P.; Li, H. Tough adhesion of freezing-and drying-tolerant transparent nanocomposite organohydrogels. *ACS Appl. Mater. Interfaces* **2021**, *13* (18), 21822−21830.
(377) Shao, Z.; Huang, A.; Cao, C.; Ji, X.; Hu, W.; Luo, H.; Bell, J.; Jin, P.; Yang, R.; Cao, X. Tri-band electrochromic smart window for energy savings in buildings. *Nat. Sustainability* **2024**, *7* (6), 796−803.
(378) Zhu, W.; Zhang, Y.; Mohammad, N.; Xu, W.; Tunc, S.; Shan, X.; Zhou, C.; Semple, K.; Dai, C.; Li, T. Large-scale industry-compatible sub-ambient radiative cooling pulp. *Cell Rep. Phys. Sci.* **2022**, *3* (11), No. 101125, DOI: 10.1016/j.xcrp.2022.101125.
(379) Aili, A.; Jiang, T.; Chen, J.; Wen, Y.; Yang, R.; Yin, X.; Tan, G. Passive daytime radiative cooling: Moving beyond materials towards real-world applications. *Next Energy* **2024**, *3*, No. 100121.
(380) Vu, T. D.; Xie, H.; Wang, S.; Hu, J.; Zeng, X.; Long, Y. Durable vanadium dioxide with 33-year service life for smart windows applications. *Mater. Today Energy* **2022**, *26*, No. 100978.
(381) Wang, K.; Liu, S.; Yu, J.; Hong, P.; Wang, W.; Cai, W.; Huang, J.; Jiang, X.; Lai, Y.; Lin, Z. Hofmeister Effect-Enhanced, Nanoparticle-Shielded, Thermally Stable Hydrogels for Anti-UV, Fast-Response, and All-Day-Modulated Smart Windows. *Adv. Mater.* **2025**, *37* (14), No. 2418372.
(382) Cui, W.; Cao, G.; Park, J. H.; Ouyang, Q.; Zhu, Y. Influence of indoor air temperature on human thermal comfort, motivation and performance. *Build. Environ.* **2013**, *68*, 114−122.
(383) Zhang, Z.; Wang, J.; Feng, X.; Chang, L.; Chen, Y.; Wang, X. The solutions to electric vehicle air conditioning systems: A review. *Renewable Sustainable Energy Rev.* **2018**, *91*, 443−463.
(384) Marty, W.; Sigrist, T.; Wyler, D. Temperature variations in automobiles in various weather conditions: An experimental contribution to the determination of time of death. *Am. J. Forensic Med. Pathol.* **2001**, *22* (3), 215−219.
(385) McLaren, C.; Null, J.; Quinn, J. Heat stress from enclosed vehicles: moderate ambient temperatures cause significant temperature rise in enclosed vehicles. *Pediatrics* **2005**, *116* (1), e109−e112.
(386) Li, J.; Wu, X.; Chow, S. K.; Zhuang, Q.; Habert, G. Thermal Comfort Comparison and Cause Analysis of Low-Temperature High-Humidity Indoor Environments of Rural Houses in Gansu Province, China. *Sustainability* **2023**, *15* (23), 16428.
(387) Mishra, S. R.; Wilson, T.; Andrabi, H.; Ait Ouakrim, D.; Li, A.; Akpan, E.; Bentley, R.; Blakely, T. The total health gains and cost savings of eradicating cold housing in Australia. *Social Sci. Med.* **2023**, *334*, No. 115954.
(388) Agency, I. E. *Future of Cooling*; Paris, 2018. https://www.iea.org/reports/the-future-of-cooling (accessed Aug 17, 2025).
(389) Duan, Z.; Wu, S.; Sun, H.; Lin, B.; Ding, P.; Cui, T.; To, J.; Zhang, X. Improvements in energy saving and thermal comfort for electric vehicles in summer through coupled electrochromic and radiative cooling smart windows. *Build. Simul.* **2024**, *17* (8), 1231−1251.
(390) Wu, T.; Lin, H.; Wu, Q.; Li, H.; Ning, S.; Zhou, L.; Zhang, S.; Zheng, H.; Jia, B. Design of radiative cooling covers for automobiles with maximized cooling power. *Int. J. Heat Mass Transfer* **2024**, *227*, No. 125601.
(391) Shi, C.; Chen, S.; Yang, X.; Qi, G.; Tu, Y.; Hu, W.; Mao, J.; Wang, Y.; Qiao, Y.; Tan, X. A transparent and flexible double-layer protective film composed of PVDF-TPU for efficient radiative cooling. *Sol. Energy Mater. Sol. Cells* **2025**, *285*, No. 113546.
(392) Xue, X.; Qiu, M.; Li, Y.; Zhang, Q.; Li, S.; Yang, Z.; Feng, C.; Zhang, W.; Dai, J. G.; Lei, D.; et al. Creating an eco-friendly building coating with smart subambient radiative cooling. *Adv. Mater.* **2020**, *32* (42), No. 1906751.
(393) Luo, C.-L.; Zheng, L.-X.; Jiao, J.-Y.; Yan, W.-G.; Zhao, J.; Jia, G.-Z.; Liu, Z.-F.; Liu, Z.-B.; Tian, J.-G. Enhanced passive radiative cooling coating with Y2O3 for thermal management of building. *Opt. Mater.* **2023**, *138*, No. 113710.
(394) Liu, C.-H.; Ay, C.; Kan, J.-C.; Lee, M.-T. The effect of radiative cooling on reducing the temperature of greenhouses. *Materials* **2018**, *11* (7), 1166.
(395) Zou, H.; Wang, C.; Yu, J.; Huang, D.; Yang, R.; Wang, R. Eliminating greenhouse heat stress with transparent radiative cooling film. *Cell Rep. Phys. Sci.* **2023**, *4* (8), No. 101539, DOI: 10.1016/j.xcrp.2023.101539.
(396) Li, J.; Jiang, Y.; Liu, J.; Wu, L.; Xu, N.; Zhang, Z.; Zhao, D.; Li, G.; Wang, P.; Li, W.; et al. A photosynthetically active radiative cooling film. *Nat. Sustainability* **2024**, *7* (6), 786−795.
(397) Zhao, B.; Hu, M.; Xuan, Q.; Kwan, T. H.; Dabwan, Y. N.; Pei, G. Tunable thermal management based on solar heating and radiative cooling. *Sol. Energy Mater. Sol. Cells* **2022**, *235*, No. 111457.
(398) Yan, C.; Li, A.; Wu, H.; Tong, Z.; Qu, J.; Sun, W.; Yang, Z. Scalable and all-season passive thermal modulation enabled by radiative cooling, selective solar absorption, and thermal retention. *Appl. Therm. Eng.* **2023**, *221*, No. 119707.
(399) Wang, J.; Xie, M.; An, Y.; Tao, Y.; Sun, J.; Ji, C. All-season thermal regulation with thermochromic temperature-adaptive radiative cooling coatings. *Sol. Energy Mater. Sol. Cells* **2022**, *246*, No. 111883.
(400) Yücel, A.; Acharya, S.; Williams, M. Natural convection and radiation in a square enclosure. *Numer. Heat Transfer* **1989**, *15* (2), 261−278.
(401) Hu, M.; Zhao, B.; Cao, J.; Wang, Q.; Riffat, S.; Su, Y.; Pei, G. Quantitative characterization of the effect of inclination angle on flat-plate radiative cooling performance in buildings. *J. Build. Eng.* **2022**, *59*, No. 105124.
(402) Tang, H.; Chen, W.; Li, C. Experimental and theoretical study on building integrated radiative cooling with a limited sky-view factor. *J. Build. Eng.* **2024**, *97*, No. 110948.
(403) Zhao, D.; Aili, A.; Zhai, Y.; Lu, J.; Kidd, D.; Tan, G.; Yin, X.; Yang, R. Subambient cooling of water: toward real-world applications of daytime radiative cooling. *Joule* **2019**, *3* (1), 111−123.
(404) Tian, L.; Li, Z.; Zhao, X. Effect of thermal resistance and infrared transparency on radiative cooling efficiency. *Energy Build.* **2024**, *323*, No. 114801.
(405) Heo, S.-Y.; Lee, G. J.; Kim, D. H.; Kim, Y. J.; Ishii, S.; Kim, M. S.; Seok, T. J.; Lee, B. J.; Lee, H.; Song, Y. M. A Janus emitter for passive heat release from enclosures. *Sci. Adv.* **2020**, *6* (36), No. eabb1906.
(406) Fu, H.; Zhang, Y.; Liu, X.; Han, H.; Kondo, H.; Zhou, H. Flexible highly thermal conductive hybrid film for efficient radiative cooling. *Sol. Energy Mater. Sol. Cells* **2024**, *266*, No. 112660.

(407) Zhang, H.; Huang, J.; Fan, D. Switchable radiative cooling from temperature-responsive thermal resistance modulation. *ACS Appl. Energy Mater.* **2022**, *5* (5), 6003−6010.
(408) Raeisi, M.; Mortazavi, B.; Podryabinkin, E. V.; Shojaei, F.; Zhuang, X.; Shapeev, A. V. High thermal conductivity in semiconducting Janus and non-Janus diamanes. *Carbon* **2020**, *167*, 51−61.
(409) Zhu, G.; Pei, S.; Li, F.; Li, Q.; Fan, D. Thermally conductive graphene-based Janus emitters with scalable fabrication for hybrid passive cooling of outdoor electronic devices. *Chem. Eng. J.* **2026**, *529*, No. 172931.
(410) Yan, X.; Liu, J.; Zhang, L.; Zhong, Y.; Ji, B.; Wu, W.; Wang, B.; Feng, X.; Rong, L.; Xu, H.; Mao, Z. Janus-structured thermally conductive radiative cooler for electronic devices heat dissipation. *Chem. Eng. J.* **2025**, *523*, No. 168743.
(411) Tian, Y.; Lei, Y.; Zeng, S.; He, Y.; Feng, C.; Li, Q.; Waller, R.; Gan, Q. Passive cooling of greenhouses in extreme climates through spectral control film. *Nexus* **2025**, *2* (1), No. 100058, DOI: 10.1016/j.ynexs.2025.100058.
(412) Wang, C.; Zou, H.; Huang, D.; Yang, R.; Wang, R. Enhancing food production in hot climates through radiative cooling mulch: A nexus approach. *Nexus* **2024**, *1* (1), No. 100002, DOI: 10.1016/j.ynexs.2023.100002.
(413) Song, Y.; Zhao, F.; Li, Z.; Cheng, Z.; Wan, H. Electrospinning preparation and near-infrared absorption properties of a silica/cesium tungsten bronze micro−nano fiber membrane. *RSC Adv.* **2021**, *11* (49), 31084−31089.
(414) Lee, K.-S.; Park, S. R.; Kim, Y. K. Effects of irradiance, temperature, and nutrients on growth dynamics of seagrasses: a review. *J. Exp. Mar. Biol. Ecol.* **2007**, *350* (1−2), 144−175.
(415) Yang, M.; Zeng, Y.; Du, Q.; Sun, H.; Yin, Y.; Yan, X.; Jiang, M.; Pan, C.; Sun, D.; Wang, Z. Enhanced radiative cooling with Janus optical properties for low-temperature space cooling. *Nanophotonics* **2024**, *13* (5), 629−637.
(416) Zhao, B.; Xuan, Q.; Zhang, W.; Hu, M.; Wang, C.; Pei, G. Low-emissivity interior wall strategy for suppressing overcooling in radiatively cooled buildings in cold environments. *Sustainable Cities Soc.* **2023**, *99*, No. 104912.
(417) Kwak, H.; Kim, D. H.; Song, Y. M. Design of Double-Sided Optical Coatings for Space Cooling Through Vertical Windows. *Adv. Photonics Res.* **2025**, *6* (6), No. 2400205.
(418) Wang, W.; Zou, Q.; Wang, N.; Hong, B.; Zhang, W.; Wang, G. P. Janus multilayer for radiative cooling and heating in double-side photonic thermal system. *ACS Appl. Mater. Interfaces* **2021**, *13* (36), 42813−42821.
(419) Yang, W.; Xiao, P.; Li, S.; Deng, F.; Ni, F.; Zhang, C.; Gu, J.; Yang, J.; Kuo, S. W.; Geng, F.; Chen, T. Engineering structural Janus MXene-nanofibrils aerogels for season-adaptive radiative thermal regulation. *Small* **2023**, *19* (30), No. 2302509.
(420) Chang, J.-Y.; Chiang, C.-C.; Liu, C.-Y.; Chen, Y.-B. Development of a Janus radiative cooler using a versatile fabrication process. *Sol. Energy Mater. Sol. Cells* **2024**, *272*, No. 112918.
(421) Yuan, L.; Jia, S.; Shao, S.; Asfahan, H. M.; Li, X. A self-cleaning janus textile for highly efficient heating and cooling management. *Nano Lett.* **2025**, *25* (19), 8019−8026.
(422) Ma, Z.; Feng, Y.; Song, A. Y.; Dinh, T.; Hong, M.; Bell, J.; Hou, B.; Song, P.; Zheng, W. A Scalable, Durable, Fire-Safe All-Day Passive Radiative Cooling Coating for Sustainable Buildings. *Adv. Funct. Mater.* **2025**, *36* (10), No. e17278.
(423) Li, M.; Lin, C.; Li, K.; Ma, W.; Dopphoopha, B.; Li, Y.; Huang, B. A UV-reflective organic−inorganic tandem structure for efficient and durable daytime radiative cooling in harsh climates. *Small* **2023**, *19* (29), No. 2301159.
(424) Li, D.; Cai, H.; Liu, J. Multifunctional daytime radiative cooler resistant to UV aging. *Sol. Energy Mater. Sol. Cells* **2024**, *276*, No. 113047.
(425) Sato, D.; Yamada, N. Review of photovoltaic module cooling methods and performance evaluation of the radiative cooling method. *Renewable Sustainable Energy Rev.* **2019**, *104*, 151−166.
(426) Alao, K. T.; Gilani, S. I. U. H.; Sopian, K.; Alao, T. O.; Aslam, Z. A comprehensive review of radiative cooling technologies and their integration with Photovoltaic (PV) systems: Challenges, opportunities, and future directions. *Sol. Energy* **2025**, *292*, No. 113445.
(427) Ahmed, S.; Li, Z.; Javed, M. S.; Ma, T. A review on the integration of radiative cooling and solar energy harvesting. *Mater. Today Energy* **2021**, *21*, No. 100776.
(428) Jia, S.; Huang, M.; Jiang, X.; Shen, C.; Chen, S.; Meng, G.; Li, X.; Guo, W. Tandem daytime radiative cooling and solar power generation. *Cell Rep. Phys. Sci.* **2025**, *6* (1), No. 102343, DOI: 10.1016/j.xcrp.2024.102343.
(429) Lee, C. H.; Kim, D. R.; Zheng, X. Transfer printing methods for flexible thin film solar cells: Basic concepts and working principles. *ACS Nano* **2014**, *8* (9), 8746−8756.
(430) Jia, Y.; Alva, G.; Fang, G. Development and applications of photovoltaic−thermal systems: A review. *Renewable Sustainable Energy Rev.* **2019**, *102*, 249−265.
(431) Xuan, Q.; Yang, N.; Kai, M.; Wang, C.; Jiang, B.; Liu, X.; Li, G.; Pei, G.; Zhao, B. Combined daytime radiative cooling and solar photovoltaic/thermal hybrid system for year-round energy saving in buildings. *Energy* **2024**, *304*, No. 132178.
(432) Hu, M.; Zhao, B.; Ao, X.; Zhao, P.; Su, Y.; Pei, G. Field investigation of a hybrid photovoltaic-photothermic-radiative cooling system. *Appl. Energy* **2018**, *231*, 288−300.
(433) Zeyghami, M.; Khalili, F. Performance improvement of dry cooled advanced concentrating solar power plants using daytime radiative cooling. *Energy Convers. Manage.* **2015**, *106*, 10−20.
(434) Aili, A.; Tan, G.; Yin, X.; Yang, R. Radiative cooling and cold storage for concentrated solar power plants. *Energy Storage Sav.* **2022**, *1* (2), 93−101.
(435) Aili, A.; Zhao, D.; Tan, G.; Yin, X.; Yang, R. Reduction of water consumption in thermal power plants with radiative sky cooling. *Appl. Energy* **2021**, *302*, No. 117515.
(436) Shaban, W. M.; Kabeel, A.; Attia, M. E. H.; Talaat, F. M. Optimizing photovoltaic thermal solar systems efficiency through advanced artificial intelligence driven thermal management techniques. *Appl. Therm. Eng.* **2024**, *247*, No. 123029.
(437) Sutanto, B.; Iacovides, H.; Nasser, A.; Cioncolini, A.; Afgan, I.; Indartono, Y. S.; Prasetyo, T.; Wijayanta, A. T. Design and analysis of passively cooled floating photovoltaic systems. *Appl. Therm. Eng.* **2024**, *236*, No. 121801.
(438) Sutanto, B.; Iacovides, H.; Nasser, A.; Cioncolini, A.; Afgan, I. Efficiency improvement of floating photovoltaic panels with natural convection cooling loops: Multi-physics thermal modelling. *Sol. Energy* **2025**, *286*, No. 113170.
(439) Hernandez-Perez, J.; Carrillo, J.; Bassam, A.; Flota-Banuelos, M.; Patino-Lopez, L. A new passive PV heatsink design to reduce efficiency losses: A computational and experimental evaluation. *Renewable Energy* **2020**, *147*, 1209−1220.
(440) Khoshvaght-Aliabadi, M.; Chamanroy, Z.; Feizabadi, A.; Kang, Y. Optimal thermal management of High-Concentrator photovoltaic systems using heat sinks with various cavity configurations. *Energy Convers. Manage.* **2025**, *345*, No. 120208.
(441) Ma, T.; Li, Z.; Zhao, J. Photovoltaic panel integrated with phase change materials (PV-PCM): technology overview and materials selection. *Renewable Sustainable Energy Rev.* **2019**, *116*, No. 109406.
(442) Sun, Y.; Javed, M.; Ji, Y.; Nawaz, M. Z.; Wang, Y.; Cai, Z.; Xu, B. Design and preparation of flexible double-layered daytime radiative cooling composite film with antifouling property. *Sol. Energy Mater. Sol. Cells* **2022**, *245*, No. 111836.
(443) Atiganyanun, S.; Plumley, J. B.; Han, S. J.; Hsu, K.; Cytrynbaum, J.; Peng, T. L.; Han, S. M.; Han, S. E. Effective radiative cooling by paint-format microsphere-based photonic random media. *ACS Photonics* **2018**, *5* (4), 1181−1187.
(444) Heo, S. Y.; Kim, D. H.; Song, Y. M.; Lee, G. J. Determining the effectiveness of radiative cooler-integrated solar cells. *Adv. Energy Mater.* **2022**, *12* (10), No. 2103258.
(445) Chen, Y. H.; Hwang, C. W.; Chang, S. W.; Tsai, M. T.; Jayakumaran, K. N.; Yang, L. C.; Lo, Y. C.; Ko, F. H.; Wang, H. C.;

Chen, H. L. Eco-Friendly Transparent Silk Fibroin Radiative Cooling Film for Thermal Management of Optoelectronics. *Adv. Funct. Mater.* **2023**, *33* (33), No. 2301924.
(446) Hamdan, M. O.; Gerner, F. M.; Abu-Nabah, B. A.; Sheikh, Y.; Moursi, K. Innovative passive cooling of photovoltaic panel using loop heat pipe technology with passive daytime radiative cooling. *Renewable Energy* **2024**, *237*, No. 121641.
(447) Walther, G.-R.; Post, E.; Convey, P.; Menzel, A.; Parmesan, C.; Beebee, T. J.; Fromentin, J.-M.; Hoegh-Guldberg, O.; Bairlein, F. Ecological responses to recent climate change. *Nature* **2002**, *416* (6879), 389−395.
(448) Biardeau, L. T.; Davis, L. W.; Gertler, P.; Wolfram, C. Heat exposure and global air conditioning. *Nat. Sustainability* **2020**, *3* (1), 25−28.
(449) Patz, J. A.; Campbell-Lendrum, D.; Holloway, T.; Foley, J. A. Impact of regional climate change on human health. *Nature* **2005**, *438* (7066), 310−317.
(450) Ji, D.; Liu, P.; Im, P.; Shin, S.; Kim, J. Thermal interface hydrogel composites mechanically compliant with curvy skins and rigid electronic modules. *Adv. Funct. Mater.* **2024**, *34* (37), No. 2402144.
(451) Tong, J. K.; Huang, X.; Boriskina, S. V.; Loomis, J.; Xu, Y.; Chen, G. Infrared-transparent visible-opaque fabrics for wearable personal thermal management. *ACS Photonics* **2015**, *2* (6), 769−778.
(452) Zhang, X.; Yang, W.; Shao, Z.; Li, Y.; Su, Y.; Zhang, Q.; Hou, C.; Wang, H. A moisture-wicking passive radiative cooling hierarchical metafabric. *ACS Nano* **2022**, *16* (2), 2188−2197.
(453) Liu, Y.; Zhang, H.; Zhang, Y.; Liang, C.; An, Q. Rendering passive radiative cooling capability to cotton textile by an alginate/CaCO3 coating via synergistic light manipulation and high water permeation. *Compos. B: Eng.* **2022**, *240*, No. 109988.
(454) Ao, S.; Li, B.; Hu, X.; Su, X.; Sun, F. Nanoengineered wool textiles with wrinkled patterns for enhanced directional radiative cooling and sun-shade effects. *ACS Appl. Eng. Mater.* **2024**, *2* (11), 2689−2697.
(455) Hsu, P.-C.; Liu, C.; Song, A. Y.; Zhang, Z.; Peng, Y.; Xie, J.; Liu, K.; Wu, C.-L.; Catrysse, P. B.; Cai, L.; et al. A dual-mode textile for human body radiative heating and cooling. *Sci. Adv.* **2017**, *3* (11), No. e1700895.
(456) Chen, Z.; Zhang, Q.; Ding, L.; Lv, G.; Liu, T.; Yang, Z.; Jiang, Y.; Li, L.; Li, W.; Ding, F.; et al. An infrared-transparent textile with high drawing processed Nylon 6 nanofibers. *Nat. Commun.* **2025**, *16* (1), No. 2009.
(457) Zeng, S.; Pian, S.; Su, M.; Wang, Z.; Wu, M.; Liu, X.; Chen, M.; Xiang, Y.; Wu, J.; Zhang, M.; et al. Hierarchical-morphology metafabric for scalable passive daytime radiative cooling. *Science* **2021**, *373* (6555), 692−696.
(458) Zhu, B.; Li, W.; Zhang, Q.; Li, D.; Liu, X.; Wang, Y.; Xu, N.; Wu, Z.; Li, J.; Li, X.; et al. Subambient daytime radiative cooling textile based on nanoprocessed silk. *Nat. Nanotechnol.* **2021**, *16* (12), 1342−1348.
(459) Zhang, Q.; Qi, C.; Wang, X.; Zhu, B.; Li, W.; Xiao, X.; Fu, H.; Hu, S.; Zhu, S.; Xu, W.; Zhu, J. Daytime radiative cooling dressings for accelerating wound healing under sunlight. *Nat. Chem. Eng.* **2024**, *1* (4), 301−310.
(460) Wang, X.; Du, X.; Xu, D.; Wei, T.; Zhang, Q.; Chen, Z.; Kong, D.; Wei, K.; Zhou, L.; Zhu, B.; et al. A Passive Sweat-Responsive Thermoregulatory Textile with the Largest Thermal Comfort Zone. *ACS Nano* **2025**, *19* (21), 19977−19988.
(461) Peng, K.; Feng, K.; Chen, B.; Shan, Y.; Zhang, N.; Wang, P.; Fang, K.; Bai, Y.; Zou, X.; Wei, W.; et al. The global power sector's low-carbon transition may enhance sustainable development goal achievement. *Nat. Commun.* **2023**, *14* (1), No. 3144.
(462) Pehl, M.; Arvesen, A.; Humpenöder, F.; Popp, A.; Hertwich, E. G.; Luderer, G. Understanding future emissions from low-carbon power systems by integration of life-cycle assessment and integrated energy modelling. *Nat. Energy* **2017**, *2* (12), 939−945.
(463) Creutzig, F.; Agoston, P.; Goldschmidt, J. C.; Luderer, G.; Nemet, G.; Pietzcker, R. C. The underestimated potential of solar energy to mitigate climate change. *Nat. Energy* **2017**, *2* (9), No. 17140.
(464) Liu, L.; He, G.; Wu, M.; Liu, G.; Zhang, H.; Chen, Y.; Shen, J.; Li, S. Climate change impacts on planned supply−demand match in global wind and solar energy systems. *Nat. Energy* **2023**, *8* (8), 870−880.
(465) Zheng, D.; Tong, D.; Davis, S. J.; Qin, Y.; Liu, Y.; Xu, R.; Yang, J.; Yan, X.; Geng, G.; Che, H.; Zhang, Q. Climate change impacts on the extreme power shortage events of wind-solar supply systems worldwide during 1980−2022. *Nat. Commun.* **2024**, *15* (1), No. 5225.
(466) Xu, N.; Zhu, P.; Sheng, Y.; Zhou, L.; Li, X.; Tan, H.; Zhu, S.; Zhu, J. Synergistic tandem solar electricity-water generators. *Joule* **2020**, *4* (2), 347−358.
(467) Zuo, H.; Bi, K.; Hao, H. A state-of-the-art review on the vibration mitigation of wind turbines. *Renewable Sustainable Energy Rev.* **2020**, *121*, No. 109710.
(468) Liu, D.; Zhao, F.-Y.; Tang, G.-F. Active low-grade energy recovery potential for building energy conservation. *Renewable Sustainable Energy Rev.* **2010**, *14* (9), 2736−2747.
(469) Kraemer, D.; Jie, Q.; McEnaney, K.; Cao, F.; Liu, W.; Weinstein, L. A.; Loomis, J.; Ren, Z.; Chen, G. Concentrating solar thermoelectric generators with a peak efficiency of 7.4%. *Nat. Energy* **2016**, *1* (11), No. 16153.
(470) Rodrigo, P.; Valera, A.; Fernández, E.; Almonacid, F. Performance and economic limits of passively cooled hybrid thermoelectric generator-concentrator photovoltaic modules. *Appl. Energy* **2019**, *238*, 1150−1162.
(471) Lekbir, A.; Hassani, S.; Ab Ghani, M. R.; Gan, C. K.; Mekhilef, S.; Saidur, R. Improved energy conversion performance of a novel design of concentrated photovoltaic system combined with thermoelectric generator with advance cooling system. *Energy Convers. Manage.* **2018**, *177*, 19−29.
(472) Zhao, B.; Pei, G.; Raman, A. P. Modeling and optimization of radiative cooling based thermoelectric generators. *Appl. Phys. Lett.* **2020**, *117* (16), No. 163903, DOI: 10.1063/5.0022667.
(473) Shi, Z.; Zhang, K.; Jiang, K.; Li, H.; Ye, P.; Yang, H.; Mahian, O. Maximizing energy generation: A study of radiative cooling-based thermoelectric power devices. *Energy* **2023**, *274*, No. 127283.
(474) Zhang, S.; Wu, Z.; Liu, Z.; Hu, Z. An emerging energy technology: self-uninterrupted electricity power harvesting from the sun and cold space. *Adv. Energy Mater.* **2023**, *13* (19), No. 2300260.
(475) Xia, Z.; Zhang, Z.; Meng, Z.; Yu, Z. A 24-hour thermoelectric generator simultaneous using solar heat energy and space cold energy. *J. Quant. Spectrosc. Radiat. Transfer* **2020**, *251*, No. 107038.
(476) Fu, Y.; Chen, L.; Guo, Y.; Shi, Y.; Liu, Y.; Zeng, Y.; Lin, Y.; Luo, D. Pyramid textured photonic films with high-refractive index fillers for efficient radiative cooling. *Adv. Sci.* **2024**, *11* (39), No. 2404900.
(477) Mu, E.; Wu, Z.; Wu, Z.; Chen, X.; Liu, Y.; Fu, X.; Hu, Z. A novel self-powering ultrathin TEG device based on micro/nano emitter for radiative cooling. *Nano Energy* **2019**, *55*, 494−500.
(478) Liu, J.-Z.; Jiang, W.; Zhuo, S.; Rong, Y.; Li, Y.-Y.; Lu, H.; Hu, J.; Wang, X.-Q.; Chen, W.; Liao, L.-S.; et al. Large-area radiation-modulated thermoelectric fabrics for high-performance thermal management and electricity generation. *Sci. Adv.* **2025**, *11* (1), No. eadr2158.
(479) Shi, X.; Luo, Y.; Liu, C.; Zhou, G.; Liu, C.; Li, M. C.; Mei, C. Sustainable All-Biomass Radiative Coolers with Biomimetic Thorny Fiber for Enhanced Thermoelectric Power Generation. *Adv. Mater.* **2025**, *38* (5), No. e16401.
(480) Chen, S.; Lin, K.; Liu, S.; Kwok, C. T.; Liang, L.; Li, Z.; Wu, S.; Liu, Z.; Wang, C.; Pan, A.; et al. Bioinspired metafilms for all-weather energy harvesting: Adaptive thermal regulation and raindrop electricity generation. *Sci. Adv.* **2025**, *11* (21), No. eadu2895.
(481) Khan, S.; Kim, J.; Roh, K.; Park, G.; Kim, W. High power density of radiative-cooled compact thermoelectric generator based on body heat harvesting. *Nano Energy* **2021**, *87*, No. 106180.
(482) Zhang, S.; Liu, Z.; Wu, Z.; Yao, Z.; Zhang, W.; Zhang, Y.; Guan, Z.; Lin, H.; Cheng, H.; Mu, E.; et al. Boosting self-powered wearable thermoelectric generator with solar absorber and radiative cooler. *Nano Energy* **2024**, *132*, No. 110381.
(483) Beysens, D. The case for alternative fresh water sources. 2000.

(484) Tu, Y.; Wang, R.; Zhang, Y.; Wang, J. Progress and expectation of atmospheric water harvesting. *Joule* **2018**, *2* (8), 1452−1475.
(485) Nilsson, T.; Vargas, W. E.; Niklasson, G. A.; Granqvist, C. Condensation of water by radiative cooling. *Renewable Energy* **1994**, *5* (1−4), 310−317.
(486) Bijarniya, J. P.; Sarkar, J.; Maiti, P. Review on passive daytime radiative cooling: Fundamentals, recent researches, challenges and opportunities. *Renewable Sustainable Energy Rev.* **2020**, *133*, No. 110263.
(487) Zhou, M.; Song, H.; Xu, X.; Shahsafi, A.; Qu, Y.; Xia, Z.; Ma, Z.; Kats, M. A.; Zhu, J.; Ooi, B. S.; et al. Vapor condensation with daytime radiative cooling. *Proc. Natl. Acad. Sci. U.S.A.* **2021**, *118* (14), No. e2019292118.
(488) Bai, S.; Tian, Y.; Zeng, Y.; Chao, L.; Pan, A.; Ho, T.; Chen, S.; Shang, J.; Tso, C. Adsorption-based atmospheric water harvesting by passive radiative condensers for continuous decentralized water production. *Appl. Therm. Eng.* **2023**, *225*, No. 120163.
(489) Bai, S.; Chao, L.; Pan, A.; Ho, T.; Lin, K.; Tso, C. Study of the relative humidity effects on the water condensation performance of adsorption-based atmospheric water harvesting using passive radiative condensers. *Appl. Therm. Eng.* **2024**, *244*, No. 122702.
(490) Dai, X.; Sun, N.; Nielsen, S. O.; Stogin, B. B.; Wang, J.; Yang, S.; Wong, T.-S. Hydrophilic directional slippery rough surfaces for water harvesting. *Sci. Adv.* **2018**, *4* (3), No. eaaq0919.
(491) Chen, G.; Wang, Y.; Qiu, J.; Cao, J.; Zou, Y.; Wang, S.; Jia, D.; Zhou, Y. A facile bioinspired strategy for accelerating water collection enabled by passive radiative cooling and wettability engineering. *Mater. Des.* **2021**, *206*, No. 109829.
(492) Wang, X.; Wei, H.; Luo, N.; Luo, H.; Zhou, X.; Qin, B.; Mei, Y.; Zhang, Y. Smart materials and micro/nanoarchitectonics for water harvesting: from fundamental mechanism to advanced application. *Composites, Part A* **2024**, *184*, No. 108241.
(493) Wang, Z.; Li, H.; Yang, X.; Guan, M.; Wang, L. Multi-bioinspired janus copper mesh for improved gravity-irrelevant directional water droplet and flow transport. *Langmuir* **2022**, *38* (6), 2137−2144.
(494) Bai, S.; Yao, X.; Wong, M. Y.; Xu, Q.; Li, H.; Lin, K.; Zhou, Y.; Ho, T. C.; Pan, A.; Chen, J.; et al. Enhancement of water productivity and energy efficiency in sorption-based atmospheric water harvesting systems: From material, component to system level. *ACS Nano* **2024**, *18* (46), 31597−31631.
(495) Kim, H.; Rao, S. R.; Kapustin, E. A.; Zhao, L.; Yang, S.; Yaghi, O. M.; Wang, E. N. Adsorption-based atmospheric water harvesting device for arid climates. *Nat. Commun.* **2018**, *9* (1), No. 1191.
(496) Wang, Y.; Gao, S.; Zhong, H.; Zhang, B.; Cui, M.; Jiang, M.; Wang, S.; Wang, Z. Heterogeneous wettability and radiative cooling for efficient deliquescent sorbents-based atmospheric water harvesting. *Cell Rep. Phys. Sci.* **2022**, *3* (5), No. 100879, DOI: 10.1016/j.xcrp.2022.100879.
(497) Huang, Y.; Li, Q.; Chen, Z.; Chen, M. Sorbent-coupled radiative cooling and solar heating to improve atmospheric water harvesting. *J. Colloid Interface Sci.* **2024**, *655*, 527−534.
(498) *Atmospheric Water Generator Market Size & Share 2025 to 2034*. 2025 (accessed 2026).
(499) Zhang, Y.; Zhu, W.; Zhang, C.; Peoples, J.; Li, X.; Felicelli, A. L.; Shan, X.; Warsinger, D. M.; Borca-Tasciuc, T.; Ruan, X.; Li, T. Atmospheric water harvesting by large-scale radiative cooling cellulose-based fabric. *Nano Lett.* **2022**, *22* (7), 2618−2626.
(500) Xiao, F.; Zhang, K.; Zhang, Z.; Jiao, S.; Zhang, Y. A comprehensive review of atmospheric water harvesting: from conventional techniques to radiative cooling solutions. *Environ. Rev.* **2025**, *33*, 1−16.
(501) Khalil, B.; Adamowski, J.; Shabbir, A.; Jang, C.; Rojas, M.; Reilly, K.; Ozga-Zielinski, B. A review: dew water collection from radiative passive collectors to recent developments of active collectors. *Sustainable Water Resour. Manage.* **2016**, *2* (1), 71−86.
(502) Kim, S.; Lee, S.; Lee, J.; Choi, H. W.; Choi, W.; Kang, Y. T. Passive isothermal film with self-switchable radiative cooling-driven water sorption layer for arid climate applications. *Nat. Commun.* **2024**, *15* (1), No. 8000.
(503) Kim, S.; Kim, M.; Jang, K.; Yoon, S. S.; Choi, W.; Lee, H.; Shim, J. H.; Kang, Y. T. Indoor CO2 capture-driven passive cooling for photovoltaics with ventilation energy reduction utilizing amine-functionalized adsorbents. *Energy Convers. Manage.* **2024**, *307*, No. 118351.
(504) Kim, S.; Park, J. H.; Lee, J. W.; Kim, Y.; Kang, Y. T. Self-recovering passive cooling utilizing endothermic reaction of NH4NO3/H2O driven by water sorption for photovoltaic cell. *Nat. Commun.* **2023**, *14* (1), No. 2374.
(505) Davies, B. Why are glaciers important? 2024.
(506) Gardner, A. S.; Moholdt, G.; Cogley, J. G.; Wouters, B.; Arendt, A. A.; Wahr, J.; Berthier, E.; Hock, R.; Pfeffer, W. T.; Kaser, G.; et al. A Reconciled Estimate of Glacier Contributions to Sea Level Rise: 2003 to 2009. *Science* **2013**, *340* (6134), 852−857.
(507) Rounce, D. R.; Hock, R.; Maussion, F.; Hugonnet, R.; Kochtitzky, W.; Huss, M.; Berthier, E.; Brinkerhoff, D.; Compagno, L.; Copland, L.; et al. Global glacier change in the 21st century: Every increase in temperature matters. *Science* **2023**, *379* (6627), 78−83.
(508) Fransen, T. 1.5 Degrees C: Understanding World's Critical Warming Threshold. 2025.
(509) Oerlemans, J.; Haag, M.; Keller, F. Slowing down the retreat of the Morteratsch glacier, Switzerland, by artificially produced summer snow: a feasibility study. *Clim. Change* **2017**, *145* (1), 189−203.
(510) Fischer, A.; Helfricht, K.; Stocker-Waldhuber, M. Local reduction of decadal glacier thickness loss through mass balance management in ski resorts. *Cryosphere* **2016**, *10* (6), 2941−2952.
(511) Xie, Y.-D.; Wang, F.-T.; Zhang, H.; Du, W.-T.; Zhao, W.-B. Assessing the impact of artificial geotextile covers on glacier mass balance and energy fluxes. *Adv. Clim. Change Res.* **2024**, *15* (6), 1147−1159.
(512) Xie, Y.; Wang, F.; Xu, C.; Yue, X.; Yang, S. Applying Artificial Cover to Reduce Melting in Dagu Glacier in the Eastern Qinghai-Tibetan Plateau. *Remote Sens.* **2023**, *15* (7), 1755.
(513) Grünewald, T.; Wolfsperger, F.; Lehning, M. Snow farming: conserving snow over the summer season. *Cryosphere* **2018**, *12* (1), 385−400.
(514) Olefs, M.; Obleitner, F. Numerical simulations on artificial reduction of snow and ice ablation *Water Resour. Res.* 2007; Vol. *43* 6 DOI: 10.1029/2006WR005065.
(515) Wang, X.; Qin, D.-H.; Ren, J.-W.; Wang, F.-T. Numerical estimation of thermal insulation performance of different coverage schemes at three places for snow storage. *Adv. Clim. Change Res.* **2021**, *12* (6), 903−912.
(516) Wang, F.-T.; Liu, S.-S.; Wang, X.; Li, H.-L.; Xu, C.-H.; Wang, L.; Xue, Y.-A.; Yue, X.-Y. Geotextile protection of glacier: Observed and simulated impacts on energy and mass balance. *Adv. Clim. Change Res.* **2023**, *14* (6), 963−975.
(517) Cao, N.; Chi, H.; Zhu, B.; Pang, H.; Ke, C.; Zhang, X.; Chen, J.; Zhu, J. Challenges to materials for local glacier conservation. *Nat. Water* **2025**, *3* (3), 251−255.
(518) Wang, F.; Yue, X.; Wang, L.; Li, H.; Du, Z.; Ming, J.; Li, Z. Applying artificial snowfall to reduce the melting of the Muz Taw Glacier, Sawir Mountains. *Cryosphere* **2020**, *14* (8), 2597−2606.
(519) Senese, A.; Azzoni, R. S.; Maragno, D.; D'Agata, C.; Fugazza, D.; Mosconi, B.; Trenti, A.; Meraldi, E.; Smiraglia, C.; Diolaiuti, G. The non-woven geotextiles as strategies for mitigating the impacts of climate change on glaciers. *Cold Reg. Sci. Technol.* **2020**, *173*, 103007.
(520) Huss, M.; Schwyn, U.; Bauder, A.; Farinotti, D. Quantifying the overall effect of artificial glacier melt reduction in Switzerland, 2005−2019. *Cold Reg. Sci. Technol.* **2021**, *184*, 103237.
(521) Li, J.; Liang, Y.; Li, W.; Xu, N.; Zhu, B.; Wu, Z.; Wang, X.; Fan, S.; Wang, M.; Zhu, J. Protecting ice from melting under sunlight via radiative cooling. *Sci. Adv.* **2022**, *8* (6), No. eabj9756.
(522) He, H.; Soden, B. J.; Vecchi, G. A.; Yang, W. Stratospheric aerosol injection can weaken the carbon dioxide greenhouse effect. *Commun. Earth Environ.* **2025**, *6* (1), No. 485.

(523) McCormick, M. P.; Thomason, L. W.; Trepte, C. R. Atmospheric effects of the Mt Pinatubo eruption. *Nature* **1995**, *373* (6513), 399−404.
(524) Dykema, J. A.; Keith, D. W.; Keutsch, F. N. Improved aerosol radiative properties as a foundation for solar geoengineering risk assessment. *Geophys. Res. Lett.* **2016**, *43* (14), 7758−7766.
(525) Laakso, A.; Niemeier, U.; Visioni, D.; Tilmes, S.; Kokkola, H. Dependency of the impacts of geoengineering on the stratospheric sulfur injection strategy − Part 1: Intercomparison of modal and sectional aerosol modules. *Atmos. Chem. Phys.* **2022**, *22* (1), 93−118.
(526) Heckendorn, P.; Weisenstein, D.; Fueglistaler, S.; Luo, B. P.; Rozanov, E.; Schraner, M.; Thomason, L. W.; Peter, T. The impact of geoengineering aerosols on stratospheric temperature and ozone. *Environ. Res. Lett.* **2009**, *4* (4), No. 045108.
(527) Pitari, G.; Aquila, V.; Kravitz, B.; Robock, A.; Watanabe, S.; Cionni, I.; Luca, N. D.; Genova, G. D.; Mancini, E.; Tilmes, S. Stratospheric ozone response to sulfate geoengineering: Results from the Geoengineering Model Intercomparison Project (GeoMIP). *J. Geophys. Res.: Atmos.* **2014**, *119* (5), 2629−2653.
(528) Weisenstein, D. K.; Keith, D. W.; Dykema, J. A. Solar geoengineering using solid aerosol in the stratosphere. *Atmos. Chem. Phys.* **2015**, *15* (20), 11835−11859.
(529) Vattioni, S.; Weber, R.; Feinberg, A.; Stenke, A.; Dykema, J. A.; Luo, B.; Kelesidis, G. A.; Bruun, C. A.; Sukhodolov, T.; Keutsch, F. N.; et al. A fully coupled solid-particle microphysics scheme for stratospheric aerosol injections within the aerosol−chemistry−climate model SOCOL-AERv2. *Geosci. Model Dev.* **2024**, *17* (21), 7767−7793.
(530) Vennes, B.; Bain, A.; Davies, J. F.; Preston, T. C. Optimizing stratospheric aerosol lifetime and albedo through particle morphology and refractive index. *Environ. Sci.: Atmos.* **2025**, *5* (9), 998−1013.
(531) Solomon, S. Stratospheric ozone depletion: A review of concepts and history. *Rev. Geophys.* **1999**, *37* (3), 275−316.
(532) Huynh, H. N.; McNeill, V. F. The potential environmental and climate impacts of stratospheric aerosol injection: a review. *Environ. Sci.: Atmos.* **2024**, *4* (2), 114−143.
(533) Vattioni, S.; Peter, T.; Weber, R.; Dykema, J. A.; Luo, B.; Stenke, A.; Feinberg, A.; Sukhodolov, T.; Keutsch, F. N.; Ammann, M.; et al. Injecting solid particles into the stratosphere could mitigate global warming but currently entails great uncertainties. *Commun. Earth Environ.* **2025**, *6* (1), No. 132.
(534) Keith, D. W.; Weisenstein, D. K.; Dykema, J. A.; Keutsch, F. N. Stratospheric solar geoengineering without ozone loss. *Proc. Natl. Acad. Sci. U.S.A.* **2016**, *113* (52), 14910−14914.
(535) Gao, R.-S.; Rosenlof, K. H.; Kärcher, B.; Tilmes, S.; Toon, O. B.; Maloney, C.; Yu, P. Toward practical stratospheric aerosol albedo modification: Solar-powered lofting. *Sci. Adv.* **2021**, *7* (20), No. eabe3416.
(536) Henry, M.; Bednarz, E. M.; Haywood, J. How does the latitude of stratospheric aerosol injection affect the climate in UKESM1? *Atmos. Chem. Phys.* **2024**, *24* (23), 13253−13268.
(537) Paik, S.; Min, S.-K.; Iles, C. E.; Fischer, E. M.; Schurer, A. P. Volcanic-induced global monsoon drying modulated by diverse El Niño responses. *Sci. Adv.* **2020**, *6* (21), No. eaba1212.
(538) Grinsted, A.; Moore, J. C.; Jevrejeva, S. Observational evidence for volcanic impact on sea level and the global water cycle. *Proc. Natl. Acad. Sci. U.S.A.* **2007**, *104* (50), 19730−19734.
(539) Asutosh, A.; Tilmes, S.; Bednarz, E. M.; Fadnavis, S. South Asian Summer Monsoon under stratospheric aerosol intervention. *npj Clim. Atmos. Sci.* **2025**, *8* (1), No. 3.
(540) Trisos, C. H.; Amatulli, G.; Gurevitch, J.; Robock, A.; Xia, L.; Zambri, B. Potentially dangerous consequences for biodiversity of solar geoengineering implementation and termination. *Nat. Ecol. Evol.* **2018**, *2* (3), 475−482.
(541) Jinnah, S.; Dove, Z. Solar radiation management: a history of the governance and political milestones. *Environ. Sci.: Atmos.* **2025**, *5* (6), 656−673.
(542) Chen, Y.; Xin, Y. Implications of geoengineering under the 1.5 °C target: Analysis and policy suggestions. *Adv. Clim. Change Res.* **2017**, *8* (2), 123−129.
(543) Huang, J.; Lin, C.; Li, Y.; Huang, B. Effects of humidity, aerosol, and cloud on subambient radiative cooling. *Int. J. Heat Mass Transfer* **2022**, *186*, No. 122438.
(544) Yang, M.; Zhong, H.; Li, T.; Wu, B.; Wang, Z.; Sun, D. Phase change material enhanced radiative cooler for temperature-adaptive thermal regulation. *ACS Nano* **2023**, *17* (2), 1693−1700.
(545) Choi, M.; Park, J.; Shin, J.; Keawmuang, H.; Kim, H.; Yun, J.; Seong, J.; Rho, J. Realization of high-performance optical metasurfaces over a large area: a review from a design perspective. *npj Nanophotonics* **2024**, *1*, No. 31.
(546) So, S.; Badloe, T.; Noh, J.; Bravo-Abad, J.; Rho, J. Deep learning enabled inverse design in nanophotonics. *Nanophotonics* **2020**, *9* (5), 1041−1057.
(547) Kang, M.; Choi, S.; Fu, K.; Liu, X.; Wei, Z.; Jin, L.; Wang, H.; J F Martin, O.; Martin, O. J. F.; K W Yang, J.; Yang, J. K. W.; So, S. AI-assisted metaphotonics. *Opto-Electron. Adv.* **2026**, *9*, No. 250263.
(548) Ma, W.; Liu, Z.; Kudyshev, Z. A.; Boltasseva, A.; Cai, W.; Liu, Y. Deep learning for the design of photonic structures. *Nat. Photonics* **2021**, *15* (2), 77−90.
(549) Keawmuang, H.; Hu, S.; Badloe, T.; So, S.; Rho, J. Hybrid Frameworks Integrating Deep Learning and Optimization Methods for Inverse Design in Nanophotonics. *ACS Appl. Mater. Interfaces* **2025**, *17* (23), 33259−33270.
(550) Jung, Y.; Ko, S. H. Radiative cooling technology with artificial intelligence. *iScience* **2024**, *27* (12), No. 111325, DOI: 10.1016/j.isci.2024.111325.
(551) Xu, Z.; Shang, W.; Kim, S.; Bobbitt, A.; Lee, E.; Luo, T. Quantum-inspired genetic algorithm for designing planar multilayer photonic structure. *Npj Comput. Mater.* **2024**, *10* (1), No. 257.
(552) Yu, S.; Zhou, P.; Xi, W.; Chen, Z.; Deng, Y.; Luo, X.; Li, W.; Shiomi, J.; Hu, R. General deep learning framework for emissivity engineering. *Light: Sci. Appl.* **2023**, *12* (1), No. 291.
(553) Li, J.; Jiang, Y.; Li, B.; Xu, Y.; Song, H.; Xu, N.; Wang, P.; Zhao, D.; Liu, Z.; Shu, S.; et al. Accelerated photonic design of coolhouse film for photosynthesis via machine learning. *Nat. Commun.* **2025**, *16* (1), No. 1396.
(554) Kim, M. J.; Kim, J. T.; Hong, M. J.; Park, S. W.; Lee, G. J. Deep learning-assisted inverse design of nanoparticle-embedded radiative coolers. *Opt. Express* **2024**, *32* (9), 16235−16247.
(555) Carne, D.; Peoples, J.; Arentz, F.; Ruan, X. True benefits of multiple nanoparticle sizes in radiative cooling paints identified with machine learning. *Int. J. Heat Mass Transfer* **2024**, *222*, No. 125209.
(556) Xiao, C.; Liu, M.; Yao, K.; Zhang, Y.; Zhang, M.; Yan, M.; Sun, Y.; Liu, X.; Cui, X.; Fan, T.; et al. Ultrabroadband and band-selective thermal meta-emitters by machine learning. *Nature* **2025**, *643* (8070), 80−88.
(557) Jiang, S.; Li, M.; Hu, Z.; Zhang, F.; Zhang, X.; Liu, W.; Omer, A. A. A.; Lv, H. A Low-Cost and Large-Scale Producible Polymer Multilayer Radiative Cooling Film for Reducing Plant Heat Stress. *ACS Photonics* **2025**, *12* (1), 528−536.

https://doi.org/10.1021/acsami.6c00074
ACS Appl. Mater. Interfaces 2026, 18, 21363−21423